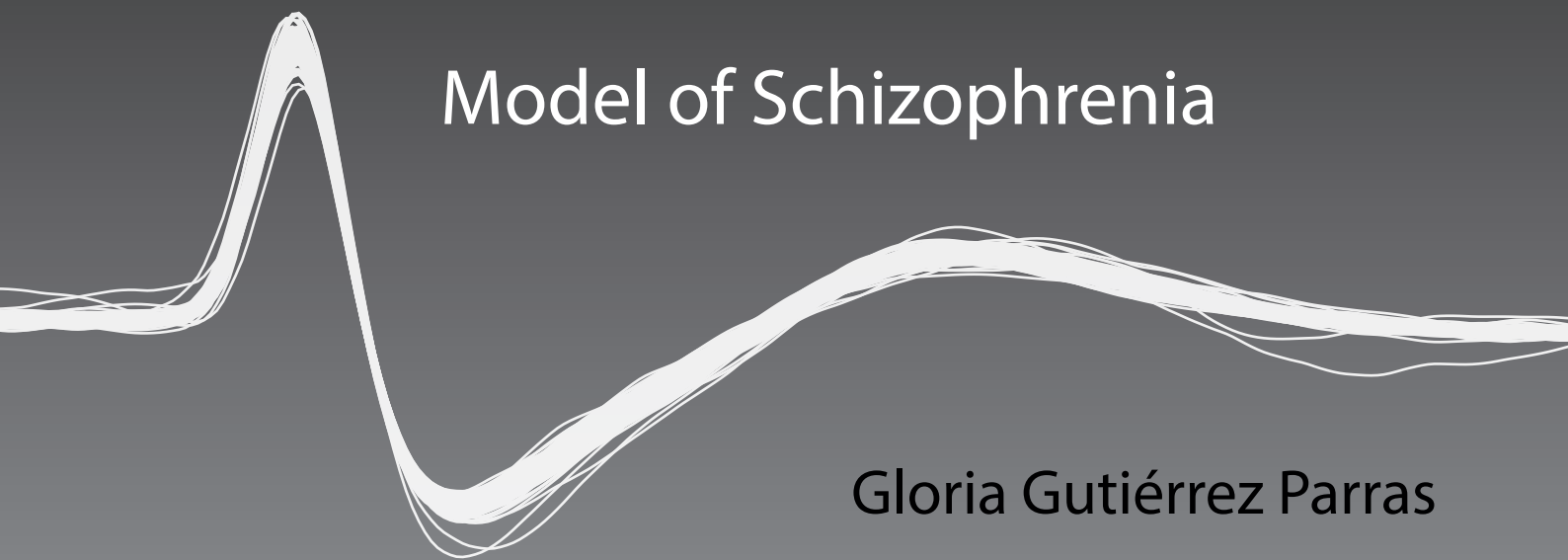
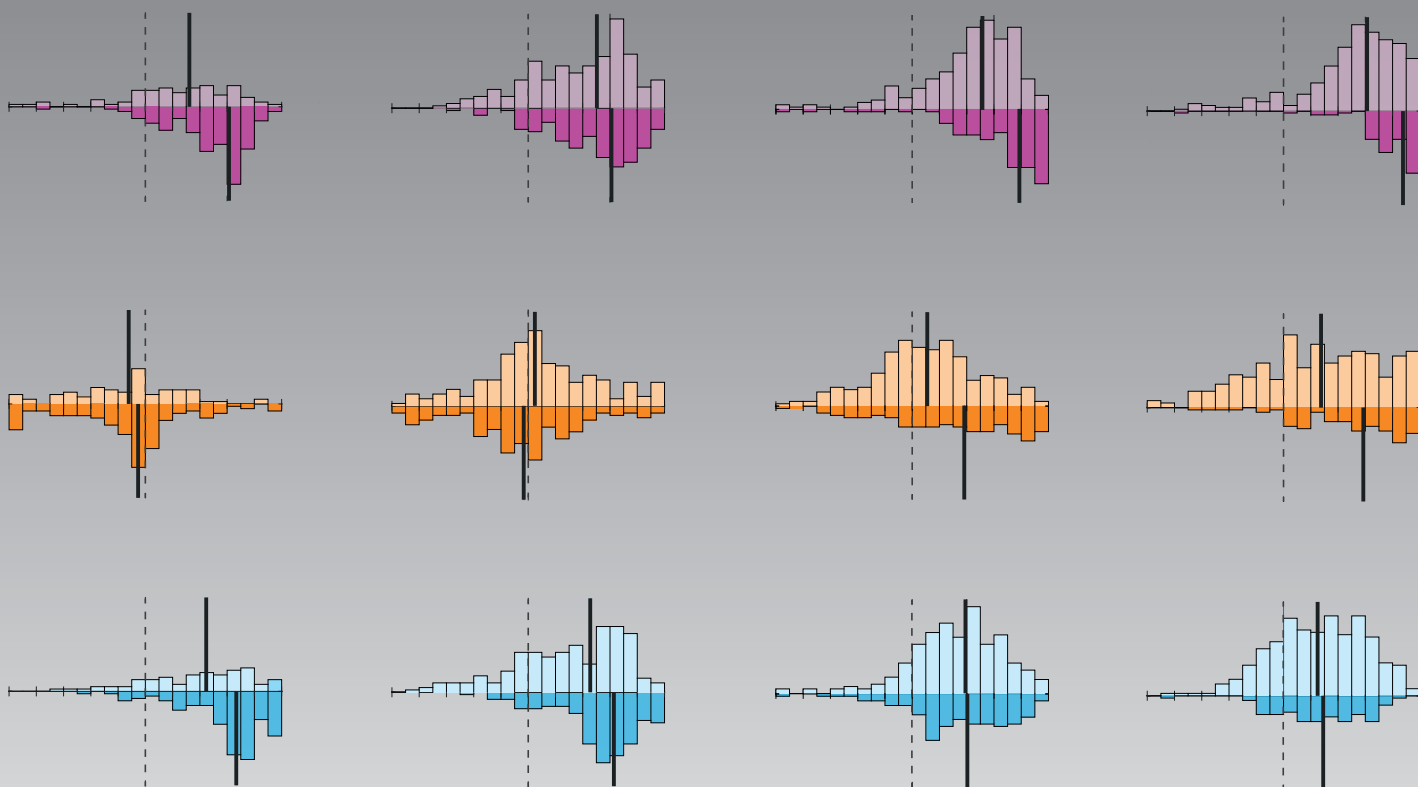


Neuronal Mismatch along the Auditory Hierarchy in an Animal Model of Schizophrenia



Gloria Gutiérrez Parras



**PhD Thesis
2019**

UNIVERSITY OF SALAMANCA

Institute of Neuroscience of Castilla y León (INCyL)

Cognitive and Auditory Neuroscience Laboratory (CANE-LAB)

Doctoral Program in Neurosciences

NEURONAL MISMATCH ALONG THE AUDITORY HIERARCHY IN AN ANIMAL MODEL OF SCHIZOPHRENIA

Thesis submitted by

Gloria Gutiérrez Parras

To obtain the degree of

PhD in Neuroscience

and International Doctor Mention

Supervised by

Dr. Manuel Sánchez Malmierca

Salamanca, April 2019

This study was funded by the Spanish MINECO (SAF2016-75803-P).

Gloria Gutiérrez Parras held a FPI fellowship for Formation PhD from the Spanish MINECO (BES-2014-069113).

Este trabajo ha sido financiado por el Gobierno de España, MINECO (SAF2016-75803-P).

Gloria Gutiérrez Parras contó con una ayuda para Formación de Personal Investigador (FPI) otorgado por el Gobierno de España, MINECO (BES-2014-069113).



Doctoral thesis supervised by

Dr. Manuel Sánchez Malmierca

Cognitive and Auditory Neuroscience Laboratory (CANE-Lab),

Institute of Neuroscience of Castilla y León.

University of Salamanca

Acknowledgements

Gracias a todos los miembros, actuales y pasados, del laboratorio, porque de todos y cada uno de ellos hay un poquito en esta tesis: Yaneri, Dani, David, Flora, Guillermo, Lorena, Cristian, Ana, Antonio, Camilo, Blanca, y en especial a Catalina por demostrarme tanta paciencia en cada una de sus explicaciones y a Javier por hacer fácil lo difícil y “empujarme” en la lucha con MATLAB.

Gracias a Manolo, por haberme dado la posibilidad de realizar esta tesis, por sus enseñanzas, sus consejos, su positividad y gran apoyo en todo momento.

Gracias a todos los miembros del INCyL, por los ratos de charla compartida, los consejos y las ayudas. Especialmente a Marianny por hacer las mejores micro-fotografías y a Nacho por su sabiduría.

Gracias a la división de neurociencias de la Universidad Pablo de Olavide, por iniciarme en este camino de la neurociencia, ayudarme, aconsejarme y recibirme siempre con los brazos abiertos.

Thank you to Pat Michie, Lauren Harms and all the University of Newcastle staff for receiving me so nicely during my stay and be extremely supportive during the manuscript preparation.

Gracias a mi familia, por su constante apoyo y comprensión. Especialmente a mis padres, por haberme dado alas para volar tan alto que yo jamás imaginaría, pero también por darme las razones para querer siempre volver.

Gracias a Guti, por animarme y creer en mí cuando ni yo misma creía. Y gracias a Estorbito Manué, por ser lo más suave, tierno y alegre de cada uno de estos días; siendo el mejor ayudante de doctorando que jamás pudiera imaginar.

La tesis titulada ‘**Discrepancia neuronal a lo largo de la jerarquía auditiva en un modelo animal de esquizofrenia**’ que presenta Gloria Gutiérrez Parras para obtener el título de Doctorado en Neurociencias corresponde a un **compendio de trabajos científicos** previamente publicados o aceptados para publicación. Los artículos se citan a continuación.

The thesis entitled ‘**Neuronal Mismatch along the Auditory Hierarchy in an animal model of Schizophrenia**’ presented by Gloria Gutiérrez Parras to obtain the degree of PhD in Neuroscience correspond to a **compendium of scientific articles** already published or accepted for publication. The articles are listed below.

Study I

Neurons along the auditory pathway exhibit a hierarchical organization of prediction error.

Authors: Gloria G. Parras^{1,2}, Javier Nieto-Diego^{1,2}, Guillermo V. Carbajal^{1,2}, Catalina Valdés-Baizabal^{1,2}, Carles Escera^{3,4,5} & Manuel S. Malmierca^{1,2,6}.

Affiliation: ¹Auditory Neuroscience Laboratory, Institute of Neuroscience of Castilla y León (INCYL), Salamanca, 37007 Castilla y León, Spain. ²The Salamanca Institute for Biomedical Research (IBSAL), Salamanca, 37007 Castilla y León, Spain. ³Brainlab-Cognitive Neuroscience Research Group, Department of Clinical Psychology and Psychobiology, University of Barcelona, Barcelona, 08035 Catalonia, Spain. ⁴Institute of Neuroscience, University of Barcelona, Barcelona, 08035 Catalonia, Spain. ⁵Institut de Recerca Sant Joan de Déu, Esplugues de Llobregat, 08950 Catalonia, Spain. ⁶Department of Cell Biology and Pathology, Faculty of Medicine, University of Salamanca, Salamanca, 37007 Castilla y León, Spain.

Journal: Nature Communications| 8:2148. 2017 Dec 15

Study II

Endocannabinoid Modulation of Stimulus-Specific Adaptation in Inferior Colliculus Neurons of the Rat.

Authors: C. Valdés-Baizabal^{1,2}, G. G. Parras^{1,2}, Y.A. Ayala^{1,4} & M.S. Malmierca^{1,2,3}.

Affiliation: ¹Auditory Neuroscience Laboratory, Institute of Neuroscience of Castilla y León (INCYL), Salamanca, 37007 Castilla y León, Spain. ²The Salamanca Institute for Biomedical Research (IBSAL), Salamanca, 37007 Castilla y León, Spain. ³Departament of Cell Biology and Pathology, Faculty of Medicine, University of Salamanca, Salamanca, 37007 Castilla y León, Spain. ⁴Present address: Instituto de Neurobiología, Universidad Nacional Autónoma de México, Querétaro, México.

Journal: Scientific Reports | 7:6997 | 2017 Aug 1.

DOI: 10.1038/s41598-017-07460-w

Study III

The effect of the NMDA-R antagonist, MK-801, on Neuronal Mismatch along the Rat Auditory Thalamocortical System.

Authors: Gloria G. Parras^{1,2}, Catalina Valdés-Baizabal^{1,2}, Lauren Harms^{3,4,5}, Patricia Michie & Manuel S. Malmierca^{1,2,6}.

Affiliation: ¹Auditory Neuroscience Laboratory, Institute of Neuroscience of Castilla y León (INCYL), Salamanca, 37007 Castilla y León, Spain. ²The Salamanca Institute for Biomedical Research (IBSAL), Salamanca, 37007 Castilla y León, Spain. ³Laboratory of Neuroimmunology. School of Psychology, University of Newcastle, Callaghan, New South Wales, Australia. ⁴Priority Research Centre for Brain and Mental Health Research, University of Newcastle, Callaghan, New South Wales, Australia

Journal: *Under Revision* in BRAIN (Manuscript ID: BRAIN-201900515).

Manuel Sánchez Malmierca, catedrático del departamento de biología celular y patología de la Universidad de Salamanca e investigador del Instituto de Neurociencias de Castilla y León.

CERTIFICA

Que la tesis doctoral titulada:

**NEURONAL MISMATCH ALONG THE AUDITORY HIERARCHY IN AN
ANIMAL MODEL OF SCHIZOPHRENIA**

Se realiza bajo el formato de compendio de artículos, ha sido redactada en inglés, contiene un resumen en español y describe el trabajo de investigación realizado por **Doña Gloria Gutiérrez Parras** bajo mi dirección durante los últimos 4 años.

La memoria de este estudio recoge un análisis detallado y exhaustivo de las respuestas neuronales del sistema auditivo central a diversos contextos auditivos en condiciones sanas y patológicas. Los datos presentados en esta memoria constituyen una aportación original y puedo afirmar que ponen de manifiesto un gran avance y progreso en el área de la Neurociencia.

Por todo ello, considero que esta tesis reúne la calidad y rigor científicos necesarios para que sea defendida en la Universidad de Salamanca como requisito para que **Doña Gloria Gutiérrez Parras** opte al grado de ‘Doctora en Neurociencias’ con ‘Mención Internacional’ por la **Universidad de Salamanca**.

Y para que así conste, firmo el presente certificado,



Department of Biological Sciences and
The Weldon School of Biomedical Engineering
206 S. Martin Jischke Dr.
Purdue University
West Lafayette, Indiana 47907-1791

Edward Bartlett
Associate Professor
Central Auditory Processing Laboratory
<http://bmew.ecn.purdue.edu/caplab/>

Voice: (765) 496-1425
Fax: (765) 496-1912
Email: ebartle@purdue.edu

April 2, 2019

To whom it may concern:

I have read the thesis of Gloria Parras, entitled, *Neuronal Mismatch along the Auditory Hierarchy in an animal model of Schizophrenia*. Her three main chapters consist of two papers that have already been published, one as first author and one as second author, and one paper that is in the review process where she is the first author.

Study I was: Neurons along the auditory pathway exhibit a hierarchical organization of prediction error. In this study, Gloria analyzed responses of neurons in the inferior colliculus (IC), auditory thalamus (MGB), and auditory cortex, both in primary, lemniscal regions and non-primary, non-lemniscal regions. She used a novel battery of sounds where she manipulated the probabilities and predictability of standard and deviant sounds. She differentiated response suppression, or the reduction in response to repeated sounds, from prediction error, or the enhanced responses to novel or low-probability, unpredictable sounds. She found that the adaptation in lemniscal IC and MGB was mainly due to repetition suppression, whereas non-lemniscal MGB, primary and especially non-primary auditory cortex was due mainly to prediction error. This is a new way to analyze and interpret these types of experiments, and it has broad application to understanding predictive coding in sensory systems and mismatch negativity in humans.

Study II was Endocannabinoid Modulation of Stimulus-Specific Adaptation in Inferior Colliculus Neurons of the Rat. In this study, Gloria and Catalina Valdes-Baizabal and colleagues recorded from IC neurons in an oddball paradigm to examine the effects of endocannabinoid modulation on stimulus-specific adaptation (SSA). They found that about half of the neurons were modified by the endogenous endocannabinoid anandamide, mainly by increasing the responses to the standard stimulus. Further testing suggested that effects were mediated primarily by CB1 receptors. This study nicely demonstrated CB1-mediated modulation of SSA, and it sets the stage for further studies to explain the variability of responses, such whether specific cell types or inputs are affected by endocannabinoids.

Study III was the effect of the NMDA-R antagonist, MK-801, on Neuronal Mismatch along the Rat Auditory Thalamocortical System. In the MGB, MK-801 reduced standard responses while maintaining deviant responses, enhancing repetition suppression. In contrast, MK-801 application in auditory cortex resulted in an enhanced deviant response in conjunction with a reduced standard response, resulting in enhanced prediction error. Comparable effects were seen in LFP recordings. These findings suggest that NMDA receptors contribute to novelty detection and prediction error in auditory cortical neurons and are consistent with NMDA dependent effects on evoked potentials in normal and schizophrenic human subjects.

In summary, in my opinion, this is an excellent body of work that merits a public defense to obtain the PhD degree.

Sincerely,

Ed Bartlett, Associate Professor, Depts. of Biological Sciences and Biomedical Engineering



UNIVERSITY OF SALAMANCA
To whom it may concern

Dr. Wolfger von der Behrens
Group leader
Phone +41 44 635 30 43
wolfger@ini.uzh.ch

Zurich, March, 31st 2019

Thesis evaluation of Ms Gloria Gutiérrez Parras

NEURONAL MISMATCH ALONG THE AUDITORY HIERARCHY IN AN ANIMAL MODEL OF SCHIZOPHRENIA

Dear Members of the thesis committee

It is my great pleasure to provide you the result of my evaluation of Ms Gutiérrez Parras thesis' submitted to obtain the degree of *PhD in Neuroscience* and *International Doctor Mention*. Ms Gutiérrez Parras submitted a cumulative thesis composed of a general introduction and discussion and three peer-reviewed journal articles that are either already published (2 articles) or in very advanced stages of publication (1 article).

In her thesis Ms Gutiérrez Parras investigates how different instances of central auditory processing (cortex, thalamus, inferior colliculus) are involved in detecting deviating and novel stimuli in the sensory environment and how this may relate to alterations of this process in the pathological condition (e.g. schizophrenia).

The result of this work is published in two articles in high-profile journals (*Nature Communication* and *Scientific Reports*) and one article is currently under review in *Brain*. These publications address very critical gaps in our understanding of novelty encoding and its relationship to pathological conditions. The two published articles are already highly cited. Overall, this is an excellent thesis with outstanding results and very high scientific quality which without any doubt merits the public defense to obtain the degree *PhD in Neuroscience* and *International Doctor Mention*.

Sincerely,

Dr. Wolfger von der Behrens

Content

1. Abbreviations	8
2. Introduction	9
a. <i>Pathways in the auditory system</i>	10
b. <i>Mismatch Negativity and Stimulus-Specific Adaptation</i>	14
c. <i>Predictive Coding</i>	19
d. <i>Schizophrenia</i>	20
3. Hypothesis	23
4. Objectives	25
5. Summary of Results	27
6. General Discussion	29
7. References	33
8. Publications	44
9. Spanish Summary	141
10. Appendix I	159

1. Abbreviations.

A1, <i>primary auditory cortex.</i>	MEG, <i>magnetoencephalography.</i>
AAF, <i>anterior auditory field.</i>	MGB, <i>medial geniculate body.</i>
AC, <i>auditory cortex.</i>	MGB _L , <i>medial geniculate body lemniscal subdivision.</i>
AC _L , <i>auditory cortex lemniscal.</i>	MGB _{NL} , <i>medial geniculate body non- lemniscal subdivision.</i>
AC _{NL} , <i>auditory cortex non-lemniscal.</i>	MGB _d , <i>medial geniculate body, dorsal subdivision.</i>
AEA, <i>anandamide.</i>	MGB _m , <i>medial geniculate body, medial subdivision.</i>
CAS, <i>cascade sequence.</i>	MGB _v , <i>medial geniculate body, ventral subdivision.</i>
CB, <i>cannabinoid.</i>	MMN, <i>mismatch negativity.</i>
CBR, <i>cannabinoid receptor.</i>	MUA, <i>multi-unit activity.</i>
CB1, <i>endocannabinoid receptor type 1.</i>	NMDA, <i>N-methyl-D-aspartate.</i>
CB2, <i>endocannabinoid receptor type 2.</i>	NMDA-R, <i>N-methyl-D-aspartate receptor.</i>
CF, <i>characteristic frequency.</i>	PAF, <i>posterior auditory field.</i>
CSI, <i>common stimulus-specific adaptation index.</i>	PSTH, <i>peri-stimulus time histogram.</i>
DEV, <i>deviant.</i>	SDF, <i>spike-density function.</i>
EEG, <i>electroencephalography.</i>	SFR, <i>spontaneous firing rate.</i>
ERP, <i>event-related potentials.</i>	SRAF, <i>supra-rhinal auditory field.</i>
FDR, <i>false discovery rate.</i>	STD, <i>standard.</i>
FRA, <i>frequency response area.</i>	TRN, <i>thalamic reticular nucleus.</i>
GABA, <i>gamma-aminobutyric acid.</i>	VAF, <i>ventral auditory field.</i>
GABA-R, <i>gamma-aminobutyric acid receptor.</i>	
IC, <i>inferior colliculus.</i>	
iMM, <i>index of neural mismatch.</i>	
iPE, <i>index of prediction error.</i>	
iRS, <i>index of repetition suppression.</i>	
LFP, <i>local field potential.</i>	
MAS, <i>many-standards sequence.</i>	

Introduction

2. Introduction.

In an ever-changing environment the ability to filter irrelevant information and to detect only the important events determine survival. To achieve this, the auditory brain has evolved to detect novel sounds that unexpectedly violate an otherwise repeated auditory scene. Understanding how a healthy auditory brain process this information is important to uncover how a pathological system is working. Thus, in this thesis I will start studying how novel auditory information is processed along the healthy central auditory system. Next, I will continue studying how these auditory responses are modulated by cannabinoid neuromodulators. Finally, I will study how the ability to detect novel sounds is altered in a rat model of schizophrenia.

a. Pathways in the Auditory System.

The mammalian auditory system is composed of several brain structures and nucleus, along which the complexity of the auditory information arriving at the two ears is processed and transferred to higher auditory centers. In brief, after the sound is transduced into electrical signals in the cochlea, the auditory information is passed through a chain of several brainstem nuclei. These include the cochlear nuclear complex, the lateral superior olive, and the nuclei of the lateral lemniscus.

From the brainstem the auditory information arrives to the inferior colliculus (IC) in the midbrain, and then ascends to the medial geniculate body in the thalamus (MGB), to finally reach the auditory cortex (AC), where the auditory objects are finally assembled. Along the way, many connections occur between the different nuclei, which comprise

connections between the two sides of the brain, top down connections, and even connections from non-auditory modulatory centers.

In this thesis, I have analyzed neuronal responses in the IC, MGB and AC. These three structures conform the upper levels of the central auditory system, and can be morpho-functionally distinguished into two parallel pathways, conforming the so-called lemniscal and non-lemniscal pathway (Calford & Aitkin, 1983; Jones, 2003; Lee & Sherman, 2011).

The lemniscal pathway arise in the central nucleus of the IC (CNIC), where it receives inputs from nuclei of the lateral lemniscus, ascends to the ventral division of the MGB (MGBv), and projects to the primary (A1), anterior (AAF) and ventral (VAF) fields of the AC. The non-lemniscal pathway receives its inputs from multiple sources, including non-auditory centers. It arises in the dorsal (DCIC), lateral (LCIC) and rostral (RCIC) cortices of the IC, projects to the dorsal (MGBd) and medial (MGBm) divisions of the MGB, the output of which is sent to the posterior (PAF) and supra-rhinal (SRAF) auditory fields of the AC (for a detailed review see Malmierca, 2015).

The lemniscal and non-lemniscal pathways exhibit different physiological responses and have distinct functional roles. The lemniscal projections carry tonotopically organized and auditory specific information, suited for the reliable and efficient transfer of information concerning the physical properties of sounds. The non-lemniscal pathway forms part of an integrative system, where temporal information and multisensorial modulation are integrated (Lee & Sherman, 2011).

Additionally, the central auditory system is organized in a hierarchical manner (Malmierca, 2015), where the information passing from the IC to the AC via the MGB is processed forwards and backwards (**Figure 1**). The highest structures, the auditory

thalamus and auditory cortex, are inextricably linked into a functional unit, the usually referred to as the thalamocortical *loop*, with extensive up- and downward communications between them (Bartlett, 2013; Huang & Winer, 2000; Imaizumi & Lee, 2014; Winer, 2006).

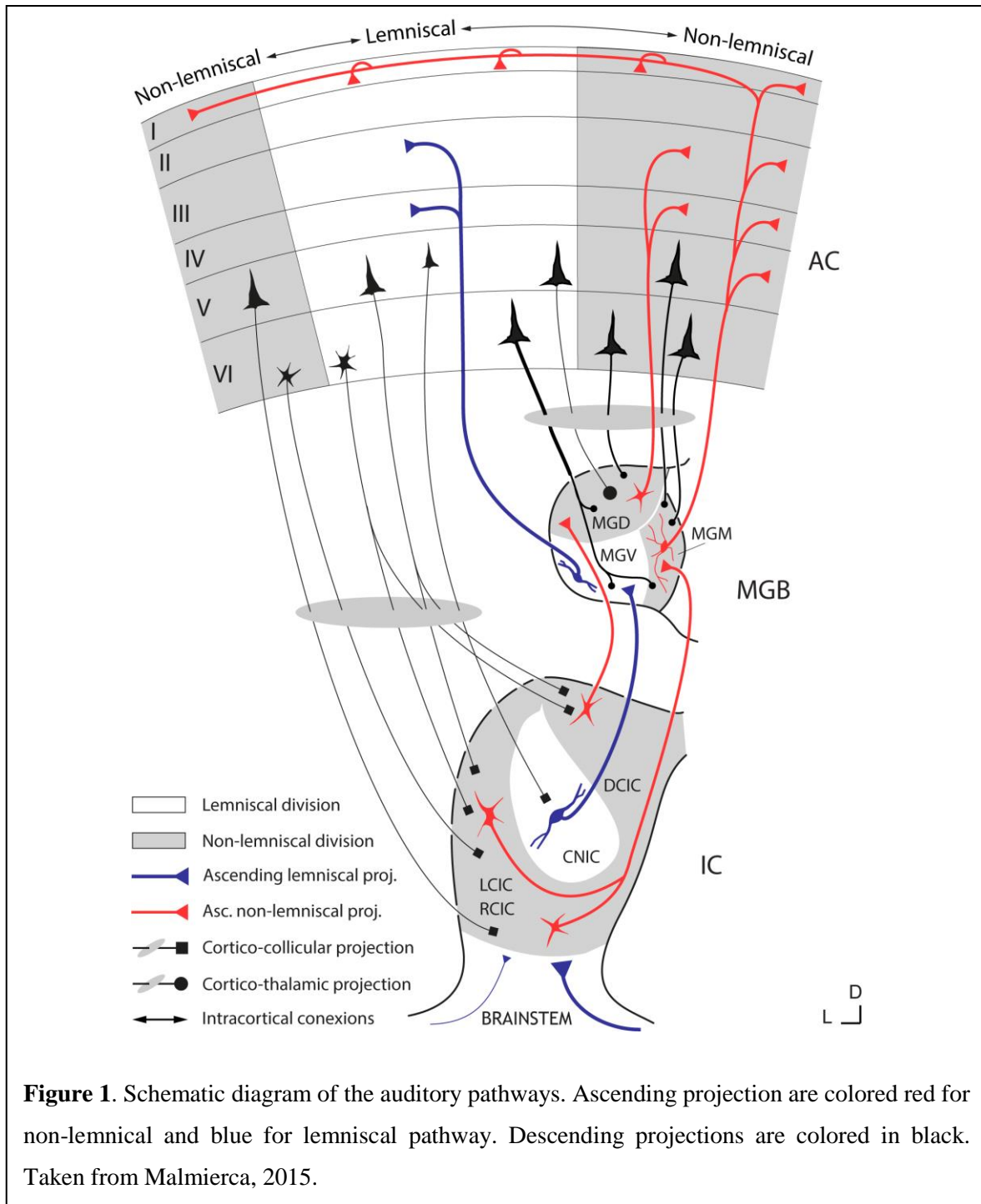


Figure 1. Schematic diagram of the auditory pathways. Ascending projection are colored red for non-lemniscal and blue for lemniscal pathway. Descending projections are colored in black. Taken from Malmierca, 2015.

The forward thalamocortical projections are not homogeneous, but different MGB neurons project to different AC layers (Llano & Sherman, 2008; Winer *et al.*, 1999). Neurons from MGBv project to layers III and IV of the lemniscal AC; while MGBd and MGBm project to layers III and IV of non-lemniscal AC areas. The MGBm also projects diffusely to layer I within all AC areas.

By contrast, corticothalamic axons originate from layers V and VI. Descending projections from layer VI give collaterals to the thalamic reticular nucleus (TRN), a sheet-like nucleus, also involved in the thalamocortical loop (He, 2003; Yu *et al.*, 2009). All TRN cells are GABAergic, receive excitatory inputs from thalamocortical and corticothalamic axons and provide inhibitory inputs to the MGB (Conley *et al.*, 1991). Thus, when viewed from the thalamus the TRN acts as cortical inhibitory feedback and, when viewed from the cortex, it acts as cortical inhibitory feedforward input to the thalamus (Cox & Sherman, 1999; Guillery *et al.*, 1998; Ohara & Lieberman, 1985).

The auditory pathway is usually described sequentially, with the ascending connections first, followed by the descending connections. However, the connections of the auditory system would be best described as a series of loops reverberating ascending and descending information (Chen *et al.*, 2015; Malmierca, 2015). Thus, the remarkable importance of bidirectional projections between auditory thalamus and auditory cortex is due to a feedback control of a lower level auditory nucleus by a center to which it sends ascending inputs. These loops of information transfer provide a “modulation” or “gating” control in the sensory evoked responses (Sherman & Guillery, 2011).

b. Mismatch Negativity and Stimulus-Specific Adaptation.

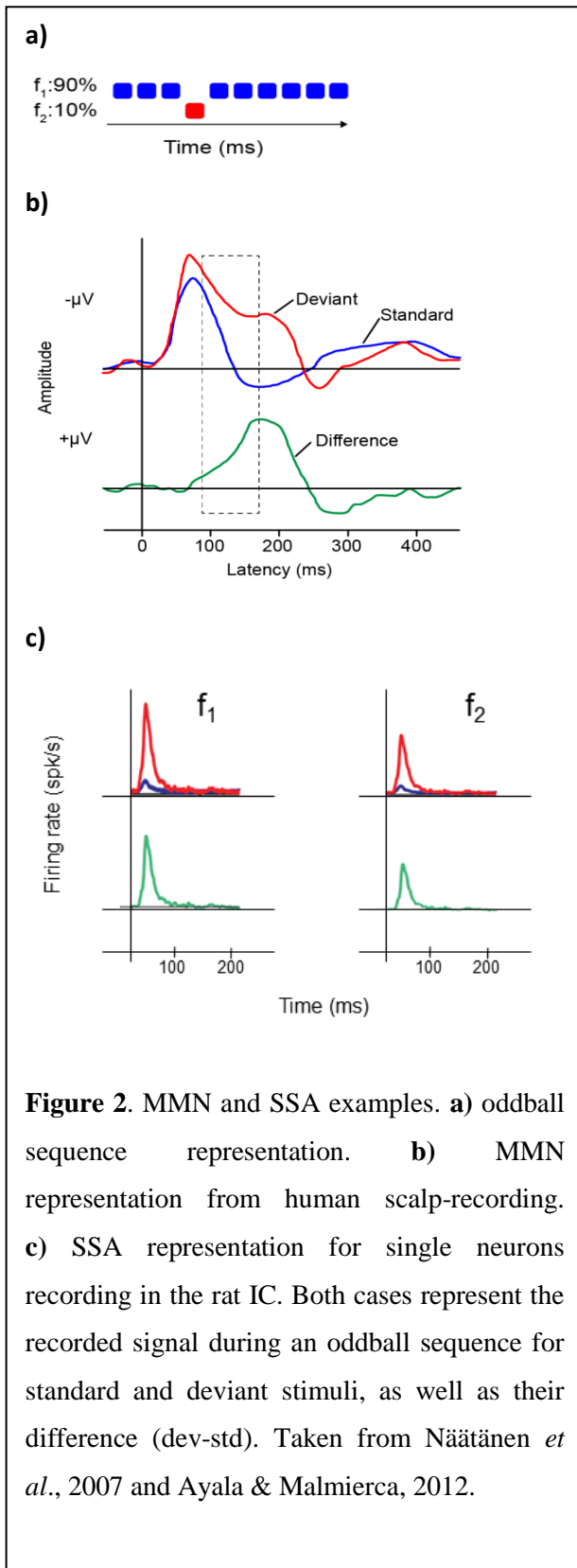
The Mismatch Negativity (MMN) is an event related potential recorded in humans that was first described in 1978 by Risto Näätänen as “*a negative shift superimposed on the evoked potential waveform*” that “*can be observed when a deviating stimulus is delivered among much more numerous, standard, stimuli*” (Näätänen *et al.*, 1978). The MMN is altered in patients with schizophrenia and other psychiatric disorders and hence is considered to be a biomarker of cognitive decline in pathological processes (Todd *et al.*, 2013). However, to understand MMN, it is crucial to understand its underlying neuronal mechanisms. Despite the large body of research dedicated to this subject the underlying neuronal mechanisms of the MMN are not yet understood but remain elusive.

In this thesis, I will study the *neuronal mismatch* along the thalamocortical system, an imitative phenomenon of the classic stimulus-specific adaptation (SSA), which has been proposed to be a neuronal correlate for the MMN (Harms *et al.*, 2014; Nieto-Diego & Malmierca, 2016; Ulanovsky *et al.*, 2003). Indeed, a large body of evidence demonstrates that SSA shares many similarities with the MMN (**Table 1**).

MMN and SSA are automatically elicited by an oddball paradigm and affected by the stimulation parameters, such as frequency, duration and intensity. Like MMN, neurons showing SSA show a stronger response to a deviant stimulus (DEV) than to a standard when stimulated by an oddball paradigm (**Figure 2b-c**). In the most classical version of the oddball paradigm, two frequencies (f_1 and f_2) are presented randomly with a different probability of occurrence within a sequence: one frequency is presented as the standard (e.g., with 90 % probability), and the second frequency presented as the deviant (e.g., with

10 % probability; **Figure 2a**). Despite their similarities, some unresolved questions precluded the recognition of SSA as a neuronal correlate for the MMN.

	SSA	MMN
Similarities	Automatic Nature	Automatic Nature
	Elicited by oddball paradigm, showing dependency of regular stimulation that is violate (Ulanovsky <i>et al.</i> , 2003).	Elicited by oddball paradigm, showing dependency of regular stimulation that is violate (Winkler <i>et al.</i> , 2001).
	Dependence of frequency, duration and intensity (Antunes <i>et al.</i> , 2010; Duque <i>et al.</i> , 2012).	Dependence of frequency, duration and intensity (Näätänen <i>et al.</i> , 1992).
	Suggested as base for perception and sensory memory representation.	Suggested as base for perception and sensory memory representation.
	Auditory and others systems.	Auditory and others systems.
	NMDA receptor dependence (Harms, 2016).	NMDA receptor dependence (Todd <i>et al.</i> , 2013).
	Understood from the Predictive Coding framework.	Understood from the Predictive Coding framework.
	Differences	Single- and multi-unit recordings.
Invasive recordings		Scalp recording (Non-invasive).
In rat peaks 50-100ms (Harms, 2016).		Peaks at about 100-250ms from change onset (Todd <i>et al.</i> , 2013).
Strongest in secondary AC areas (Nieto-Diego & Malmierca, 2016).		Strongest intensity in temporal and frontal areas of topographic scalp maps (Sams <i>et al.</i> , 1985).
		Used as clinical tool: -Schizophrenia (Umbricht & Krljes, 2005). -Dyslexia (Baldeweg <i>et al.</i> 1999)



Although the concept of SSA arose in 1979, when Movshon and Lennie described the responses of single neurons in the cat visual cortex after stimulation by grating patterns, as “*Our most surprising observation is that the loss of sensitivity in cortical neurons can be specific to the adapting stimulus*”, this pioneering study of SSA was largely neglected for 25 years (Pérez-González *et al.*, 2005; Ulanovsky *et al.*, 2003).

Since then, many labs contributed prolifically to the study of SSA, including our lab (Antunes & Malmierca, 2011, 2014; Antunes *et al.*, 2010; Ayala & Malmierca, 2015; Ayala & Malmierca, 2012; Ayala *et al.*, 2016; Duque & Malmierca, 2015; Duque *et al.*, 2014; Duque *et al.*, 2018; Duque *et al.*, 2012; Malmierca *et al.*, 2019; Pérez-González *et al.*, 2012; Valdés-Baizabal *et al.*, 2017).

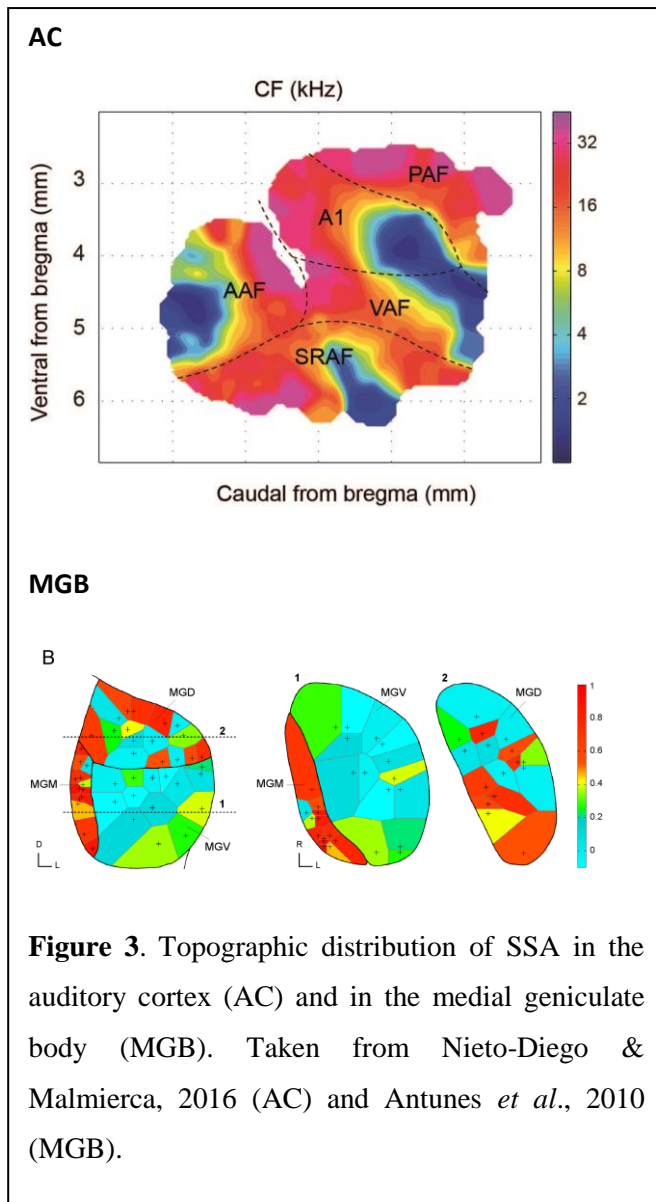


Figure 3. Topographic distribution of SSA in the auditory cortex (AC) and in the medial geniculate body (MGB). Taken from Nieto-Diego & Malmierca, 2016 (AC) and Antunes *et al.*, 2010 (MGB).

SSA is a rather complex phenomenon of adaptation that differs from a mere firing rate adaptation (Ulanovsky *et al.*, 2004). SSA implies a reduction in the response to a repetitive stimulus, while the responses to an infrequent stimulus are not affected (Malmierca *et al.*, 2009; Ulanovsky *et al.*, 2003). It cannot be generated exclusively by the intrinsic membrane properties of a neuron, which will affect all stimuli similarly, but needs the involvement of the neuronal network.

SSA has been found in the IC (Pérez-González *et al.*, 2005), MGB (Antunes *et al.*, 2010) and AC (Nieto-

Diego & Malmierca, 2016; Polley *et al.*, 2007), (**Figure 3**).

SSA is not homogeneously expressed along these nuclei but has a hierarchical organization, in which an *in crescendo level of SSA is displayed from the IC to the MGB reaching the highest levels in the AC, and from lemniscal to non-lemniscal regions*. SSA is considered a form of short-term plasticity (Ogawa & Oka, 2015), modulated by acetylcholine (Ayala & Malmierca, 2015) and GABA-A mediated inhibition (Pérez-González *et al.*, 2012).

SSA and MMN were initially described in different species and pointing the relevance into different aspects of auditory processing. While the MMN has long been recognized to reflect the detection of novel stimuli, SSA has been viewed as a simple mechanism of adaptation to a repeated stimulus. However, recent studies support the hypothesis that SSA does indeed reflect deviance detection, as reflected by an enhancement of the responses to the deviant stimulus, thus meeting a fundamental criterion of the MMN (Ayala & Malmierca, 2012; Taaseh *et al.*, 2011).

The predictive coding framework has emerged as an appealing explanation of how sensory information is processed in the auditory brain (Auksztulewicz & Friston, 2016; Auksztulewicz *et al.*, 2018; Bastos *et al.*, 2012; Friston, 2005; Kort *et al.*, 2017; Shipp, 2016; Wacongne, 2016). According to the predictive coding framework, two mechanisms that previously were considered mutually exclusive, can actually act together to generate the MMN, and therefore SSA: *repetition suppression* and *prediction error*.

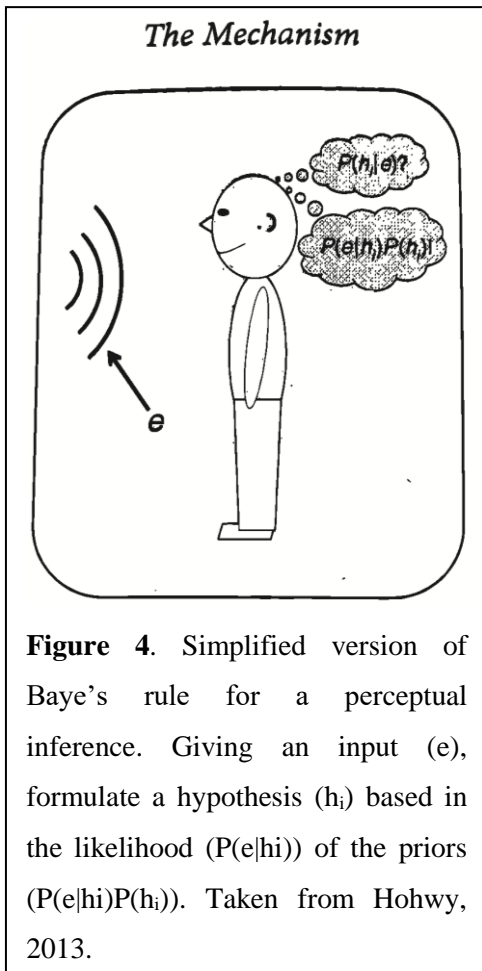
When the same auditory stimulus is repeatedly presented, the neuronal populations originally sensitive to that stimulus undergo adaptation and decrease their responses due to *repetition suppression*. At the same time, a sensory memory based on the history of the stimulation is created (by the repetition of the standard stimulus) and it is used to establish a predictive model of the stimulation. When a rare or deviant stimulus occurs, an error signal emerges i.e., a *prediction error*, which increases the neural response to the deviant stimulus. Therefore, violations of this prediction upon presentation of an unexpected deviant sound, results in a neural response that tracks the unexpectedness of the stimuli.

In the present work I will try to disentangle whether any or both of these mechanisms occur in the neuronal mismatch (an imitative index of SSA). Furthermore, I

will study how these mechanisms are affected when NMDA receptor functioning is disrupted, by using NMDA antagonists.

c. *Predictive Coding*

The predictive coding encompasses MMN and SSA. Even if it was estimated a millennial ago by Ibn al Haytham, who developed the view that “*many visible properties are perceived by judgement and inference*”, or when Hermann von Helmholtz clutched on the idea of the brain as a hypothesis tester (**Figure 4**; Hohwy, 2013), it has been only in



recent years that the predictive coding has gained strength in neurosciences, mainly catapulted by the works of Friston (2005).

According to this theory, the brain works as a Bayesian inference system (Friston, 2005) that uses the hierarchy of the auditory processing (Auksztulewicz & Friston, 2016; Friston 2005; Garrido *et al.* 2008), where higher stations are constantly trying to anticipate the future by generating predictions (likelihood based in the priors) about what is going to happen in the future (inferences). Priors are pushed down leading to perceptual inference, and perceptual inference

shapes the priors, in order to minimize the prediction errors (Hohwy, 2013).

This approach assumes that mismatches between prior beliefs and incoming signals constitute prediction errors. MMN is effortlessly fitting it as the sum of thousands of neuronal prediction error (PE) signals (Bendixen *et al.*, 2012). Since predictions and prediction errors operate in a hierarchical manner (Friston, 2005; Garrido *et al.*, 2008), in Bayesian terms, the PE corresponds to the difference between the prior and the likelihood, where predictive signals may be sent from higher hierarchical levels predominantly via glutamatergic NMDA receptors (Bastos *et al.*, 2012). Thus, in this thesis I will study whether prediction error signals can be tracked at a single neuron level, and whether this prediction error signals are processed in a hierarchical manner along the auditory system or not.

d. Schizophrenia

Schizophrenia is a severe mental disorder affecting more than 21 million people worldwide. It is characterized by distortion in thinking, perception, emotions, language, sense of self and behavior, including hearing voices (hallucinations) and delusions (World Health Organization, 2014). Recent evidence suggests that deficits in thalamocortical connectivity contribute to auditory dysfunction in schizophrenia (Lee *et al.* 2017).

Current theories in the framework of hierarchical predictive coding propose that positive symptoms of schizophrenia, such as delusions and hallucinations, arise from an alteration in Bayesian inference (predictions) (Erickson *et al.*, 2017; Horga *et al.*, 2014; Sterzer *et al.*, 2018). These studies argue that reduced precision of predictions, relative to

sensory inputs may be the cause for the positive symptoms of schizophrenia (Sterzer *et al.*, 2016).

In healthy subjects, the higher levels of the hierarchy system encode predictions and send them as predictive signals to lower levels. Whenever the incoming sensory data (likelihood) violate these predictions, a prediction error signal is sent to update the predictive model at higher levels. But, in psychosis states the balance between predictions and incoming sensory data has been proposed to be disrupted, with a decreased precision in the priors and with an increase in the likelihood, resulting in the abnormal strong weighting of prediction errors (Sterzer *et al.*, 2018).

Interesting, humans with schizophrenia have consistently been observed to have a reduced MMN (Umbricht & Krljes, 2005). In humans, acute exposure to the NMDA antagonist ketamine reduces the size of the MMN (Todd *et al.*, 2013), an observation consistent with the NMDA hypothesis for schizophrenia (Harms, 2016), that posits that NMDA hypofunction underlies the neuropathology of schizophrenia (Kantrowitz & Javitt, 2012). This hypothesis was originally based on observations that NMDA antagonists, such as ketamine or phencyclidine, administered to healthy participants mimic the full range of schizophrenia symptoms (Andine *et al.*, 1999; Krystal *et al.*, 2005). Such schizophrenia-like impairments are also found in the MMN equivalent from a rodent model after the administration of NMDA antagonists to the animals (Harms *et al.*, 2016) (**Figure 5**). Nevertheless, no studies have examined the impact of the drug on prediction error versus repetition suppression.

Thus, in this thesis I will study the effects of NMDA-R antagonists on neuronal mismatch responses, analyzing separately whether they have an effect on prediction error

and/or repetition suppression, and importantly, how they affect neuronal responses in the different lemniscal and non-lemniscal nuclei along the thalamocortical axis.

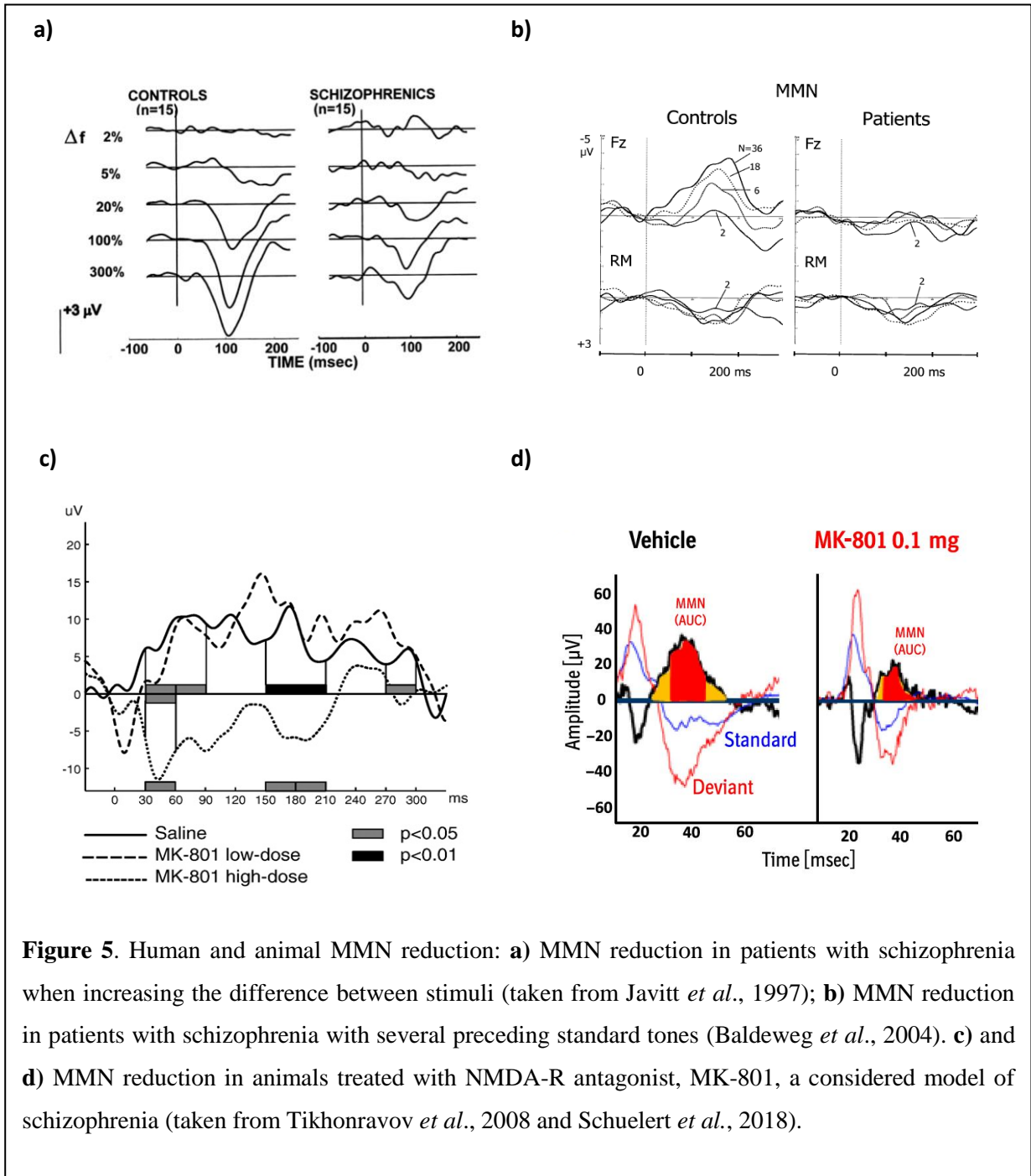


Figure 5. Human and animal MMN reduction: **a)** MMN reduction in patients with schizophrenia when increasing the difference between stimuli (taken from Javitt *et al.*, 1997); **b)** MMN reduction in patients with schizophrenia with several preceding standard tones (Baldeweg *et al.*, 2004). **c)** and **d)** MMN reduction in animals treated with NMDA-R antagonist, MK-801, a considered model of schizophrenia (taken from Tikhonravov *et al.*, 2008 and Schuelert *et al.*, 2018).

Hypothesis

3. Hypothesis.

Considering that the central auditory system is hierarchically organized, with higher levels of SSA in the upper structures and in the non-lemniscal pathway, and that the SSA have been proposed as the neuronal correlate of the MMN, an event related potential that have been found altered in persons with schizophrenia and in animal models, which is fashioned by *repetition suppression* and *prediction errors*, we propose the following hypothesis:

- I. Prediction errors can be recorded from single neurons. We also propose that prediction error will increase from lower to higher stations in the auditory pathway as the predictive coding framework propose.
- II. Since the IC neurons express cannabinoid receptors, we propose that cannabinoid drugs can modulate SSA responses in the IC.
- III. Prediction error and repetition suppression are affected in an animal model of schizophrenia.

Objectives

4. Objectives

Based on my hypothesis, my objectives were the following:

- I.** Determine whether or not single neurons exhibit prediction error in the IC, MGB and AC, and dividing it in two parallel pathways, lemniscal or non-lemniscal. To do that, we will use an oddball paradigm and two control sequences, the many-standard and the cascade.
- II.** To avoid the possible effects of anesthesia in our results, we will record awake animals using same paradigms, to establish that neuronal prediction errors are independent of awareness states.
- III.** Determine if SSA can be modulated in the IC using agonists and antagonist cannabinoids.
- IV.** Examine the impact of an NMDA-R antagonism, such the MK-801 on single unit responses in the MGB and AC during an auditory oddball, many standards and cascade control sequences were presented. This will allow us to delineate effects on repetition suppression and prediction error.

Summary of Results

5. Summary of Results.

Our results are based on two published works and one actually under revision.

Study I

We recorded individual responses from cortical and subcortical neurons in anaesthetized rats and awake mice while oddball and control sequences were played. Data evidence prediction error in single auditory neurons, showing an increase along the hierarchical organization, from lower to higher stations and from lemniscal to non-lemniscal. The analysis also revealed that the hierarchical prediction error signal is conserved across species and arousal.

Study II

Results demonstrate that cannabinoid agonist increase the neuronal response to standard tones, while responses to deviants are unaffected, leading a reduction in the neuronal adaptation (SSA).

Study III

We report the data from a large sample of single neurons in control animals (non-treated) and animals treated with a non-competitive antagonist of NMDA receptors (MK-801). Our data show that MK-801 produces differential effects on responses to DEV and STD tones in oddball sequences, affecting the mismatch index along the thalamocortical system. These changes consist of an increase in the repetition suppression at the thalamic regions, while prediction error responses are enhanced in the auditory cortex.

General Discussion

6. General Discussion.

In my thesis I demonstrate that single neurons from the midbrain level and upwards of the auditory pathway exhibit prediction error responses that mimic those recorded in MMN studies. This finding supports the hypothesis that single neurons along the auditory brain take their part in the computations of MMN and predictive activity in the brain. Moreover, these prediction error responses are organized in a hierarchical manner, consistent across species and awareness states. Similarly, my results agree with evidences showing that mismatch responses are dependent on NMDA receptor activity (Javitt *et al.*, 1996; Garrido, 2009). All these results agree with the general predictive coding framework (Friston, 2005). Furthermore, I demonstrate that stimulus-specific adaptation at the single neuron level in the inferior colliculus are modulated by cannabinoids, adding evidences of cannabinoids neuromodulatory activity.

Here, I demonstrate that prediction errors at the neuronal level are hierarchically organized along the pathway, in a way that matches the hierarchical organization of auditory information proposed by the predictive coding framework (Auksztulewicz & Friston, 2016). In anaesthetized and awake animals, the central auditory system, at least from the IC to the MGB and then to the AC, and from lemniscal to non-lemniscal regions, exhibits an *in crescendo* level of prediction errors.

By contrast, when NMDA-R hypofunction is assumed, this hierarchical organization fails, as was demonstrated after applying a low dose of NMDA antagonist (MK-801). MK-801 increases the prediction error signal in the AC, while increasing repetition suppression in the MGB. Moreover, we have found that MK-801 alters the dynamics of neuronal adaptation along the thalamocortical axis, becoming faster and stronger especially at the thalamic level. These results are in accordance with other works that suggest thalamocortical activity deficits in schizophrenia (Lee *et al.* 2017). Similarly, our results fit those theories proposing that positive symptoms of

schizophrenia, such as delusions and hallucinations, arise from alteration in Bayesian inference due to a reduced precision in generating predictions that leads to an increase in prediction errors (Sterzer *et al.*, 2016; 2018).

Furthermore, we have found that cannabinoid agonists reduce SSA in the IC, while cannabinoid antagonists increase SSA in the IC. Thus, the endocannabinoid system can modulate the generation of SSA in a similar way to GABA (via GABA-A receptors) and acetylcholine (Ayala & Malmierca, 2015; Perez-Gonzalez *et al.* 2012). It could well be that endocannabinoids interact with these neurotransmitters to shape SSA. Indeed, the cannabinoid neuromodulators have been suggested to comprise a system that functionally interacts with other neurotransmitters (Lutz, 2002). The complexity of the cannabinoid system is far from being understood. However, considering our results showing that cannabinoids modulate SSA, and that SSA is likely a neuronal correlate of MMN (Nieto-Diego & Malmierca, 2016; Ulanovsky *et al.*, 2003; Harms *et al.*, 2016), it would be interesting to study cannabinoid modulation in the context of the neuronal mismatch and the predictive coding. For example, to investigate if cannabinoids play a role in the generation of some psychotic syndromes known to alter MMN responses (Sánchez-Blazquez *et al.*, 2014; Javitt *et al.*, 2008).

Overall, the data from my doctoral thesis show that single neurons along the auditory hierarchy have the ability to filter irrelevant repetitive information in order to detect novel stimuli, by generating enhanced error signals. This activity is NMDA-dependent and modulated by cannabinoids. When these systems are manipulated, for example by the administration of NMDA-R antagonists, we generate a pathological system that alters the normal hierarchy of repetition suppression and prediction errors, and therefore the neural mismatch.

What are the implications of our findings for schizophrenia? If a safe drug were available that targeted the relevant NMDA-R subunit, and facilitated neuroplasticity as indexed by an increased MMN even for a short time period, it offers opportunities for interventions to remediate

cognitive deficits that are a core feature of schizophrenia (Green *et al.*, 2000). Memantine which has been shown to increase MMN amplitude in healthy individuals and in schizophrenia has been used as an adjunctive therapy in schizophrenia for some time to improve cognition in particular. While effects of adjunctive therapy are small, recent meta-analysis suggests that there are improvements in global measures of cognition, but improvements in more sensitive composite cognitive test scores were not observed (Kishi *et al.*, 2018). To date, there have been no attempts to utilize MMN response to memantine as an index of neuroplasticity that could be exploited in remediation studies. Interestingly, both the moderate affinity antagonist, memantine, and high affinity antagonist, MK-801, bind to the NR2B subunit of the NMDA-R at very similar binding locations (Song *et al.*, 2018) but only memantine has been approved for use in humans given evidence of neurotoxic effects of MK-801 in humans (Olney *et al.*, 1989). One avenue of future research is the development of safe compounds for human use that target similar binding locations to memantine and MK-801.

References

7. References.

- Andine, P., Widermark, N., Axelsson, R., Nyberg, G., Olofsson, U., Martensson, E., & Sandberg, M. (1999). Characterization of MK-801-Induced Behavior as a Putative Rat Model of Psychosis. *J. Pharmacol. Exp. Ther.*, 290(3), 1393–1408.
- Antunes, F. M., & Malmierca, M. S. (2011). Effect of auditory cortex deactivation on stimulus-specific adaptation in the medial geniculate body. *The Journal of Neuroscience : The Official Journal of the Society for Neuroscience*, 31(47), 17306–17316.
- Antunes, F. M., & Malmierca, M. S. (2014). An Overview of Stimulus-Specific Adaptation in the Auditory Thalamus. *Brain Topography*, 27(4), 480–499.
- Antunes, F. M., Nelken, I., Covey, E., & Malmierca, M. S. (2010). Stimulus-Specific Adaptation in the Auditory Thalamus of the Anesthetized Rat. *PLoS ONE*, 5(11), e14071.
- Auksztulewicz, R., & Friston, K. (2016). Repetition suppression and its contextual determinants in predictive coding. *Cortex; a Journal Devoted to the Study of the Nervous System and Behavior*, 80, 125–140.
- Auksztulewicz, R., Schwiedrzik, C. M., Thesen, T., Doyle, W., Devinsky, O., Nobre, A. C., ... Melloni, L. (2018). Not all predictions are equal: ‘What’ and ‘When’ predictions modulate activity in auditory cortex through different mechanisms. *The Journal of Neuroscience*, 38(40), 0369–18.
- Ayala, YA., & Malmierca, MS. (2015). Cholinergic Modulation of Stimulus-Specific

- Adaptation in the Inferior Colliculus. *Journal of Neuroscience*, 35(35), 12261–12272.
- Ayala, YA, & Malmierca, MS. (2012). Stimulus-specific adaptation and deviance detection in the inferior colliculus. *Frontiers in Neural Circuits*, 6, 89.
- Ayala, YA, Pérez-González, D., & Malmierca, MS. (2016). Stimulus-specific adaptation in the inferior colliculus: The role of excitatory, inhibitory and modulatory inputs. *Biological Psychology*, 116, 10–22.
- Baldeweg T., Richardson A., Watkins S., Foale C. & Gruzelier J. (1999). Impaired Auditory Frequency Discrimination in Dyslexia Detected with Mismatch Evoked Potentials. *Annals of Neurology*, 45(4):495-503.
- Baldeweg T, Klugman A, Gruzelier J & Hirsch S. (2004). Mismatch Negativity potentials and cognitive impairment in schizophrenia. *Schizophrenia research*, 69(2-3):203-217.
- Bartlett, EL. (2013). The organization and physiology of the auditory thalamus and its role in processing acoustic features important for speech perception. *Brain and Language*, 126(1), 29–48.
- Bastos, AM., Usrey, WM., Adams, R A., Mangun, GR., Fries, P., & Friston, KJ. (2012). Canonical Microcircuits for Predictive Coding. *Neuron*, 76(4), 695–711.
- Bendixen, A., SanMiguel, I., & Schröger, E. (2012). Early electrophysiological indicators for predictive processing in audition: A review. *International Journal of Psychophysiology* 83:120-131
- Calford, MB., & Aitkin, LM. (1983). Ascending projections to the medial geniculate body of the cat: evidence for multiple, parallel auditory pathways through thalamus. *The*

Journal of Neuroscience : The Official Journal of the Society for Neuroscience, 3(11), 2365–2380.

Chen, IW., Helmchen, F., & Lutcke, H. (2015). Specific Early and Late Oddball-Evoked Responses in Excitatory and Inhibitory Neurons of Mouse Auditory Cortex. *Journal of Neuroscience*, 35(36), 12560–12573.

Conley, M., Kupersmith, AC., & Diamond, IT. (1991). The Organization of Projections from Subdivisions of the Auditory Cortex and Thalamus to the Auditory Sector of the Thalamic Reticular Nucleus in Galago. *European Journal of Neuroscience*, 3(11), 1089–1103.

Cox, CL., & Sherman, SM. (1999). Glutamate inhibits thalamic reticular neurons. *The Journal of Neuroscience : The Official Journal of the Society for Neuroscience*, 19(15), 6694–6699.

Duque, D., & Malmierca, MS. (2015). Stimulus-specific adaptation in the inferior colliculus of the mouse: anesthesia and spontaneous activity effects. *Brain Structure and Function*, 220(6), 3385–3398.

Duque, D., Malmierca, MS., & Caspary, DM. (2014). Modulation of stimulus-specific adaptation by GABA(A) receptor activation or blockade in the medial geniculate body of the anaesthetized rat. *The Journal of Physiology*, 592(4), 729–743.

Duque, D., Pais, R., & Malmierca, MS. (2018). Stimulus-specific adaptation in the anesthetized mouse revealed by brainstem auditory evoked potentials. *Hearing Research*, 370, 294–301.

Duque, D., Pérez-González, D., Ayala, YA., Palmer, AR., & Malmierca, MS. (2012).

- Topographic Distribution, Frequency, and Intensity Dependence of Stimulus-Specific Adaptation in the Inferior Colliculus of the Rat. *Journal of Neuroscience*, 32(49), 17762–17774.
- Erickson, MA., Albrecht, M., Ruffle, A., Fleming, L., Corlett, P., & Gold, J. (2017). No association between symptom severity and MMN impairment in schizophrenia: A meta-analytic approach. *Schizophrenia Research. Cognition*, 9, 13–17.
- Friston, K. (2005). A theory of cortical responses. *Philosophical Transactions of the Royal Society B: Biological Sciences*, 360(1456), 815–836.
- Friston, K. (2005). Models of Brain Function in Neuroimaging. *Annual Review of Psychology*, 56(1), 57–87.
- Garrido, MI., Friston, K., Kiebel, SJ., Stephan, KE., Baldeweg, T., & Kilner, JM. (2008). The functional anatomy of the MMN: a DCM study of the roving paradigm. *NeuroImage*, 42(2), 936–944.
- Guillery, RW., Feig, S L., & Lozsádi, DA. (1998). Paying attention to the thalamic reticular nucleus. *Trends in Neurosciences*, 21(1), 28–32.
- Harms, L. (2016). Mismatch responses and deviance detection in N-methyl-D-aspartate (NMDA) receptor hypofunction and developmental models of schizophrenia. *Biological Psychology*, 116, 75–81.
- Harms, L., Fulham, WR., Todd, J., Budd, TW., Hunter, M., Meehan, C., ... Michie, PT. (2014). Mismatch negativity (MMN) in freely-moving rats with several experimental controls. *PloS One*, 9(10), e110892.

- Harms, L., Michie, P.T., & Näätänen, R. (2016). Criteria for determining whether mismatch responses exist in animal models: Focus on rodents. *Biological Psychology*, *116*, 28–35.
- He, J. (2003). Corticofugal modulation of the auditory thalamus. *Experimental Brain Research*, *153*(4), 579–590.
- Hohwy, J. (2013). *The Predictive Mind*. Oxford University Press.
- Horga, G., Schatz, K., Abi-Dargham, A., & Peterson, B.S. (2014). Deficits in Predictive Coding underlie Hallucinations in Schizophrenia. *The Journal of Neuroscience*, *34*(24), 8072–8082.
- Huang, C.L., & Winer, J.A. (2000). Auditory thalamocortical projections in the cat: Laminar and areal patterns of input. *The Journal of Comparative Neurology*, *427*(2), 302–331.
- Imaizumi, K., & Lee, C.C. (2014). Frequency transformation in the auditory lemniscal thalamocortical system. *Frontiers in Neural Circuits*, *8*.
- Javitt, D.C., Steinschneider, M., Schroeder, C.E., & Arezzo, J.C. (1996). Role of cortical N-methyl-D-aspartate receptors in auditory sensory memory and mismatch negativity generation: implications for schizophrenia. *Proceedings of the National Academy of Sciences of the United States of America*, *93*(21), 11962–11967.
- Jones, E.G. (2003). Chemically Defined Parallel Pathways in the Monkey Auditory System. *Annals of the New York Academy of Sciences*, *999*(1), 218–233.
- Kantrowitz, J., & Javitt, D.C. (2012). Glutamatergic transmission in schizophrenia: from basic research to clinical practice. *Current Opinion in Psychiatry*, *25*(2), 96–102.

- Kort, NS., Ford, JM., Roach, BJ., Gunduz-Bruce, H., Krystal, J. H., Jaeger, J., ... Mathalon, D. H. (2017). Role of N-Methyl-D-Aspartate Receptors in Action-Based Predictive Coding Deficits in Schizophrenia. *Biological Psychiatry*, *81*(6), 514–524.
- Krystal, JH., Perry, EB., Gueorguieva, R., Belger, A., Madonick, SH., Abi-Dargham, A., ... Cyril D'Souza, D. (2005). Comparative and interactive human psychopharmacologic effects of ketamine and amphetamine: Implications for glutamatergic and dopaminergic model psychoses and cognitive function. *Archives of General Psychiatry*, *62*(9), 985–995.
- Lee, C., & Sherman, SM. (2011). On the classification of pathways in the auditory midbrain, thalamus, and cortex. *Hearing Research*. NIH Public Access.
- Lee, M., Sehatpour, P., Hoptman, MJ., Lakatos, P., Dias, EC., Kantrowitz, JT., ... Javitt, D. C. (2017). Neural mechanisms of mismatch negativity dysfunction in schizophrenia. *Molecular Psychiatry*, *22*(11), 1585–1593.
- Llano, DA., & Sherman, SM. (2008). Evidence for nonreciprocal organization of the mouse auditory thalamocortical-corticothalamic projection systems. *The Journal of Comparative Neurology*, *507*(2), 1209–1227.
- Malmierca, MS. (2015). Auditory System. In *Chapter 29-The Rat Nervous System* (pp. 865–946). Academic Press.
- Malmierca, MS., Cristaudo, S., Perez-Gonzalez, D., & Covey, E. (2009). Stimulus-Specific Adaptation in the Inferior Colliculus of the Anesthetized Rat. *Journal of Neuroscience*, *29*(17), 5483–5493.
- Malmierca, MS., Niño-Aguillón, BE., Nieto-Diego, J., Porteros, Á., Pérez-González, D., &

- Escera, C. (2019). Pattern-sensitive neurons reveal encoding of complex auditory regularities in the rat inferior colliculus. *NeuroImage*, *184*, 889–900.
- Movshon JA, & Lennie P. (1979). Pattern-selective adaptation in visual cortical neurones. *Nature* Vol.278:850-852.
- Näätänen, R., Gaillard, AWK., & Mäntysalo, S. (1978). Early selective-attention effect on evoked potential reinterpreted. *Acta Psychologica*, *42*(4), 313–329.
- Näätänen R., Paavilainen P., Rinne T. & Alho K. (2007). The mismatch negativity (MMN) in basic research of central auditory processing: A review. *Clinical Neurophysiology*, *118*(12):2544-2590.
- Näätänen, R., Teder, W., Alho, K., & Lavikainen, J. (1992). Auditory attention and selective input modulation: a topographical ERP study. *Neuroreport*, *3*(6), 493–496.
- Nieto-Diego, J., & Malmierca, MS. (2016). Topographic Distribution of Stimulus-Specific Adaptation across Auditory Cortical Fields in the Anesthetized Rat. *PLOS Biology*, *14*(3), e1002397.
- Ogawa, H., & Oka, K. (2015). Direction-Specific Adaptation in Neuronal and Behavioral Responses of an Insect Mechanosensory System. *Journal of Neuroscience*, *35*(33), 11644–11655.
- Ohara, PT., & Lieberman, AR. (1985). The thalamic reticular nucleus of the adult rat: experimental anatomical studies. *Journal of Neurocytology*, *14*(3), 365–411.
- Pérez-González, D., Hernández, O., Covey, E., & Malmierca, MS. (2012). GABA A-mediated inhibition modulates stimulus-specific adaptation in the inferior colliculus.

PLoS ONE, 7(3).

Pérez-González, D., Malmierca, MS., & Covey, E. (2005). Novelty detector neurons in the mammalian auditory midbrain. *European Journal of Neuroscience*, 22(11), 2879–2885.

Polley, DB., Read, HL., Storace, DA., & Merzenich, MM. (2007). Multiparametric Auditory Receptive Field Organization Across Five Cortical Fields in the Albino Rat. *J Neurophysiol*, 97, 3621–3638.

Sams, M., Paavilainen, P., Alho, K., & Näätänen, R. (1985). Auditory frequency discrimination and event-related potentials. *Electroencephalography and Clinical Neurophysiology*, 62(6), 437–448.

Schuelert N., Dorner-Ciossek C., Brendel M. & Rosenbrock H. (2018). A comprehensive analysis of auditory event-related potentials and network oscillations in an NMDA receptor antagonist mouse model using a novel wireless recording technology. *Physiological Reports*, 6(16), e13782.

Sherman, SM., & Guillery, RW. (2011). Distinct functions for direct and transthalamic corticocortical connections. *Journal of Neurophysiology*, 106(3), 1068–1077.

Shipp, S. (2016). Neural elements for predictive coding. *Frontiers in Psychology*. 7:1792.

Sterzer, P., Adams, RA., Fletcher, P., Frith, C., Lawrie, SM., Muckli, L., ... Corlett, PR. (2018). The Predictive Coding Account of Psychosis. *Biological Psychiatry*, 84:634-643.

Sterzer, P., Mishara, AL., Voss, M., Heinz, A., Corlett, PR., & Friston, K. (2016). Thought

Insertion as a Self-Disturbance: An Integration of Predictive Coding and Phenomenological Approaches, *Frontiers in human neuroscience*, 10:502.

Taaseh, N., Yaron, A., & Nelken, I. (2011). Stimulus-specific adaptation and deviance detection in the rat auditory cortex. *PloS One*, 6(8), e23369. <https://doi.org/10.1371/journal.pone.0023369>

Tikhoravov D., Neuvonen T., pertovaara A., Savioja K., Ruusuvirta T., Näätänen R & Carlson S.(2008). Effects of an NMDA-receptor antagonist MK-801 on an MMN-like response recorded in anesthetized rats. *Brain Research*, 1203.97-102

Todd, J., Harms, L., Schal l, U., & Michie, P. T. (2013). Mismatch negativity: Translating the potential. *Frontiers in Psychiatry*. Frontiers.

Ulanovsky, N., Las, L., Farkas, D., & Nelken, I. (2004). Multiple Time Scales of Adaptation in Auditory Cortex Neurons. *The Journal of Neuroscience*, 24(46), 10440–10453.

Ulanovsky, N., Las, L., & Nelken, I. (2003). Processing of low-probability sounds by cortical neurons. *Nature Neuroscience*, 6(4), 391–398.

Umbrecht, D., & Krljes, S. (2005). Mismatch negativity in schizophrenia: a meta-analysis. *Schizophrenia Research*, 76(1), 1–23.

Valdés-Baizabal, C., Parras, GG., Ayala, YA., & Malmierca, MS. (2017). Endocannabinoid Modulation of Stimulus-Specific Adaptation in Inferior Colliculus Neurons of the Rat. *Scientific Reports*, 7(1), 1–14.

Wacongne, C. (2016). A predictive coding account of MMN reduction in schizophrenia.

Biological Psychology, 116, 68–74.

Winer, J. A. (2006). Decoding the auditory corticofugal systems. *Hearing Research*, 212(1–2), 1–8.

Winer, J. A., Kelly, J.B., & Larue, D.T. (1999). Neural architecture of the rat medial geniculate body. *Hearing Research*, 130(1–2), 19–41.

Winkler, I., Schröger, E., & Cowan, N. (2001). The role of large-scale memory organization in the mismatch negativity event-related brain potential. *Journal of Cognitive Neuroscience*, 13(1), 59–71.

World Health Organization. (2014). Schizophrenia. Retrieved February 18, 2019, from https://www.who.int/mental_health/management/schizophrenia/en/

Yu, X., Xu, X., He, S., & He, J. (2009). Change detection by thalamic reticular neurons. *Nature Neuroscience*, 12(9), 1165–1170.





Publications

ARTICLE

DOI: 10.1038/s41467-017-02038-6

OPEN

Neurons along the auditory pathway exhibit a hierarchical organization of prediction error

Gloria G. Parras ^{1,2}, Javier Nieto-Diego^{1,2}, Guillermo V. Carbajal ^{1,2}, Catalina Valdés-Baizabal^{1,2}, Carles Escera ^{3,4,5} & Manuel S. Malmierca ^{1,2,6}

Perception is characterized by a reciprocal exchange of predictions and prediction error signals between neural regions. However, the relationship between such sensory mismatch responses and hierarchical predictive processing has not yet been demonstrated at the neuronal level in the auditory pathway. We recorded single-neuron activity from different auditory centers in anaesthetized rats and awake mice while animals were played a sequence of sounds, designed to separate the responses due to prediction error from those due to adaptation effects. Here we report that prediction error is organized hierarchically along the central auditory pathway. These prediction error signals are detectable in subcortical regions and increase as the signals move towards auditory cortex, which in turn demonstrates a large-scale mismatch potential. Finally, the predictive activity of single auditory neurons underlies automatic deviance detection at subcortical levels of processing. These results demonstrate that prediction error is a fundamental component of singly auditory neuron responses.

¹ Auditory Neuroscience Laboratory, Institute of Neuroscience of Castilla y León (INCYL), Salamanca, 37007 Castilla y León, Spain. ² The Salamanca Institute for Biomedical Research (IBSAL), Salamanca, 37007 Castilla y León, Spain. ³ Brainlab-Cognitive Neuroscience Research Group, Department of Clinical Psychology and Psychobiology, University of Barcelona, Barcelona, 08035 Catalonia, Spain. ⁴ Institute of Neurosciences, University of Barcelona, Barcelona, 08035 Catalonia, Spain. ⁵ Institut de Recerca Sant Joan de Déu, Esplugues de Llobregat, 08950 Catalonia, Spain. ⁶ Department of Cell Biology and Pathology, Faculty of Medicine, University of Salamanca, Salamanca, 37007 Castilla y León, Spain. Gloria G. Parras and Javier Nieto-Diego contributed equally to this work. Correspondence and requests for materials should be addressed to M.S.M. (email: msm@usal.es)

Unexpected events tend to convey relevant information, making their prompt detection fundamental for survival¹. Brain responses to a perceptual mismatch between expected and actual sensory inputs have been extensively recorded in all sensory systems, including auditory, visual, somatosensory and olfactory modalities^{2,3}. In the case of audition, these responses are thought to underlie the brain's ability to identify what sounds or auditory objects are⁴, suggesting that they may be a key feature of perceptual processing^{3,5}. Auditory prediction errors can be induced using oddball sequences⁵, in which a repetitive (standard) tone is replaced randomly by a different (deviant) tone with a low probability. Neural responses, recorded from the human scalp with electroencephalography while people heard such oddball stimuli, have revealed a characteristic pattern of activity, the so-called mismatch negativity (MMN) response⁶.

The MMN response is widely considered to represent a prediction error signal, a member of a hierarchy of prediction errors^{3,7,8}. Hierarchical predictive coding is a neurobiologically informed theory of general brain function^{9,10} that unifies many concepts and experimental evidence about perceptual systems into a common framework. According to this framework, cortical processing stations send predictions to lower hierarchical levels to aid the suppression of any ascending neuronal activity evoked by sensory events that can be anticipated. These stations also forward prediction errors to higher hierarchical levels whenever their current predictions fail. This framework explains both repetition suppression, or response attenuation with stimulus repetition^{11,12}, and deviance detection, or automatic enhancement of responses to sensory inputs that deviate from a strong prediction^{13,14}. Because it encompasses these different facets, the main concepts of predictive coding have been used to describe a variety of brain responses and brain dynamics, including the MMN^{3,4,13}. Thus, it is now widely accepted that large-scale mismatch responses such as those seen in humans or animals listening to an auditory oddball stimulus^{15,16}, reflect the predictive activity of the auditory and other sensory systems^{3,7}. These responses can be seen even at early processing stages⁸, including subcortical midbrain and thalamus².

However, at the cellular level, such mismatch responses could also arise from a simpler neurophysiological mechanism^{17,18}, namely, stimulus-specific adaptation (SSA)^{19,20}, which is response decrement to a stimulus repetition¹ that leaves neuronal responses to novel stimuli almost unaffected. SSA is a widespread property of auditory neurons, increasing from midbrain^{21–24} through the thalamus²⁵ to primary^{26,27} and non-primary²⁷ auditory cortices, and is assumed to be due to synaptic depression^{2,26}. Due to SSA, single neuron responses along the auditory pathway show a differential response to standard (highly repeated sounds) and deviant (low probability sounds) tones under oddball stimulation, thereby resembling a cellular version of the MMN but at the neuronal level^{2,19}. This similarity has caused some researchers to suggest that SSA is all the brain needs to generate the MMN¹⁷. Yet, this theory does not take into account predictive activity in single neurons, which has been demonstrated in different contexts and systems. Single neurons in primary auditory cortex have also been probed for predictive activity^{15,19}, but the results, have been controversial¹⁸. Some studies did not find evidence for deviance detection^{28,29}, while others found similar results but interpreted them differently and suggested that auditory cortical neurons do detect deviance²⁶. Only one recent study in mouse primary auditory cortex explicitly showed deviance detection in late responses of layer II/III excitatory cortical neurons³⁰.

Auditory signals follow an ascending pathway and are interrupted at least three times: at the cochlear nuclei, the superior olivary complex, the nuclei of the lateral lemniscus, and the

inferior colliculus. The different nuclei in these structures encode specific features of the acoustic stimulus. However, the system is even more complex, as the ascending auditory pathway can actually be divided into two broad categories of parallel processing stations. These have been referred to as the “lemniscal line system” and “lemniscal adjunct system”³¹ and have been identified in both the auditory (referring to the lateral lemniscus) and somatosensory systems (referring to the medial lemniscus). Currently, the terms “lemniscal” and “non-lemniscal” are widely used to refer to two general categories of pathways between the IC and the forebrain^{32,33}. Neurons in the lemniscal areas of the auditory system (“cochleotopic” or core areas) tend to be sharply tuned and tonotopically organized, whereas neurons in the non-lemniscal areas (“diffuse” or belt areas) are broadly tuned and tonotopy is not evident. In general, the lemniscal part of the inferior colliculus projects to the lemniscal part of the auditory thalamus, which projects to the core or primary auditory cortex, and the non-lemniscal inferior colliculus projects to the non-lemniscal areas of the auditory thalamus, which project to the non-primary or belt areas of auditory cortex³⁴.

In this study, we recorded the individual responses of subcortical and cortical neurons along the auditory pathway while anaesthetized rats and awake mice were played a recently-developed auditory oddball sequences, which are designed to separate repetition suppression from prediction error³⁵. We report the data from a large sample of anesthetized rats and from a smaller sample of awake mice to assess the generalizability of any findings across rodent species and arousal states. Our data show that differential responses to deviant and standard tones in oddball sequences indeed reflect active predictive activity and not simply SSA in single neurons, and that this predictive activity follows a hierarchical pattern that extends to subcortical structures. These results unify three coexisting views of perceptual deviance detection at different levels of description: neuronal physiology, cognitive neuroscience and the theoretical predictive coding framework.

Results

Evidence of prediction error in single auditory neurons. The goal of the present experiments was to test responses of single neurons of the central auditory system of the rat for signs of predictive activity under oddball stimulation. We recorded extracellular single neuron activity in response to sinusoidal tones in different auditory centers of the rat brain (Fig. 1a). Rats were deeply anesthetized prior to surgery preparation and during the whole recording session. One single neuron was recorded at a time, using one tungsten electrode inserted into the brain, and local field potential (LFP) activity was simultaneously recorded from the same electrode.

The predictive coding framework assumes that the generation of both predictions and prediction errors takes place at every hierarchical level of a sensory system¹⁰. In principle, this assumption could include subcortical processing stations¹². Unfortunately, there is little evidence supporting this possibility, since most previous research on predictive brain activity was focused on cortical responses^{7,8}. In order to collect a representative sample from different processing stations along the auditory pathway, we recorded a total of 210 neurons (Table 1) from the following: the auditory midbrain—specifically the inferior colliculus (IC), the auditory thalamus—specifically the medial geniculate body (MGB), and the auditory cortex (AC) of anesthetized rats while the animal was played sequences of pure tones (Fig. 1b). According to the well-established functional and anatomical organization of the auditory system³⁴, recorded neurons in the IC, MGB and AC were grouped as lemniscal (L) or

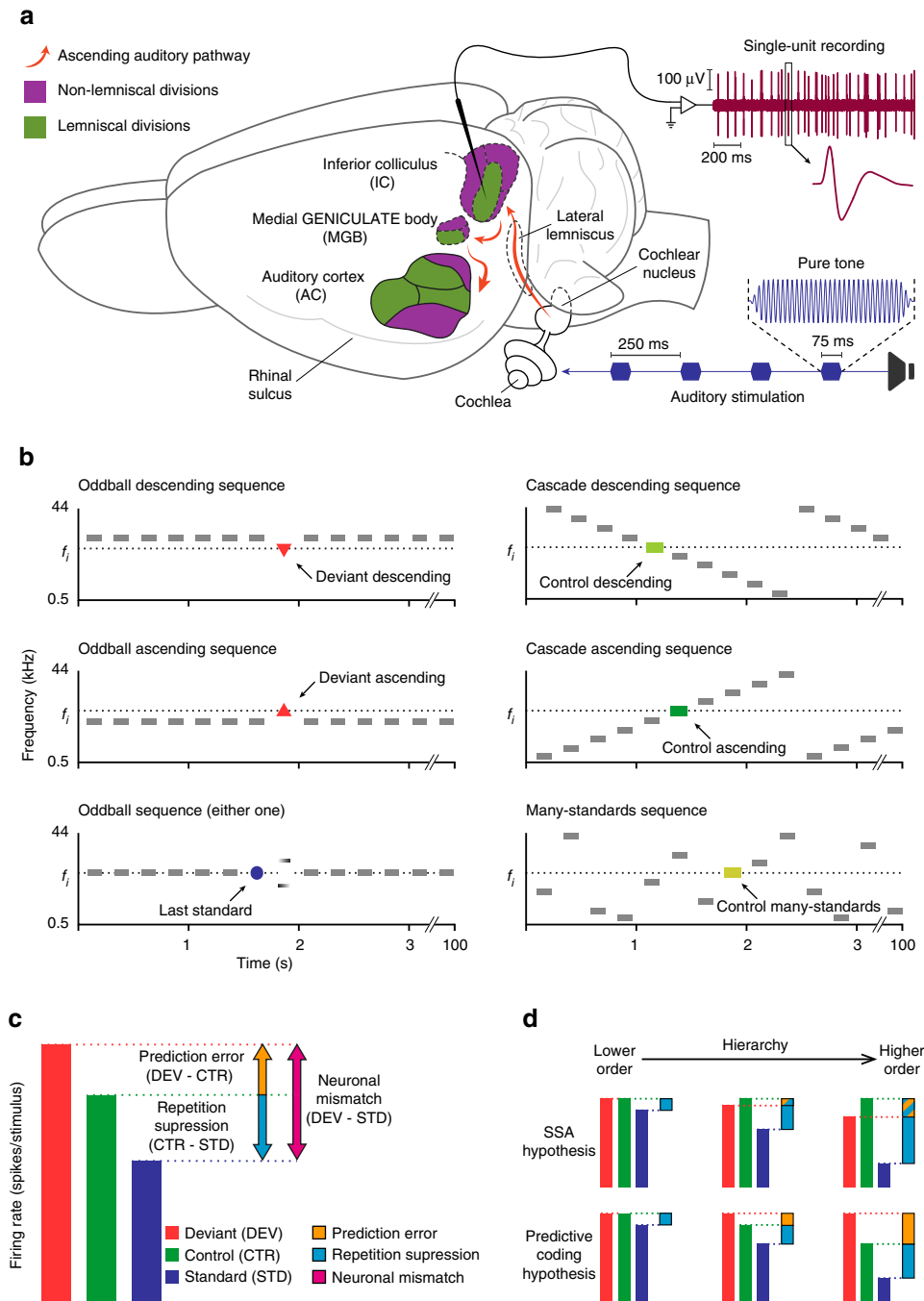


Fig. 1 Experimental design. **a** Sketch of experimental setup. While stimulating with sequences of pure tones, isolated neurons were recorded from three auditory nuclei of anesthetized rats: IC, MGB and AC (colored). The schematic representation of the ascending auditory pathway information flow (orange) shows how lemniscal (green) and non-lemniscal (purple) subdivisions can be distinguished in the IC, MGB and AC. **b** Stimulation sequences. For each neuron, 10 tones of evenly-spaced frequencies were selected to construct the stimulation sequences. Each tone f_i ($i = 1 \dots 10$) lying inside the neuron's receptive field could be presented in two experimental conditions (deviant and standard, in separated oddball sequences, left column), and two control conditions (cascade and many-standards, right column) for adaptation effects. Note that ascending and descending deviant tones will be compared to the control ascending or control descending sequences, respectively. They will also be compared to the many-standards sequence for both types of deviants (see Methods). **c** Decomposition of neuronal mismatch responses (DEV-STD) to the oddball sequence using either one of the control conditions. Under the assumption of predictive coding, CTR-STD (if positive) represents repetition suppression, and DEV-CTR (if positive) represents prediction error. **d** Two hypothetical scenarios according to two possible competing mechanisms accounting for the neuronal mismatch: SSA (top) and predictive coding (bottom). For SSA, there is response suppression to the standard (blue bars), which progressively increases from lower order to higher order. In addition, due to suppression of the deviant relative to control, the prediction error is increasingly negative (blue and orange bars) as one progresses to higher-order regions. For predictive coding, repetition suppression of the standard (blue bars) increases from lower to higher-order regions. Unlike SSA, responses to deviants are higher than controls, especially in higher-order regions, leading to a positive prediction error (orange bars)

Table 1 Summary of principal urethane data set

	IC _L	IC _{NL}	MGB _L	MGB _{NL}	AC _L	AC _{NL}
Neurons	26	56	25	33	34	36
Points/required	149/104	523/401	79/69	211/153	250/125	307/29
DEV (spikes)	1.37	0.99	0.72	0.69	0.95	0.98
STD (spikes)	1.25	0.22	0.20	0.16	0.24	0.21
Cascade (spikes)	1.66	0.97	0.74	0.57	0.77	0.59
Many-standards (spikes)	1.91	0.95	0.90	0.65	0.85	0.52
Spike count differences						
DEV-STD	0.12	0.78	0.52	0.54	0.71	0.76
<i>p</i> value	0.000	0.000	0.000	0.000	0.000	0.000
Cascade-STD	0.41	0.76	0.53	0.42	0.53	0.38
<i>p</i> value	0.000	0.000	0.000	0.000	0.000	0.000
DEV-Cascade	-0.29	0.02	-0.01	0.12	0.18	0.38
<i>p</i> value	0.000	0.024	0.021	0.019	0.017	0.000
Many-standards-STD	0.57	0.73	0.70	0.50	0.60	0.31
<i>p</i> value	0.003	0.000	0.000	0.000	0.000	0.000
DEV-Many-standards	0.04	0.04	-0.26	0.03	0.11	0.46
<i>p</i> value	0.190	0.155	0.003	0.671	0.049	0.000
Differences using Cascade controls						
iMM	0.14	0.49	0.34	0.52	0.50	0.60
<i>p</i> value	0.000	0.000	0.000	0.000	0.000	0.000
iRS	0.22	0.46	0.46	0.46	0.39	0.33
<i>p</i> value	0.000	0.000	0.000	0.000	0.000	0.000
iPE	-0.08	0.03	-0.12	0.06	0.11	0.27
<i>p</i> value	0.000	0.024	0.021	0.019	0.017	0.000
Differences using Many-standards						
iMM	0.14	0.48	0.30	0.50	0.50	0.61
<i>p</i> value	0.000	0.000	0.000	0.000	0.000	0.000
iRS	0.16	0.46	0.44	0.49	0.43	0.34
<i>p</i> value	0.003	0.000	0.000	0.000	0.000	0.000
iPE	-0.02	0.02	-0.14	0.01	0.07	0.27
<i>p</i> value	0.190	0.155	0.003	0.671	0.049	0.000

For each auditory station: Number of recorded neurons and tested neuron/tone combinations (points), along with estimated minimum sample size (of points) required for a statistical power of 0.8 (see Methods subsection on 'Statistical Analyses'). Median values for baseline-corrected spike counts (spikes) to the different conditions. Median differences between the former measures, and associated *p* values against zero (Friedman test with post hoc multiple comparison, Fisher's Least Significant Difference method, uncorrected for 6 independent tests). All *p* values are rounded to 3 decimal figures, so a value of 0.000 means "*p* < 0.0005". Median indices of neuronal mismatch (iMM), repetition suppression (iRS) and prediction error (iPE), computed from each of the two control sequences (cascade or many-standards), and their corresponding *p* values (note that *p* values are the same for absolute differences and normalized indices, since these indices are median differences between normalized responses, and the non-parametric test is independent of scaling). Values related to predictive neuronal activity are highlighted in bold case, since they represent the most significant result of this research

non-lemniscal (NL)^{2, 27, 34}, thus leading to six different processing stations. These included the following: (1) the central nucleus of the IC, i.e., the lemniscal division of the IC (IC_L); (2) the dorsal, lateral, and rostral cortices of the IC, i.e., the non-lemniscal divisions of the IC (IC_{NL}); (3) the ventral division of the MGB, i.e., the lemniscal division of the auditory thalamus, (MGB_L); (4) the medial and dorsal divisions of the MGB, i.e., the non-lemniscal regions of the MGB (MGB_{NL}); (5) the primary auditory cortical fields: primary, anterior, and ventral auditory fields, which collectively constitute the core or lemniscal AC (AC_L), and finally, (6) the posterior and the suprarhinal auditory field, which together form the belt or non-lemniscal division of the AC (AC_{NL}); for a full list of abbreviations, refer to Supplementary Table 1; Fig. 2; see Methods section).

For each recorded neuron, we presented a set of oddball sequences, using tones selected from the neuron's frequency-response area, and we computed a "neuronal mismatch response" as the difference between responses to deviant (DEV) and standard (STD) conditions for each tone (Fig. 1c). To determine whether this difference (usually DEV > STD) reflected predictive activity, instead of (or in addition to) SSA, we also presented two cascaded sequences (ascending and descending) and one many-standards sequence as controls^{35, 36} (Fig. 1b). These latter sequences contained all tones used in oddball sequences (see Methods section). The main rationale behind this design is that, in the control conditions, each tone has the same low (10%)

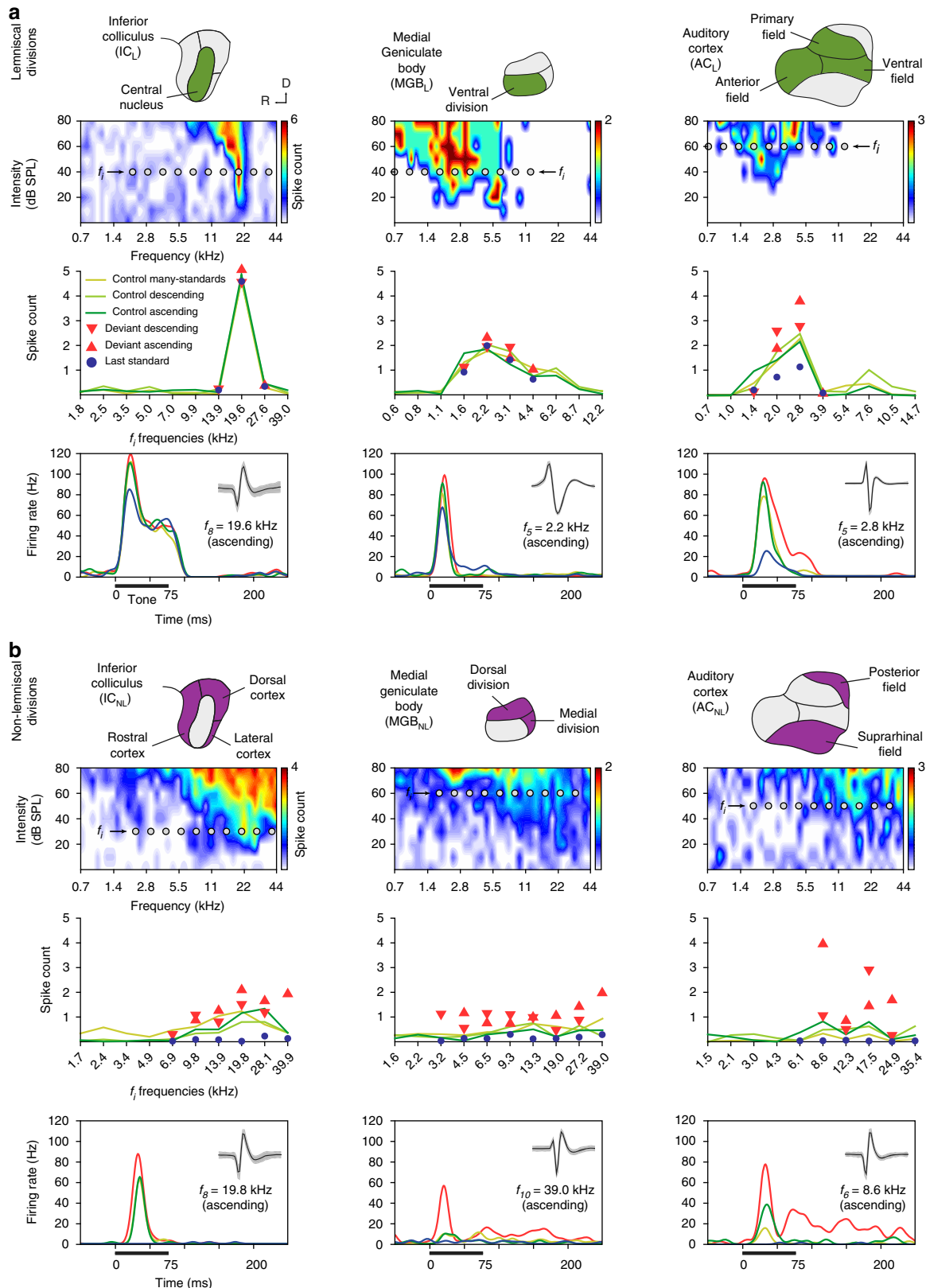
probability of occurrence as a DEV tone in the oddball sequence, so it is not repetitive (as the STD), and therefore is free of repetition effects (e.g., repetition suppression); at the same time, it does not stand out from the statistical context (as the DEV), and therefore it is not perceived as a deviant^{35, 36}. Thus, we used responses to cascades and many-standards control conditions as the reference with which to discriminate between repetition suppression and prediction error effects (Fig. 1c). If the neuronal mismatch response (DEV-STD) is caused entirely by SSA to the STD tone, responses to DEV and control conditions should remain comparable through all hierarchical levels, or if anything, the response to DEV tones should undergo a slightly stronger suppression than to the controls, due to cross-frequency adaptation²⁶ (Fig. 1d). By contrast, under the predictive coding framework, deviance detection is based on Bayesian inference¹⁰, such that stronger prediction errors will be produced as more sensory input accumulates to increase the confidence and precision of current predictions^{3, 12, 13}. Therefore, stronger prediction errors should be elicited by DEV than by cascades or many-standards tones, due to the lack of sequential stimulus repetitions in the controls^{3, 35}, and this effect should increase up the hierarchy (Fig. 1d), since higher-order processing stations are more sensitive to all forms of regularity, including complex and global regularities^{2, 8, 14, 37, 38}.

Our results show that the responses of lemniscal neurons were mostly dependent on tone frequency, with little sensitivity to the

different conditions. This was particularly true at subcortical levels (See Fig. 2 for individual responses of representative neurons). However, in the auditory cortex (Fig. 2, right column), strong response suppression to STD was apparent in both AC_L and AC_{NL}, although the suppression was clearest and strongest in the non-lemniscal regions (Fig. 2b). Also, a higher firing rate in

response to DEV tones, as compared to both many-standards and cascades control conditions, was consistent across tested frequencies. These results demonstrate the hypothesized signature of prediction error at the single neuron level^{15, 26}.

Neuronal responses to many-standards and cascades conditions were not statistically different from each other, either in the



whole sample (Wilcoxon signed-rank test, $n = 1495$ $z = -0.125$, $p = 0.9$), or within each station separately (Wilcoxon signed-rank test, $n(\text{IC}_L) = 149$; $n(\text{IC}_{NL}) = 522$; $n(\text{MGB}_L) = 77$; $n(\text{MGB}_{NL}) = 211$; $n(\text{AC}_L) = 250$ and $n(\text{AC}_{NL}) = 307$ $p > 0.1$ within all stations). Additionally, the results using either cascades or many-standards conditions as a control were largely comparable (Table 1). Therefore, we will limit our results to those obtained using the cascaded sequence as control (CTR), since this sequence controls for additional factors beyond presentation rate of the deviant tone^{35, 36} (see Methods subsection ‘Experimental design’).

Prediction error increases along the auditory hierarchy. In order to demonstrate deviance detection at the cellular level, responses to deviant tones must exceed responses to control tones at the population level. To determine whether this was true for our data, we first performed a within-station multiple comparison (Friedman test), between responses to DEV, STD, and CTR conditions such that each pair of conditions, within each station, was tested for a difference in medians (Table 1). As expected, responses to DEV condition were stronger than to STD condition within all stations (Friedman test and median values from $\text{IC}_L = 0.12$ $p = 4.8 \times 10^{-5}$; $\text{IC}_{NL} = 0.78$ $p = 1.8 \times 10^{-92}$; $\text{MGB}_L = 0.52$ $p = 8.4 \times 10^{-6}$; $\text{MGB}_{NL} = 0.54$, $p = 7.4 \times 10^{-26}$; $\text{AC}_L = 0.71$ $p = 5.3 \times 10^{-42}$ and $\text{AC}_{NL} = 0.76$, $p = 6.7 \times 10^{-56}$; Table 1). This neuronal behavior has been described along the auditory pathway², but has been referred to as SSA in previous studies^{19, 21, 22, 27}. However, as we demonstrate, these responses could also arise from deviance detection. Indeed, the neuronal mismatch results we showed were mostly due to the suppression of the response to the repetitive STD condition (repetition suppression), since responses to STD were significantly weaker than to CTR condition within all stations (Friedman test and median values from $\text{IC}_L = 0.41$ ($p = 2.6 \times 10^{-21}$); $\text{IC}_{NL} = 0.76$ $p = 1.6 \times 10^{-73}$; $\text{MGB}_L = 0.53$ $p = 1.3 \times 10^{-11}$; $\text{MGB}_{NL} = 0.42$ $p = 2.9 \times 10^{-16}$; $\text{AC}_L = 0.53$ $p = 4.8 \times 10^{-29}$ and $\text{AC}_{NL} = 0.38$ $p = 9.1 \times 10^{-19}$; Table 1). Critically, responses to DEV tones were already significantly higher than to CTR within the IC_{NL} (median = 0.02 $p = 0.024$), and this difference increased progressively in the MGB_{NL} (median = 0.12 $p = 0.019$), and AC_{NL} (median = 0.38 $p = 4.9 \times 10^{12}$) (Table 1). Therefore, neuronal responses showed clear signs of prediction error at the population level, within all non-lemniscal stations, (i.e., the dorsal, lateral and rostral regions of IC, the dorsal and medial divisions of the MGB, and posterior auditory field and suprarhinal auditory field in AC) and also within AC_L ; Table 1), which is consistent with the observed effects in the example neurons shown in Fig. 2, corresponding with AC_L , IC_{NL} , MGB_{NL} and AC_{NL} .

To both quantify the relative contribution of repetition suppression and prediction error to neuronal mismatch in

observed neuronal responses, and to facilitate comparisons between different neurons/stations, we normalized the neuronal responses to the three conditions (DEV, STD, CTR) for each neuron/tone combination. We applied Euclidean vector normalization (Supplementary Fig. 1) such that all normalized responses ranged between 0 and 1. Then, we computed three indices as the difference between normalized responses to pairs of conditions, ranging between -1 and $+1$ (Fig. 3a). The “index of neuronal mismatch”, $\text{iMM} = \text{DEV} - \text{STD}$, is the relative difference in responses to STD and DEV tones in the oddball paradigm. The iMM is quantitatively equivalent to the typical SSA index¹⁹, used in previous studies (Supplementary Fig. 2). The “index of neuronal repetition suppression”, $\text{iRS} = \text{CTR} - \text{STD}$, is the relative reduction of the response to a standard tone, as compared to the control. Thus, the iRS quantifies repetition effects¹¹. Finally, and most importantly for this study, the “index of neuronal prediction error”, $\text{iPE} = \text{DEV} - \text{CTR}$, is the relative increase in the response to a deviant tone, compared to the control. A positive iPE reflects predictive activity³⁵, as opposed to SSA, and quantifies the proportion of prediction error accounting for neuronal mismatch. Therefore, the relation $\text{iMM} = \text{iRS} + \text{iPE}$ provides a functional, quantitative decomposition of neuronal mismatch (Fig. 1d). The distribution of these indices across stations revealed that both the index of neuronal mismatch (the relative difference in responses to STD and DEV tones in the oddball paradigm) and index of prediction error (the relative increase in the response to a deviant tone, compared to the control) increase along the auditory pathway, from IC_L to AC_{NL} (Fig. 3b). Medians of iMM for $\text{IC}_L = 0.14$; $\text{IC}_{NL} = 0.49$; $\text{MGB}_L = 0.34$; $\text{MGB}_{NL} = 0.52$; $\text{AC}_L = 0.50$ and $\text{AC}_{NL} = 0.60$. Medians of iPE along the auditory pathway $\text{IC}_L = -0.08$; $\text{IC}_{NL} = 0.03$; $\text{MGB}_L = -0.12$; $\text{MGB}_{NL} = 0.06$; $\text{AC}_L = 0.11$ and $\text{AC}_{NL} = 0.27$.

Summary statistics for these normalized responses and indices are shown in Fig. 4a, b, respectively. Critically, median iPE was significantly greater than zero within AC_L ($p = 0.01$) and within the three non-lemniscal stations (Friedman test to IC_{NL} $p = 0.024$; $\text{MGB}_{NL} = 0.019$ and $\text{AC}_{NL} = 4.9 \times 10^{-12}$) (Table 1; Fig. 4b), which is consistent with a significant difference in absolute spike counts (median and p values from $\text{IC}_{NL} = 0.02$ $p = 0.024$; $\text{MGB}_{NL} = 0.12$ $p = 0.019$; $\text{AC}_L = 0.18$ $p = 0.017$ and $\text{AC}_{NL} = 0.38$ $p = 4.9 \times 10^{-12}$) (DEV-CTR in Table 1). Moreover, the iPE showed a distinct increase in two ways: (1) from lemniscal ($\text{IC} = -0.08$; $\text{MGB} = -0.12$ and $\text{AC} = 0.11$) to non-lemniscal stations ($\text{IC} = 0.03$; $\text{MGB} = 0.06$ and $\text{AC} = 0.27$); and (2) from IC to MGB to AC (Fig. 4b). To validate these observations statistically, we fitted a linear model for the iPE using “nucleus” (IC, MGB, AC) and “hierarchy” (Lemniscal “L”, Non-Lemniscal “NL”) as categorical factors. Using ‘L’ and ‘IC’ as reference levels for these factors, the resulting

Fig. 2 Prediction error in representative examples of neuronal responses in anaesthetized rat. **a** Examples of lemniscal neuronal responses in each recorded auditory station (columns). The first row contains schematics of the lemniscal subdivisions (green) within each nuclei. The second row shows the frequency-response area (representation of neuronal sensitivity to different frequency-intensity combinations) of representative lemniscal neurons from each nucleus. Ten grey dots within each frequency-response area represent the ten tones (f_i) selected to build the experimental sequences (see Methods). The third row displays the measured responses of the particular neuron to each f_i tone (baseline-corrected spike counts, averaged within 0–180 ms after tone onset) for all conditions tested. Note that measured conditions tend to overlap in the subcortical stations (IC_L and MGB_L), and only start differentiating from each other once auditory information reaches the cortex (AC_L). The fourth row contains sample peri-stimulus histograms comparing the neuronal responses to each condition tested for an indicated f_i tone. A thick horizontal line represents stimulus duration. A small inset within the upper right corner of each panel features the isolated spike (mean \pm SEM) of that single neuron. **b** Examples of non-lemniscal neuronal responses in each recorded auditory nuclei, organized as in **a**. The first row highlights non-lemniscal divisions in purple. In the second row, note frequency-response areas tend to be more broadly tuned, as compared to lemniscal neurons. In the third row, responses to deviant conditions tend to relatively increase and distance themselves from their corresponding controls as information ascends in the auditory pathway. Also note that responses to last standards are feeble or even completely missing across all non-lemniscal stations (IC_{NL} , MGB_{NL} and AC_{NL}). In the last row, the strong influence of the experimental condition over the neuronal response to the same tone can be clearly appreciated in the three nuclei

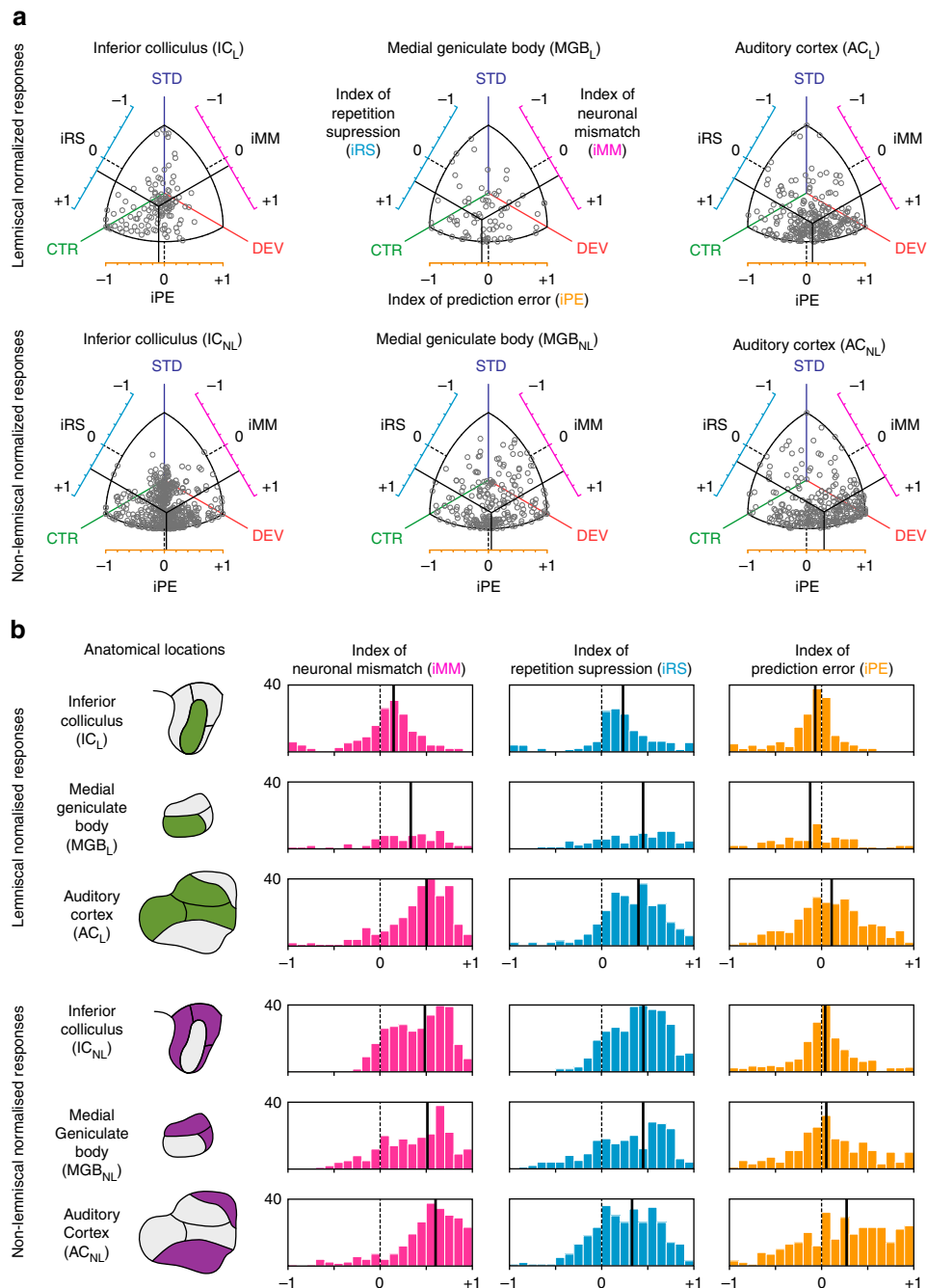


Fig. 3 Prediction error at population level for each station in anaesthetized rat. Distribution of normalized responses and related indices of neuronal mismatch (iMM), repetition suppression (iRS) and prediction error (iPE). **a** Each grey dot in these scatter plots represents the three normalized responses of a single neuron to the same tone played as deviant (DEV), as standard (STD) and as control (CTR). Indexes result from the difference between two of these normalized responses, represented in the axes surrounding the scatter plots, where the dotted black lines marks the absence of difference between conditions (index = 0). Solid black lines represent the mean of each index, corresponding their intersection to the center of gravity of the distribution of responses in the normalized space. Note how, while the intersection for lemniscal subcortical stations (IC_L and MGB_L) is skewed towards CTR, in their non-lemniscal counterparts (IC_{NL} and MGB_{NL}) as well as all over the cortex (AC_L and AC_{NL}) the center of gravity of the distribution shifts closer and closer to DEV as it moves up in the auditory pathway, increasing the iPE as auditory information reaches higher-order stations. **b** Histograms represent distributions within stations of the three indexes for each neuronal response. Solid black lines indicate medians. The noticeable overall tendency of the median indexes to shift towards more positive values, from IC through MGB to AC, and from lemniscal to non-lemniscal divisions, unveils a hierarchy of processing in the auditory pathway

model was:

$$iPE = 0.012 + 0.020 \times NL - 0.136 \times MGB + 0.092 \times AC + 0.185 \times NL \times MGB + 0.158 \times NL \times AC$$

where the constant term 0.012 is the reference level in IC_L. Then, we applied an ANOVA to this model and revealed a significant effect of hierarchy ($F = 36.43$, $p = 2.01 \times 10^{-9}$) and nucleus ($F = 45.74$, $p = 5.53 \times 10^{-20}$), and a significant hierarchy × nucleus

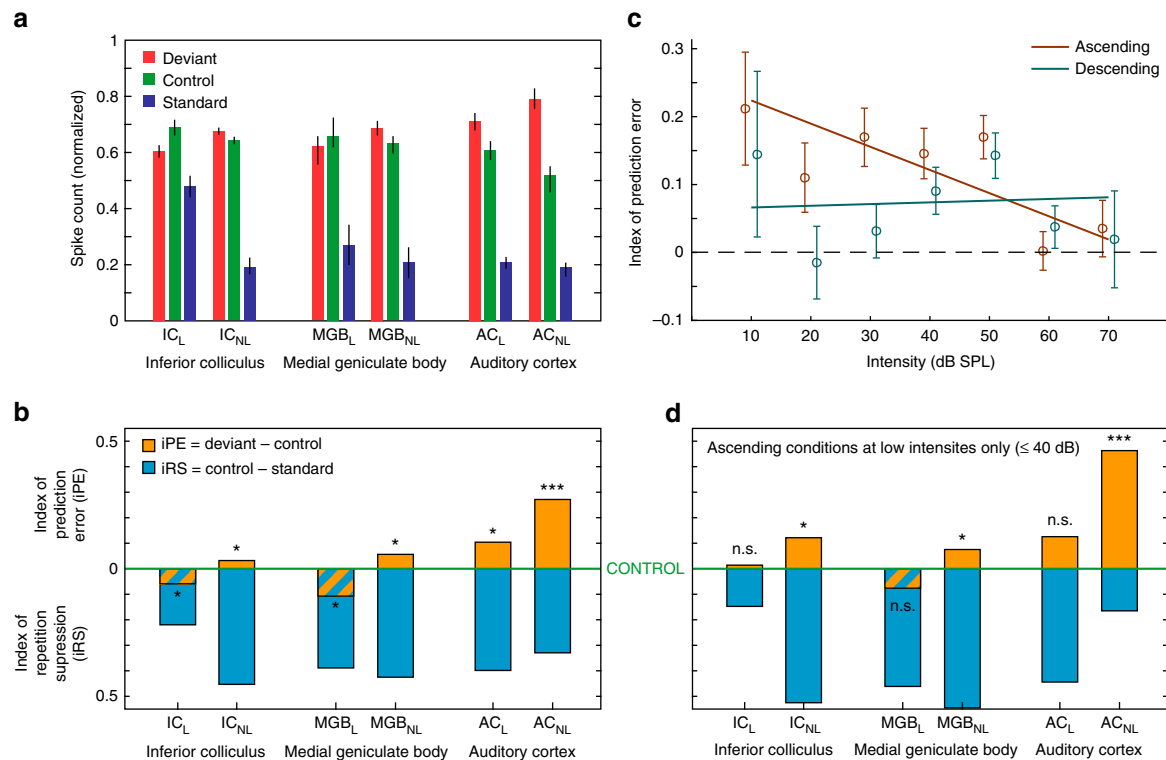


Fig. 4 Emergence of prediction error along the auditory hierarchy. **a** Median normalized responses (lines indicate SEM) to the deviant, standard and control within each station. **b** Median indices of prediction error (orange) and repetition suppression (cyan), represented with respect to the baseline set by the control. Thereby, iPE is upwards-positive while iRS is downwards-positive. Each median index corresponds to differences between normalized responses in **a**. Asterisks denote statistical significance of iPE against zero median (* $p = 0.05$, ** $p = 0.01$, *** $p = 0.001$, see Table 1). **c** Linear model fitted for the iPE using SPL and direction (ascending / descending) as predictors. Error bars denote mean and SEM for each SPL and direction. Note the model predicts greater iPE values for ascending conditions at low intensities. **d** Same as in **b**, but only representing ascending conditions at intensities equal or lower than 40 dB SPL

interaction ($F = 3.7$, $p = 0.024$). Therefore, both tendencies, from lemniscal to non-lemniscal and from IC to MGB to AC, were significant and robust from midbrain to cortex. Specific post hoc comparisons confirmed that median iPE was higher in AC_{NL} than in AC_L ($n = 557$ ranksum test, $p = 2.2 \times 10^{-5}$) or MGB_{NL} ($n = 518$ $p = 1.9 \times 10^{-5}$), and higher in AC_L than in IC_{NL} ($n = 773$, $p = 2.2 \times 10^{-13}$). Although iPE was numerically higher in MGB_{NL} than in IC_{NL}, this difference was not quite statistically significant ($n = 734$, ranksum test, $p = 0.151$).

Overall, this analysis demonstrates a systematic increase of prediction error in responses of single neurons as information progresses along the auditory pathway. This was true, both from the IC to the MGB to cortex (bottom-up processing) and from lemniscal to non-lemniscal regions, with a mutual potentiation of these two effects.

According to previous modeling work, single neurons were expected to be maximally sensitive to change for stimulus ranges, where the firing rate of the neuron is below saturation³⁹. Consistent with this hypothesis, we observed that deviance specific-responses were easier to produce with low stimulation intensities, particularly for ascending deviants (e.g., Fig. 2d, IC_{NL}). To test these observations at the population level, we fitted a different model for the iPE, using SPL (in Bels = dB SPL/10) and direction (ascending or descending) of deviant tones (see Fig. 1b) as predictors. The model showed a significant effect of SPL ($F = 4.59$, $p = 0.03$) and a SPL \times direction interaction ($F = 6.66$, $p = 0.01$):

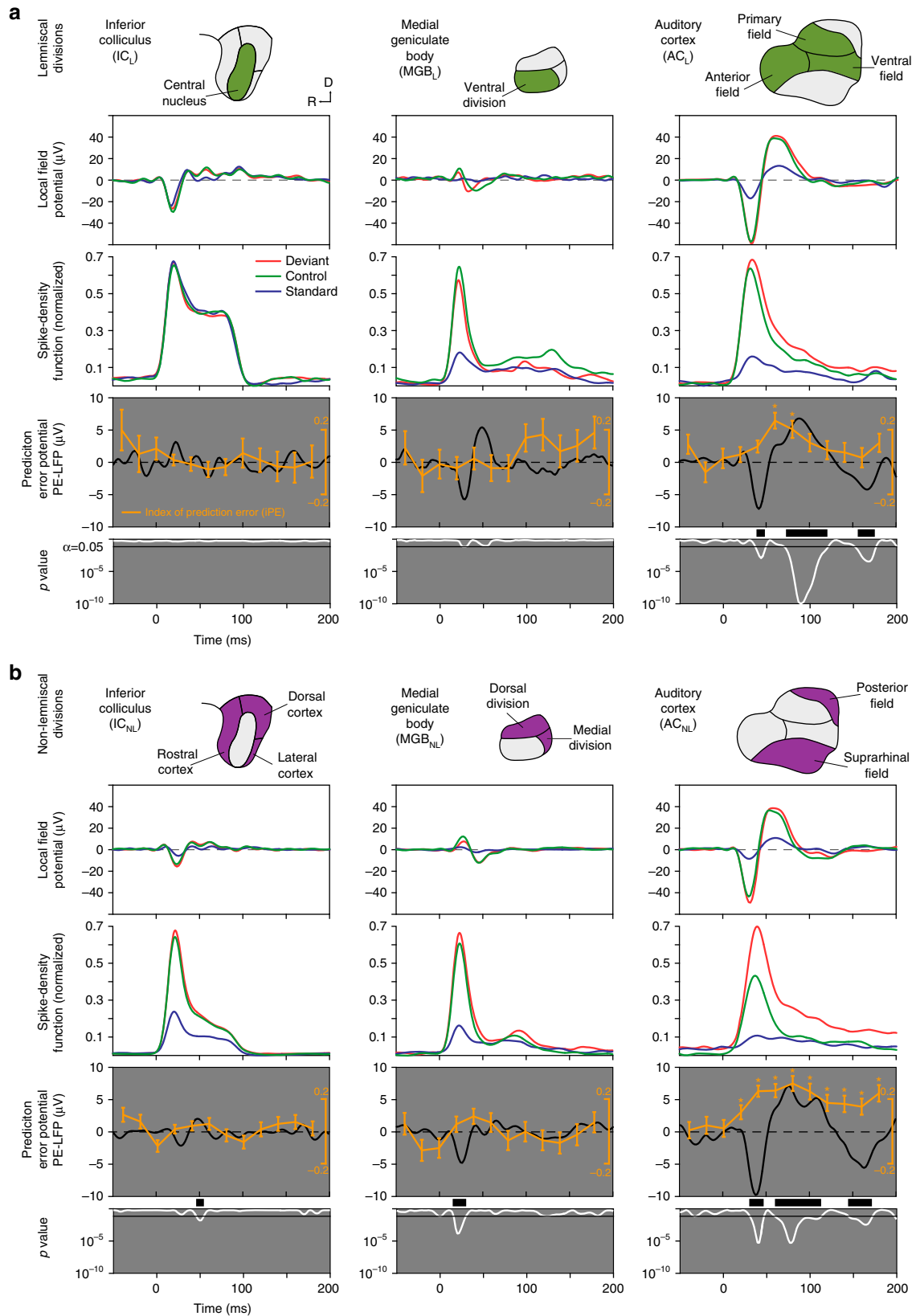
$$\text{iPE} = 0.064 + 0.194 \times \text{ascending} + 0.003 \times \text{SPL} - 0.037 \times \text{ascending} \times \text{SPL}$$

which indicates that the iPE is expected to be much higher for ascending deviants at intensities equal or below 40 dB SPL (Fig. 4c). Indeed, we observed a distinct increase in the iPE within all stations (medians and Friedman test from IC_L $n = 15$; median = -0.003 and $p = 1$; IC_{NL} $n = 113$; median = 0.1174 and $p = 0.0052$; MGB_L $n = 12$; median = -0.0739 and $p = 0.6831$; MGB_{NL} $n = 40$; median = 0.1041 and $p = 0.0442$ and AC_L $n = 61$; median = 0.1364 and $p = 0.0629$), under these stimulation conditions (Fig. 4d), particularly in AC_{NL} ($n = 38$ median = 0.5048 and $p = 1.01 \times 10^{-4}$), where prediction error accounted for around two thirds of the iMM.

We also wanted to test the relationship between a neuron's deviance sensitivity and its tuning width, since broadly tuned neurons have wider spectral integration capabilities, which in turn might facilitate the task of deviance detection. Specifically, broadly tuned neurons would be activated by more of the control tones than narrowly tuned neurons, which in turn could reduce neuronal responses to the control condition in broadly tuned neurons (compared to narrowly tuned neurons, which are more abundant in lemniscal stations). However, we did not find any significant correlation between neuronal tuning bandwidth (measured as a quality factor Q_{30} , see Methods section) and iPE in our sample (Spearman correlation coefficient, $\rho = -0.0067$, $p = 0.93$). Interestingly, however, a subset of neurons with highly disorganized and fragmented frequency-response area, for which a Q_{30} factor could not be measured, showed iPE levels significantly higher than the rest (median iPE, ranksum test; untuned neurons: iPE = 0.31 , tuned neurons: iPE = 0.024 , $p = 1.6 \times 10^{-5}$). This indicates that the functional role of these neurons are more concerned with contextual integration at a higher level than with spectral processing.

Single neuron PE and large-scale mismatch response in AC. We used the same electrodes from which we recorded the single neuron spike to simultaneously record local field potentials (LFPs). We then leveraged these latter signals to explore the direct correlation between the prediction error demonstrated in the

spike responses and large-scale mismatch responses (such as the MMN). We averaged LFP responses for each condition and station, as well as the difference between DEV and CTR conditions, which we called the “prediction error potential”^{16, 36}: $PE-LFP = LFP_{DEV} - LFP_{CTR}$ (Fig. 5). A significant early PE-LFP using a two-



tailed t test was already detectable within IC_{NL} (median = 0.0480 and $p < 0.05$) and MGB_{NL} (median = 0.0550 and $p < 0.05$) (Fig. 5b, left and central columns). In the auditory cortex, the PE-LFP was strong and significant in both AC_L and AC_{NL} (median = 0.1269 and 0.4929 respectively and $p < 0.05$), showing three major deflections (Fig. 5, right column): a fast negative deflection (N1; 35–50 ms after change onset), a slower positive deflection (P2; 70–120 ms), and a third, late, negative deflection (N2; beyond 150 ms; paired t test, FDR-corrected for 200 comparisons). Epidural MMN peaks between 60 and 120 ms in rats¹⁵, the same range of the P2 recorded here for the PE-LFP, and can be positive when recorded from inside the brain²⁹. Then, we recomputed the iPE for 12 different time windows (20 ms width, from –50 to 190 ms respect to stimulus onset), for each neuron/ tone combination separately, and we averaged within each station (Fig. 5). The iPE showed a clear modulation over time in both AC_L and AC_{NL} stations (Friedman test, not corrected for 6 independent tests). Each individual iPE value was also tested against zero (signrank test, FDR-corrected for 12 comparisons), and this analysis revealed a significant iPE ($p < 0.05$ in both asterisks) within AC_L between 60–100 ms after change onset, and in AC_{NL} ($p < 0.01$ for all asterisks) between 25–200 ms, and seemingly beyond (Fig. 5, right column). In summary, the highest iPE values, which reflect prediction error in single neuron responses, correlate in time and location with a large-scale mismatch wave (the PE-LFP), which is the putative MMN in rats^{15, 16}.

Hierarchical prediction is conserved across species and arousal.

The pattern of results shown in Fig. 4b suggests that the auditory system adheres to the general predictive coding framework. To confirm both that these results held different species of rodent, and to exclude the potential biasing influence of anesthesia, we performed identical experiments in awake, restrained mice. We recorded multi-unit activity and LFP from IC (49 recordings from 5 animals) and AC (42 recordings from 5 animals). Representative sample recordings are shown in Fig. 6. As in single-unit cases recorded in the anesthetized preparation (Fig. 2), we observed clear signs of prediction error (DEV > CTR) across different frequencies in the multi-unit recordings (Fig. 6).

Normalized responses and indices of prediction error and repetition suppression for the awake mice are shown in Fig. 7 and Table 2. Similarly to the results obtained from the anesthetized rats, median iPE was significantly greater than zero within IC_{NL} and both AC stations (median iPE, Friedman test with post hoc multiple comparisons, Fisher's Least Significant Difference method; IC_L : –0.13, $p = 0.023$; IC_{NL} : 0.12, $p = 0.018$; AC_L : 0.17, $p = 0.001$; AC_{NL} : 0.32, $p = 5 \times 10^{-7}$). Also, iPE was significantly higher in AC_{NL} than in AC_L (ranksum test, $p = 0.015$), or in IC_{NL} ($p = 0.0004$). Therefore, the two extremes of the hierarchical organization of the iPE (IC and AC) coincide in awake mice and anesthetized rats (compare Figs. 4a, b and 7b, c). This finding is consistent with the hypothesis that neurons along the auditory

pathway exhibit a hierarchical organization of prediction error is a general pattern across rodent species and states of awareness. Indeed, median iPE levels in both AC_L and AC_{NL} were not statistically different between the two preparations (ranksum test, $p > 0.1$). However, median iPE levels were significantly higher in awake than in anesthetized IC_{NL} (ranksum test, $p = 0.048$; compare above values with Table 1). Thus, iPE tended to be higher in the awake condition, within each processing station (compare Figs. 4a, b and 7b, c), especially in subcortical IC_{NL} . Finally, as was the case in the anesthetized rat, a difference between DEV and CTR conditions was also observed in the LFP, at the level of the AC (t test $p < 0.05$ for lemniscal and non-lemniscal regions. Fig. 7a, third row); and the difference was significant during similar time windows: 35–42 ms (N1) and 95–118 ms (P2) in AC_L , 86–116 ms (P2) and beyond 165 ms (N2) in AC_{NL} (compare with Fig. 5, right column).

Discussion

This study demonstrates that predictive activity of single neurons responding to an auditory oddball paradigm can be tracked along the ascending auditory pathway. These prediction error signals are organized hierarchically and are consistent across species and awareness states. Furthermore, our data suggests that this predictive activity underlies large-scale mismatch responses, such as the MMN. Quantitatively decomposing neuronal mismatch responses into repetition suppression and prediction error revealed a systematic increase in the proportion of prediction error that explained the neuronal mismatch responses as the sensory signal traveled along the ascending auditory pathway. The increase in explanatory power of the prediction error signal occurred not only from the inferior colliculus to auditory thalamus and cortex, but also from lemniscal (first order) to non-lemniscal (high order) divisions within each level. Thus, the highest prediction error values are found in the higher-order auditory cortex, where they correlate with a large-scale prediction error potential including late evoked potentials.

This latter finding suggests an influence from prefrontal cortices⁴⁰. This view is consistent with a recent study that recorded from humans subdural electrocorticographic electrodes located in frontal and temporal cortex while they listened to trains of repeated tones that were interrupted by two types of deviant: predictable and unpredictable^{41, 42}. Using high gamma (H γ -band, > 60 Hz) activity as an index of local spiking these authors found more evidence for a hierarchical organization of mismatch signals⁴², highlighting the role of frontal cortex and H γ -band activity in deviance detection and in the generation of predictive activity. Interestingly, a recent study using LFP recordings in the parietal and frontal cortex in rats also supports this notion⁴⁰. Our finding that prediction error contributes to neuronal mismatch response supersedes repetition suppression within the higher-order auditory cortex is also consistent with studies of the neuroanatomical location of the MMN in animals¹⁶ and humans³⁷.

Fig. 5 Correlation of iPE and prediction error potential (PE-LFP). **a** Population grand-averages for different response measures, computed for each lemniscal station (in columns, represented in first row highlighted in green). The second row shows the average LFP across all tested tones and single neurons from each station for different conditions. The third row displays the average firing rate profiles for each station as normalized spike-density functions. The fourth row contains the prediction error potentials (PE-LFP, black trace), which is the difference wave of the deviant and the control LFP. Along PE-LFP, the time course of the average iPE is plotted in orange (mean \pm SEM, asterisks indicating significant iPE for the corresponding time window; Wilcoxon signed-rank test for 12 comparisons, corrected for FDR = 0.1). Next row shows an instantaneous p value (white trace) of the corresponding PE-LFP (paired t test against equal means, corrected for FDR = 0.1, critical threshold for significance set at 0.05 represented as a horizontal bar). Thick black bars of the grey panel mark time intervals for which the average PE-LFP is significant. Note that only AC_L shows a significant prediction error signal. **b** Same as in **a** but computed for each non-lemniscal station (highlighted in purple in the first row). Note in the last row significant PE-LFPs appear in all three stations (IC_{NL} , MGB_{NL} and AC_{NL}), and prominently in AC_{NL} . Note also how highest iPE values are concurrent with the strongest PE-LFPs in time and location (auditory cortex, both AC_L and AC_{NL})

Taken together, results from previous studies cohere with our findings and present strong evidence for the predictive coding account of mismatch responses. Our study also extends this work, highlighting the role of subcortical structures in perception⁴³, providing a novel extension of the exclusively cortical perspective of the predictive coding literature^{9, 10, 44}. Although lemniscal and non-lemniscal pathways process different aspects of the auditory signal in parallel, the non-lemniscal auditory regions represent a higher hierarchical level of processing³³ and are known to be more sensitive to acoustic change and contextual influences than lemniscal ones^{2, 22, 25, 27, 45}. In fact, the involvement of higher-order areas in predictive processes has been hypothesized

previously⁴, but until now, this hypothesis had not been tested directly.

The response patterns we observed confirm that subcortical, first-order nuclei are mostly sensitive to global or pattern probability generated in the classical oddball paradigm, while higher levels are more sensitive to local relationships between sounds (transitional probabilities), exactly as observed in human MMN studies^{42,46}. Thus, our data are consistent with a passive stimulus-specific adaptation underlying oddball responses in the lemniscal midbrain and thalamus^{26,47}. By contrast, the responses we observe in high-order regions support a generative mechanism of Bayesian inference being at play in auditory cortex and high-order subcortical stations of perceptual processing³. The contrast between first-order and high-order neuronal mismatch is particularly clear within the auditory thalamus. Responses to the deviant condition are more adapted than to the cascade sequence condition, exactly as predicted by the SSA model in narrow frequency channels²⁶. However, median of the index of neuronal prediction error is significantly positive at the high-order thalamus, indicating actual prediction error. Thus, in the case of prediction error, we have shown that the higher-order midbrain and thalamus behave like the auditory cortex. It is likely that the enhancement of responses to deviant tones seen at subcortical levels is modulated, at least in part, by top-down cortical influences^{48–51}, and this is precisely what the hierarchical predictive coding framework would suggest^{12, 51}. Indeed, the lower levels of prediction error seen in the high-order midbrain in the anesthetized preparation, as compared to the awake condition, suggests that descending connections play a role deviance detection, and are therefore reduced by anesthesia.

The enhanced prediction error for low intensities of stimulation could facilitate perception under challenging sensory conditions, by increasing the gain of prediction error responses at early processing stages¹². These findings parallel previous observations of single neurons of the primary visual cortex⁵². The former study showed that cortical feedback improves figure-background discrimination of low-salience stimuli⁵². The dependence of prediction error on intensity conforms with previous studies showing a bias to deviance detection being stronger at the high-frequency edges of the frequency-response areas in collicular neurons²². Finally, asymmetries in the direction of frequency-change detection (ascending vs. descending) have also been found in both animal³⁶ and human⁵³ MMN studies, although this asymmetry was only weak for frequency modulation tones similar to our cascaded condition⁵⁴. Moreover, as discussed elsewhere³⁶ the asymmetry with respect to the direction of the deviant indicates an overall trend towards a higher sensitivity of the rodents brain to increments in frequency. The auditory system of the rodents may therefore be primed to perceive high-frequency noises like the ultrasonic vocalizations that these species use to communicate with each other³⁶.

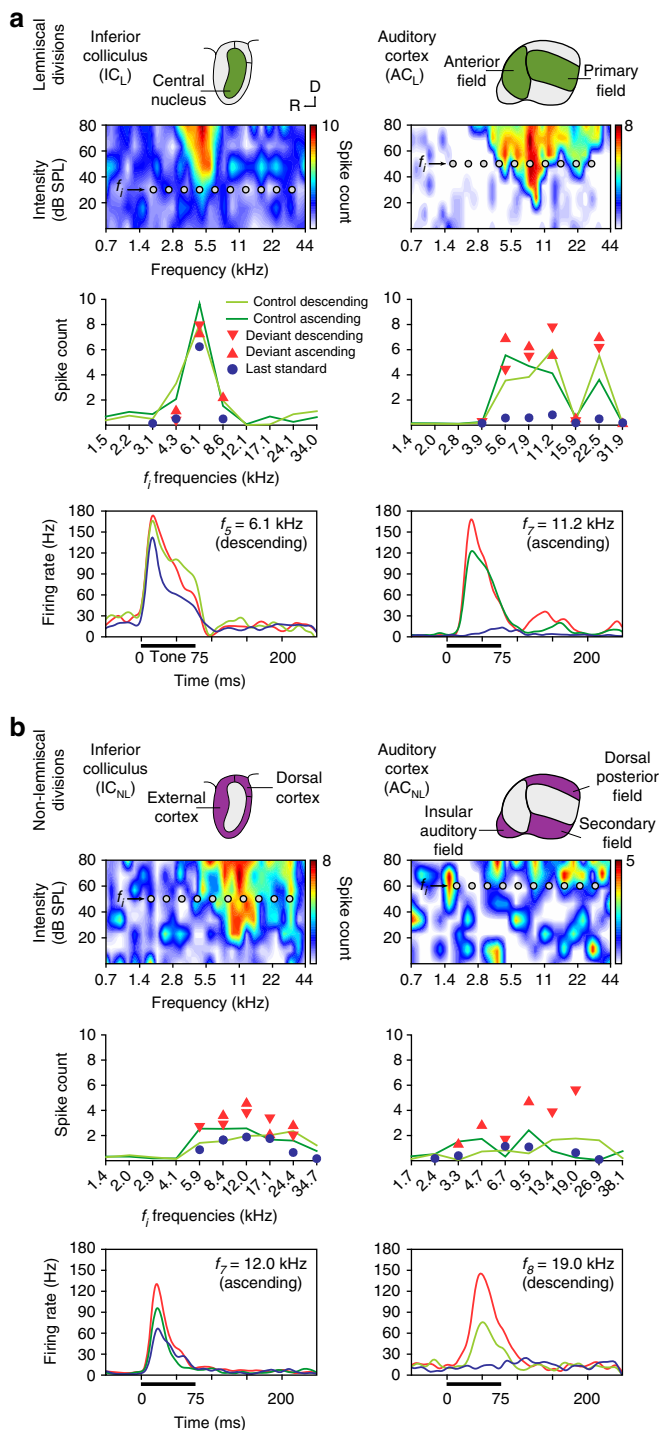


Fig. 6 Prediction error in representative examples of neuronal responses in awake mouse. **a** Examples of lemniscal multiunit activity recorded in two auditory nuclei (columns). The first row contains schematics of the lemniscal subdivisions (green) within each station. The second row shows a frequency-response area of each nuclei. Ten grey dots within those frequency-response area represent the ten tones (f_i) selected to build the experimental sequences (see Methods). The third row displays the measured responses to each f_i tone (baseline-corrected spike counts, averaged within 0–180 ms after tone onset) for all conditions tested. The fourth row contains sample peri-stimulus histograms comparing the neuronal responses to each condition tested for an indicated f_i tone. Stimulus duration is represented by a thick horizontal line. **b** Examples of multiunit activity recorded in non-lemniscal divisions (first row, colored purple) of each auditory nuclei, organized as in **a**

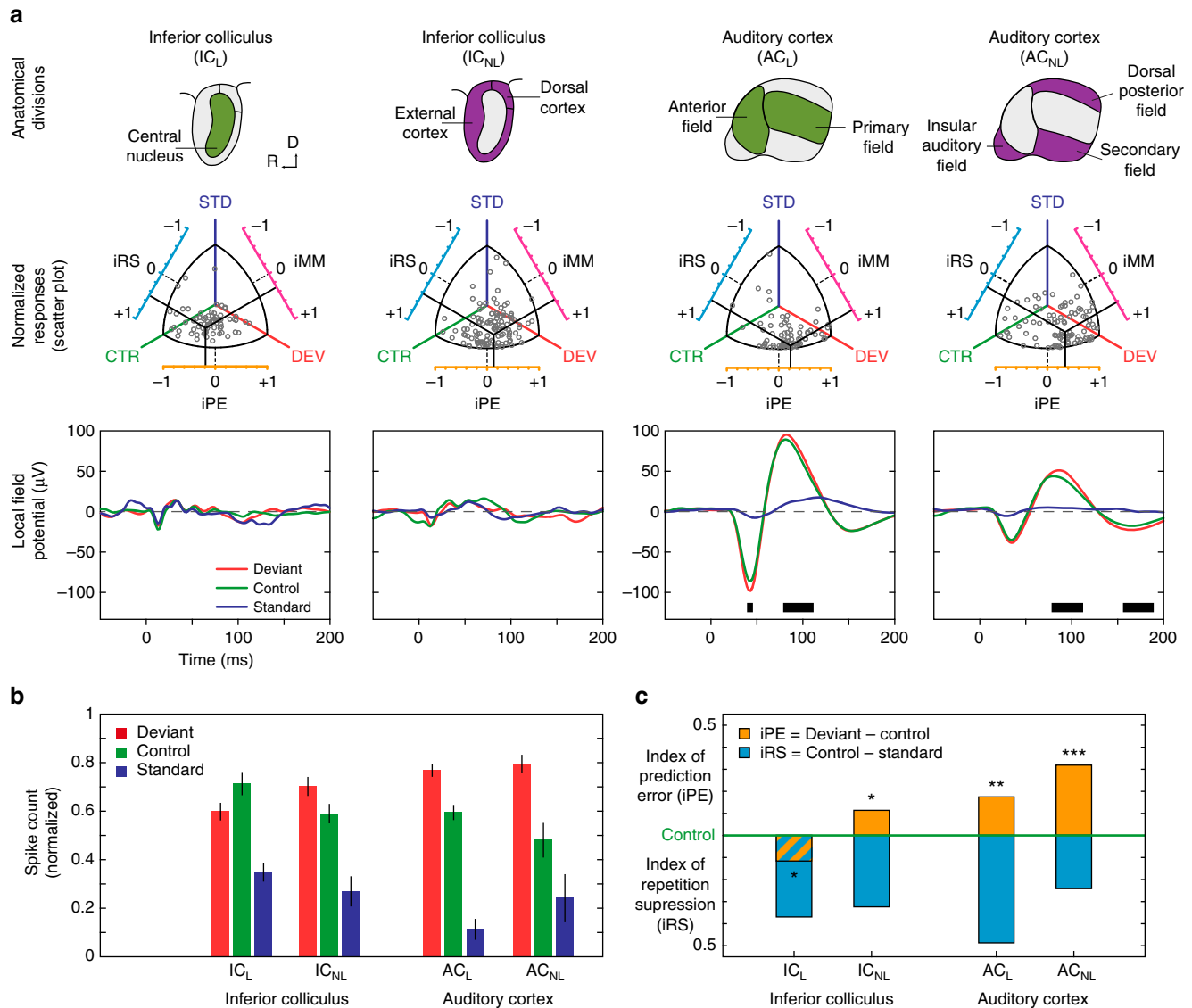


Fig. 7 Population results for awake mouse. **a** Summary of population results for each recorded station (columns). The first row displays lemniscal (green) and non-lemniscal (purple) subdivisions of two recorded auditory nuclei of the mouse brain. The second row contains scatter plots featuring normalized responses of each multiunit recording to the same tone played as DEV, STD and CTR (grey dots) and the mean population values of each index (solid black bars). The third row contains the average LFP across all tested tones from each station for different conditions. Thick black bars at the bottom of the panels mark the time intervals where the difference between the deviant LFP and the control LFP is significant, thereby producing a prediction error potential. **b** Median normalized responses (bar indicate interquartile range) to the deviant, standard and control within each station. **c** Median indices of prediction error (orange) and repetition suppression (cyan), represented with respect to the baseline set by the control. Asterisks denote statistical significance of iPE against zero median ($*p = 0.05$, $**p = 0.01$, $***p = 0.001$). Note the overall similarities with results in the anaesthetized rat (Figs. 3–5), confirming a hierarchical generation of prediction error also in awake preparations

Previous studies of deviance detection in rat auditory neurons were limited to primary auditory cortex, and yielded inconclusive results. In most of these studies, responses to deviant tones were not different from control tones, pointing to a purely-SSA explanation of oddball responses^{26, 28}, although this result was interpreted by some of these authors²⁶ as indicative of deviance detection, based on theoretical considerations. In this context, it is worth noting that in some experiments in rats, anesthesia with ketamine (an NMDA-antagonist) has shown a weakened MMN⁵⁵ and abolition of global mismatch responses⁵⁶. This pattern of effects has been called a disruption of predictive coding⁵⁷. Indeed, we observed that prediction error tended to be higher in the awake condition and this might be one important reason why deviance detection was not apparent in previous rat studies^{26, 28}.

A recent study in mouse primary auditory cortex has unambiguously demonstrated signs of deviance detection in late responses of single units, using the many-standards control sequence³⁰. The cascade sequence is arguably a better control for repetition effects than the many-standards sequence³⁵. This is so because the many-standards sequence overestimates the true state of refractoriness in the oddball whereas the cascading control is highly comparable to the deviant without violating any regularity³⁵. However, so far the cascade sequence has been used in only a single animal study that yielded inconclusive results³⁶. Several reasons may explain the ambiguous results. First, the use of the cascade control sequence may result in an underestimation of deviance detection, with the stimuli used as deviants are sitting at the outer extremes of the range of stimuli³⁶. A second reason is

Table 2 Summary of awake data set

	IC _L	IC _{NL}	AC _L	AC _{NL}
Neurons	20	27	16	23
Points	61	104	75	77
DEV (spikes)	1.3481	1.5188	3.0306	0.7589
STD (spikes)	0.8515	0.5961	0.4807	0.2141
CAS (spikes)	1.8504	1.4219	2.0772	0.4999
DEV-STD (spikes)	0.4966	0.9227	2.5499	0.5448
<i>p</i> value	0.000	0.000	0.000	0.000
CTR-STD (spikes)	0.9989	0.8258	1.5965	0.2858
<i>p</i> value	0.000	0.000	0.0015	0.0048
DEV-CTR (spikes)	-0.5023	0.09669	1.5965	0.2590
<i>p</i> value	0.024	0.018	0.000	0.000
iMM	0.2387	0.4292	0.6612	0.5773
<i>p</i> value	0.000	0.000	0.000	0.000
iRS	0.3663	0.3048	0.4910	0.2552
<i>p</i> value	0.000	0.000	0.000	0.0048
iPE	-0.1276	0.1244	0.1702	0.3222
<i>p</i> value	0.024	0.018	0.001	0.000

For IC and AC stations: Number of multi-unit activity recorded and tested neuron/tone combinations (points). Median values for baseline-corrected spike counts to the different conditions. Median differences between the former measures, and associated *p* values against zero (Friedman test with post-hoc multiple comparison, Fisher's Least Significant Difference method, uncorrected for 6 independent tests). All *p* values are rounded to 3 decimal figures, so a value of 0.000 means "*p* < 0.0005". Median indices of neuronal mismatch (iMM), repetition suppression (iRS) and prediction error (iPE), computed using the cascade control sequence, and their corresponding *p* values (note that *p* values are the same for absolute differences and normalized indices, since these indices are median differences between normalized responses, and the non-parametric test is independent of scaling). Values related to predictive neuronal activity are highlighted in bold case, since they represent the most significant result of this research

that the cascade control required the use of a higher frequency deviant for the ascending oddball condition. Finally, it could be arguable that the pattern of regularity established by the cascade sequence could be modeled by the rat brain³⁶. Our results, using single-unit recordings, were comparable or even more robust for the cascade than for the many-standard control, in agreement with human studies³⁵. Thus, although the rat brain may not be capable of fully encoding the complex regularity of the cascade control condition³⁶, this regularity may serve to boost the index of neuronal prediction error levels at subcortical structures just enough to make them detectable and statistically significant. This observation suggests that future research of subcortical deviance detection should use the cascade sequence as a control.

A fundamental theme in cognitive neuroscience is the generalization of predictive coding across sensory modalities and animal models. Importantly, predictive activity using a design similar to ours has been shown in sensory modalities other than audition, such as in rat barrel cortex⁵⁸, mouse visual cortex⁵⁹ and both primary and non-primary rat visual cortex⁶⁰. The latter study found clear signs of deviance detection in latero-intermediate area in extrastriate cortex, a higher-order visual area, but only SSA in the primary visual cortex, demonstrating also a hierarchical organization, i.e., neural responses along the rat ventral visual stream become increasingly sensitive to changes in the visual environment. Although the visual system does not have the lemniscal/non-lemniscal organization^{32, 33} of the auditory and somatosensory systems, recent reports have demonstrated distinct adaptation effects cascading through the visual system^{60, 61}. This suggests that our results generalize across the senses and types of organization. Moreover, a mouse model of visual MMN found that both MMN and schizophrenia are based on the same underlying sensory deficits⁵⁹. Despite these similarities, caution should be taken when equating sensory modalities

between species⁵⁹. Indeed, our results also contrast with previous studies that show little or no evidence of predictive coding in the auditory cortex of monkeys and humans^{28, 29, 42, 62}. Anatomical/functional and/or methodological differences likely account for some of the discrepant findings. Rodents and primates have different auditory anatomical/functional organizations. These differences are most apparent and pronounced at the cortical level³⁴ such that more complex or sophisticated functions may occur at lower levels of the system in rodents⁶³. Specifically, the complex computational machinery of the subcortical auditory system led some authors to speculate a comparable computational role of the inferior colliculus and the primary visual cortex⁶³. Technical differences may also account for the discrepancies with our current results. While we used mostly single-unit recordings, previous studies carried out in monkeys and humans^{29, 62} and even previous rodent studies^{26, 28} used local field potentials, current source density components, multiunit activity, and/or Hy-band responses. These techniques are excellent for population activity, but they measure aggregate local synaptic input rather than neuronal output and do not pick up activity patterns that are present at a finer neuronal level.

Our study suffers from some technical limitations as well. While we made electrolytic lesions in IC and MGB consistently, we did not mark recording sites in AC and therefore our results are inconclusive about the layer organization of our AC recordings. According to the canonical circuit of predictive coding, error units and prediction units are differentially located in supra-granular and infragranular layers, respectively^{9, 41, 64}. Future studies using, for example, patch-clamp recording to label the individual neurons (including their axonal arborizations) could address this issue and would help to disentangle the differences between local feedforward and feedback processing within and across layers. Another important caveat to our study is that we do not investigate the relationship between prediction and attention. Although this question was outside the scope of the study, it is worth mentioning that predictive coding is associated with different cortical rhythms^{9, 41}. Error units seem to propagate messages forward via gamma-band (high frequency) while prediction units propagate via lower beta-band (low frequency)⁶⁴. The selective Hy-band amplitude modulation to unpredictable deviants mentioned above might also reflect a switch of attention⁴². Future experiments using recordings in animals to study cortical rhythms and frontal cortex responses might provide a more detailed and refined picture for the relation between predictive coding and attention.

In conclusion, our results demonstrate that prediction error is a fundamental component of responses of single auditory neurons to an auditory oddball paradigm. This prediction-error signal is detectable even at subcortical levels, thereby adding additional evidence in support of the predictive coding framework of perceptual processing. In addition, we show that neuronal predictive activity underlies the generation of large-scale mismatch responses in animal models, paralleling fundamental properties of the human MMN such as the hierarchically organization of prediction error along the central auditory pathway. Critically, we have shown that our results hold across rodent species and arousal and hence, we have validated rodent preparations as animal models of MMN. These are promising results for translational research into the cellular mechanisms of neural disorders characterized by reductions in large-scale mismatch responses, such as the MMN.

Methods

Experimental design. Experiments in anesthetized rats were performed on 36 adult, female Long-Evans rats with body weights between 200–250 g (aged 9 to 15 weeks). The experimental protocols were approved by, and used methods

conforming to the standards of, the University of Salamanca Animal Care Committee and the European Union (Directive 2010/63/EU) for the use of animals in neuroscience research.

Sounds used for stimulation were white noise bursts or pure tones with 5 ms rise-fall ramps. Sounds used for searching for neuronal activity were trains of noise bursts or pure tones (1–8 stimulus per second). We used short stimulus duration for searching (30 ms) to prevent strong adaptation. In addition, type (white noise, narrowband noise, pure tone) and parameters (frequency, intensity, presentation rate) of the search stimuli were varied manually when necessary to facilitate release from adaptation, and thus prevent overlooking responses with high SSA. All stimuli presented were sinusoidal pure tones of 75 ms duration, including 5 ms raise/fall ramps.

For each recorded neuron, the frequency-response area that is the map of response magnitude for each frequency/intensity combination was first computed (Fig. 2, second and sixth rows). To obtain this frequency-response area, a randomized sequence of tones was presented at a 4 Hz rate, randomly varying frequency and intensity of the presented tones (3–5 repetitions of all tones). Then, we selected 10 evenly-spaced tones (0.5 octave separation) at a fixed sound intensity (usually 20–30 dB above minimal response threshold), so that at least two of them fell within the frequency-response area or close to its limits (Figs. 1b and 2). These 10 frequencies were used to create the control sequences shown in Fig. 1c. Additionally, adjacent pairs of them were used to present different oddball sequences. All sequences were 400 tones in length, at the same, constant presentation rate of 3 Hz (for AC) or 4 Hz (for IC and MGB). A faster presentation rate was used for subcortical recordings, to compensate for the relative slowing down of preferred repetition rates from brainstem to cortex³⁴.

We used oddball sequences^{5,19} (Fig. 1b) to test the specific contribution of deviance to the neuronal responses. An oddball sequence consisted of a repetitive tone (standard 90% probability), occasionally replaced by a different tone (deviant 10% probability), in a pseudorandom manner. The first 10 tones of the sequence were always the standard tone, and a minimum of 3 standard tones always preceded each deviant. Oddball sequences were either ascending or descending, depending on whether the deviant was a higher or lower frequency than the standard, respectively (Fig. 1b). To control for the overall presentation rate of the target tone, we used two different control sequences, namely, the many-standards and cascaded sequences^{26,35} (Fig. 1b). The many-standards control sequence was a random presentation of the 10 selected tones, such that each of them were played the same number of times in an unpredictable order but a single tone was never repeated. Two cascaded control sequences, ascending and descending, contained the same 10 tones but were arranged according to ascending/descending frequency, respectively (Fig. 1b). Since all sequences were 400 stimuli long, a tone was played with the same overall presentation rate (4 Hz) in the deviant, many-standard control sequence and cascade control sequence conditions, a total of 40 times along the 400-stimuli sequence. The tone immediately preceding a deviant is the same in the oddball (a standard) and cascaded sequences. The cascaded sequence was recently designed as an improvement to the many-standards, by controlling for the state of refractoriness and the regularity of the deviant tone in the oddball paradigm^{35,36}. This improves the estimation of the overall adaptation state of the system by the time the deviant tone is played, and controls for the potential sensitivity of the neuron to a rise or fall in frequency between two successive tones. Second, the cascaded sequence mimics the regular structure of the oddball sequence, with the important difference that now the target tone conforms to the rule, instead of being a deviant. Thus, using this design, every tone presented as a deviant was also presented as a standard (in a different oddball sequence) and in the context of both the many-standards and cascaded control sequences. These four conditions, and by extension response measures to them, will be denoted as deviant (DEV), standard (STD), many standard control and cascade control (CTR). Note that there were two variants of the DEV condition (ascending/descending), which were compared with the corresponding ascending/descending cascade condition. The STD condition was averaged, for each frequency, across ascending/descending versions of the oddball sequence (as indicated in Fig. 1b). The order of presentation of these sequences was randomized across neurons, with a silent pause of ~30 s between sequences. If the neuron could be held for long enough, the same protocol was repeated at different sound intensities.

Surgical procedures in anaesthetized rats. Surgical anesthesia was induced and maintained with urethane (1.5 g/kg, i.p.), with supplementary doses (0.5 g/kg, i.p.) given as needed. Dexamethasone (0.25 mg/kg) and atropine sulfate (0.1 mg/kg) were administered at the beginning of the surgery and every 10 h thereafter to reduce brain edema and the viscosity of bronchial secretions, respectively. The initial surgical procedures were identical in each case, and the electrophysiological procedures differed only in the location of the craniotomy, and placement/orientation of the recording electrode, for each different station. After the animal reached a surgical stage of anesthesia, the trachea was cannulated for artificial ventilation and a cistern drain was introduced to prevent brain hernia. The animal was then placed in a stereotaxic frame in which the ear bars were replaced by hollow specula that accommodated a sound delivery system. Corneal and hind-paw withdrawal reflexes were monitored to ensure that a deep anesthetic level was maintained as uniformly as possible throughout the recording procedure. Isotonic glucosaline solution was administered periodically (5–10 ml every 6–8 h, s.c.)

throughout the experiment to prevent dehydration. Body temperature was monitored with a rectal probe and maintained between 37–38°C with a homeothermic blanket system (Cibertec).

For IC and MGB recordings, a craniotomy was performed in the left parietal bone to expose the cerebral cortex overlying the left IC/MGB. The dura was removed, and the electrode was advanced with an angle of 20° for the IC, and in a vertical direction for the MGB. For AC recordings, the skin and temporal muscles over the left side of the skull were reflected and a 6 × 5 mm craniotomy was made in the left temporal bone to expose the entire auditory cortex (see Fig. 1 in ref. 27). The dura was removed and the exposed cortex and surrounding area were covered with a transparent layer of agar to prevent desiccation and to stabilize the recordings. The electrode was positioned orthogonal to the pia surface, forming a 30° angle with the horizontal plane, to penetrate through all the cortical layers of one same cortical column.

Surgical procedures in awake mice. Experiments in awake mice were performed in 10 CBA/J mice aged between 8 and 12 weeks. Animal handling and surgical procedures for this preparation followed the procedures detailed in previous experiments^{65,66}. Briefly, animals were handled and trained to stay in a customized foam bed, adapted to the animal body, and placed into the stereotaxic frame for 5–7 consecutive days. For the initial surgery, anesthesia was induced using a mixture of ketamine (50 mg/kg) and xylazine (10 mg/kg, i.m.). Animals were fixed to the stereotaxic frame, skull was exposed, and coordinates for IC or AC (between 2 and 4 mm posterior to bregma, and about 2 mm ventral to linea temporalis), according to refs. 67,68 were taken. A head-post was implanted as in ref. 66, and a craniotomy was performed, sparing the dura. Analgesic buprenorphine (Buprex™, RB Pharmaceuticals Limited) was injected every 12 h after surgery. The exposed area was protected with a removable silicone elastomer (Kwik-Cast™ & Kwik-Sil™, WPI). At least 3 days after recovery, animals were acclimated to the recording environment with their head and body restrained^{65,66,68}. Only well-acclimated animals were used to collect data, and mild sedative acepromazine (2 mg/kg, i.p., Equipromacina, Fatro Iberica) was injected in case the mouse showed signs of apprehension during the recordings. Recording sessions were no longer than 3 h, during 2–3 consecutive days.

Electrophysiological recording procedures. Each individual animal was used to record from only one auditory station, either IC, MGB or AC. Once a single neuron was isolated and confirmed to be stable, the whole stimulation protocol was applied, as described in the first section “Experimental Design”.

Experiments in anaesthetized rats were performed inside a sound-insulated and electrically-shielded chamber. All sounds were generated using an RX6 Multifunction Processor (Tucker-Davis Technologies) and delivered monaurally (to the right ear) in a closed system through a Beyer DT-770 earphone (0.1–45 kHz) fitted with a custom-made cone and coupled to a small tube (12 gauge hypodermic) sealed in the ear.

The sound system response was flattened with a finite impulse response filter, and the output of the system was calibrated in situ using a ¼-inch condenser microphone (model 4136, Brüel & Kjær), a conditioning amplifier (Nexus, Brüel & Kjær) and a dynamic signal analyzer (Photon +, Brüel & Kjær). The output of the system had a flat spectrum at 76 dB SPL (± 3 dB) between 500 Hz and 45 kHz, and the second and third harmonic components in the signal were ≤ 40 dB below the level of the fundamental at the highest output level (90 dB SPL). Prior to surgery and recording sessions, we recorded auditory brainstem responses with subcutaneous electrodes to ensure the animal had normal hearing. Auditory brainstem responses were collected using a Tucker-Davis Technologies software (BioSig) and hardware (RX6 Multifunction Processor) following standard procedures (0.1 ms clicks presented at a 21/s rate, delivered in 10 dB ascending steps from 10 to 90 dB SPL).

The experimental procedure for the awake mice was similar to that used for the rats; the main difference was that auditory stimulation in the awake condition was free field (at ~1 cm), presented monaurally to the contralateral ear (the left ear) using an electrostatic loudspeaker (TDT-EC1: Tucker-Davis Technologies) driven by a RZ6 processor. The free field recording was necessary because the mice's heads were immobilized by fixing the head post to a custom-made clamp during recordings. The output of the system at the left ear was calibrated as described above and its maximum output was flat from 1 to 44 kHz ($\sim 89 \pm 4.3$ dB SPL). The highest frequency produced by this system was limited to 44 kHz and the second and third harmonic components in the signal were at least 40 dB lower than the level of the fundamental at the highest output level⁶⁵.

Action potentials and local field potentials were recorded with hand-manufactured, glass-coated tungsten electrodes (1–4 M Ω impedance at 1 kHz). One individual electrode was used to record one single neuron at a time. The electrode was advanced using a piezoelectric micromanipulator (Sensapex) until we observed a strong spiking activity synchronized with the train of searching stimuli. The signal was amplified (1000 \times) and band-pass filtered (1 Hz to 3 kHz) with an alternate current differential amplifier (DAM-80, WPI). This analog signal was digitized at a 12 K sampling rate and further band-pass filtered (with a second TDT-RX6 module) separately for action potentials (between 500 Hz and 3 kHz) and LFP (between 3 and 50 Hz). Stimulus generation and neuronal response processing and visualization were controlled online with custom software created

with the OpenEx suite (Tucker-Davis Technologies) and Matlab (Mathworks). A unilateral threshold for automatic action potential detection was manually set at about 2–3 standard deviations of the background noise. Spike waveforms were displayed on the screen, and overlapped on each other in a pile-plot to facilitate isolation of single units. Only when all spike waveforms were identical and clearly separable from other smaller units and the background noise, the recorded action potentials were considered to belong to a single unit.

To confirm that our recordings corresponded to well-isolated single units, we used 2552731 individual spike waveforms from 5871 record files from all stations to measure spike isolation quality. Inter-spike interval distribution for all recorded spike waveforms (Supplementary Fig. 3a) shows that only 0.85% spikes occurred less than 4 ms after the previous spike. To show that waveform variability was low in our recordings (as indicated by the sample spike waveform in Fig. 2), and that spike amplitude was well above background noise level, we computed a spike-amplitude-to-noise-ratio (SNR), for all sets of spike waveforms S recorded:

$$\text{SNR} = \frac{\max(\bar{x}(S)) - \min(\bar{x}(S))}{\text{Std}(S)}$$

Spike-amplitude-to-noise-ratio distribution in our sample (Supplementary Fig. 3b) shows that 96% of our recorded spikes had at least 5 times more amplitude than the background noise, and that 61% of them were well above 10 times that. Finally, to ensure that all spike waveforms of every record belonged to a single neuron, Mahalanobis distance was computed for each of them. Mahalanobis distance is a normalized measure separation between a point and a cluster of point in a multidimensional space. If more than two neurons were recorder together, the spike waveforms would follow a multimodal Gaussian distribution, and the median Mahalanobis distance would be larger than for a single Gaussian distribution. Our spike waveforms were streams of 32 samples (5 ms at 12 K sampling rate); thus, in our case, Mahalanobis distance is a normalized measure of separation between a spike waveform and a cluster of spike waveforms in a 32-D space. If our spikes were purely normally distributed following a single 32-dimensional Gaussian distribution, the distribution of mahal (w, S) values for all spike waveforms w would look like the red dotted line in Supplementary Fig. 3c. However, the real distribution (blue histogram) is a left-skewed version of the former, indicating that our spike waveforms were even closer to each other in shape than in a standardized single-spike cluster (Supplementary Fig. 3d, e).

Histological procedures and localization of recording sites. For AC experiments, a magnified picture (25 \times) of the exposed cortex was taken at the end of the surgery with a digital single-lens reflex camera (D5100, Nikon) coupled to the surgical microscope (Zeiss) through a lens adapter (TTI Medical)²⁷. The picture included a pair of reference points—previously marked prior surgery on the dorsal ridge of the temporal bone - indicating the absolute scale and position of the image with respect to bregma. This picture was displayed on a computer screen and a micrometric grid was overlapped to guide and mark the placement of the electrode for every recording made (Supplementary Figs. 4a and 5a). Recording sites (250–500 μm spacing) were evenly distributed across the cortical region of interest and avoided blood vessels. The vascular pattern was used as a local reference to mark the position of every recording site in the picture, but otherwise differed between animals.

At the end of the experiment, the limits and relative position of the auditory fields were determined for each animal. This was done using the characteristic frequency, the tone frequency that elicits a significant neuronal response at the lowest intensity gradient, as the main reference landmark. Five auditory cortical fields were identified according to tone frequency-response topographies both in rats^{27, 69} and mice^{67, 68}. In rats, we consistently observed distinct tonotopic gradients within the different fields with a high-frequency reversal between ventral and anterior auditory field (rostrally), a low-frequency reversal between primary and posterior auditory field (dorsocaudally) and a high-frequency reversal between ventral and suprarhinal auditory field (ventrally) (Supplementary Fig. 4a). We identified the boundary between primary and ventral auditory field as a 90° shift in the characteristic frequency gradient in the ventral low-frequency border of primary auditory cortex, and the boundary between primary and anterior auditory field as an absence of tone-evoked responses in the ventral, high-frequency border of primary auditory cortex²⁷. We used these boundaries to assign each recording to a given field. The characteristic frequency of each recording track was computed as the average characteristic frequency of all neurons recorded in that track, including a fast multi-unit activity frequency-response area recording made between 400–550 μm depth, corresponding to layers IIb-IV of the AC.

Similar tonotopic gradients were observed in mice (Supplementary Fig. 5a) in accordance with previous studies^{67, 68}. Inversions of the characteristic frequency progression define the limits between cortical fields^{67, 68} so that most recordings could be assigned to a particular field: primary, secondary, dorsal posterior, or insular auditory field. Tonotopic maps were less distinct in mice because the mice data sample was smaller than in rats. Furthermore, since mice AC is smaller, mappings are less detailed than those in rat.

For IC and MGB experiments, each recording track was marked with electrolytic lesions for subsequent histological localization of the recorded neurons. At the end of the experiment, the animal was given a lethal dose of sodium

pentobarbital and perfused transcardially with phosphate buffered saline (0.5% NaNO₃ in Phosphate Buffered Saline) followed by fixative (a mixture of 1% paraformaldehyde and 1% glutaraldehyde in rat Ringer's solution). After fixation and dissection, the brain tissue was cryoprotected in 30% sucrose and sectioned on a freezing microtome in the transverse or sagittal planes into 40 μm -thick sections. Sections were Nissl stained with 0.1% cresyl violet to facilitate identification of cytoarchitectural boundaries (Supplementary Figs. 4b–e and b, c). Recording sites were marked on standard sections from a rat/mouse brain atlas^{70, 71} and neurons were assigned to one of the main divisions of the IC (central nucleus, dorsal, lateral or rostral cortex) or the MGB (ventral, dorsal and medial division), respectively. The stained sections with the lesions were used to localize each track mediolaterally, dorsoventrally and rostrocaudally in the Paxinos atlas. To determine the main IC or MGB subdivisions, cytoarchitectonic criteria, i.e., cell shape and size, Nissl staining patterns and cell packing density were used. This information was complemented and confirmed by the stereotaxic coordinates used during the experiment to localize the IC/MGB. After assigning a section to each track/lesion, the electrophysiological coordinates from each experiment and recording unit, i.e., beginning and end of the IC/MGB, as well as the depth of the neuron, were used as complementary references to localize each neuron within a track.

Statistical analysis. All the data analyses were performed with the MatlabTM software, using the built-in functions, the Statistics and Machine Learning toolbox, or custom scripts and functions developed in our laboratory. A peri-stimulus histogram was a histogram of action potential density over time (in action potentials per second, or Hz) from –75 to 250 ms around stimulus onset, using the 40 trials available for each tone and condition. Every peri-stimulus histogram was smoothed with a 6 ms gaussian kernel (“ksdensity” function in Matlab) in 1 ms steps to estimate the spike-density function over time, and the baseline spontaneous firing rate was determined as the average firing rate (in Hz) during the 75 ms preceding stimulus onset. Peri-stimulus histograms were generated for each stimulus/condition tested. Only the last STD tones preceding each DEV tone were used for the analyses. The excitatory response was measured as the area below the spike-density function and above the baseline spontaneous firing rate, between 0 and 180 ms after stimulus onset (positive area patches only, to avoid negative response values). This measure will be referred to as “baseline-corrected spike count”.

We only analyzed excitatory responses, since we look primarily for enhancement of responses to deviant tones. Neuron/frequency combinations with no significant excitatory response to at least one of the conditions (DEV, STD, CTR) were excluded from the analyses ($p > 0.05$ for all three conditions). To test for statistical significance of the baseline-corrected spike count, we used a Monte Carlo approach, a probability simulation that obtain numerical results from several random sampling. First, 1000 simulated peri-stimulus histograms were generated using a Poisson model with a constant firing rate equal to the spontaneous firing rate. Then, a null distribution of baseline-corrected spike count was generated from this collection of peri-stimulus histograms, following these same steps. Finally, the p value of the original baseline-corrected spike count was empirically computed as $p = (g + 1)/(N + 1)$, where g is the count of null measures greater than or equal to baseline-corrected spike count and $N = 1000$ is the size of the null sample.

We used two types of sequences to control for repetition effects namely the many-standards and cascaded sequences (Fig. 1b). However, it is possible to decompose the neuronal mismatch into repetition suppression and prediction error using either of these sequences alone (Fig. 1c). Here we describe the analysis performed using the cascade condition as control (CTR), since the analysis using the many-standards sequence was completely analogous. Baseline-corrected spike count responses of a neuron to the same tone in the three conditions (DEV, STD, CTR) were normalized using the formulas:

$$\text{DEV}_{\text{Normalized}} = \text{DEV}/N;$$

$$\text{STD}_{\text{Normalized}} = \text{STD}/N;$$

$$\text{CTR}_{\text{Normalized}} = \text{CTR}/N;$$

where

$$N = \sqrt{\text{DEV}^2 + \text{STD}^2 + \text{CTR}^2}$$

is the Euclidean norm of the vector (DEV, STD, CTR) defined by the three responses. This normalization procedure always results in a value ranging 0–1, and has a straightforward geometrical interpretation (Fig. 3a): Normalized values were the coordinates of a 3D unit vector ($\text{DEV}_{\text{Normalized}}, \text{STD}_{\text{Normalized}}, \text{CTR}_{\text{Normalized}}$) with the same direction of the original vector (DEV, STD, CTR), and thus the same proportions between the three response measures. From these normalized responses, indices of neuronal mismatch (iMM), repetition suppression (iRS), and

prediction error (iPE) were computed as:

$$iMM = DEV_{Normalized} - STD_{Normalized},$$

$$iRS = CTR_{Normalized} - STD_{Normalized},$$

$$iPE = DEV_{Normalized} - CTR_{Normalized},$$

These indices, consequently, always range between -1 and 1 , and provide the following quantitative decomposition of neuronal mismatch (Fig. 1d) into repetition suppression and prediction error:

$$iMM = iRS + iPE$$

As shown in Supplementary Fig. 2, the iMM was largely equivalent to the typical "SSA index", commonly used in most previous studies of SSA in single units^{29, 37}:

$$SSA\ index = (DEV - STD)/(DEV + STD)$$

For the analysis of the LFP signal, we aligned the recorded wave to the onset of the stimulus for every trial, and computed the mean LFP for every recording site and stimulus condition (DEV, STD, CTR), as well as the "prediction error potential" (PE-LFP = LFP_{DEV} - LFP_{CTR}). Then, grand-averages were computed for all conditions, for each auditory station separately. The p value of the grand-averaged PE-LFP was determined for every time point with a two-tailed t test (Bonferroni-corrected for 200 comparisons, with family-wise error rate FWER < 0.05), and we computed the time intervals, where PE-LFP was significantly different from zero (Fig. 5).

Our data set was not normally distributed so we used distribution-free (non-parametric) tests. These included the Wilcoxon signed-rank test and Friedman test (for baseline-corrected spike counts, normalized responses, indices of neuronal mismatch, repetition suppression and prediction error). Only the difference wave for the LFPs (PE-LFP in Fig. 5) was tested using a t test, since each LFP trace is itself an average of 40 waves, and thus approximately normal (according to the Central Limit Theorem). For multiple comparison tests, p values were corrected for false discovery rate (FDR = 0.1) using the Benjamini-Hochberg method. Linear models used to test significant average iPE within each auditory station (Fig. 4b, d) and significant effects of nucleus, hierarchy, SPL, direction, and interactions between them, were fitted using the 'fitlm' function in Matlab, with robust options. To estimate final sample sizes required for the observed effects after the initial exploratory experiments, we used the 'sampsizepwr' function in Matlab. The central measure of this study was the iPE, and thus we adjusted sample sizes, for each station, to obtain a statistical power of 0.8 for this index, given the observed effect:

$$\text{MinSampleSize} = \text{sampsizepwr}(t, [0\ \text{std}(iPE)], \max(.05, \text{abs}(\text{mean}(iPE))), .8);$$

where iPE is the distribution of iPE values in the sample, including all frequencies tested for all neurons ("points" in Table 1). Sample sizes were enlarged with additional experiments until they were just greater than the minimum required (number of points recorded and the minimum required for each station: IC_L = 149/104; IC_{NL} = 523/401; MGB_L = 79/69; MGB_{NL} = 211/153; AC_L = 250/125 and AC_{NL} = 307/29). In some cases, such as AC_{NL}, final sample sizes were much larger than required (307 points recorded for 29 required), due to four very productive experiments.

Code availability. The scripts and functions written in Matlab to generate the results and analysis during the current study are available from the corresponding author on reasonable request.

Data availability. The data sets generated and analyzed during the current study are available from the corresponding author on reasonable request.

Received: 26 January 2017 Accepted: 2 November 2017

Published online: 15 December 2017

References

- Whitmore, C. J. & Stanley, G. B. Rapid sensory adaptation redux: A circuit perspective. *Neuron* **92**, 298–315 (2016).
- Escera, C. & Malmierca, M. S. The auditory novelty system: An attempt to integrate human and animal research. *Psychophysiology* **51**, 111–123 (2014).
- Stefanics, G., Kremláček, J. & Czigler, I. Visual mismatch negativity: a predictive coding view. *Front. Hum. Neurosci.* **8**, 666 (2014).
- Winkler, I., Denham, S. L. & Nelken, I. Modeling the auditory scene: predictive regularity representations and perceptual objects. *Trends Cogn. Sci.* **13**, 532–540 (2009).
- Dehaene, S., Meyniel, F., Wacongne, C., Wang, L. & Pallier, C. The neural representation of sequences: From transition probabilities to algebraic patterns and linguistic trees. *Neuron* **88**, 2–19 (2015).
- Näätänen, R., Paavilainen, P., Rinne, T. & Alho, K. The mismatch negativity (MMN) in basic research of central auditory processing: A review. *Clin. Neurophysiol.* **118**, 2544–2590 (2007).
- Phillips, H. N. et al. Convergent evidence for hierarchical prediction networks from human electrocorticography and magnetoencephalography. *Cortex* **82**, 192–205 (2016).
- Bendixen, A., SanMiguel, I. & Schröger, E. Early electrophysiological indicators for predictive processing in audition: A review. *Int. J. Psychophysiol.* **83**, 120–131 (2012).
- Bastos, A. M. et al. Canonical microcircuits for predictive coding. *Neuron* **76**, 695–711 (2012).
- Friston, K. The free-energy principle: a rough guide to the brain? *Trends Cogn. Sci.* **13**, 293–301 (2009).
- Baldeweg, T. Repetition effects to sounds: Evidence for predictive coding in the auditory system [1]. *Trends Cogn. Sci.* **10**, 93–94 (2006).
- Auksztulewicz, R. & Friston, K. Repetition suppression and its contextual determinants in predictive coding. *Cortex* **80**, 125–140 (2016).
- Garrido, M. I., Kilner, J. M., Stephan, K. E. & Friston, K. J. The mismatch negativity: A review of underlying mechanisms. *Clin. Neurophysiol.* **120**, 453–463 (2009).
- Wacongne, C., Changeux, J.-P. & Dehaene, S. A neuronal model of predictive coding accounting for the mismatch negativity. *J. Neurosci.* **32**, 3665–3678 (2012).
- Harms, L., Michie, P. T. & Näätänen, R. Criteria for determining whether mismatch responses exist in animal models: Focus on rodents. *Biol. Psychol.* **116**, 28–35 (2016).
- Shiramatsu, T. I., Kanzaki, R., Takahashi, H., Sams, M. & Näätänen, R. Cortical mapping of mismatch negativity with deviance detection property in rat. *PLoS ONE* **8**, e82663 (2013).
- May, P. J. C. & Tiitinen, H. Mismatch negativity (MMN), the deviance-elicited auditory deflection, explained. *Psychophysiology* **47**, 66–122 (2010).
- Fishman, Y. I. The mechanisms and meaning of the mismatch negativity. *Brain Topogr.* **27**, 500–526 (2014).
- Ulanovsky, N., Las, L. & Nelken, I. Processing of low-probability sounds by cortical neurons. *Nat. Neurosci.* **6**, 391–398 (2003).
- Malmierca, M. S., Sánchez-Vives, M. V., Escera, C. & Bendixen, A. Neuronal adaptation, novelty detection and regularity encoding in audition. *Front. Syst. Neurosci.* **8**, 111 (2014).
- Malmierca, M. S., Cristaudo, S., Pérez-González, D. & Covey, E. Stimulus-specific adaptation in the inferior colliculus of the anesthetized rat. *J. Neurosci.* **29**, 5483–5493 (2009).
- Duque, D., Perez-Gonzalez, D., Ayala, Y. A., Palmer, A. R. & Malmierca, M. S. Topographic distribution, frequency, and intensity dependence of Stimulus-Specific adaptation in the inferior colliculus of the rat. *J. Neurosci.* **32**, 17762–17774 (2012).
- Ayala, Y. A. & Malmierca, M. S. Stimulus-specific adaptation and deviance detection in the inferior colliculus. *Front. Neural Circuits* **6**, 1–16 (2013).
- Ayala, Y. A., Pérez-González, D., Duque, D., Nelken, I. & Malmierca, M. S. Frequency discrimination and stimulus deviance in the inferior colliculus and cochlear nucleus. *Front. Neural Circuits* **6**, 119 (2013).
- Antunes, F. M. & Malmierca, M. S. An overview of Stimulus-Specific adaptation in the auditory thalamus. *Brain Topogr.* **27**, 480–499 (2014).
- Taaseh, N., Yaron, A. & Nelken, I. Stimulus-Specific adaptation and deviance detection in the rat auditory cortex. *PLoS ONE* **6**, e23369 (2011).
- Nieto-Diego, J. & Malmierca, M. S. Topographic distribution of Stimulus-Specific adaptation across auditory cortical fields in the anesthetized rat. *PLoS Biol.* **14**, 1–30 (2016).
- Farley, B. J., Quirk, M. C., Doherty, J. J. & Christian, E. P. Stimulus-Specific adaptation in auditory cortex is an NMDA-Independent process distinct from the sensory novelty encoded by the mismatch negativity. *J. Neurosci.* **30**, 16475–16484 (2010).
- Fishman, Y. I. & Steinschneider, M. Searching for the mismatch negativity in primary auditory cortex of the awake monkey: Deviance detection or stimulus specific adaptation? *J. Neurosci.* **32**, 15747–15758 (2012).
- Chen, I.-W., Helmchen, F. & Lutcke, H. Specific early and late Oddball-Evoked responses in excitatory and inhibitory neurons of mouse auditory cortex. *J. Neurosci.* **35**, 12560–12573 (2015).
- Graybiel, A. M. The thalamo-cortical projection of the so-called posterior nuclear group: A study with anterograde degeneration methods in the cat. *Brain Res.* **49**, 229–244 (1973).

32. Jones, E. G. Chemically defined parallel pathways in the monkey auditory system. *Ann. N. Y. Acad. Sci.* **999**, 218–233 (2003).
33. Lee, C. C. & Sherman, S. M. On the classification of pathways in the auditory midbrain, thalamus, and cortex. *Hear. Res.* **276**, 79–87 (2011).
34. Malmierca, M. S. in *The Rat Nervous System* (ed. Paxinos, G.), 3rd ed., Elsevier Academic Press, San Diego, pp 996–1081 (2004).
35. Ruhnau, P., Herrmann, B. & Schröger, E. Finding the right control: The mismatch negativity under investigation. *Clin. Neurophysiol.* **123**, 507–512 (2012).
36. Harms, L. et al. Mismatch negativity (MMN) in freely-moving rats with several experimental controls. *PLoS ONE* **9**, e110892 (2014).
37. Opitz, B., Schröger, E. & Von Cramon, D. Y. Sensory and cognitive mechanisms for preattentive change detection in auditory cortex. *Eur. J. Neurosci.* **21**, 531–535 (2005).
38. Recasens, M., Grimm, S., Wollbrink, A., Pantev, C. & Escera, C. Encoding of nested levels of acoustic regularity in hierarchically organized areas of the human auditory cortex. *Hum. Brain Mapp.* **35**, 5701–5716 (2014).
39. Abbott, L. F., Varela, J. A., Sen, K. & Nelson, S. B. Synaptic depression and cortical gain control. *Science* **275**, 221–224 (1997).
40. Imada, A., Morris, A. & Wiest, M. C. Deviance detection by a P3-like response in rat posterior parietal cortex. *Front. Integr. Neurosci.* **6**, 127 (2013).
41. Heilbron, M. & Chait, M. Great expectations: Is there evidence for predictive coding in auditory cortex? *Neuroscience* <https://doi.org/10.1016/j.neuroscience.2017.07.061> (2017).
42. Dürschmid, S. et al. Hierarchy of prediction errors for auditory events in human temporal and frontal cortex. *Proc. Natl. Acad. Sci.* **113**, 6755–6760 (2016).
43. Güntürkün, O. & Bugnyar, T. Cognition without Cortex. *Trends Cogn. Sci.* **20**, 291–303 (2016).
44. Parvizi, J. Corticocentric myopia: old bias in new cognitive sciences. *Trends Cogn. Sci.* **13**, 354–359 (2009).
45. Ayala, Y. A. et al. Differences in the strength of cortical and brainstem inputs to SSA and non-SSA neurons in the inferior colliculus. *Sci. Rep.* **5**, 10383 (2015).
46. Mittag, M., Takegata, R. & Winkler, I. Transitional probabilities are prioritized over Stimulus/Pattern Probabilities in auditory deviance detection: memory basis for predictive sound processing. *J. Neurosci.* **36**, 9572–9579 (2016).
47. Duque, D., Wang, X., Nieto-Diego, J., Krumbholz, K. & Malmierca, M. S. Neurons in the inferior colliculus of the rat show stimulus-specific adaptation for frequency, but not for intensity. *Sci. Rep.* **6**, 24114 (2016).
48. Ayala, Y. A., Pérez-González, D. & Malmierca, M. S. Stimulus-specific adaptation in the inferior colliculus: The role of excitatory, inhibitory and modulatory inputs. *Biol. Psychol.* **116**, 10–22 (2016).
49. Duque, D., Malmierca, M. S. & Caspary, D. M. Modulation of stimulus-specific adaptation by GABA(A) receptor activation or blockade in the medial geniculate body of the anaesthetized rat. *J. Physiol.* **592**, 729–743 (2014).
50. Ayala, Y. A. & Malmierca, M. S. Cholinergic Modulation of Stimulus-Specific Adaptation in the Inferior Colliculus. *J. Neurosci.* **35**, 12261–12272 (2015).
51. Malmierca, M. S., Anderson, L. A. & Antunes, F. M. The cortical modulation of stimulus-specific adaptation in the auditory midbrain and thalamus: a potential neuronal correlate for predictive coding. *Front. Syst. Neurosci.* **9**, 1–14 (2015).
52. Hupe, J. M. et al. Cortical feedback improves discrimination between figure and background by V1, V2 and V3 neurons. *Nature* **423**, 979–982 (2003).
53. Peter, V., McArthur, G. & Thompson, W. F. Effect of deviance direction and calculation method on duration and frequency mismatch negativity (MMN). *Neurosci. Lett.* **482**, 71–75 (2010).
54. Klein, C., Von Der Behrens, W. & Gaese, B. H. Stimulus-specific adaptation in field potentials and neuronal responses to frequency-modulated tones in the primary auditory cortex. *Brain Topogr.* **27**, 599–610 (2014).
55. Umbricht, D., Koller, R., Vollenweider, F. X. & Schmid, L. Mismatch negativity predicts psychotic experiences induced by NMDA receptor antagonist in healthy volunteers. *Biol. Psychiatry* **51**, 400–406 (2002).
56. Uhrig, L., Janssen, D., Dehaene, S. & Jarraya, B. Cerebral responses to local and global auditory novelty under general anesthesia. *Neuroimage* **141**, 326–340 (2016).
57. Strauss, M. et al. Disruption of hierarchical predictive coding during sleep. *Proc. Natl. Acad. Sci.* **112**, E1353–E1362 (2015).
58. Musall, S., Haiss, F., Weber, B. & von der Behrens, W. Deviant processing in the primary somatosensory cortex. *Cereb. Cortex* **27**, 863–879 (2015).
59. Hamm, J. P. & Yuste, R. Somatostatin interneurons control a key component of mismatch negativity in mouse visual cortex. *Cell Rep.* **16**, 597–604 (2016).
60. Vinken, K., Vogels, R. & Op de Beeck, H. Recent visual experience shapes visual processing in rats through stimulus-specific adaptation and response enhancement. *Curr. Biol.* **27**, 914–919 (2017).
61. Dhruv, N. T. & Carandini, M. Cascaded effects of spatial adaptation in the early visual system. *Neuron* **81**, 529–535 (2014).
62. Eliades, S. J. et al. Adaptation of high-gamma responses in human auditory association cortex. *J. Neurophysiol.* **112**, 2147–2163 (2014).
63. King, A. J. & Nelken, I. Unraveling the principles of auditory cortical processing: can we learn from the visual system? *Nat. Neurosci.* **12**, 698–701 (2009).
64. Bastos, A. M. et al. A DCM study of spectral asymmetries in feedforward and feedback connections between visual areas V1 and V4 in the monkey. *Neuroimage* **108**, 460–475 (2015).
65. Duque, D. & Malmierca, M. S. Stimulus-specific adaptation in the inferior colliculus of the mouse: anesthesia and spontaneous activity effects. *Brain Struct. Funct.* **220**, 3385–3398 (2015).
66. Ayala, Y. A., Pérez-González, D., Duque, D., Palmer, A. R. & Malmierca, M. S. Extracellular recording of neuronal activity combined with microiontophoretic application of neuroactive substances in awake mice. *J. Vis. Exp.* (111), e53914 (2016).
67. Guo, W. et al. Robustness of cortical topography across fields, laminae, anesthetic states, and neurophysiological signal types. *J. Neurosci.* **32**, 9159–9172 (2012).
68. Joachimsthaler, B., Uhlmann, M., Miller, F., Ehret, G. & Kurt, S. Quantitative analysis of neuronal response properties in primary and higher-order auditory cortical fields of awake house mice (*Mus musculus*). *Eur. J. Neurosci.* **39**, 904–918 (2014).
69. Polley, D. B., Read, H. L., Storace, D. A. & Merzenich, M. M. Multiparametric auditory receptive field organization across five cortical fields in the albino rat. *J. Neurophysiol.* **97**, 3621–3638 (2007).
70. Paxinos, G. & Watson, C. *The Rat Brain in Stereotaxic Coordinates*. (Elsevier Science, 2013).
71. Franklin, K. B. J. & Paxinos, G. *The Mouse Brain In Stereotaxic Coordinates*. (Boston, 2008).

Acknowledgements

We thank Drs. Ryszard Aukstulewicz, Edward L. Bartlett, Nell Cant, Javier Cudeiro, Bernhard Englitz, Yonatan Fishman, Patrick May, Alan Palmer, José Luis Peña, Daniel Polley, Adrian Rees, Iria SanMiguel, Christoph Schreiner, and Juanita Todd for their comments and many fruitful discussions on previous versions of the manuscript and for their constructive criticisms. Financial support was kindly provided by the Spanish MINECO (SAF2016-75803-P) to MSM and an Explora-Ciencia grant (PSI2013-49348-EXPLORA) to MSM and CE. CE was also supported by the Generalitat de Catalunya (SGR2014-177) and by the Icrea Acadèmia Distinguished Professor Award. JND held a fellowship from the European Social Fund/Spanish JCYL (Operational Programme ESF Castilla y León 2007–2013). GGP held a fellowship from the Spanish MINECO (BES-2014-069113) and CVB held a fellowship from Mexican CONACyT (216652).

Author contributions

The experiments were performed at the Auditory Neuroscience Laboratory, Institute of Neuroscience of Castilla y León- INCYL, University of Salamanca, Salamanca, Spain. The contribution of each author to the following aspects of the study is as stated: (1) conception and design of experiments: J.N.D. and M.S.M.; (2) collection of data: J.N.D., G.G.P., G.V.C. and C.V.B.; (3) analysis, interpretation of data and conceptual advice: J.N.D., G.V.C., G.G.P., C.E. and M.S.M.; (5) writing of the manuscript: J.N.D. and M.S.M. (6) project supervision: M.S.M. All authors approved the final version of the manuscript.

Additional information

Supplementary Information accompanies this paper at <https://doi.org/10.1038/s41467-017-02038-6>.

Competing interests: The authors declare no competing financial interests.

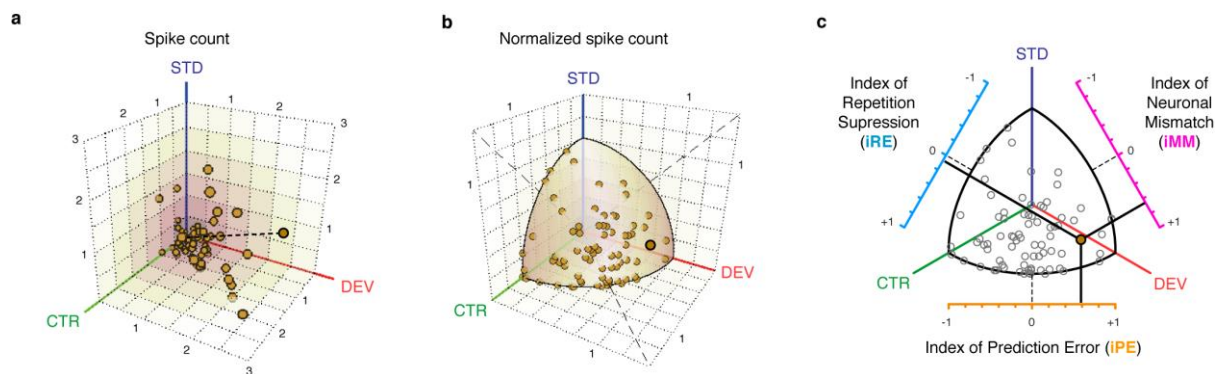
Reprints and permission information is available online at <http://npg.nature.com/reprintsandpermissions/>

Publisher's note: Springer Nature remains neutral with regard to jurisdictional claims in published maps and institutional affiliations.

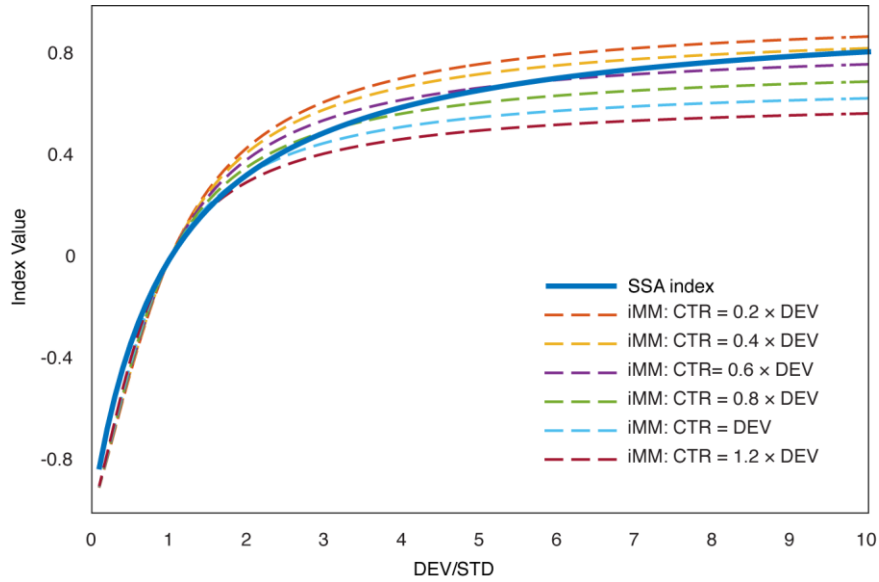


Open Access This article is licensed under a Creative Commons Attribution 4.0 International License, which permits use, sharing, adaptation, distribution and reproduction in any medium or format, as long as you give appropriate credit to the original author(s) and the source, provide a link to the Creative Commons license, and indicate if changes were made. The images or other third party material in this article are included in the article's Creative Commons license, unless indicated otherwise in a credit line to the material. If material is not included in the article's Creative Commons license and your intended use is not permitted by statutory regulation or exceeds the permitted use, you will need to obtain permission directly from the copyright holder. To view a copy of this license, visit <http://creativecommons.org/licenses/by/4.0/>.

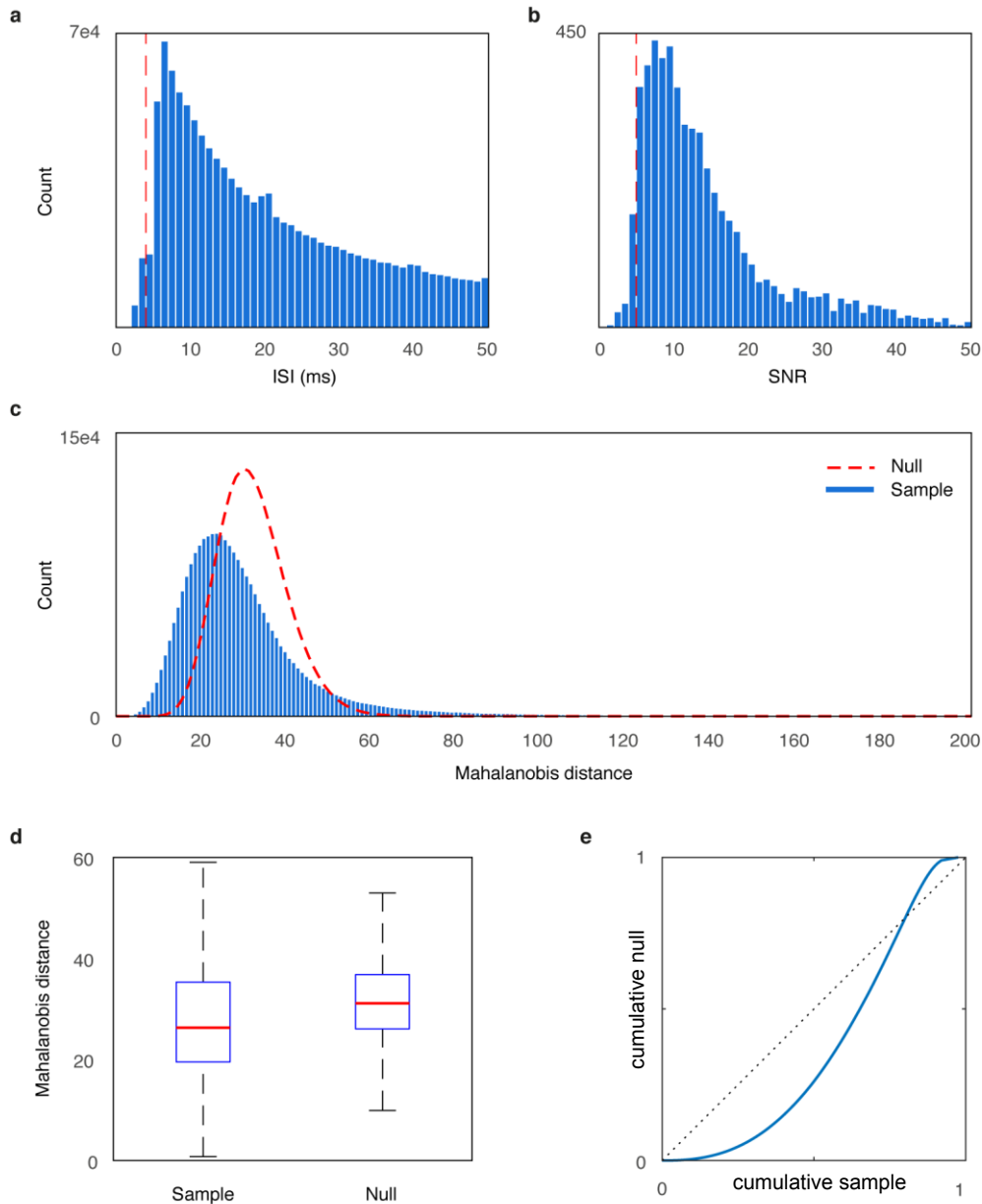
© The Author(s) 2017



Supplementary Figure 1: Example of a population normalization procedure and representation. **a.** The response of each neuron to each tested tone recorded in deviant (DEV), standard (STD) and control (CTR) conditions defines a point in 3D space. **b.** Normalization of these three associated responses to a value between 0 and 1. Each point represented in (a) appears now radially projected onto a unit sphere centered on origin. **c.** Indexes result from the difference between two of these normalized responses, represented as color axes surrounding the scatter plots. The dotted black lines marks the absence of difference between conditions (index=0). Index values for each individual neuronal response (grey dots) can be consulted in the color axes as exemplified with the highlighted response (brown dot, solid black bar projecting from it to each index axis). The scatter plot is represented flattened from a zenith view of the unit sphere in order to simplify and facilitate overall legibility.

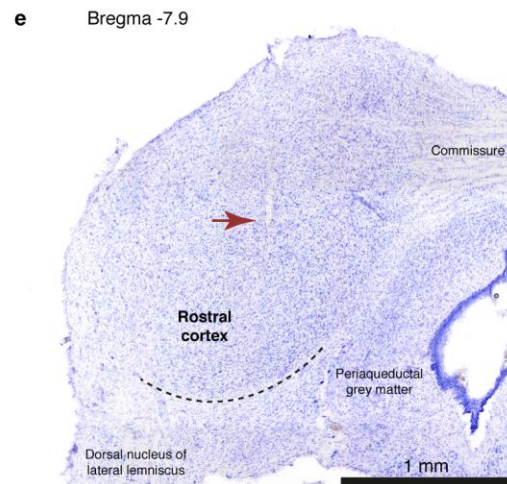
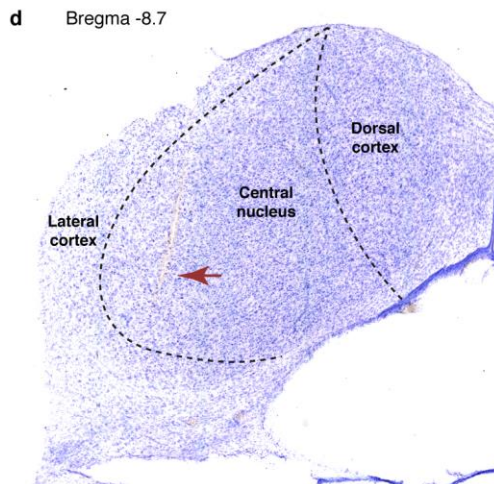
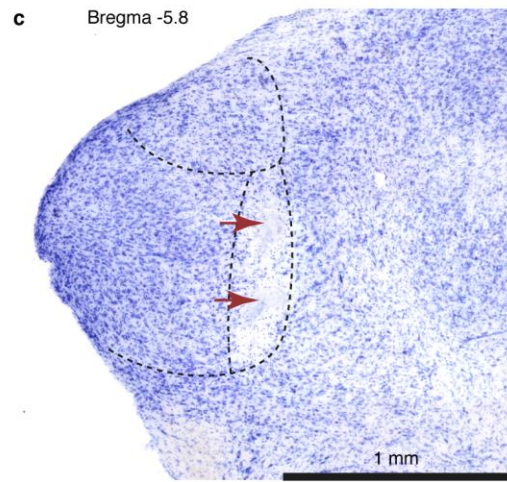
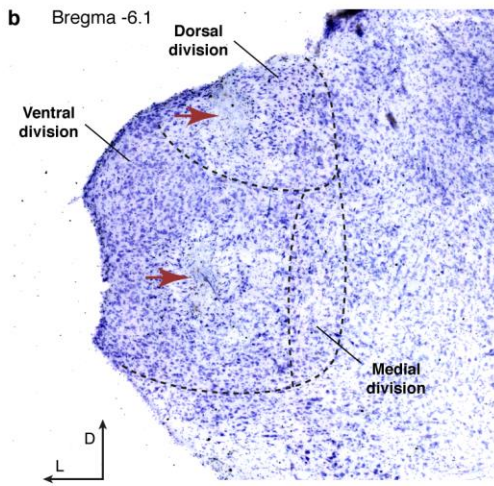
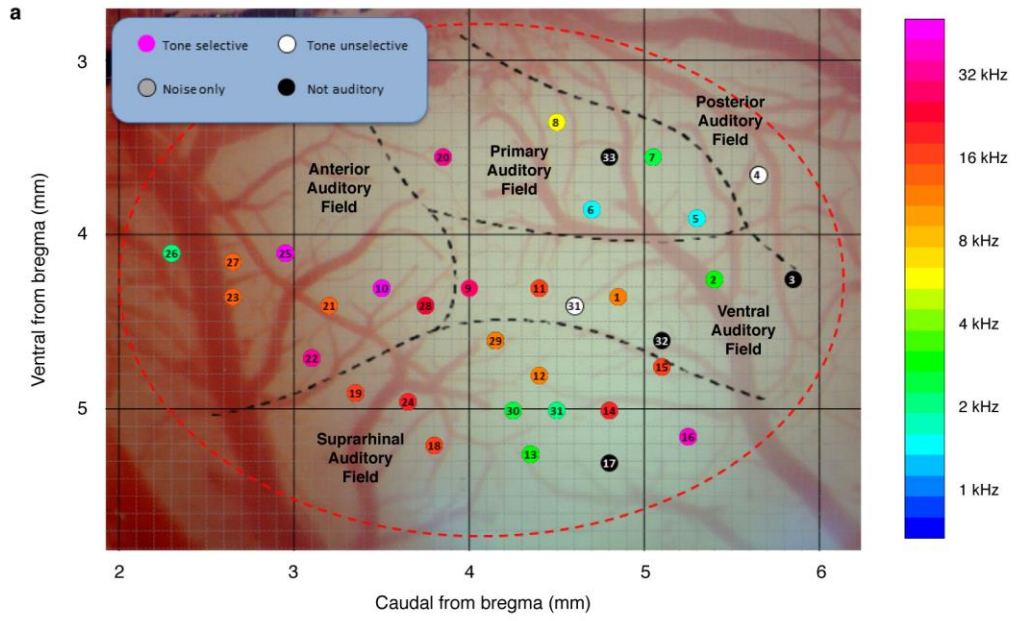


Supplementary Figure 2: Quantitative comparison between iMM and the “classical” SSA index. Quantitative comparison between iMM and the “classical” SSA index. The SSA index trace is plotted as a function of the DEV/STD ratio, since SSA does not take into account the control condition. Different iMM traces are plotted (dashed lines), as a function of the relative magnitude of the response to control condition with respect to deviant response (CTR/DEV), from low ($CTR=0.2*DEV$) to high ($CTR=1.2*DEV$) hypothetical responses to the control. Note that the two indices (the SSA index and the iMM for different CTR response magnitudes) tend to take values very close to each other.

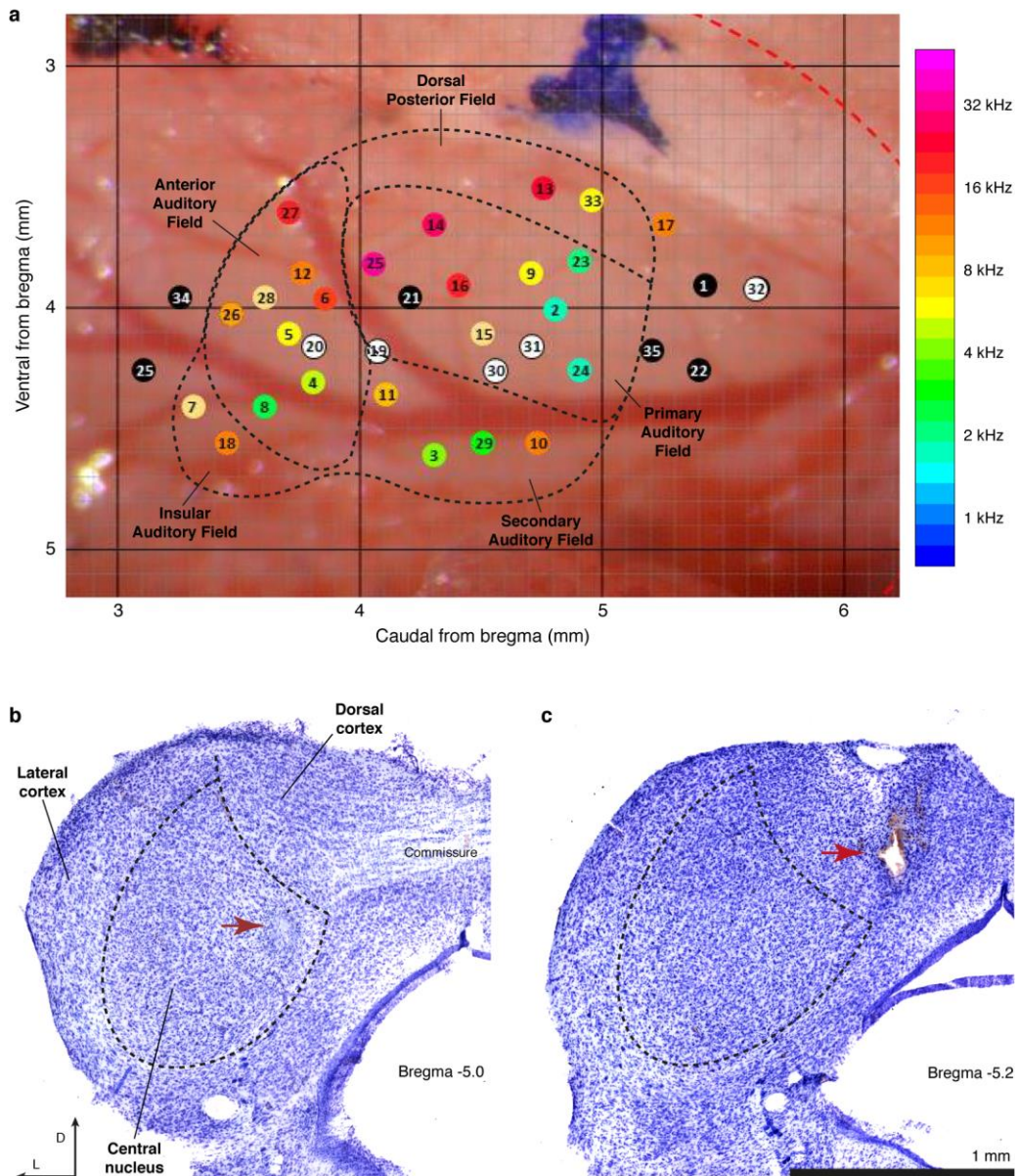


Supplementary Figure 3: Measures of spike isolation quality. **a.** Inter-spike interval (ISI) distribution for all our anesthetized recordings (2552731 individual spike waveforms from 5871 record files from all stations). For each individual spike, the time interval (in ms) to the previous spike is computed, and all these (2 million+) values are represented in the histogram. The long, thin tail beyond 50 ms is not shown for clarity, to show that less than 2% single spikes waveform occurred less than 4 ms (a reasonable refractory period) after the previous spike. **b.** Distribution of spike-amplitude-to-noise-ratio (SNR), for all sets of spikes waveform S recorded. More than 96% of our recorded spikes had at least 5 times more amplitude than the 2-3 std deviations set as threshold. **c.** Distribution of Mahalanobis distance for each single spikes waveform w recorded (blue histogram). If our spikes were purely normally distributed following a single 32-dimensional Gaussian distribution, the distribution of mahal (w, S) values for all spikes waveform w would look like the red dotted line. The real distribution is a left-skewed version of the former, indicating that our spikes waveform were even closer to each other in shape than in a standard single-spike cluster. **d.** This is confirmed by the boxplot comparative, showing that median and inter-quartile range were closer to zero

than the reference (null) distribution. **e.** As Mahalanobis distance d increases from 0 to $+\text{Inf}$, a point of the blue trace is defined as $[\text{cdf_sample}(d), \text{cdf_null}(d)]$, where cdf is the cumulative density function of each distribution. Thus, the blue line compares all quantiles of these distributions, and shows that all quantiles of the sample distribution up to $Q_{0.8}$ correspond to lower quantiles of the reference distribution.



Supplementary Figure 4: Anatomy for anesthetized rat preparations. a. Localization of all recordings made in the AC of one rat, in coordinates with respect to bregma. The characteristic frequency) of each track was determined (from all recordings made in that track, see Methods). Inversions of the characteristic frequency progression define the limits between cortical fields^{1,2}, so that all or most recordings can eventually be assigned to a particular field: primary, anterior, ventral, posterior or suprarhinal auditory field. **b.** Sample Nissl-stained histological slice showing electrolytic lesions along one electrode track (red arrows). Applying depth interpolation, all recordings made in that track could be assigned to either ventral or dorsal divisions of the MGB³. **c.** Same as in (b), showing lesions along a track that traverses the medial division of the MGB³. **d.** In this case, the whole electrode track through the central nucleus of the inferior colliculus can be clearly seen up to the point where the lesion was made (red arrow; lateral cortex of the IC^{4,5}). **e.** Sample of a lesion marking a neuron recorded in the rostral cortex of the IC^{4,5}). Scale bars: 1 mm in each case.



Supplementary Figure 5: Anatomy for awake mice. **a.** Localization of all recordings made in the AC of one mouse, in coordinates with respect to bregma. The characteristic frequency of each track was determined (from all recordings made in that track, see Methods). Inversions of the characteristic frequency progression define the limits between cortical fields^{6,7}, so that all or most recordings can eventually be assigned to a particular field: primary, secondary, anterior, dorsal posterior or insular auditory field. **b, c.** Sample Nissl-stained histological slice showing an electrolytic lesion (red arrow) in central nucleus in one case (b) or dorsal cortex in a different mouse (c). Scale bar: 1 mm.


Supplementary Table 1: List of abbreviations

Abbreviation	Definition
AC	Auditory Cortex
AC _L	Lemniscal areas of the Auditory Cortex
AC _{NL}	Non-lemniscal areas of the Auditory Cortex
CTR	Control
DEV	Deviant
FDR	False Discovery Rate
IC	Inferior Colliculus
ICL	Lemniscal region of the Inferior Colliculus
ICNL	Non-lemniscal regions of the Inferior Colliculus
iMM	Index of Neuronal Mismatch.
iPE	Index of Prediction Error
iRS	Index of Repetition Suppression
L	Lemniscal pathway
LFP	Local Field Potential
MGB	Medial Geniculate Body
MGB _L	Lemniscal regions of the Medial Geniculate Body
MGB _{NL}	Non-Lemniscal regions of the Medial Geniculate Body
MMN	Mismatch Negativity
NL	Non-Lemniscal pathway
PE-LFP	Prediction error potential
SPL	Sound Pressure Level
SSA	Stimulus-Specific Adaptation
STD	Standard

Supplementary References:


1. Nieto-Diego, J. & Malmierca, M. S. Topographic Distribution of Stimulus-Specific Adaptation across Auditory Cortical Fields in the Anesthetized Rat. *PLoS Biol.* 14, 1–30 (2016).
2. Paxinos, G. & Watson, C. *The Rat Brain in Stereotaxic Coordinates*. (Elsevier Science, 2013).
3. Antunes, F. M., Nelken, I., Covey, E. & Malmierca, M. S. Stimulus-specific adaptation in the auditory thalamus of the anesthetized rat. *PLoS One* 5, e14071 (2010).
4. Malmierca, M. S., Blackstad, T. W. & Osen, K. K. Computer-assisted 3-D reconstructions of Golgi-impregnated neurons in the cortical regions of the inferior colliculus of rat. *Hear. Res.* 274, 13–26 (2011).
5. Loftus, W. C., Malmierca, M. S., Bishop, D. C. & Oliver, D. L. The cytoarchitecture of the inferior colliculus revisited: A common organization of the lateral cortex in rat and cat. *Neuroscience* 154, 196–205 (2008)
6. Joachimsthaler, B., Uhlmann, M., Miller, F., Ehret, G. & Kurt, S. Quantitative analysis of neuronal response properties in primary and higher-order auditory cortical fields of awake house mice (*Mus musculus*). *Eur. J. Neurosci.* 39, 904–918 (2014).
7. Polley, D. B., Read, H. L., Storace, D. A. & Merzenich, M. M. Multiparametric Auditory Receptive Field Organization Across Five Cortical Fields in the Albino Rat. *J. Neurophysiol.* 97, 3621–3638 (2007).

SCIENTIFIC REPORTS



OPEN

Endocannabinoid Modulation of Stimulus-Specific Adaptation in Inferior Colliculus Neurons of the Rat

C. Valdés-Baizabal^{1,2}, G. G. Parras^{1,2}, Y. A. Ayala^{1,4} & M. S. Malmierca^{1,2,3} 

Cannabinoid receptors (CBRs) are widely distributed in the brain, including the inferior colliculus (IC). Here, we aim to study whether endocannabinoids influence a specific type of neuronal adaptation, namely, stimulus-specific adaptation (SSA) found in some IC neurons. SSA is important because it has been found as early as the level of the midbrain and therefore it may be a neuronal correlate of early indices of deviance detection. Furthermore, recent studies have demonstrated a direct link between SSA and MMN, that is widely used as an outcome measure in a variety of human neurodegenerative disorders. SSA is considered a form of short-term plasticity, and CBRs have been shown to play a role in short-term neural plasticity. Therefore, it is reasonable to hypothesize that endocannabinoids may play a role in the generation or modulation of SSA. We recorded single units in the IC under an oddball paradigm stimulation. The results demonstrate that cannabinoid agonists lead to a reduction in the neuronal adaptation. This change is due to a differential increase of the neuronal firing rate to the standard tone alone. Furthermore, we show that the effect is mediated by the cannabinoid receptor 1 (CBR1). Thus, cannabinoid agonists down-modulate SSA in IC neurons.

Anatomical and physiological studies have demonstrated that endocannabinoids (ECBs) modulate neural processing in sensory systems^{1–4}, including the auditory system. Indeed, many nuclei in the auditory brainstem and midbrain, such as cochlear nuclei (CN), superior olivary complex (SOC) and inferior colliculus (IC), express cannabinoid receptors (CBRs). Moreover, previous *in vitro* studies have shown that ECBs modulate electrophysiological properties in CN^{5,6} and SOC neurons⁷. For example, in CN cartwheel neurons, ECBs selectively suppress glutamatergic synapses⁶, while endocannabinoid signaling attenuates both glycinergic and glutamatergic postsynaptic currents in SOC neurons⁷. IC neurons express CBRs^{8,9} and therefore, ECBs probably modulate their responses, but, to date, effects of ECBs in the mammalian IC have not been electrophysiologically studied.

The canonical view of the mechanism of action of the CB system (ECBs, and receptor types 1 and 2, CBR1 and CBR2) is that the ligand is released by a postsynaptic neuron and acts as a retrograde messenger on receptors located on presynaptic terminals. Both receptor types are coupled to G-proteins⁵. CBR1s are expressed predominantly in the mammalian central nervous system while CBR2s are located mainly in the peripheral nervous system and immune tissues. ECBs are produced on demand in an activity-dependent manner. When a neuron is stimulated synaptically, ECB synthesis is initiated via a Ca²⁺-dependent activation of ECB-synthesizing enzymes, and the ECBs are then released into the synaptic cleft. The released ECBs act as retrograde messengers at central synapses¹⁰, resulting in the activation of presynaptic CBRs^{4,11}, which attenuates Ca²⁺ influx into the presynaptic terminal, blocking vesicle fusion, and thus decreasing transmitter release¹². This retrograde mechanism is called depolarization-induced suppression of inhibition^{13,14} or depolarization-induced suppression of excitation¹⁵, depending on whether the ECBs act on an inhibitory or excitatory input¹⁶.

Here, we aim to examine whether ECBs influence a specific type of neuronal adaptation found in the IC and beyond along the auditory pathway, namely, stimulus-specific adaptation (SSA). SSA in IC^{17–25} and primary

¹Auditory Neuroscience Laboratory, Institute of Neuroscience of Castilla y León, Calle Pintor Fernando Gallego 1, 37007, Salamanca, Spain. ²The Salamanca Institute for Biomedical Research (IBSAL), 37007, Salamanca, Spain.

³Department of Biology and Pathology, Faculty of Medicine, Campus Miguel de Unamuno, University of Salamanca, 37007, Salamanca, Spain. ⁴Present address: Instituto de Neurobiología, Universidad Nacional Autónoma de México, Querétaro, Mexico. Correspondence and requests for materials should be addressed to M.S.M. (email: msm@usal.es)

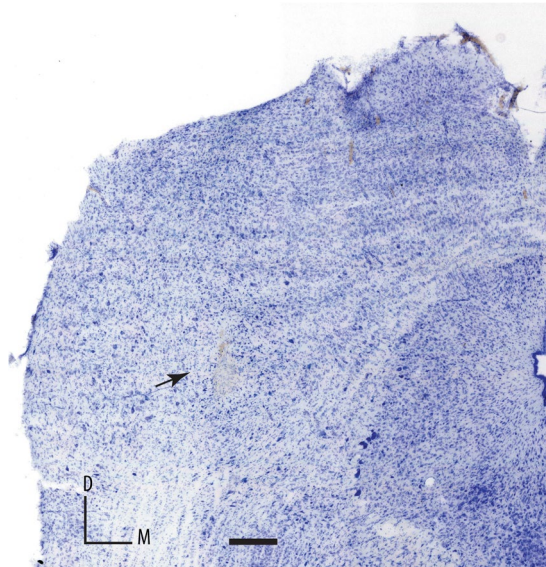


Figure 1. Photomicrograph of a coronal section through the rostral cortex of the IC showing a typical electrolytic lesion of a recording site for a neuron with a high CSI value. Scale bar, 1 mm. M, medial; D, dorsal.

auditory cortex (A1)^{26–33} occurs mainly in early responses (20–40 ms), so it may be a neuronal correlate of early indices of deviance detection^{30, 31, 34–36}. However, SSA in non-primary AC occurs within, and beyond, the MMN time window³³. Hence a direct link between SSA and MMN has already been established.

SSA is elicited under oddball paradigm stimulation and consists of a rapid and pronounced decrement of neural responsiveness to trains of identical stimuli (standard stimuli), even at low repetition rates on the order of seconds^{24, 26}. SSA neurons recover their responsiveness whenever certain stimulus parameters are changed (deviant stimuli)¹⁷. SSA also occurs in other sensory systems^{37–39}. Over the last decade, a series of studies from our lab has reported the principal electrophysiological properties and the details of organization of SSA in auditory midbrain neurons^{17–25, 30–32}. SSA in the IC is mainly a property of non-lemniscal IC neurons (the IC cortical regions) and SSA is not homogeneously distributed throughout the neuron's frequency response area, such that higher levels of SSA are found at low intensity levels and at the high frequency edges of the neurons' receptive fields. SSA is modulated by acetylcholine²⁵ and GABA-A mediated inhibition³⁹. Moreover, SSA in the IC is not a property inherited from the AC^{32, 40} as originally suggested²⁶.

Because SSA is considered a form of short-term plasticity⁴¹ and ECBs have been shown to play a role in short-term plasticity^{4, 7}, it is plausible that ECBs play a role in the generation or modulation of SSA. Moreover, since cannabinoid receptors are expressed in the IC, we hypothesize that cannabinoid drugs modulate SSA responses of the IC neurons. To document a functional role of endocannabinoid system on IC neuronal activity and, more specifically, to discover how ECBs affect SSA, we performed two sets of complementary experiments; namely, intravenous and intracerebral microiontophoretic applications of cannabinoid drugs while testing for SSA. The results demonstrate that the endocannabinoid system down-modulates SSA responses in rat IC neurons.

Results

To determine the influence of ECBs on SSA, we recorded the response of 154 well-isolated IC neurons under the oddball paradigm before, during and after the application of the CB1R agonists anandamide ($n = 50$, *i.v.*), and O-2545 ($n = 40$, microiontophoretically), and the CB1R antagonist AM251 ($n = 49$, *i.v.*) as well as a drug cocktail made of the CB1R agonist anandamide and CB1R antagonist AM251 ($n = 15$, *i.v.*). (Anandamide and AM251 were administered *i.v.* because they are not water soluble and so could not be administered iontophoretically.) Because previous studies have shown that SSA is maximum in the cortical regions of the IC^{17–19}, we specifically attempted to record neurons from these regions. The subsequent histological verification of the recording sites, marked by lesions showed that 67% were in the rostral cortex (e.g., Fig. 1) and 33% were in the lateral cortex of the IC. Overall, there were no differences between the effects obtained in these two cortices, and so the data were pooled into a single sample. We also analyzed the effect of the drugs on some properties other than SSA, such as spontaneous activity and spectral sensitivity (FRA).

The effect of anandamide on firing rate and SSA level. Figure 2A shows a typical example of a single-unit response before, during and after drug application. The injection of anandamide elicited a significant increase in the response to standard stimuli that resulted in a significant decrease of the CSI, from 0.58 to 0.28. For most neurons, as it is the case shown in Fig. 2A, the firing rate was only partially recovered. However, we considered an almost or partial recovery when the firing rate values were not significantly different to those in the control condition.

An analysis of the CSI of the whole sample ($n = 50$) showed that there is a marked tendency toward a decrease of the CSI after drug application (Fig. 2B). To determine the significance of the effects, we performed

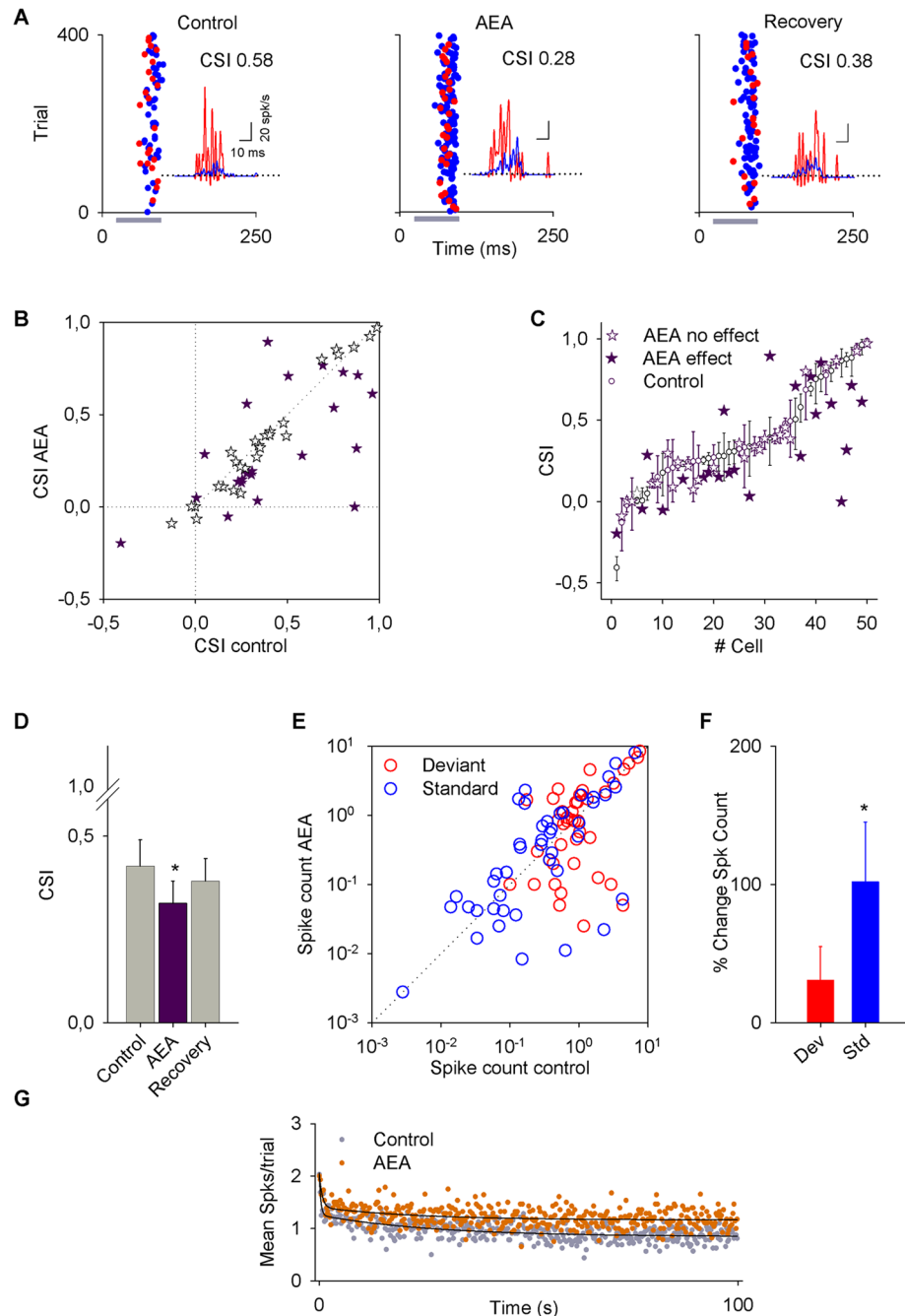


Figure 2. Effect of anandamide (AEA) on the activity of inferior colliculus (IC) neurons. **(A)** Typical recording of an IC neuron under an oddball stimulation paradigm before (control), during (AEA) and after (recovery) an i.v. application of AEA. (For this neuron, the standard frequency was 2105 Hz and the deviant frequency was 1724 Hz.) Application of AEA decreased the CSI from 0.58 to 0.28. For this and subsequent figures, the gray horizontal bars indicate the duration of sound stimulation and asterisks indicate a P-value less than 0.05. The insets are PSTHs that represent the mean response to the oddball sequence, in all conditions showing a significantly larger neuronal response to the deviant tone (red) than to the standard (blue). **(B)** Scatter plot of the CSI in control condition versus drug application. It can be seen that the CSI of most neurons decreases. **(C)** Bootstrapping analysis for each neuron. White dots indicate the control CSI and stars indicate the AEA application (purple stars: significant change; white stars: no change). **(D)** Bars represent the average value \pm SE of the change for the population that had significant changes in the CSI. **(E)** Scatter plot of the spike count in the control condition versus AEA application for standard (blue dots) and deviant (red dots) stimuli. **(F)** Percent change in the responses to deviant and standard stimuli (vertical bars represent the % change \pm SE). The AEA significantly increases the response to the standard stimulus. **(G)** Time course of adaptation for the mean response to the standard frequency for each position (time) in the oddball sequence of neurons significantly affected by anandamide. The baseline (gray circles) and anandamide data (orange circles) had fast and slow decay components and a steady-state component that were fitted by a double exponential function (black lines).

Drug	n	CSI		
		# neurons with significant change	Total change	Segregated changes
Anandamide (agonist)	50	23	↓ 0.42 to 0.32 (P = 0.048) (parametric test)	16/23 ↓ 0.51 to 0.27 (P < 0.001) (non-parametric test)
				7/23 ↑ 0.22 to 0.44 (P = 0.008) (parametric test)
O-2545 (agonist)	40	13	↓ 0.53 to 0.29 (P = 0.012) (parametric test)	11/13 ↓ 0.61 to 0.31 (P = 0.003) (parametric test)
				2/13 ↑ 0.21 to 0.4 (no statistical analysis)
AM251 (antagonist)	49	7	↑ 0.17 to 0.43 (P = 0.017) (parametric test)	N/A*

Table 1. Summary of effects of cannabinoid drugs on the CSI. *N/A Does not apply.

a bootstrapping analysis evaluating the effect of anandamide on each individual neuron (Fig. 2C). This analysis showed that anandamide affected 23/50 neurons, and the population *t*-test showed that overall anandamide decreased the CSI from 0.42 ± 0.07 to 0.32 ± 0.06 ($P = 0.048$; Fig. 2D). In this group of neurons, the CSI decreased in 16/23 and increased in 7/23 (details provided in Table 1).

Next, we analyzed how the firing rate of the neurons showing a change in their CSI ($n = 23$) was affected. The firing rates for both standard and deviant stimuli are plotted in Fig. 2E. The spike count increased significantly in response to standard stimuli (by $102 \pm 43\%$, $P = 0.013$), while the spike count in response to deviant stimuli was unchanged. The bar plots in Fig. 2F show the percent change in the responses to deviant and standard stimuli after anandamide application.

In order to study the dynamics of adaptation to the repetitive stimuli, we averaged responses to standard stimuli across recordings for every trial within the sequence. The response to the standard frequency was fit by a double exponential function under the baseline ($R^2 = 0.65$) and anandamide ($R^2 = 0.43$) conditions, displaying a rapid and a slow decay as well as a steady state component (Fig. 2G). Anandamide increased the steady-state component of the response from 0.84 spikes per trial to 1.16 (95% CIs) without affecting either the timing or the magnitude of the fast (baseline, $\tau_r = 0.37$ trial, $A_r = 0.77$ spikes per trial; anandamide $\tau_r = 0.67$ trial, $A_r = 0.65$) or slow (baseline, $\tau_s = 27.23$ trial, $A_s = 0.41$ spikes per trial; anandamide $\tau_s = 23.68$ trial, $A_s = 0.24$) components of the adaptation (Fig. 2G).

The effect of O-2545 on firing rate and CSI. Since anandamide was administered intravenously instead of microiontophoretically due to its poor water solubility, the changes observed might reflect not only direct effects on IC neural activity but also actions on other brain regions projecting directly or indirectly to the IC neurons. To address this issue we conducted a second experimental series using the microiontophoretic injection of 25 mM O-2545 while recording single unit responses from a total of 40 IC neurons. A typical example of a single-unit recording is illustrated in Fig. 3A under the control condition, after drug application and during recovery. In this particular neuron, the O-2545 drug significantly decreased the CSI from 0.44 to 0.11 followed by a recovery to basal levels after the injection was terminated.

We first analyzed the average change in CSI for the entire population ($n = 40$). This analysis revealed that overall the CSI showed a marked decrease (Fig. 3B). As with anandamide, we performed a bootstrapping analysis to determine the effect on each individual neuron (Fig. 3C). This analysis showed that the CSI significantly decreases from 0.53 ± 0.1 to 0.29 ± 0.1 ($n = 13$; $P = 0.012$) and thus, the reduction is about 50% (Fig. 3D). Table 1 contains the details of the effect of O-2545.

Figure 3E shows the firing rate of the neurons with a significant change in CSI ($n = 13$). O-2545 significantly increased the response to the standard stimulus by $138 \pm 55\%$ ($P = 0.037$, Fig. 3F) without changes in the firing rate to the deviant stimulus.

We also analyzed the effect of O-2545 on the time course of the response to the standard stimulus for the neurons with a significant change in their CSI. The dynamics of the response to the standard frequency was fit by a double exponential function under the baseline ($R^2 = 0.38$) and O2545 ($R^2 = 0.26$) conditions, displaying a rapid and a slow decay as well as a steady state component (Fig. 3G). O-2545 increased the response during the steady-state component of the response from 0.48 spikes per trial to 0.53 (95% CIs) without affecting either the timing or the magnitude of the fast (baseline, $\tau_r = 0.21$ trial, $A_r = 0.74$ spikes per trial; O-2545 $\tau_r = 0.003$ trial, $A_r = 0.34$) or slow (baseline, $\tau_s = 9.58$ trial, $A_s = 0.24$ spikes per trial; O-2545 $\tau_s = 0.63$ trial, $A_s = 0.70$) components of the adaptation (Fig. 3G). O-2545 seems to change the variance more than anandamide.

AM251 decreases the firing rate but not the CSI. AM251 was applied to a total of 49 IC neurons. An example of its effect on the single-unit response is shown in Fig. 4A. The application of AM251 on IC neurons did not show a clear tendency to change the CSI at the population level (Fig. 4B). However, when a bootstrapping analysis was performed (Fig. 4C), 7/49 neurons displayed a significant change, with an increase in the CSI from 0.17 ± 0.2 to 0.43 ± 0.13 (Fig. 4D; Table 1). Non-significant changes were observed in the firing rate to deviant and standard stimuli (Fig. 4E and F). Although the effects on the firing rate of the neurons are not significant, there is a tendency for a decrease in the firing rate to the standard stimulus (36%; $P = 0.105$), leading to changes in the CSI.

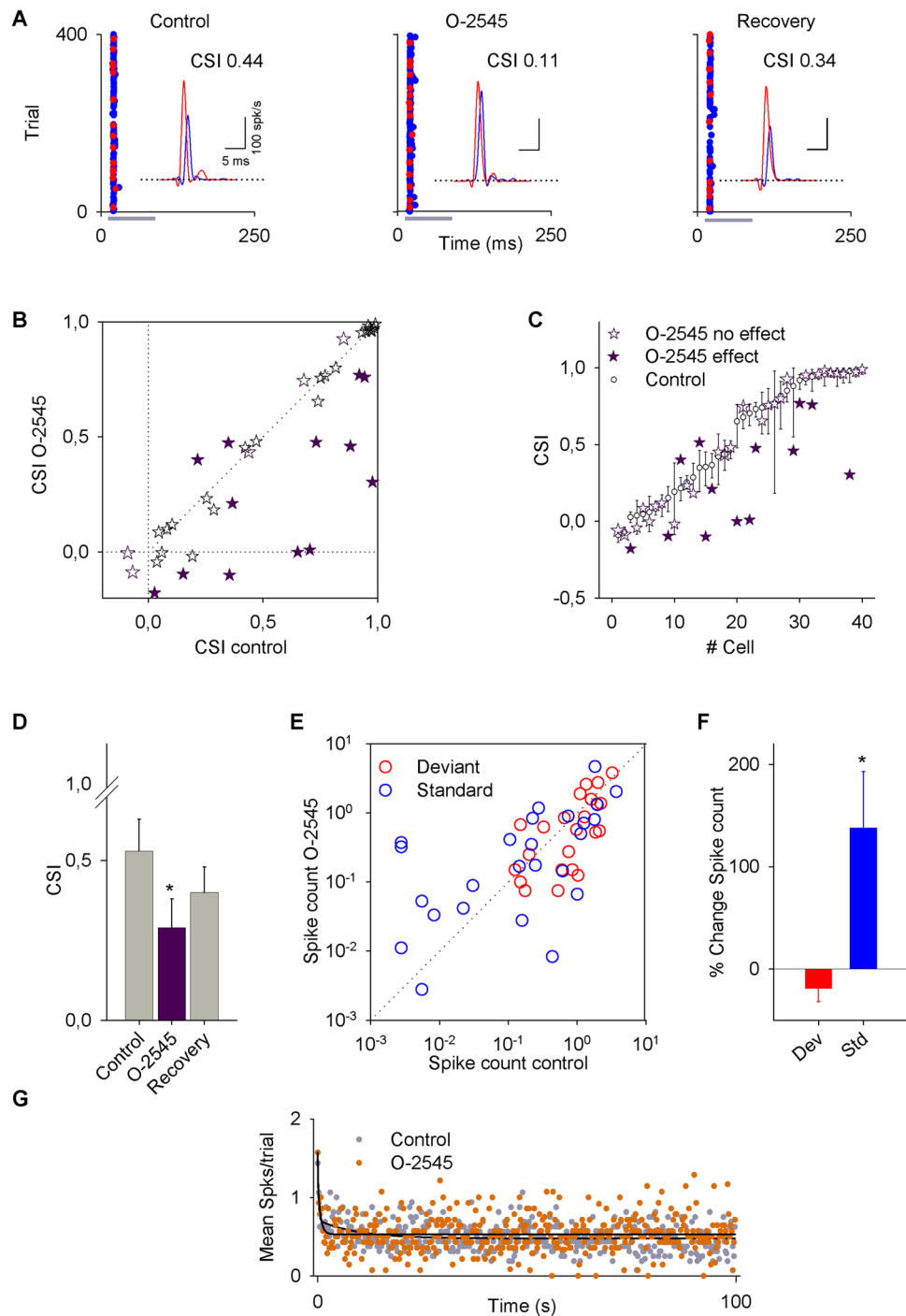


Figure 3. Effect of O-2545 on the activity of IC neurons. **(A)** Typical recording of an IC neuron under an oddball stimulation paradigm before (control), during (O-2545), and after (recovery) microiontophoretic application of O-2545. (For this neuron, the standard frequency was 34544 Hz and the deviant frequency was 28284 Hz.) Insets represent the PSTH of the response in which the CSI decreased from 0.44 to 0.11 and recovered to 0.34. **(B)** Scatter plot of the CSI in the control condition versus O-2545 application. The CSI of most of the neurons decreased. **(C)** Bootstrapping analysis for each neuron recorded in control condition (white dots) and with O-2545 application (purple stars: significant change; white stars: no change). **(D)** Bars represent the averaged CSI \pm SE of the neurons in which there were significant changes. **(E)** Scatter plot of the spike count in control condition versus drug application for deviant (red dots) and standard (blue dots) stimuli. **(F)** Bars represent the percent change in the spike count for deviant (red bar) and standard (blue bar) stimuli. Vertical bars represent the % change \pm SE. **(G)** Time course of adaptation of O-2545. The baseline (gray circles) and O-2545 data (orange circles) had fast and slow decay components and a steady-state component that were fitted by a double exponential function (black lines).

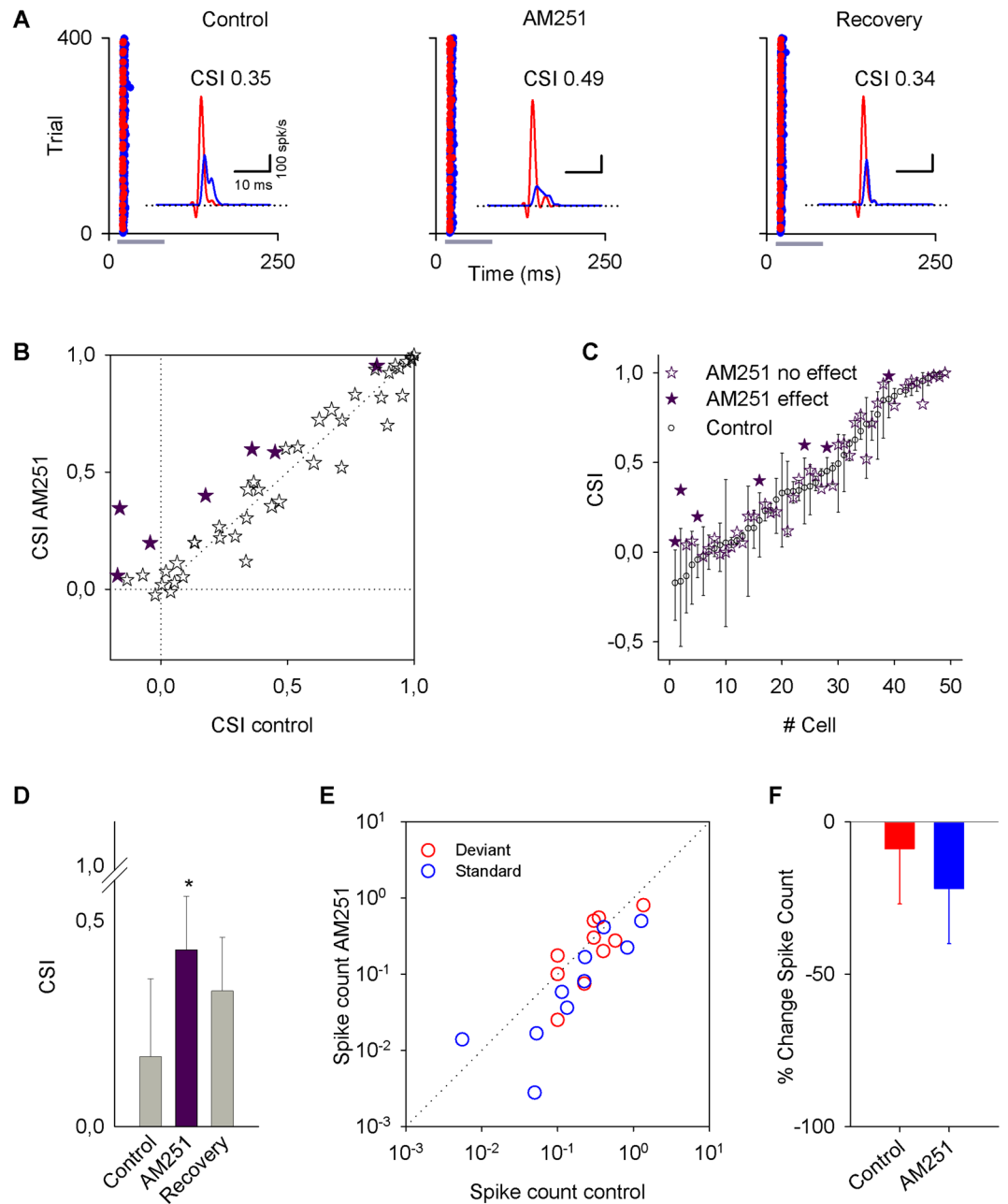


Figure 4. Effects of AM251 on the activity of IC neurons. **(A)** Typical recordings of an IC neuron under an oddball stimulation paradigm before (control), during (AM251), and after (recovery) an i.v. application of AM251. (For this neuron, the standard frequency was 8574 Hz, and the deviant frequency was 10472 Hz.) The insets show the PSTH of the responses. **(B)** Scatter plot of the CSI in control condition versus AM251 application. **(C)** Bootstrapping analysis showing that AM251 produced significant changes in the CSI only in 7/49 neurons. **(D)** Bars represent the average of the CSI values \pm SE in control condition, AM251 application and recovery. **(E)** Scatter plot of the firing rate showing the spike count for deviant and standard frequencies in control condition versus AM251 application. **(F)** Bars show the percent change in the spike count averaged for deviant and standard stimuli by AM251 application. There is a tendency for a decrease in the firing rate for both frequencies. Vertical bars represent the % change \pm SE.

Next, we injected a drug cocktail made of anandamide and AM251. Its application produced no significant changes in any of the measured parameters ($n = 15$), including CSI (Fig. 5A and B) and spike counts (Fig. 5C). This result demonstrates that the effects we observed were specifically mediated by CB1R.

Effect of cannabinoid drugs on latency, spontaneous activity and other properties of IC neurons. Neither the agonists nor the antagonist affected the first spike latency (FSL), which was shorter in response to the deviant stimulus compared to the standard stimulus, as previously described^{17,39} (Fig. 5D–F).

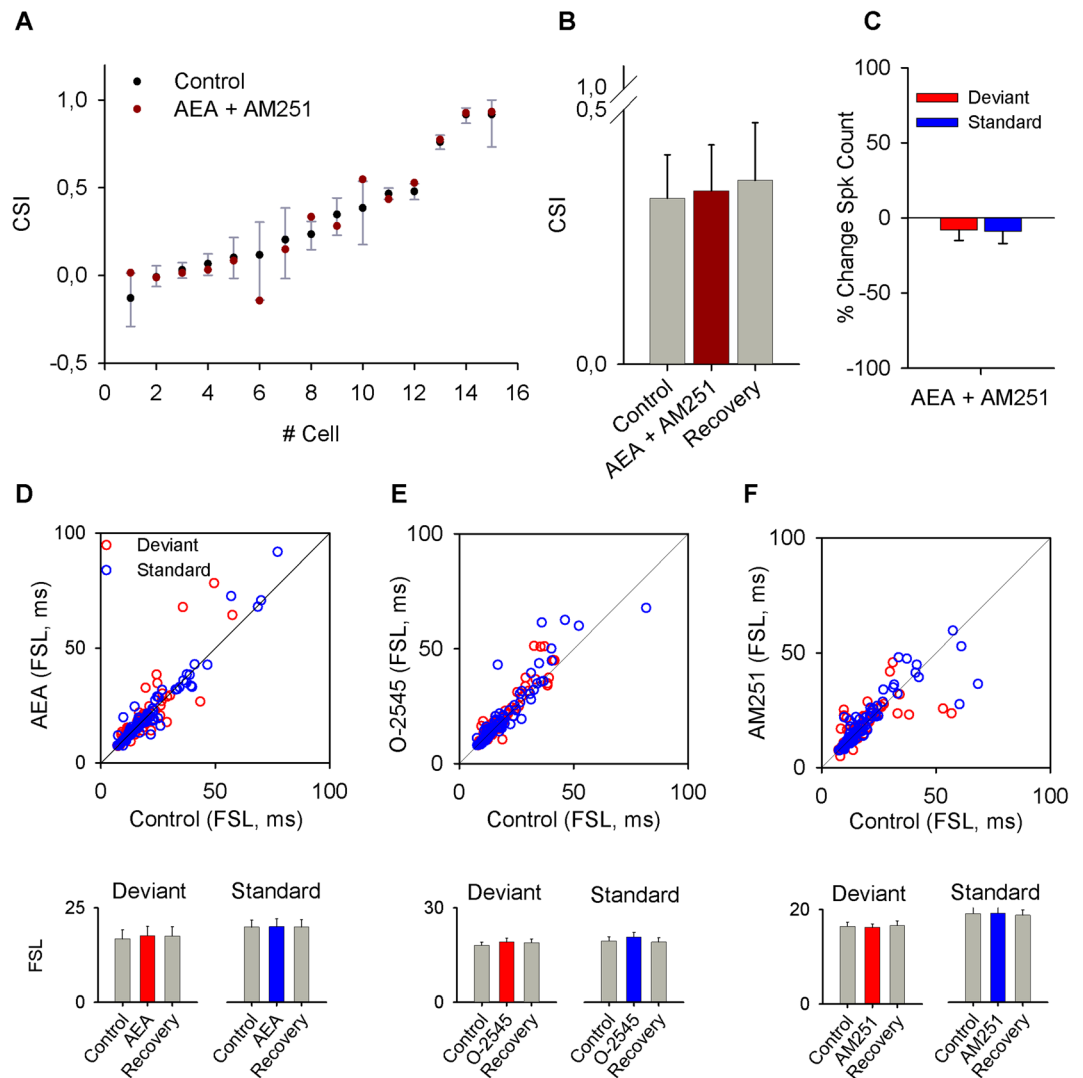


Figure 5. Effects of the co-application of AEA and AM251. **(A)** Bootstrap analysis of the effect of the combination of agonist plus antagonist showing that co-application did not produce effects on the CSI of the IC neurons. **(B)** Bar graph representation of the effect of the combination of drugs on the average value of CSI. **(C)** Percent change of the spike count in response to standard and deviant frequencies after application of agonist plus antagonist. **(D–F)** Scatter plots that represent the FSL in control condition versus drug application, for AEA, O-2545 and AM251 respectively. Below are bar plots of the average values of FSL for deviant and standard stimuli in control condition, with drug application and during recovery.

A small percentage of all recorded neurons (23%, 32/139) exhibited spontaneous activity (0.51 ± 0.16 spikes per second). There were no detectable effects on the spontaneous activity after application of the agonists. However, when the antagonist AM251 was applied, the spontaneous activity significantly increased by $7 \pm 4\%$ ($P = 0.023$). Finally, the properties of several different parameters including FRA shape, BE, CF, threshold, Q_{10} , Q_{30} , BW₁₀ and BW₃₀ analyzed in 118 neurons, remained unchanged.

Discussion

The results of this study demonstrate that ECBs exert an effect on SSA in non-lemniscal IC neurons of the rat. When IC neurons are stimulated under the oddball paradigm, cannabinoid agonists affect the neuronal firing of IC neurons mostly increasing the responses to standard stimuli but not the response to the deviant one. This differential effect leads to a decrease in the level of SSA. Based on the pharmacological properties of the agonists and antagonists, we conclude that the effect of anandamide is specifically mediated by CB1 receptors, because the SSA levels did not change with the co-application of the agonist plus antagonist.

The retrograde modulation of inhibitory and excitatory inputs by cannabinoids has been previously described for both glutamatergic and GABAergic synapses in the auditory pathway⁵. It is well known that the IC receives excitatory and inhibitory inputs and that the interplay between them determines the activity of IC neurons⁴². These inputs may be under the influence of a delicate neuromodulation. It is also known that IC neurons express CBRs, but their functional expression and their effects on SSA remained unknown.

Here we report for the first time that the cannabinoid agonists anandamide (an endogenous CB1R agonist) and O-2545 (a high affinity synthetic CB1R agonist) decrease neuronal adaptation in the IC as measured by the CSI, i.e., the SSA index^{17,26}. In the IC, this effect is due to a differential increase in the spike count to repetitive stimuli. There are at least three possibilities that could account for these results. The first is based on the well-known mechanism through which cannabinoids act on presynaptic receptors. The second depends on the combined action of cannabinoids and other neuromodulatory substances such as acetylcholine. A potential third mechanism requires the presence of postsynaptic CBRs in addition to the known presynaptic receptors. Although it is currently unknown whether mammalian IC neurons express postsynaptic CBRs, we cannot rule out this possibility. These three mechanisms are not mutually exclusive. In the following we discuss each possibility in the context of our main results.

Based on well-established mechanisms of cannabinoid drugs in other parts of the brain, anandamide and O-2545 could be acting on CB1Rs expressed on presynaptic inhibitory neurons, leading to the observed increases in neuronal responses to repetitive stimuli. Previous studies have shown that GABA_A-mediated inhibition plays a role in shaping SSA by acting as a gain control system^{23,39}. Our results suggest that the postsynaptic neurons from which we recorded are likely to receive inhibitory inputs (probably GABAergic) expressing CB1Rs⁴³. These inputs would normally inhibit the postsynaptic neuron, but the application of the cannabinoid agonists would activate the CB1Rs on the presynaptic terminals, decreasing GABA release and so increasing the activity of the postsynaptic neuron (Fig. 6.I). We cannot rule out an effect mediated by glycinergic inputs, but this is unlikely because results from our lab have shown that glycine-mediated inhibition has only a weak effect, if any, on SSA^{44,45}. Further, glycinergic receptors are expressed mainly in the ventral part of the central IC^{43,46} where SSA is almost negligible^{17,19,24}.

A wealth of data supports the idea that modulation of GABA-mediated inhibition is a common mechanism in the central nervous system. It is known that endocannabinoids modulate GABA release in many CNS regions, including the hippocampus, basal ganglia, cerebellum and brainstem^{12,14,47-51}. Likewise, anatomical studies have demonstrated that high levels of CB1R mRNA and immunoreactivity are associated with GABAergic neurons^{12,47,52}. Hence, a GABA suppression-mediated mechanism is a plausible explanation for the action of cannabinoid agonist drugs on SSA in IC neurons (Fig. 6.I). The specific increase on standard response might be explained by an activity-dependent CBRs-activation. Considering that SSA can be accounted for by differential activation of afferent inputs (Duque *et al.*²¹), repetitively activated afferents by the standard frequency would lead to a 'larger' release of ECBs at their synapse with the IC neurons than those released by inputs activated by deviant frequencies. The CBRs activation would in turn decrease the inhibition locally recruited by standard-activated frequency channels acting on SSA neuron. In this context it is worth to mention that a growing body of evidence suggests that perturbations in GABAergic synaptic transmission, such as reduced CB1R expression, are linked to schizophrenia^{51,53}. Since MMN is altered in schizophrenia⁵⁴ and SSA may be a neuronal correlate of MMN²⁷⁻²⁹ our study may open new avenues for future studies on the relationship between ECBs, SSA, MMN and schizophrenia. We did observe decreases in firing to the repetitive stimulus in a few neurons; this result could be explained by an effect on excitatory (glutamatergic) inputs expressing CB1Rs. Agonists would promote a blockade of excitation through action on CB1R receptors expressed on glutamatergic presynaptic neurons, for this small population of neurons. There is electrophysiological evidence that CBR activation inhibits glutamate release in many brain regions, including the Purkinje neuron-parallel fiber synapse in the cerebellum and also at synapses in the striatum, midbrain periaqueductal gray, and nucleus accumbens^{15,49,55,56}. This possibility could explain the mixed effects that we have observed when we applied anandamide or O-2545. Also it is plausible that ECBs modulate both excitatory and inhibitory inputs and that the final increase or decrease of the firing rate depends on the ratio of ECB modulation to both inputs.

A second possibility that could explain some of our results is synergistic activity of the ECB system and other neuromodulators. We collected a large sample of neurons (154), but only a relatively small number showed significant changes in the CSI. It is possible that CB1Rs are differentially expressed in presynaptic neurons and that there is a population that does not express CB1Rs. But it is also possible that the endocannabinoid system, although functionally expressed, requires other modulatory substances to exert its effects. Interestingly, and similar to what we observed here with CB1R, previous work from our lab has demonstrated a differential increase in the response to a standard stimulus is also elicited by the activation of cholinergic (muscarinic) receptors²⁵ such that SSA is reduced by ACh blockade. Moreover, a recent psychopharmacological study⁵⁷ to test specific and formal predictions about the effect of cholinergic manipulations on MMN and repetition suppression has shown that by assigning ACh the role of signaling sensory precision, its augmentation can reduce adaptation to surprising stimuli in sensory cortices, i.e., MMN. We cannot confirm or rule out that the previously reported cholinergic effect on SSA²⁵ and MMN⁵⁷ is mediated by the CB1R activation, but many *in vitro* studies have demonstrated a close functional relationship between cannabinoids and acetylcholine. Co-activation of glutamate and acetylcholine receptors increases the release of ECBs^{58,59}. Further, co-treatment with glutamate and carbachol (a cholinergic agonist) stimulates the anandamide biosynthesis pathway in primary cultured cortical neurons⁵⁸. Patch clamp recordings in hippocampal slices have demonstrated that the activation of cholinergic neurons (through muscarinic receptors) and retrograde signaling by ECBs act cooperatively to regulate GABAergic transmission through the blockade of CB1Rs or M2-type mAChRs, decreasing the probability of GABA release⁵⁰. At the cellular level, this mechanism is mediated by cAMP/PKA (cyclic adenosine monophosphate/protein kinase A). It is known that CB1Rs are coupled to a G_{i/o} protein that induces the inhibition of cAMP with consequent non-activation of PKA. In hippocampal synapses, the decrease of PKA contributes to the decrease of ECB-dependent GABA release⁵⁰. It is also possible that the ECB system requires the presence of other neuromodulator substances such as dopamine or serotonin to produce its effects. Future studies are necessary to test this hypothesis.

Finally, a third possible CB1Rs activation mechanism would involve the postsynaptic expression of cannabinoid receptors in IC neurons. In this case, since CB1Rs are coupled to G_{i/o} protein, one would expect that their

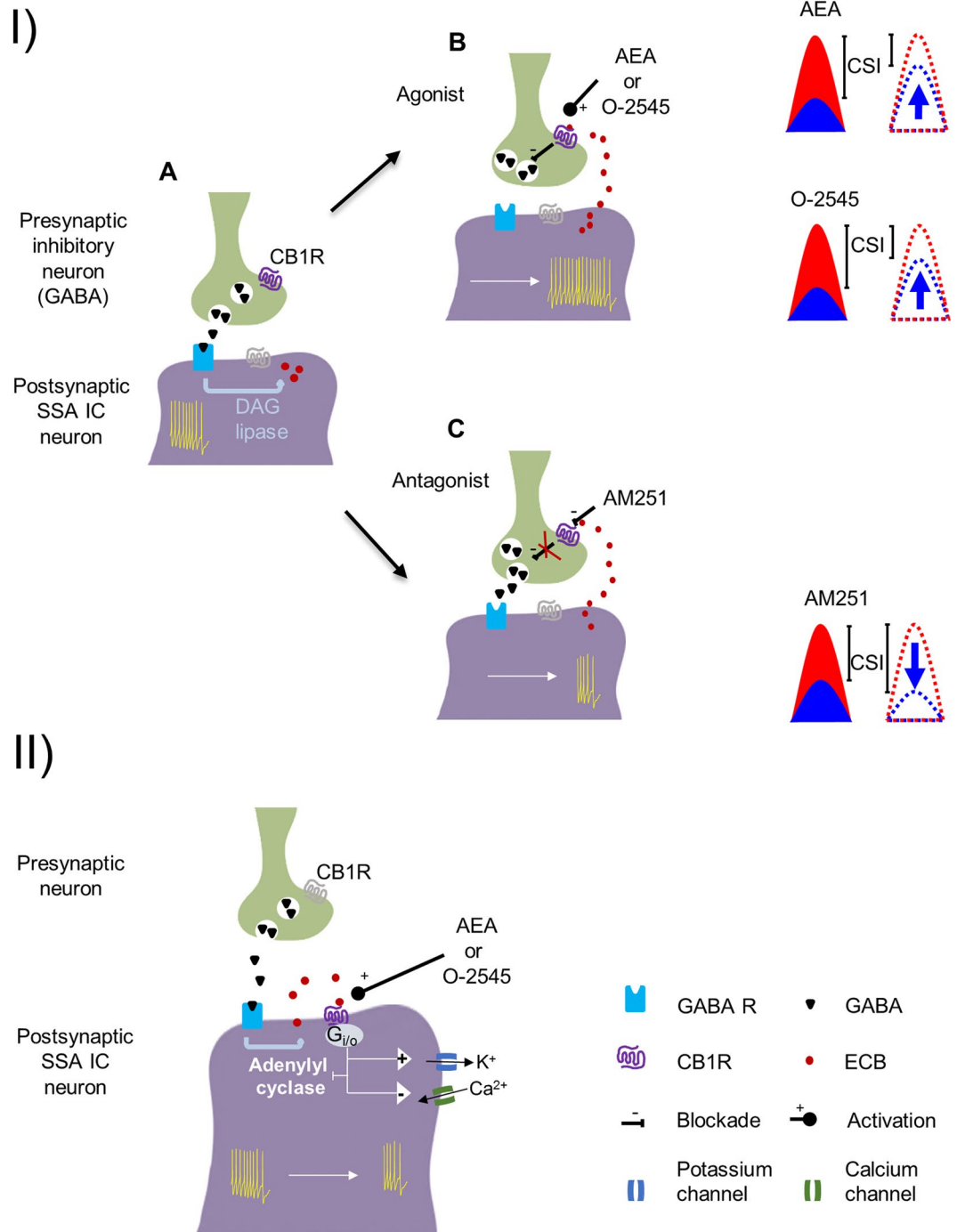


Figure 6. Schematic representation of hypothetical action mechanisms of cannabinoids on IC neurons that exhibit SSA. (I.A) An inhibitory input (probably GABAergic, green) contacting a postsynaptic IC neuron (purple). Basal activity is shown as action potentials (yellow) in the postsynaptic neuron. GABA release affects the activity of the neuron by acting on postsynaptic receptors. (I.B) Agonist drugs that activate presynaptic CB1R on the inhibitory terminal lead to an increase in the firing rate of the postsynaptic neuron due to a decrease in the GABA release. Both agonists produce an increase of the firing rate in response to the standard frequency; thus, the CSI of the postsynaptic SSA IC neuron decreases. We cannot rule out the possible involvement of other neuromodulatory substances in the final result. (I.C) Injection of the CB1R antagonist AM251 produces a blockade of the basal ECB and/or the constitutive activity of the receptors, hence GABA is released, decreasing the firing rate for standard stimuli that results in a CSI increase. (II) If CBRs are located in the postsynaptic neurons, their activation should promote both an inhibition of adenylyl cyclase, and a change in the open probability of ionic channels (K⁺ and Ca²⁺) that would lead to a decrease in neuronal activity.

activation would promote the inhibition of adenylyl cyclase, an increase in the open probability of potassium channels and a decrease in the open probability of calcium channels. Under this scenario, the expected effect on neuronal firing rate would be a decrease (Fig. 6.II). Although, this effect was not the main observation in our data set, there was a small subpopulation of IC neurons in which CB1R agonists led to a decrease in the spike count to standard stimuli, thus increasing the CSI (Table 1).

An important limitation of our study is that in most cases, only, partial recovery was obtained after drug application. Although we record the neurons for as long as possible, some also were lost without achieving full recovery. This could be because CB1 receptors undergo agonist-induced desensitization involving G-protein uncoupling due to phosphorylation by G-protein-coupled receptor kinases (GRKs) and receptor internalization. GRK-mediated receptor phosphorylation leads to the binding of beta-arrestins, which uncouple receptors from heterotrimeric G-proteins and target CB1 receptors for internalization in clathrin-coated vesicles⁶⁰.

The effects elicited by the antagonist AM251 on the CSI of some neurons suggest the possibility that there is some sound-evoked endogenous ECB release, unless the CBRs are constitutively active. Such constitutive activity is a common feature in receptors with seven transmembrane segments like histamine receptors⁶¹, dopamine receptors⁶² and others. On the other hand, the fact that only some neurons were affected by the antagonist could indicate that the endogenous ECB release may not occur in all neurons in our anesthetized preparation². A similar conclusion was reached by Dasilva and colleagues² during recordings in the visual thalamus.

In summary, it is likely that ECBs have mixed and complex modulatory effects in the IC, with a major effect being a decrease in SSA. We conclude that the cannabinoid system has a role in a down-regulation of SSA in some IC neurons. The degree of modulation would depend on the strength and nature of the inputs that each neuron receives.

Methods

Surgical procedures. Experiments were performed on 35 adult rats (body weights: 150–250 g). All experimental procedures were carried out at the University of Salamanca using methods conforming to the standards of, and approved by, the University of Salamanca Animal Care Committee.

Surgical anesthesia was induced with a mixture of ketamine/xylazine (100 and 20 mg/kg, respectively, i.m.) and maintained with urethane (1.5 g/kg, i.p.). Supplementary urethane doses (0.5 g/kg, i.p.) were given as needed. Urethane was selected as an anesthetic because effects on multiple aspects of neural activity, including inhibition and spontaneous firing, are less apparent than with barbiturates and other anesthetic drugs^{21, 25, 44}. The trachea was cannulated, and atropine sulphate (0.05 mg/kg, s.c.) was administered to reduce bronchial secretions. Body temperature was maintained at $38\text{ }^{\circ}\text{C} \pm 1\text{ }^{\circ}\text{C}$. Details of surgical preparation were as described elsewhere^{17, 18, 23, 24, 39, 40, 42, 63–68}.

The animal was placed in a stereotaxic frame in which the ear bars were replaced by hollow specula that accommodated a sound delivery system. A craniotomy was performed to expose the cerebral cortex overlying the IC. A tungsten electrode⁴⁴ (1–2 M Ω) was lowered through the cortex and used to record extracellular single unit responses in the IC. Recording sites in the IC were based on stereotaxic coordinates and physiological criteria including tonotopicity and response reliability^{17, 18, 63, 65}.

Acoustic delivery and electrophysiological recording. Stimuli were delivered through a sealed acoustic system^{17, 19–21, 25}. Pure tone bursts were delivered to the contralateral ear under computer control using TDT (Tucker-Davis Technologies) System 2 hardware and custom software. Two electrostatic loudspeakers (TDT-EC1) were driven by two TDT-ED1 modules. The sound system was calibrated using a $\frac{1}{4}$ " condenser microphone (model 4136, Brüel&Kjær) and a dynamic signal analyzer (Photon +, Brüel&Kjær). The maximum sound system output was flat between 0.3–5 kHz ($\sim 100 \pm 7$ dB SPL) and between 5–40 kHz ($\sim 90 \pm 5$ dB SPL). The system's maximum frequency output was 40 kHz. The second and third harmonic components of the signal were at least 40 dB re maximum output (i.e., lower than the level of the fundamental frequency at the highest output level¹⁷).

The electrode was advanced using a Sensapex microdrive. Action potentials were recorded with a Bioamp amplifier (Tucker-Davis Technologies; TDT) whose 10X output was further amplified and bandpass-filtered (TDT PC1; fc, 500 Hz and 3 kHz) before passing through a spike discriminator (TDT SD1). Spike times were logged on a computer by feeding the output of the spike discriminator into an event timer (TDT ET1) synchronized to a timing generator (TDT TG6).

Stimulus generation and on-line data visualization were controlled with custom software. Spike times were displayed as dot rasters ordered by the acoustic parameter varied during testing.

Auditory stimulation. Search stimuli were pure tones or noise bursts. To the extent possible, the approximate frequency tuning of the neuron was determined audiovisually. The minimum threshold and best frequency (BF) of the neuron were then obtained by an automated procedure with 2–5 stimulus repetitions at each frequency and intensity step.

The monaural frequency response area (FRA), i.e., the combination of frequencies and intensities capable of evoking a response, was then obtained automatically using a randomized stimulus presentation paradigm and plotted using Excel, SigmaPlot and Matlab software. The stimuli used to generate FRAs for single units were pure tones with a duration of 75 ms (5 ms rise/fall time). Frequency and intensity of the stimulus were varied randomly (0–100 dB attenuation in 5 or 10 dB steps and in 25 frequency steps from 0.1–40 KHz to cover approximately 2–3 octaves above and below the BF⁶⁵).

Oddball paradigm. We presented trains of 400 stimuli containing two different frequencies (f_1 and f_2) presented in a pseudo-random order at a specific repetition rate (4 Hz) and at a level of 10–40 dB above threshold. Both frequencies were within the excitatory FRA previously determined for the neuron. One frequency (f_1) was

presented as standard (i.e., high probability within the sequence, $p = 0.9$); interspersed randomly with the second frequency (f_2) presented as deviant (i.e., low probability within the sequence, $p = 0.1$). After obtaining one data set, the relative probabilities of the two stimuli were reversed, with f_2 as the standard and f_1 as the deviant (total number of stimuli for the frequency pair = 400). The frequency contrasts were chosen with variations between 0.14–0.53 octaves, as in previous studies¹⁷.

Analysis of neuronal responses (f_1 and f_2). The level of SSA for both frequencies at each condition (Common SSA Index, CSI) was calculated as:

$$CSI = \frac{\sum DEV(f_i) - \sum STD(f_i)}{\sum DEV(f_i) + \sum STD(f_i)}; i = 1, 2$$

where $DEV(f_i)$, $STD(f_i)$ are spike counts in response to frequency f_i when it was a deviant and standard, respectively. CSI reflects the extent to which the response to the standard stimulus was suppressed. The index ranges between -1 to $+1$, being positive if the response to the deviant stimulus was greater than the response to the standard stimulus. To test for effects of the drugs on each individual neuron, the 95% confidence intervals (CIs) for the baseline CSI were calculated using a bootstrapping method^{39, 68} (10000 repetitions). The CSI is a special statistic, resulting from a complex combination of the single-trial responses to deviants and standards in a specific way; thus, the sample distribution of CSI for any neuron is highly non-normal, and confidence intervals or standard error of the sample CSI cannot be easily determined using analytical methods. For this reason, we use a bootstrap approach to determine empirical confidence intervals for our sample CSI values, and to assess statistical significance of changes in the neuronal CSI. We have used the bootstrapping method previously^{22, 25, 33, 39, 68, 72}, it is very robust and yields accurate results for high resampling size (e.g. 10000 resamplings).

To characterize the time course of adaptation, we plotted the averaged response to the standard frequency from the neurons with significant change after drug application as a function of time. We performed a nonlinear least-square fit to this population mean curve to find the best-fitting double exponential function as follows: $f(t) = A_{ss} + A_r \cdot e^{-t/\tau(r)} + A_s \cdot e^{-t/\tau(s)}$, where A_{ss} , A_r , and A_s are the magnitudes of the steady state and the rapid and slow components, respectively, and $\tau_{(r)}$ and $\tau_{(s)}$ are the time constants of the rapid and slow components (for details, see ref. 39).

Spontaneous activity. Drug-induced effects on spontaneous activity were measured by averaging the firing rate over a time window of 150 ms at the end of each sound presentation trial in the control condition and comparing this to that obtained in the same time window during the drug application.

Drugs. We used two CB1R agonists: anandamide [AEA, N-(2-Hydroxyethyl)-5Z,8Z,11Z,14Z-eicosatetraenamide, Tocris, UK] and O-2545 hydrochloride [(6aR,10aR)-6a,7,10,10a-Tetrahydro-3-(5-{1H-imidazol-1-yl}-1,1-dimethylpentyl)-6,6,9-trimethyl-6H-dibenzo[b,d]pyran-1-ol hydrochloride, Tocris, UK] and one CB1R antagonist: AM251 [N-(Piperidin-1-yl)-5-(4-iodophenyl)-1-(2,4-dichlorophenyl)-4-methyl-1H-pyrazole-3-carboxamide, Tocris, UK].

The two agonists were applied through different administration pathways due to differences in their water solubility. Microiontophoresis is a technique that can be used only for water soluble drugs. We used anandamide, which is not water soluble, since it is the endogenous agonist of CBR, although it had to be injected into the circulatory system. We administered O-2545, a water soluble compound that is a potent synthetic agonist, by microiontophoresis.

Anandamide and AM251 were administered through the tail vein² (0.5 mg/kg each). Anandamide was supplied pre-dissolved in anhydrous ethanol and dissolved to a final concentration of 1:19 ethanol/saline. AM251 was dissolved in 1:19 DMSO/saline and sonicated for 30 minutes to make a homogeneous solution. Control experiments were performed using the solution vehicles alone, and no changes were apparent (data not shown).

O-2545 hydrochloride was applied iontophoretically through multi-barreled pipettes attached to the recording electrode so that it was released into the micro-domain of the recorded neuron^{25, 39}. The tip of the recording electrode protruded 15–25 μm from the pipette tip. The glass pipette consisted of five barrels in an H configuration (World Precision Instruments, catalog no. 5B120F-4) with the tip broken to a diameter of 30–40 μm ⁴⁴. The center barrel was filled with saline for current compensation (165 mM NaCl), whereas the others were filled with 25 mM O-2545. The drug was dissolved in distilled water and its pH adjusted to 3 with HCl. The drug was retained in the pipette with a -20 nA current and was ejected, typically, using 10–20 nA currents (Neurophore BH-2 system, Harvard Apparatus). This drug concentration has been previously demonstrated to be effective in *in vivo* studies in the mammalian visual thalamus². The duration of the drug ejection was usually 5–10 min. After the drug ejection, we repeated the stimulation protocol until we observed recovery.

Recovery of drug application was considered when spike counts returned to levels that did not differ significantly from control values.

Histological verification of recording sites. At the end of each experiment, electrolytic lesions (5 μA , 5 s) were made with the tungsten recording electrode. Then, animals were sacrificed using a lethal dose of pentobarbital and decapitated the animal so that brains were immediately fixed using a mixture of 1% paraformaldehyde and 1% glutaraldehyde diluted in 0.4 M PBS (0.5% NaNO_3 in PBS). After fixation, tissue was cryoprotected in 30% sucrose and sectioned in the coronal or sagittal plane at a thickness of 40 μm on a freezing microtome. Slices were stained with 0.1% cresyl violet to facilitate identification of cytoarchitectural boundaries. The recorded units were assigned to one of the main subdivisions of the IC using as reference the standard sections from a rat brain atlas^{66, 69–72}.

Statistics. Results were analyzed using the *Student t-test* comparing control condition versus drug application and reported as mean \pm SE. When data failed to pass the normality test, a non-parametric *Mann-Whitney rank sum test* was performed.

All analyses were done with Sigma Plot software, except bootstrapping which was done using MATLAB.

Data availability statement. The datasets generated during and/or analyzed during the current study are available from the corresponding author on reasonable request.

References

- Czesnik, D., Schild, D., Kuduz, J. & Manzini, I. Cannabinoid action in the olfactory epithelium. *Proc. Natl. Acad. Sci. USA* **104**, 2967–72 (2007).
- Dasilva, M. A., Grieve, K. L., Cudeiro, J. & Rivadulla, C. Endocannabinoid CB1 receptors modulate visual output from the thalamus. *Psychopharmacology (Berl)* **219**, 835–45 (2012).
- Dasilva, M., Grieve, K. L., Cudeiro, J. & Rivadulla, C. Anandamide activation of CB1 receptors increases spontaneous bursting and oscillatory activity in the thalamus. *Neuroscience* **265**, 72–82 (2014).
- Castillo, P. E., Younts, T. J., Chávez, A. E. & Hashimoto, Y. Endocannabinoid Signaling and Synaptic Function. *Neuron* **76**, 70–81 (2012).
- Zhao, Y., Rubio, M. E. & Tzounopoulos, T. Distinct functional and anatomical architecture of the endocannabinoid system in the auditory brainstem. *J. Neurophysiol.* **101**, 2434–46 (2009).
- Sedlacek, M., Tipton, P. W. & Brenowitz, S. D. Sustained firing of cartwheel cells in the dorsal cochlear nucleus evokes endocannabinoid release and retrograde suppression of parallel fiber synapses. *J. Neurosci.* **31**, 15807–17 (2011).
- Trattner, B., Gravot, C. M., Grothe, B. & Kunz, L. Metabolic Maturation of Auditory Neurons in the Superior Olivary Complex. *PLoS One* **8**, e67351 (2013).
- Moldrich, G. & Wenger, T. Localization of the CB1 cannabinoid receptor in the rat brain. An immunohistochemical study. *Peptides* **21**, 1735–42 (2000).
- Penzo, M. A. & Peña, J. L. Endocannabinoid-mediated long-term depression in the avian midbrain expressed presynaptically and postsynaptically. *J. Neurosci.* **29**, 4131–9 (2009).
- Kano, M., Ohno-Shosaku, T., Hashimoto, Y., Uchigashima, M. & Watanabe, M. Endocannabinoid-mediated control of synaptic transmission. *Physiol. Rev.* **89**, 309–80 (2009).
- Alger, B. E. & Kim, J. Supply and demand for endocannabinoids. *Trends Neurosci.* **34**, 304–15 (2011).
- Katona, I. & Freund, T. F. Multiple Functions of Endocannabinoid Signaling in the Brain. *Annu. Rev. Neurosci.* **35**, 529–558 (2012).
- Pitler, T. A. & Alger, B. E. Depolarization-induced suppression of GABAergic inhibition in rat hippocampal pyramidal cells: G protein involvement in a presynaptic mechanism. *Neuron* **13**, 1447–55 (1994).
- Wilson, R. I., Kunos, G. & Nicoll, R. A. Presynaptic specificity of endocannabinoid signaling in the hippocampus. *Neuron* **31**, 453–62 (2001).
- Kreitzer, A. C. & Regehr, W. G. Cerebellar depolarization-induced suppression of inhibition is mediated by endogenous cannabinoids. *J. Neurosci.* **21**, RC174 (2001).
- Ohno-Shosaku, T., Tanimura, A., Hashimoto, Y. & Kano, M. Endocannabinoids and retrograde modulation of synaptic transmission. *Neuroscientist* **18**, 119–32 (2012).
- Malmierca, M. S., Cristaudo, S., Perez-Gonzalez, D. & Covey, E. Stimulus-Specific Adaptation in the Inferior Colliculus of the Anesthetized Rat. *J. Neurosci.* **29**, 5483–5493 (2009).
- Pérez-González, D., Malmierca, M. S. & Covey, E. Novelty detector neurons in the mammalian auditory midbrain. *Eur. J. Neurosci.* **22**, 2879–85 (2005).
- Duque, D., Pérez-González, D., Ayala, Y. A., Palmer, A. R. & Malmierca, M. S. Topographic distribution, frequency, and intensity dependence of stimulus-specific adaptation in the inferior colliculus of the rat. *J. Neurosci.* **32**, 17762–74 (2012).
- Duque, D., Ayala, Y. A. & Malmierca, M. S. Deviance detection in auditory subcortical structures: what can we learn from neurochemistry and neural connectivity? *Cell Tissue Res.* **361**, 215–32 (2015).
- Duque, D., Wang, X., Nieto-Diego, J., Krumbholz, K. & Malmierca, M. S. Neurons in the inferior colliculus of the rat show stimulus-specific adaptation for frequency, but not for intensity. *Sci. Rep.* **6**, 24114 (2016).
- Ayala, Y. A., Pérez-González, D., Duque, D., Nelken, I. & Malmierca, M. S. Frequency discrimination and stimulus deviance in the inferior colliculus and cochlear nucleus. *Front. Neural Circuits* **6**, 119 (2012).
- Duque, D., Malmierca, M. S. & Caspary, D. M. Modulation of stimulus-specific adaptation by GABA(A) receptor activation or blockade in the medial geniculate body of the anaesthetized rat. *J. Physiol.* **592**, 729–43 (2014).
- Ayala, Y. A. & Malmierca, M. S. Stimulus-specific adaptation and deviance detection in the inferior colliculus. *Front. Neural Circuits* **6**, 89 (2013).
- Ayala, Y. A. & Malmierca, M. S. Cholinergic Modulation of Stimulus-Specific Adaptation in the Inferior Colliculus. *J. Neurosci.* **35**, 12261–12272 (2015).
- Ulanovsky, N., Las, L. & Nelken, I. Processing of low-probability sounds by cortical neurons. *Nat. Neurosci.* **6**, 391–398 (2003).
- Todd, J., Harms, L., Schall, U. & Michie, P. T. Mismatch negativity: translating the potential. *Front. psychiatry* **4**, 171 (2013).
- Harms, L. *et al.* Mismatch negativity (MMN) in freely-moving rats with several experimental controls. *PLoS One* **9**, e110892 (2014).
- Harms, L., Michie, P. T. & Näätänen, R. Criteria for determining whether mismatch responses exist in animal models: Focus on rodents. *Biol. Psychol.* **116**, 28–35 (2016).
- Escera, C. & Malmierca, M. S. The auditory novelty system: an attempt to integrate human and animal research. *Psychophysiology* **51**, 111–23 (2014).
- Malmierca, M. S., Sanchez-Vives, M. V., Escera, C. & Bendixen, A. Neuronal adaptation, novelty detection and regularity encoding in audition. *Front. Syst. Neurosci.* **8**, 111 (2014).
- Malmierca, M. S., Anderson, L. A. & Antunes, F. M. The cortical modulation of stimulus-specific adaptation in the auditory midbrain and thalamus: a potential neuronal correlate for predictive coding. *Front. Syst. Neurosci.* **9**, 19 (2015).
- Nieto-Diego, J. & Malmierca, M. S. Topographic Distribution of Stimulus-Specific Adaptation across Auditory Cortical Fields in the Anesthetized Rat. *PLoS Biol.* **14**, e1002397 (2016).
- Grimm, S. & Escera, C. Auditory deviance detection revisited: Evidence for a hierarchical novelty system. *Int. J. Psychophysiol.* **85**, 88–92 (2012).
- Grimm, S., Escera, C., Slabu, L. & Costa-Faidella, J. Electrophysiological evidence for the hierarchical organization of auditory change detection in the human brain. *Psychophysiology* **48**, 377–384 (2011).
- Slabu, L., Grimm, S. & Escera, C. Novelty Detection in the Human Auditory Brainstem. *J. Neurosci.* **32**, 1447–1452 (2012).
- Martin-Cortecero, J. & Nuñez, A. Tactile response adaptation to whisker stimulation in the lemniscal somatosensory pathway of rats. *Brain Res.* **1591**, 27–37 (2014).

38. Musall, S., Haiss, F., Weber, B. & von der Behrens, W. Deviant Processing in the Primary Somatosensory Cortex. *Cereb. Cortex* **23**, 283. doi:10.1093/cercor/bhv283 (2015).
39. Pérez-González, D., Hernández, O., Covey, E. & Malmierca, M. S. GABA(A)-mediated inhibition modulates stimulus-specific adaptation in the inferior colliculus. *PLoS One* **7**, e34297 (2012).
40. Anderson, L. A. & Malmierca, M. S. The effect of auditory cortex deactivation on stimulus-specific adaptation in the inferior colliculus of the rat. *Eur. J. Neurosci.* **37**, 52–62 (2013).
41. Ogawa, H. & Oka, K. Direction-Specific Adaptation in Neuronal and Behavioral Responses of an Insect Mechanosensory System. *J. Neurosci.* **35**, 11644–55 (2015).
42. Malmierca, M. S. In *The Rat Nervous System* 865–946, doi:10.1016/B978-0-12-374245-2.00029-2 (2015).
43. Merchán, M., Aguilar, L. A., Lopez-Poveda, E. A. & Malmierca, M. S. The inferior colliculus of the rat: quantitative immunocytochemical study of GABA and glycine. *Neuroscience* **136**, 907–25 (2005).
44. Ayala, Y. A., Pérez-González, D., Duque, D., Palmer, A. R. & Malmierca, M. S. Extracellular Recording of Neuronal Activity Combined with Microiontophoretic Application of Neuroactive Substances in Awake Mice. *J. Vis. Exp.* doi:10.3791/53914 (2016).
45. Ayala, Y. A. & Malmierca, M. S. The effect of inhibition on stimulus-specific adaptation in the inferior colliculus. *Brain Struct. & Funct.* (In press) 2017.
46. Choy Buentello, D., Bishop, D. C. & Oliver, D. L. Differential distribution of GABA and glycine terminals in the inferior colliculus of rat and mouse. *J. Comp. Neurol.* **523**, 2683–97 (2015).
47. Katona, I., Sperlág, B., Sik, A., Káfalvi, A., Vizi, E.S., Mackie, K. & Freund, T.F. Presynaptically located CB1 cannabinoid receptors regulate GABA release from axon terminals of specific hippocampal interneurons. *J. Neurosci.* **19**, 4544–58 (1999).
48. Hoffman, A. F. & Lupica, C. R. Mechanisms of cannabinoid inhibition of GABA(A) synaptic transmission in the hippocampus. *J. Neurosci.* **20**, 2470–9 (2000).
49. Takahashi, K. A. & Linden, D. J. Cannabinoid receptor modulation of synapses received by cerebellar Purkinje cells. *J. Neurophysiol.* **83**, 1167–80 (2000).
50. Ahumada, J. F., de Sevilla, D., Couve, A., Buño, W. & Fuenzalida, M. Long-term depression of inhibitory synaptic transmission induced by spike-timing dependent plasticity requires coactivation of endocannabinoid and muscarinic receptors. *Hippocampus* **23**, 1439–52 (2013).
51. Younts, T. J. & Castillo, P. E. Endogenous cannabinoid signaling at inhibitory interneurons. *Curr. Opin. Neurobiol.* **26**, 42–50 (2014).
52. Herkenham, M., Lynn, A.B., Johnson, M.R., Melvin, L.S., de Costa, B.R. & Rice, K.C. Characterization and localization of cannabinoid receptors in rat brain: a quantitative *in vitro* autoradiographic study. *J. Neurosci.* **11**, 563–83 (1991).
53. Laviolette, S. R. & Grace, A. A. The roles of cannabinoid and dopamine receptor systems in neural emotional learning circuits: implications for schizophrenia and addiction. *Cell. Mol. Life Sci.* **63**, 1597–613 (2006).
54. Michie, P. T., Malmierca, M. S., Harms, L. & Todd, J. The neurobiology of MMN and implications for schizophrenia. *Biol. Psychol.* **116**, 90–97 (2016).
55. Lévénés, C., Daniel, H., Soubrié, P. & Crépel, F. Cannabinoids decrease excitatory synaptic transmission and impair long-term depression in rat cerebellar Purkinje cells. *J. Physiol.* **867**–79 (1998).
56. Robbe, D., Alonso, G., Duchamp, F., Bockaert, J. & Manzoni, O. J. Localization and mechanisms of action of cannabinoid receptors at the glutamatergic synapses of the mouse nucleus accumbens. *J. Neurosci.* **21**, 109–16 (2001).
57. Moran, R.J., Jones, M.W., Blockeel, A.J., Adams, R.A., Stephan, K.E. & Friston, K.J. Free energy, precision and learning: the role of cholinergic neuromodulation. *J. Neurosci.* **33**, 8227–36 (2013).
58. Stella, N. & Piomelli, D. Receptor-dependent formation of endogenous cannabinoids in cortical neurons. *Eur. J. Pharmacol.* **425**, 189–96 (2001).
59. Kim, J., Isokawa, M., Ledent, C. & Alger, B. E. Activation of muscarinic acetylcholine receptors enhances the release of endogenous cannabinoids in the hippocampus. *J. Neurosci.* **22**, 10182–91 (2002).
60. Ferguson, S. S. G. Evolving Concepts in G Protein-Coupled Receptor Endocytosis: The Role in Receptor Desensitization and. *Am. Soc. Pharmacol. Exp. Ther.* **53**, 1–24 (2001).
61. Arrang, J.-M., Morisset, S. & Gbahou, F. Constitutive activity of the histamine H3 receptor. *Trends Pharmacol. Sci.* **28**, 350–357 (2007).
62. Valdés-Baizabal, C., Soto, E. & Vega, R. Dopaminergic modulation of the voltage-gated sodium current in the cochlear afferent neurons of the rat. *PLoS One* **10**, e0120808 (2015).
63. Malmierca, M. S. Hernández, O., Falconi, A., Lopez-Poveda, E. A., Merchán, M. & Rees, A. The commissure of the inferior colliculus shapes frequency response areas in rat: an *in vivo* study using reversible blockade with microinjection of kynurenic acid. *Exp. Brain Res.* **153**, 522–9 (2003).
64. Malmierca, M. S., Saint Marie, R. L., Merchan, M. A. & Oliver, D. L. Laminar inputs from dorsal cochlear nucleus and ventral cochlear nucleus to the central nucleus of the inferior colliculus: two patterns of convergence. *Neuroscience* **136**, 883–94 (2005).
65. Hernández, O., Espinosa, N., Pérez-González, D. & Malmierca, M. S. The inferior colliculus of the rat: a quantitative analysis of monaural frequency response areas. *Neuroscience* **132**, 203–17 (2005).
66. Izquierdo, M. A., Gutiérrez-Conde, P. M., Merchán, M. A. & Malmierca, M. S. Non-plastic reorganization of frequency coding in the inferior colliculus of the rat following noise-induced hearing loss. *Neuroscience* **154**, 355–69 (2008).
67. Antunes, F. M., Nelken, I., Covey, E. & Malmierca, M. S. Stimulus-Specific Adaptation in the Auditory Thalamus of the Anesthetized Rat. *PLoS One* **5**, e14071 (2010).
68. Antunes, F. M. & Malmierca, M. S. Effect of auditory cortex deactivation on stimulus-specific adaptation in the medial geniculate body. *J. Neurosci.* **31**, 17306–16 (2011).
69. Malmierca, M. S., Seip, K. L. & Osen, K. K. Morphological classification and identification of neurons in the inferior colliculus: a multivariate analysis. *Anat. Embryol. (Berl.)* **191**, 343–50 (1995).
70. Malmierca, M. S., Blackstad, T. W. & Osen, K. K. Computer-assisted 3-D reconstructions of Golgi-impregnated neurons in the cortical regions of the inferior colliculus of rat. *Hear. Res.* **274**, 13–26 (2011).
71. Loftus, W. C., Malmierca, M. S., Bishop, D. C. & Oliver, D. L. The cytoarchitecture of the inferior colliculus revisited: a common organization of the lateral cortex in rat and cat. *Neuroscience* **154**, 196–205 (2008).
72. Ayala, Y.A., Udeh, A., Dutta, K., Bishop, D., Malmierca, M.S. & Oliver, D.L. Differences in the strength of cortical and brainstem inputs to SSA and non-SSA neurons in the inferior colliculus. *Sci. Rep.* **5**, 10383 (2015).

Acknowledgements

We thank Drs Flora M. Antunes, Edward Bartlett, Nell B. Cant, Daniel Duque, Douglas L. Oliver, Javier Nieto-Diego, David Pérez-González, and Alan R. Palmer for their comments on a previous version of the manuscript and for their constructive criticisms. We also thank Ms. Marianny Janiree Pernía Rosales for helping with the histological section photomicrography. Financial support was provided by the Spanish MINECO (SAF2016-75803-P) and JCYL (SA343U14) to MSM. CVB held a fellowship from the Mexican CONACyT (216652). GGP held a fellowship from the Spanish MINECO (BES-2014-069113) and YAA held fellowships from the Mexican CONACyT (216106) and SEP.

Author Contributions

The experiments were performed in the Auditory Neuroscience Laboratory, Institute of Neuroscience of Castilla y León, University of Salamanca, Salamanca, Spain. The contribution of each author to the following aspects of the study is as stated: (1) collection of data: C.V.B.; G.G.P., Y.A.A. (2) conception and design of experiments: C.V.B.; G.G.P., Y.A.A., M.S.M.; (3) analysis and interpretation of data: C.V.B.; G.G.P., Y.A.A. and M.S.M.; (4) writing of the manuscript: C.V.B. and M.S.M. All authors approved the final version of the manuscript.

Additional Information

Competing Interests: The authors declare that they have no competing interests.

Publisher's note: Springer Nature remains neutral with regard to jurisdictional claims in published maps and institutional affiliations.



Open Access This article is licensed under a Creative Commons Attribution 4.0 International License, which permits use, sharing, adaptation, distribution and reproduction in any medium or format, as long as you give appropriate credit to the original author(s) and the source, provide a link to the Creative Commons license, and indicate if changes were made. The images or other third party material in this article are included in the article's Creative Commons license, unless indicated otherwise in a credit line to the material. If material is not included in the article's Creative Commons license and your intended use is not permitted by statutory regulation or exceeds the permitted use, you will need to obtain permission directly from the copyright holder. To view a copy of this license, visit <http://creativecommons.org/licenses/by/4.0/>.

© The Author(s) 2017

The effect of the NMDA-R antagonist, MK-801, on Neuronal Mismatch along the Rat Auditory Thalamocortical System

Journal:	<i>Brain</i>
Manuscript ID	BRAIN-2019-00515
Manuscript Type:	Original Article
Date Submitted by the Author:	25-Mar-2019
Complete List of Authors:	Parras, Gloria; Institute of Neurosciences of Castilla and Leon, Valdés-Baizabal, Catalina; Institute of Neurosciences of Castilla and Leon, Harms, Lauren; University of Newcastle Michie, Patricia; University of Newcastle, School of Psychology, Malmierca, Manuel; University of Salamanca, ; Institute of Neurosciences of Castilla and Leon,
Subject category:	Systems/Development/Physiology
To search keyword list, use whole or part words followed by an *:	Sensory systems < SYSTEMS/DEVELOPMENT/PHYSIOLOGY, Hearing < SYSTEMS/DEVELOPMENT/PHYSIOLOGY, Auditory system < SYSTEMS/DEVELOPMENT/PHYSIOLOGY, Schizophrenia < NEUROPSYCHIATRY, Event-related potentials < SYSTEMS/DEVELOPMENT/PHYSIOLOGY, Neuroanatomy < SYSTEMS/DEVELOPMENT/PHYSIOLOGY, Thalamus < SYSTEMS/DEVELOPMENT/PHYSIOLOGY, Plasticity < SYSTEMS/DEVELOPMENT/PHYSIOLOGY

SCHOLARONE™
 Manuscripts

1 **Title**2 **The effect of NMDA-R antagonist, MK-801, on Neuronal**
3 **Mismatch along the Auditory Thalamocortical System**4 **Authors**5 Gloria G Parras^{1,2}, MSc; Catalina Valdés-Baizabal^{1,2}, PhD, Lauren Harms³, PhD,
6 Patricia Michie³, PhD & Manuel S Malmierca, PhD^{1,2,4*}

7

8 **Affiliations**9 ¹ Cognitive and Auditory Neuroscience Laboratory, Institute of Neuroscience of Castilla
10 y León (INCYL), Salamanca, Spain.11 ² The Salamanca Institute for Biomedical Research (IBSAL), Salamanca, Spain.12 ³ School of Psychology, University of Newcastle, Callaghan, NSW, Australia; Priority
13 Centre for Brain and Mental Health Research, Callaghan, NSW, Australia; Hunter
14 Medical Research Institute, Newcastle, NSW, Australia.15 ⁴ Department of Cell Biology and Pathology, Faculty of Medicine, University of
16 Salamanca, Salamanca, Spain.

17

18 **Corresponding author: msm@usal.es*

19

20

21

22

23 According to predictive coding, the brain constantly generates top-down
24 predictions that are compared with sensory bottom-up signals. Stimuli that match
25 predictions are suppressed, whereas unexpected stimuli that do not match generate an
26 enhanced error signal. The predictive coding framework has emerged as an appealing
27 model of MMN, an ERP potential recorded in humans in an oddball paradigm. It has
28 been repeatedly observed that MMN is reduced in persons with schizophrenia. It is
29 believed that the molecular correlate of this reduction is glutamate NMDA-R
30 hypofunction, now a major model of the pathophysiology of schizophrenia. We have
31 previously demonstrated that the neuronal index of mismatch negativity is composed of
32 two elements i.e., repetition suppression and prediction error, while others have shown
33 that these MMN-like responses are reduced after administration of acute high doses of
34 NMDA antagonists in animal models. Therefore, our main goal was to test whether and
35 how a low acute dose of the NMDA-R antagonist, MK-801 affects repetition
36 suppression and prediction errors along the rat auditory thalamocortical pathway.
37 Results demonstrate enhanced prediction error neuronal responses at cortical level,
38 while repetition suppression is profoundly affected in the thalamus. Moreover, our
39 results demonstrate that MK-801 alters the dynamics of neuronal adaptation along the
40 thalamocortical axis, becoming faster and stronger especially at thalamic level. These
41 single unit data correlate with the recordings of large-scale responses. Our study opens
42 new avenue for future research in the development of safe compounds for human use
43 that target similar binding locations to MK-801.

44

45

46

47

48 **Keywords:** Mismatch negativity, predictive coding, prediction error, repetition
49 suppression, schizophrenia, auditory.

50

51 **Abbreviations:** **AC**, auditory cortex; **AC_L**, auditory cortex lemniscal; **AC_{NL}**, auditory
52 cortex non-lemniscal; **CAS**, cascade paradigm; **DEV**, deviant stimulus; **ERP**, event-
53 related potential; **FDR**, false discovery rate; **iMM**, index of neural mismatch; **iPE**,
54 index of prediction error; **iRS**, index of repetition suppression; **LFP**, local field
55 potential; **MGB**, medial geniculate body; **MGB_L**, medial geniculate body lemniscal
56 subdivision; **MGB_{NL}**, medial geniculate body non-lemniscal subdivision; **MMN**,
57 mismatch negativity; **NMDA-R**, N-methyl-D-aspartate Receptor; **PSTH**, peri-stimulus
58 time histogram; **SDF**, spike-density function; **STD**, standard stimulus; **TRN**, thalamic
59 reticular nucleus;

60

61

62

63

64

65

66

67 INTRODUCTION

68 The mismatch negativity (MMN) is an auditory event-related potential (ERP)
69 that occurs when an unexpected stimulus (the deviant, DEV) interrupts a train of
70 expected stimuli (standards, STD) in an *oddball* sequence. The MMN is commonly
71 quantified as the difference between the size of the DEV ERP response and the size of
72 the STD response (Näätänen *et al.*, 1978).

73 The predictive coding framework has emerged as an appealing model of MMN
74 (Randeniya *et al.*, 2018) and of how sensory information is processed. According to
75 predictive coding, the brain constantly generates top-down predictions from any regular
76 ascending input that is compared with the actual sensory bottom-up signals. Stimuli
77 that match predictions are suppressed, whereas unexpected stimuli discrepant with the
78 prediction generate an enhanced error signal (Carbajal & Malmierca, 2018; Friston,
79 2005; Garrido *et al.*, 2008; Michie *et al.*, 2016). NMDA-R dependent plasticity is
80 believed to underpin the capacity of the brain to adjust internal predictions and use
81 memory of recent past inputs to anticipate future stimuli (Wacongne, 2016).

82 There are two likely mechanisms underlying the MMN signal according to the
83 predictive coding model. First, MMN could reflect *repetition suppression*. When the
84 same stimulus is repeatedly presented, neuronal populations originally sensitive to that
85 stimulus undergo adaptation and neural responses decrease (Bendixen *et al.*, 2007). The
86 repetition suppression has been conclusively demonstrated in the auditory cortex (AC)
87 of animal models, surface recordings in humans as well as along multiple levels of the
88 auditory hierarchy in rodents, including the inferior colliculus in midbrain and medial
89 geniculate body (MGB) in thalamus (Parras *et al.*, 2017).

90 At the same time, MMN could reflect a process of *prediction error*, where the
91 sensory memory of the previously-heard stimuli establishes a predictive model, and the
92 violation of this prediction upon presentation of an unexpected DEV stimuli, results an
93 enhanced neural response that reflects the unexpectedness of the stimuli. Prediction
94 error has been observed in human and rodent surface recordings when suitable control
95 conditions have been included in the design of sound sequences (Lauren Harms et al.,
96 2014; Kurkela et al., 2018; Nakamura et al., 2011; Parras et al., 2017). Single- and
97 multiunit recordings in the rodent auditory system have demonstrated that prediction
98 error responses are hierarchically organized, from midbrain to auditory cortex, and
99 predominate in non-lemniscal areas (Carbajal & Malmierca, 2018; Parras et al., 2017).
100 Therefore, there is strong evidence in both humans and rodents that MMN when
101 extracted as a difference between STD and DEV responses receives contributions from
102 both prediction error and repetition suppression.

103 MMN is found to be altered in number of different clinical conditions. Most
104 notably, persons with schizophrenia have consistently been observed to have reduced
105 MMN amplitude (Bodatsch et al., 2015; Erickson et al., 2016; Umbricht & Krljes,
106 2005). This finding has been replicated in over 100 independent research. For persons
107 with an established illness a large effect size approaching 1 has been observed (Erickson
108 et al., 2016) attesting to the replicability and substantive nature of reduced MMN in
109 schizophrenia. Smaller MMN in schizophrenia has also been found to correlate with
110 impaired cognition, and poorer psychosocial functioning (Light & Braff, 2005; Rasser
111 et al., 2011), leading to the suggestion that MMN may be a useful biomarker for disease
112 progression or risk (Light & Swerdlow, 2015). In humans, acute exposure to the NMDA
113 antagonist ketamine or phencyclidine mimic the full range of schizophrenia symptoms

114 in healthy participants (Krystal et al., 2005), including reduced MMN size (for review
115 see Todd et al., 2013). An observation that posits that NMDA hypofunction underlies
116 the neuropathology of the disorder (Javitt et al., 1996). Importantly, schizophrenia-like
117 impairments and equivalent MMN reduction have been observed after acute
118 administration of NMDA antagonists in animal (Featherstone et al., 2018; Mouri et al.,
119 2007; Harms, 2016; Siegel et al., 2013).

120 Our primary interest in this paper is whether NMDA-R antagonists
121 differentially affect repetition suppression and prediction error. While some studies
122 have demonstrated that MMN-like responses in rodents are altered by NMDA-R
123 antagonists (Ehrlichman et al., 2008; Sivarao et al., 2014; Tikhonravov et al., 2010),
124 only one report has examined the impact of prediction error on the MMN in surface
125 recordings (Harms et al., 2018). There are no reports that have examined their effects on
126 single-unit activity and local field potential recordings from the thalamus and auditory
127 cortex.

128 Thus, it is unknown (i) whether there are differential effects of NMDA-R
129 antagonism on prediction error as opposed to repetition suppression at the single unit or
130 local field potential level, and (ii) the regional specificity of where effects of NMDA-R
131 antagonists occur, for example, in the lemniscal *vs.* non-lemniscal auditory areas, or the
132 thalamus *vs.* cortex. Therefore, in the current study, we use an acute exposure to a low
133 dose of MK-801 to examine the impact of NMDA antagonism on individual responses
134 of MGB and AC neurons while auditory oddball, many standards and cascade control
135 sequences were presented. This design allowed us to delineate effects on repetition
136 suppression *vs.* prediction error (Harms et al., 2016; Opitz et al., 2005; Parras et al.,

137 2017; Ruhnau et al., 2012). Our data show that MK-801 produces differential effects on
138 responses to DEV and STD tones in oddball sequences, affecting the mismatch index
139 along the thalamocortical system. Furthermore, we found an increase in repetition
140 suppression in the thalamic regions, while prediction error responses were enhanced in
141 the cortex.

142

143

144 **MATERIAL AND METHODS**

145 Experiments were performed on 48 (control=25; MK-801=23) adult, female Long-
146 Evans rats with body weights between 200-250g (aged 9 to 15 weeks). All experimental
147 procedures were performed at the University of Salamanca, and all procedures and
148 experimental protocols were in accordance with the guidelines of the European
149 Communities Directive (86/609/EEC, 2003/65/EC and 2010/63/EU) and the RD
150 53/2013 Spanish legislation for the use and care of animals. All the details of the study
151 were approved by the Bioethics Committee of the University of Salamanca (ref#
152 USAL-ID-195).

153 **Surgical procedures:** Anesthesia was induced and maintained with urethane (1.5g/kg,
154 i.p), with supplementary doses (0.5g/kg, i.p) given as needed. Dexamethasone
155 (0.25mg/kg) and atropine (0.1mg/kg) were administered at the beginning of the surgery
156 to reduce brain edema and bronchial secretions, respectively. Isotonic glucosaline
157 solution was administered periodically (5-10ml every 6-8h, s.c) to avoid dehydration.
158 During all experimental procedures, animals were artificially ventilated, and CO₂ and

159 temperature monitored (Ayala & Malmierca, 2015, 2018; Duque & Malmierca, 2015;
160 Duque et al., 2016; Pérez-González et al., 2012).

161 The initial procedure was the same in each case, and the subsequent procedures differed
162 only in the craniotomy location, and the placement/orientation for the recording
163 electrode (animals per group/location: control MGB=16, AC=9; MK-801 MGB=15,
164 AC=8). For MGB recordings, a craniotomy (~2x2mm, from -5 to -6.5mm bregma and -
165 3.5mm lateral) was performed in the left parietal bone, dura was removed and the
166 electrode advanced in a vertical direction (Antunes & Malmierca, 2011, 2010). For AC
167 recordings, the skin and muscle over the left temporal bone was retracted and a 6x5mm
168 craniotomy was performed (between -2 and -6 from Bregma) over the temporal bone
169 (Nieto-Diego & Malmierca, 2016) dura was removed and the area was covered with a
170 thin, transparent layer of agar to prevent desiccation and stabilize recordings. Electrodes
171 for AC recording were inserted using a triple axis micromanipulator (Sensapex),
172 forming a 30° angle with the horizontal plane, to penetrate through all cortical layers of
173 the same cortical column.

174 For this study, animals in MK-801-treated group receive a systemic intraperitoneal
175 injection (0.1mg/kg) of a noncompetitive NMDA-R antagonist (MK-801 hydrogen
176 maleate, M107 Sigma-Aldrich). Control animals did not receive any injection.

177 MGB neurons were localized using Nissl stained cresyl violet and AC neurons were
178 localized after determining the boundaries of tonotopic changes (see Supplementary
179 Material).

180 **Electrophysiological recording procedures.** During all procedures, animals were
181 placed in a stereotaxic frame fixed with hollow specula ear bars that housed the sound

182 delivery system. One single neuron and local field potential (LFP) was recorded at a
183 time, using the same tungsten electrode (1-4M Ω) inserted into a single auditory station
184 (MGB or AC) in each individual animal.

185 For each animal treated with MK-801 the first single neuron was recorded ~15 min after
186 the drug injection (Vezzani et al., 1989). Ten evenly-spaced pure tones (0.5 octaves
187 separation) at a fixed sound intensity (usually 20-30dB above the threshold) were
188 selected to each neuron recorded to create the control sequences, cascades and many-
189 standard (Parras et al., 2017; Ruhnau et al., 2012), and additionally, adjacent pairs of
190 them were used to present various oddball sequences. All sequences were 400 tones in
191 length (75ms duration, 5ms rise-fall ramp and 250ms interstimulus interval), each tone
192 in the control sequences was played 40 times, with the same overall presentation rate as
193 deviants in the oddball sequence (see Supplementary Material).

194 Oddball sequences were used to test the specific contribution of deviant tones in an
195 adaptation context. An oddball sequence consisted of a repetitive tone (standard 90%
196 probability), occasionally replaced by a tone of a different frequency (deviant 10%
197 probability), in a pseudorandom manner. We used two types of control sequences: the
198 many-standard and cascade sequences. Both containing the same 10 frequencies but
199 differing in the order of presentation. The many-standard control was randomly
200 presented, mimicking the presentation rate and the unpredictability of the deviant tones.
201 While cascades were played always in the same presentation order, ascending or
202 descending in frequency (see figure 2b in Supplementary Material). Hence the cascade
203 contains a regularity, mimic the presentation rate of deviant sounds but in a predictable
204 context and consequently do not violate a regularity. These four conditions, and by

205 extension responses to them, will be denoted as deviant (DEV), standard (STD),
206 cascade (CAS) and many-standard. Finally, if the neuron could be held for long enough,
207 the same protocol was repeated for different frequencies and/or intensity.

208 **Statistical analysis.** All the data analyses were performed with MatlabTM software,
209 using the built-in functions, the Statistics and Machine Learning toolbox, or custom
210 scripts and functions developed in our laboratory. A PSTH was used, showing action
211 potential density over time (in action potentials per second) from -75 to 250 ms around
212 stimulus onset, for the 40 trials available for each tone and condition (DEV, STD,
213 CAS). Every PSTH was smoothed with a 6ms gaussian kernel (“ksdensity” function in
214 Matlab) in 1ms steps to estimate the spike-density function (SDF) over the time, and the
215 baseline spontaneous firing rate was determined as the average firing rate during the
216 75ms preceding stimulus onset.

217 The excitatory response was measured as the area below the SDF and above the
218 baseline spontaneous firing rate, between 0 and 180ms after stimulus onset (positive
219 area patches only, to avoid negative response values). This measure will be referred to
220 as “baseline-corrected spike count” (details in Supplementary Material).

221 Baseline-corrected spike count responses of a neuron to the same tone in the three
222 conditions (DEV, STD, CAS) were normalized using the formulas:

223
$$\text{DEV}_{\text{Normalized}} = DEV/N;$$

224
$$\text{STD}_{\text{Normalized}} = STD/N;$$

225
$$\text{CAS}_{\text{Normalized}} = CAS/N;$$

226 Where $N = \sqrt{DEV^2 + STD^2 + CAS^2}$, is the Euclidean norm of the vector (DEV,
 227 STD, CAS) defined by the three responses. This normalization procedure always results
 228 in a value ranging 0–1, and has a straightforward geometrical interpretation.

229 From these normalized responses, indices of neuronal mismatch (iMM), repetition
 230 suppression (iRS), and prediction error (iPE) were computed as:

$$231 \quad iMM = DEV_{Normalized} - STD_{Normalized};$$

$$232 \quad iPE = DEV_{Normalized} - CAS_{Normalized};$$

$$233 \quad iRS = CAS_{Normalized} - STD_{Normalized};$$

234 These indices, consequently, always range between –1 and 1, and provide the
 235 following quantitative decomposition of neuronal mismatch into repetition suppression
 236 and prediction error: $iMM = iRS + iPE$. To test these indices over time, we divided the
 237 whole response into 12 time windows, 20ms width, from -50 to 190ms with respect to
 238 the stimulus onset. Then, we compared each time window against zero using a sign-rank
 239 test, false discovery rate (FDR=0.1) corrected for the 12 windows.

240 For the analysis of the LFP signal, we aligned the recorded wave to the onset of the
 241 stimulus for every trial, and computed the mean LFP for every recording site and
 242 stimulus condition (DEV-LFP, STD-LFP and CTR-LFP), as well as the differences
 243 between them, resulting in the three LFP-indices: “neuronal mismatch” (MM-LFP =
 244 DEV-LFP – STD-LFP), “prediction error” (PE-LFP = DEV-LFP – CAS-LFP) and
 245 “repetition suppression” (RS-LFP = CAS-LFP – STD-LFP). Then, grand-averages were

246 computed for all conditions and auditory station separately. The p value of the grand-
247 averaged for the three LFP-indices (MM-LFP, PE-LFP and RS-LFP) was determined
248 for every time point with a two-tailed t test (FDR corrected).

249 Our data set was not normally distributed, so we used distribution-free (non-
250 parametric) tests. These included the Wilcoxon signed-rank test and Friedman test (for
251 baseline-corrected spike counts, normalized responses, indices of neuronal mismatch,
252 repetition suppression and prediction error). Only the difference wave for the LFPs was
253 tested using a t -test, since each LFP trace is itself an average of 40 waves. For multiple
254 comparison tests, p values were FDR corrected using the Benjamini-Hochberg method.
255 Linear models were used to test for significant average iMM, iPE and iRS within each
256 auditory station. Significant effects of station, pathway, and interactions between them
257 were fitted using the ‘fitlm’ function in Matlab, with robust options. To estimate final
258 sample sizes required for the observed effects after the initial exploratory experiments,
259 we used the ‘sampsizepwr’ function in Matlab adjusted for the iPE for each region, to
260 obtain a statistical power of 0.8 for this index. Sample sizes were enlarged with
261 additional experiments until they were just greater than the minimum required (number
262 of points recorded, and the minimum required for each station; see Table 1).

263 To analyze the time course of adaptation we computed an averaged time course for all
264 the standard stimuli presented. Then, we fitted a power law function with a three
265 parameters model, $y(t) = a \cdot t^b + c$, where a indicates the responses beginning or the
266 first spike strength; b the sensitivity to repetitive stimuli, or the adaptation velocity, and
267 c the steady-state response. R^2 values indicated that the model fits very well for standard

268 responses in both groups, explaining between 60% and 78% of the response variability
269 within all regions.

270 To analyze spikes differences between MK-801 and control group we computed the
271 median values for each condition tested (DEV, STD and CAS) and their differences
272 (iMM, iRS and iPE) and calculated a ranksum test. To compare each time window
273 between groups a two-sample *t*-test (from 0 to 200ms, Bonferroni corrected for 200
274 comparisons with family-wise error rate FWER < 0.05) was used for the SDF and LFPs
275 to each stimulus condition and indices, using the 'ttest2' function in Matlab, for every
276 time point.

277 **Data availability.** The data that support the findings of this study are available from the
278 corresponding author on reasonable request.

279

280 **RESULTS**

281 We recorded a total of 290 well isolated neurons, 143 from the control group and 147
282 from the MK-801-treated group. Since we found no statistically significant differences
283 between the use of the cascade and many-standards sequences for the control group and
284 MK-801 group, except for the MGB_{NL} from the MK-801 group (table 1), the CAS
285 sequence was chosen to control for repetition effects. This is because the CAS paradigm
286 not only controlled for the presentation rate of the deviant stimuli, but also the
287 frequency difference (ascending or descending) between standards and deviants in the
288 oddball sequences.

289 **Effects of MK-801 on the neuronal firing rate.** MK-801 injection significantly
290 reduced the responses to STD tones within all regions. By contrast, for responses to the
291 DEV tones, we observed a significant increment in responses in AC but not for the
292 MGB. When the firing rate of the cascade sequence was considered, MK-801
293 differentially affected the AC and MGB such that CAS responses were significantly
294 increased in the MGB_{NL} but decreased in AC. These results reveal a differential effect
295 of MK-801 on the refractoriness and salience of infrequent events at the single neuron
296 level (Figure 1a, table 2).

297 **Effects of MK-801 on neuronal mismatch and its components.** Next we analyzed the
298 differences between these normalized responses and computed three indexes (ranging
299 between -1 and +1): 1) the index of neuronal mismatch ($iMM = DEV - STD$), similar to the
300 typical SSA index used in previous single neurons studies; 2) the index of prediction
301 error ($iPE = DEV - CAS$), that shows the relative enhancement of DEV tones compared
302 with CAS tones and 3) the index of repetition suppression ($iRS = CAS - STD$) that
303 reflects the level of response suppression due to the repetition effect, and is obtained by
304 comparing the normalized responses to CAS and STD. It should be noted that the iMM
305 is the sum of iRS and iPE ($iMM = iRS + iPE$).

306 The analysis of the iMM after the injection of MK-801 demonstrated that iMM values
307 are significantly different from zero for all recording sites (figure 1b, table 1: Friedman
308 test). But when comparisons between groups were considered, the analysis revealed that
309 MK-801 increased the neuronal iMM (figure 1b- iMM ; table 2). As described above,
310 these changes are largely due to a reduced response to STD tones in all recording
311 locations and an enhanced response to DEV in the AC.

312 Since $iMM=iRS+iPE$, an important advantage of these metrics is that we can determine
313 how much of the mismatch index is due to the regularity of the context (RS) and/or to
314 the occurrence of an infrequent event (PE). Thus, to determine which of these two
315 components of the iMM is affected by MK-801, we computed the indices of iPE and
316 iRS separately.

317 Interestingly, MGB neurons in the MK-801 group did not show any sign of genuine
318 deviance detection, as iPE values were almost zero and negative. While both AC
319 showed a significant positive iPE (figure 1c; iPE values in table 1). When comparison
320 between groups were analyzed an increased iPE for the MK-801 group in the AC were
321 found, and even a further decreased iPE for the MGB_{NL} in the MK-801 group (figure 1c
322 and e light and bright oranges; iPE in table 2). These data suggest that the MK-801
323 produces an augmentation of saliency for novel stimuli processed in the AC.

324

325 Yet, the detection of rare or novel stimuli requires the establishment of a regular context
326 or pattern. Therefore, we were also interested to find out if the refractoriness due to
327 regularity was altered by MK-801. We calculated the iRS by assessing the response of
328 the same tone when it was presented as CAS, with a 10% probability in a regular pattern
329 and presented as STD with a probability of 90%, within an oddball paradigm, so it is in
330 a much more regular context (Harms et al., 2014; Ruhnau et al., 2012). In both cases,
331 we assume some level of regularity adaptation, but only a genuine repetition
332 suppression can be determined if the responses to STD tones are lower than responses
333 to CAS. Our results demonstrate that there is a significant repetition suppression effect
334 in the MK-801 group along the thalamocortical pathway (figure 1d bright blue; iRS in

335 table 1). The analysis also revealed that MK-801 produced a significant increase in
336 repetition suppression at thalamic level but did not affect repetition suppression in the
337 AC when compared with controls (figure 1d-e light and bright blues; results in table 2).

338 These results show that the auditory thalamus and cortex differ in the way repetition
339 effects and prediction errors are processed. To confirm this hypothesis and considering
340 that we have previously found an increase in the level of iPE along the thalamocortical
341 hierarchy in awake and anesthetized animals (Parras et al., 2017), we fitted a linear
342 model to assess if there is a similar increase in iPE along the thalamocortical pathway
343 under MK-801. Using station (MGB and AC) and pathway (Lemniscal vs. Non-
344 lemniscal) and their interaction as categorical factors, if MGB_L is used as reference
345 level for these factors, the fitted model is as follows: $iPE = -$
346 $0.131 + 0.094 \cdot NL + 0.469 \cdot AC + 0.091 \cdot NL \cdot AC$. Next, we applied an ANOVA to this model
347 and found a significant effect of station ($F=196.85$, $p=3.65 \times 10^{-39}$) and pathway
348 ($F=13.19$, $p=3.02 \times 10^{-4}$) but not for the interaction ($F=1.54$, $p=0.2138$). A subsequent
349 *post hoc* analysis confirmed that the iPE was higher at the MGB_{NL} and AC ($p < 0.05$
350 within all comparisons). These results indicate that indeed, the sensitivity to detect
351 novel stimuli increase significantly along the thalamocortical axis in the MK-801 group
352 (figure 1e, iPE in orange).

353 Similarly, we also fitted a linear model for iRS in the MK-801 group. The resulting
354 model was: $iRS = 0.6412 - 0.0987 \cdot NL - 0.2753 \cdot AC + 0.0180 \cdot AC \cdot NL$. The ANOVA
355 demonstrate a significant effect for both categories (Station $F=108.07$, $p < 0.000$,
356 Pathway $F=13.23$, $p < 0.000$), but not for the interaction ($F=0.1211$, $p=0.7280$). The *post*
357 *hoc* comparisons confirmed decreasing levels of repetition suppression as one ascends

358 along the hierarchy from thalamus to cortex and from lemniscal to non-lemniscal
359 [figure 1e, iRS in blue; $MGB_L > MGB_{NL}$ ($p < 0.000$), from $MGB_L > AC_L$ ($p < 0.000$) and
360 from $MGB_{NL} > AC_{NL}$ ($p < 0.000$); but not from AC_L to AC_{NL} ($p = 0.0810$)].

361 In summary, the changes described above demonstrate that NMDA-R antagonism has
362 distinct effects on auditory scene analysis, as measured by the iPE and iRS, at different
363 levels of the thalamocortical hierarchy.

364

365 **Effect of MK-801 on Spike-Density Function and indexes.** Next, we sought to
366 identify how MK-801 affected the temporal responses to auditory stimuli (DEV, STD
367 and CAS) by comparing spike-density functions (SDF) to each condition between
368 groups. Analysis revealed the latency of the main peak for the SDF to DEV tones was
369 mostly unaffected by MK-801 in the MGB, but it was clearly delayed by 40 and 60 ms
370 in the AC_L and AC_{NL} , respectively. Furthermore, the magnitude of the SDF was altered
371 at the AC and MGB_{NL} , with the early component being reduced and the later sustained
372 component being enhanced (figure 2a, horizontal white line for significant differences
373 at $p < 0.05$). When the STD tones were considered, we observed a distinct and significant
374 decrease of the SDF mostly at the AC and only marginally at the subcortical levels
375 (figure 2b). Finally, MK-801 affected mostly the initial responses to cascade tones at all
376 regions, being reduced in the auditory cortex but was earlier and increased in MGB_L
377 (figure 2c). The sustained portion of the SDF was only significantly increased in the
378 MGB_{NL} . Results show that MK-801 has a profound effect on the spike-density
379 functions to DEV, STD and cascade stimuli.

380 Next, we studied where and when the MK-801 effect on the neuronal indices of iMM,
381 iPE and iRS was significantly different from control. Thus, we examined whether in
382 each group independently (MK-810 and control) these indices are different from zero,
383 *i.e.*, is there a significant iMMN, iPE or iRS at each time point. Figure 2d-f highlights
384 the significant time windows ($p < 0.01$) with white and black asterisks for control and
385 MK-801, respectively. The analysis revealed that under MK-801, there was a significant
386 iMM along the thalamocortical axis (between 20-40ms for MGB_L, 20-80ms in MGB_{NL}
387 and from 20-190ms in both AC; Figure 2d, bright purple lines) and a significant iPE
388 between 20 and 180ms in both AC, and a late iPE in the lemniscal thalamus between
389 60-80ms and 140-190ms (Figure 2e, bright orange lines). We also found significant
390 thalamocortical iRS (figure 2f, bright cyan lines; between 20-40ms for MGB_L, 0-100ms
391 in MGB_{NL}, from 20-120ms in AC_L and between 40-100ms in AC_{NL}).

392 When we compared the two groups, the analysis revealed that MK-801 produced a
393 significant enhancement of iMM and iPE at both AC subdivisions ($p < 0.000$ for iMM
394 between 60-190ms in both AC; and $p < 0.05$ for iPE ranging between 100 and 190ms in
395 AC_L and between 60-190ms in AC_{NL}; white horizontal lines in Figures 2 d-f). By
396 contrast, iRS was affected more in the MGB ($p < 0.000$ between 5-35ms in MGB_L;
397 $p < 0.000$ between 40-110ms in MGB_{NL}; $p < 0.05$ between 60-130ms in AC_L; and $p < 0.05$
398 at 80ms in AC_{NL}; white horizontal lines in Figure 2f). Thus, MK-801 produce an
399 increase of iMM and iPE mostly in the late time window in AC, while iRS is much
400 affected in the MGB.

401

402 **MK-801 affects the dynamics of adaptation.** Since MK-801 lowered and flattened
403 responses to STD tones across the response window, we sought to assess the dynamics
404 and the time course of adaptation (figure 3a). Results show that the control group (light
405 gray arrows) exhibit a hierarchical timing for adaptation responses, becoming faster in
406 higher order areas (from top to down, responses reach the half of the initial values at the
407 fourth, ninth, twelfth and fourteenth standard tone, respectively). By contrast, results
408 from the MK-801 group exhibited much faster adaptation dynamics (figure 3b; 50% of
409 the initial response occurred at the third and second standard tones in MGB and AC,
410 respectively; *b* values for control group: $MGB_L = -0.1769$, $MGB_{NL} = -0.4174$, $AC_L = -$
411 0.6824 and $AC_{NL} = -1.175$; and for MK-801 group: $MGB_L = -0.8499$, $MGB_{NL} = -0.8853$,
412 $AC_L = -1.712$ and $AC_{NL} = -1.418$).

413 These data reveal that MK-801 alters the timing across the hierarchical organization of
414 the auditory system, resulting in the lemniscal thalamus having almost the same
415 adaptation velocity as the non-lemniscal cortex (arrows in Figure 3-b). Furthermore,
416 MK-801 reduces (almost by half) the steady-state plateau in the AC (dotted lines in
417 Figure 3b; *c* values for control group: $MGB_L = 0.0776$, $MGB_{NL} = 0.2908$, $AC_L = 0.6084$
418 and $AC_{NL} = 0.7740$; and for MK-801 group: $MGB_L = 0.1428$, $MGB_{NL} = 0.2884$,
419 $AC_L = 0.3523$ and $AC_{NL} = 0.3834$).

420 All these results together support the idea that MK-801 produces a differential effect on
421 adaptation and deviance detection along the thalamocortical axis, providing new
422 evidence of a change in the firing pattern and temporal responses at single neuron level.

423

424 **Delayed and broader larger-scaled LFP responses.** Next, we wanted to check if the
425 single unit responses correlated with larger-scale measurements of neuronal activity.
426 The analysis of local field potentials (LFP) revealed that MK-801 produced significant
427 changes in MGB_{NL} and AC (both in the lemniscal and non-lemniscal portions) for the
428 deviant, standard and cascade LFPs (Figure 4a-c), such that they exhibited broader and
429 longer responses for DEV-LFP and CAS-LFP in the auditory cortex, while the
430 waveforms of these LFPs were shifted in latency for the MGB_{NL} due to a progressive
431 delay of N1, P1 and N2 (note that this terminology refers to the first negative peak, first
432 positive peak and second negative peak), showing delayed peaks of 8, 14 and 57ms for
433 DEV-LFP and 6, 26 and 45ms delay for CAS-LFP in N1, P1 and N2, respectively
434 (DEV-LFP: N1 peak for MK-801= $-6.6\mu V$ at 20ms and control= $-1.5\mu V$ at 12ms; P1
435 peak for MK-801= $6.9\mu V$ at 41ms and control= $6.8\mu V$ at 28ms; finally, N2 peak for MK-
436 801= $-5.4\mu V$ at 102ms and control= $-10.2\mu V$ at 45ms. CAS-LFP: N1 peak for MK-
437 801= $-6.5\mu V$ at 18ms and control= $-1.2\mu V$ at 12ms; P1 peak for MK-801= $5.1\mu V$ at
438 53ms and control= $10.6\mu V$ at 27ms; finally, N2 peak for MK-801= $-5.0\mu V$ at 91ms and
439 control= $-10.3\mu V$ at 45ms).

440 Similarly, we also sought significant LFP signals for each computed index (Figure 4d-
441 f). The horizontal colored lines highlight the time at which significant deflections occur
442 to each index-LFP for control and MK-801 groups independently (light and bright
443 horizontal lines, respectively). Additionally, we compared these LFP indices between
444 groups. The analysis of the MM-LFP shows that MK-801 elicited stronger and broader
445 deflections within all regions (horizontal bright purple lines; Figure 4d) and abolished
446 the late negative component (N2) in the AC (MGB_L : N2 = 114-157ms; MGB_{NL} : N1 =

447 12-21ms, P1 = 32-63ms and N2 = 75-135ms; AC_L: N1 = 10-57ms and P1 = 60-147ms;
448 AC_{NL} N1 = 20-53 and P1 = 60-144ms). Our data also demonstrate that MK-801
449 produced a higher MM-LFP for virtually the whole LFP response within MGB_{NL} and
450 both AC, while no differences occurred in MGB_L.

451 Similar to the spike population analysis, and considering that the PE-LFP and RS-LFP
452 both contribute to the MM-LFP, we also wanted to understand how MK-801 shapes the
453 LFP for prediction error and repetition suppression. In response to MK-801, the PE-LFP
454 waveform was reduced at the early component of the MGB_{NL}, while it was increased
455 and delayed for the AC (orange horizontal lines in Figure 4e). Moreover, MK-801 also
456 abolished the N2 deflection (MGB_{NL}: N1 = 99-146ms; AC_L: N1 = 30-65ms and P1 =
457 87-180ms; AC_{NL} N1 = 30-67 and P1 = 106-180ms). When PE-LFP was compared
458 between groups, we only found differences in AC, mainly at the early (50-70ms) and
459 late components (120-180ms). In other words, the lemniscal thalamus does not exhibit
460 deviance detection, neither at the single neuron level nor at large-scale responses. Hence
461 PE-LFP confirm single unit population data, where MK-801 produced greater levels of
462 deviance detection in the auditory cortex (figure 1e).

463 Finally, MK-801 had similar effects on RS-LFP to those described above for MM-LFP
464 and PE-LFP, eliciting broader and larger waveforms for MGB_{NL} and AC (Figure 4f;
465 MGB_{NL}: N1 = 10-28ms, P1 = 34-63ms and N2 = 73-108ms; AC_L: N1 = 10-55ms, P1 =
466 67-140ms and N2 = 148-180ms; AC_{NL}: N1 = 10-51, P1 = 55-132ms and N2 = 141-
467 180ms). When differences between groups are considered, the non-lemniscal thalamus
468 exhibited a shift in the waveform between 15-100ms, while for the cortex, responses
469 over virtually the whole temporal window were increased by MK-801.

470 **DISCUSSION**

471 In this study, we demonstrate that the neuronal index derived from single cell
472 recordings of mismatch is profoundly affected along the auditory thalamocortical
473 system in rats treated acutely with a low dose of the NMDA-R antagonist, MK-801.
474 Importantly, we also reveal that the two elements that make up the index of mismatch
475 negativity, i.e., repetition suppression and prediction error, are differentially affected by
476 MK-801 in single neurons at auditory thalamus and cortex. MK-801 increases repetition
477 suppression in thalamus and prediction error in cortex. The increase in repetition
478 suppression is more prominent in lemniscal areas of the thalamus, while the increase in
479 prediction error is more evident in the non-lemniscal areas of cortex. Furthermore, our
480 results demonstrate that MK-801 alters the dynamics of neuronal adaptation along the
481 thalamocortical axis, becoming faster and stronger especially at thalamic level. These
482 single unit data correlate with the recordings of large-scale responses, LFPs, as they
483 exhibit delayed and broader deflections. In summary, our work demonstrates that the
484 MK-801 increase of the neuronal mismatch in the auditory cortex 60ms after stimulus
485 onset is due to the combined effect of an increment in the sustained responses to deviant
486 tones and a decrease to standard tones. It should be noted that, in contrast to most
487 previous studies using large scale recording procedures to study neuronal population
488 activity in rodents such as LFPs or EEG via skull screws, we have also recorded single-
489 unit activity, an excellent technique for revealing activity patterns that are present at the
490 single neuron level.

491 It is well established that NMDA-R plays a fundamental role in neuronal
492 plasticity, controlling long-term potentiation and depression (Blanke & VanDongen,

493 2009). Further, it is generally accepted that human MMN is reduced after NMDA-R
494 antagonist treatments because NMDA-R antagonist blocks synaptic plasticity,
495 precluding the formation of a memory trace for the standard tones (Todd et al., 2013).
496 As we have seen in our results, MK-801 reduces responses to standard tones thus
497 increasing repetition suppression.

498 Although this finding supports the hypothesis that NMDA-R antagonists alter
499 sensory-memory formation (Aukstulewicz & Friston, 2016), the findings that low dose
500 (0.1 mg/kg) MK-801 treatment produces a significant increment in the response to the
501 deviant tones, in prediction error and hence, an increment in the neuronal mismatch are
502 in the opposite direction to those expected. It is clear that the role of NMDA-R in the
503 generation of MMN is considerably more complex than thought (Näätänen et al., 2007).
504 There have been suggestions in the literature of precedents for our observations. Even
505 considering that MK-801 has 160 times the affinity of ketamine to NMDA-R,
506 necessitating higher ketamine doses for similar drug effect (Schuelert et al., 2018), our
507 results conform with those that report an increment in amplitude and latencies to deviant
508 responses after the acute ketamine treatment in rats (Ahnaou et al., 2017) and with a
509 sub-anaesthetic dose of ketamine in healthy humans producing larger N100 to deviant
510 tones but not MMN (Oranje et al., 2000). Interestingly, a dose response study of the
511 MK-801 effects on MMR-like responses in male rats showed that while a high dose
512 (0.5mg/kg) reduced late deviance detection (around 55ms), a medium dose (0.3mg/kg)
513 significantly enhanced early deviance detection effects (at about 13 ms) and some
514 evidence of enhanced late effects although not significantly (Harms et al., 2018). We
515 used a single dose of 0.1mg/kg, as it has been demonstrated that female rats are more
516 sensitive to MK-801 than males (Andine et al., 1999) and that this dose is enough to

517 induce behavioral/sex effects (Meehan et al., 2017). Importantly, memantine, a low
518 affinity uncompetitive agonist of NMDA-R, has been shown to increase (i) the duration
519 of rodent MMN-like responses (Tikhonravov et al., 2010), (ii) increase MMN amplitude
520 in healthy individuals (Korostenskaja et al., 2007), and (iii) in persons with
521 schizophrenia (Swerdlow et al., 2016).

522 The memantine results suggest an interpretation of our findings in terms of the
523 mechanisms underpinning synaptic plasticity (Slutsky et al., 2004). Partial blockade of
524 NMDA-R channels (such as mediated by memantine, or low dose MK-801) is also
525 likely to reduce background calcium flux resulting in homeostatic upregulation of
526 NR2B-containing NMDA-Rs leading in turn to the conversion of synapses to a plastic
527 state. That is, while these drugs reduce calcium influx during uncorrelated activity,
528 there is increased calcium influx during correlated activity (produced by physiological
529 stimuli), increased signal to noise, facilitated transmission and increased plasticity
530 (Abumaria et al., 2011; Slutsky et al., 2010).

531 Other characteristics of the neuronal mechanisms and microcircuitry involving
532 the glutamate NMDA-R system are relevant to the effects we have observed on the
533 neuronal mismatch after the MK-801 treatment. NMDA-R are located, not only at
534 postsynaptic and presynaptic sites in excitatory neurons, but they are also found at
535 GABAergic inhibitory interneurons in neocortex (DeBiasi et al., 1996). MK-801 have
536 demonstrated a preferential regulation of the firing rate of cortical GABA interneurons,
537 increasing the firing rate of the majority of pyramidal neurons (Homayoun &
538 Moghaddam, 2007) and therefore producing an imbalance in the excitatory/inhibitory
539 networks in the cortices (Javitt et al., 2018; Okada et al., 2019). It is well known that
540 cortical GABAergic interneurons differentially amplify stimulus-specific adaptation (a

541 similar phenomenon to iMM) in excitatory pyramidal neurons in auditory cortex (Chen
542 et al., 2015). Moreover, a model of a mutually coupled excitatory/inhibitory network
543 can explain distinct mechanisms that allow cortical inhibitory neurons to enhance the
544 brain's sensitivity to deviant or unexpected sounds (Natan et al., 2015). Further MK-
545 801 would alter the tonic inhibitory control of NMDA-R in cortical areas leading to the
546 activation of pyramidal neurons by subsequent deviant tones.

547 The increased repetition suppression we observed in the medial geniculate body
548 can also be by the altered excitatory/inhibitory balance. Although the rat MGB lacks
549 GABAergic neurons, it receives GABAergic input from the thalamic reticular nucleus
550 (TRN) and the inferior colliculus (Malmierca, 2003; Winer et al., 1999). The latter is a
551 source of bottom-up inhibitory influences while the TRN provides the MGB with an
552 indirect and inhibitory feedback activation from AC (Bartlett, 2013). Cortical
553 stimulation hyperpolarizes TRN neurons and increases their inhibitory output to the
554 MGB (Crabtree et al., 2013) and furthermore, TRN has been demonstrated to
555 profoundly influence SSA in the MGB (Yu et al., 2009). Changes in the thalamocortical
556 neuronal firing pattern of thalamic neurons into bursts have been suggested to provide
557 an alerting signal to the cortex to enhance stimulus detection (Hu & Agmon, 2016).
558 Overall our results match the general concept that when the system is adapted, it is more
559 sensitive to detect changes in the environment (Musall et al., 2014), where a stronger
560 thalamic repetition suppression (or inhibition) support the increase in the prediction
561 error signals (excitatory) at cortical level, or vice versa. It would be very interesting to
562 test whether thalamic repetition suppression is correlated with cortical prediction error
563 signals, but this question awaits future experiments.

564 Our study is important because it has revealed the involvement of two basic
565 mechanisms, i.e., repetition suppression and prediction error; and two different
566 pathways, lemniscal and non-lemniscal, underlying the neuronal mismatch in the
567 thalamocortical hierarchy. Accordingly, with the predictive coding theory which
568 suggest that the brain is constantly trying to minimize the discrepancy between actual
569 sensory input and internal representations of the environment (Friston, 2005; Rauss &
570 Pourtois, 2013). What is new in our data is the critical importance of the hierarchical
571 organization of the auditory system in sharing the ‘responsibility’ for generating the
572 representation and detecting the discrepancy, largely attributable to thalamic and
573 cortical processes. While altering the balance between the predictive signal and
574 predictive-error signal may underlie the aberrant perception of psychotic disorders
575 (Sterzer et al., 2018), our data provide evidence that the NMDA-synaptic plasticity and
576 MMN relationship is not as simple as previously surmised from human studies.
577 Moreover, here we have only tackled the functional role of the NMDA-R under a
578 particular experimental manipulation and we cannot exclude the possibility that larger
579 doses of MK-801 would have generated different results. It is also well known that
580 other neuromodulatory systems such as the dopaminergic, cholinergic and/or
581 cannabinoid systems maybe altered and interact with the NMDA receptors in normal
582 brain function (Ayala et al., 2016; Valdés-Baizabal et al., 2017) and schizophrenia
583 patients (Coyle et al., 2010; Howes & Kaar, 2018; Lucatch et al., 2018; Musty et al.,
584 2000; Okada et al., 2019; Parr & Friston, 2018)). Thus, futures studies of schizophrenia
585 in animal models should also consider these interactions.

586 What are the implications of our findings for schizophrenia? If a safe drug
587 were available that targeted the relevant NMDA-R subunit, and facilitated

588 neuroplasticity as indexed by an increased MMN even for a short time period, it offers
589 opportunities for interventions to remediate cognitive deficits that are a core feature of
590 schizophrenia (Green et al., 2000). Memantine which has been shown to increase
591 MMN amplitude in healthy individuals and in schizophrenia has been used as an
592 adjunctive therapy in schizophrenia for some time to improve cognition in particular.
593 While effects of adjunctive therapy are small, recent meta-analysis suggests that there
594 are improvements in global measures of cognition, but improvements in more sensitive
595 composite cognitive test scores were not observed (Kishi et al., 2018). To date, there
596 have been no attempts to utilize MMN response to memantine as an index of
597 neuroplasticity that could be exploited in remediation studies. Interestingly, both the
598 moderate affinity antagonist, memantine, and high affinity antagonist, MK-801, bind to
599 the NR2B subunit of the NMDA-R at very similar binding locations (Song et al., 2018)
600 but only memantine has been approved for use in humans given evidence of neurotoxic
601 effects of MK-801 in humans (Olney et al., 1989). One avenue of future research is the
602 development of safe compounds for human use that target similar binding locations to
603 memantine and MK-801.

604

605 **Acknowledgements**

606 We thank Drs. Javier Nieto-Diego and David Perez-Gonzalez for their technical support
607 and constructive criticisms; and Nashat Abumaria and Juanita Todd for advice and
608 constructive comments on the discussion. We also thank Ms. Marianny Janiree Pernía
609 Rosales for helping with the histological photomicrography and Mr. Antonio Rivas
610 Cornejo for the technical support.

611 **Funding**

612 Financial support was kindly provided by the Spanish MINECO (SAF2016-75803-P)
613 and JCYL (SA023P17) to MSM. GGP held a fellowship from the Spanish MINECO
614 (BES-2014-069113) and CVB held a fellowship from Mexican CONACyT (216652).
615 LH was supported by an NHMRC project grant: APP1109283.

616

617 **Competing interest.**

618 The authors report no competing interests.

619

620 **REFERENCES**

621 Abumaria, N., Yin, B., Zhang, L., Li, X.-Y., Chen, T., Descalzi, G., ... Liu, G. (2011).
622 Effects of elevation of brain magnesium on fear conditioning, fear extinction, and
623 synaptic plasticity in the infralimbic prefrontal cortex and lateral amygdala. *The*
624 *Journal of Neuroscience : The Official Journal of the Society for Neuroscience*,
625 *31*(42), 14871–14881.

626 Ahnaou, A., Huysmans, H., Van de Castele, T., & Drinkenburg, W. H. I. M. (2017).
627 Cortical high gamma network oscillations and connectivity: a translational index
628 for antipsychotics to normalize aberrant neurophysiological activity. *Translational*
629 *Psychiatry*, *7*(12), 1285.

630 Andine, P., Widermark, N., Axelsson, R., Nyberg, G., Olofsson, U., Martensson, E., &
631 Sandberg, M. (1999). Characterization of MK-801-Induced Behavior as a Putative

- 632 Rat Model of Psychosis. *J. Pharmacol. Exp. Ther.*, 290(3), 1393–1408.
- 633 Antunes, F. M., & Malmierca, M. S. (2011). Effect of auditory cortex deactivation on
634 stimulus-specific adaptation in the medial geniculate body. *The Journal of*
635 *Neuroscience : The Official Journal of the Society for Neuroscience*, 31(47),
636 17306–17316.
- 637 Antunes, F. M., Nelken, I., Covey, E., & Malmierca, M. S. (2010). Stimulus-Specific
638 Adaptation in the Auditory Thalamus of the Anesthetized Rat. *PLoS ONE*, 5(11),
639 e14071.
- 640 Auksztulewicz, R., & Friston, K. (2016). Repetition suppression and its contextual
641 determinants in predictive coding. *Cortex; a Journal Devoted to the Study of the*
642 *Nervous System and Behavior*, 80, 125–140.
- 643 Ayala, Y. A., & Malmierca, M. S. (2015). Cholinergic Modulation of Stimulus-Specific
644 Adaptation in the Inferior Colliculus. *Journal of Neuroscience*, 35(35), 12261–
645 12272.
- 646 Ayala, Yaneri A., & Malmierca, M. S. (2018). The effect of inhibition on stimulus-
647 specific adaptation in the inferior colliculus. *Brain Structure and Function*, 223(3),
648 1391–1407.
- 649 Ayala, Yaneri A., Pérez-González, D., Duque, D., Palmer, A. R., & Malmierca, M. S.
650 (2016). Extracellular Recording of Neuronal Activity Combined with
651 Microiontophoretic Application of Neuroactive Substances in Awake Mice.
652 *Journal of Visualized Experiments*, (111), 1–10.
- 653 Bartlett, E. L. (2013). The organization and physiology of the auditory thalamus and its

- 654 role in processing acoustic features important for speech perception. *Brain and*
655 *Language*, 126(1), 29–48.
- 656 Bendixen, A., Roeber, U., & Schröger, E. (2007). Regularity extraction and application
657 in dynamic auditory stimulus sequences. *Journal of Cognitive Neuroscience*,
658 19(10), 1664–1677.
- 659 Blanke, M. L., & VanDongen, A. M. J. (2009). *Activation Mechanisms of the NMDA*
660 *Receptor (Chapter 13). Biology of the NMDA Receptor*. CRC Press/Taylor &
661 Francis.
- 662 Bodatsch, M., Brockhaus-Dumke, A., Klosterkötter, J., & Ruhrmann, S. (2015).
663 Forecasting Psychosis by Event-Related Potentials—Systematic Review and
664 Specific Meta-Analysis. *Biological Psychiatry*, 77(11), 951–958.
- 665 Carbajal, G. V., & Malmierca, M. S. (2018). The Neuronal Basis of Predictive Coding
666 Along the Auditory Pathway: From the Subcortical Roots to Cortical Deviance
667 Detection. *Trends in Hearing*. SAGE Publications.
- 668 Chen, I.-W., Helmchen, F., & Lutcke, H. (2015). Specific Early and Late Oddball-
669 Evoked Responses in Excitatory and Inhibitory Neurons of Mouse Auditory
670 Cortex. *Journal of Neuroscience*, 35(36), 12560–12573.
- 671 Coyle, J. T., Balu, D., Benneyworth, M., Basu, A., & Roseman, A. (2010). Beyond the
672 dopamine receptor: novel therapeutic targets for treating schizophrenia. *Dialogues*
673 *in Clinical Neuroscience*, 12(3), 359–382.
- 674 Crabtree, J. W., Lodge, D., Bashir, Z. I., & Isaac, J. T. R. (2013). GABAA, NMDA and
675 mGlu2 receptors tonically regulate inhibition and excitation in the thalamic

- 676 reticular nucleus. *European Journal of Neuroscience*, 37(6), 850–859.
- 677 DeBiasi, S., Minelli, A., Melone, M., & Conti, F. (1996). Presynaptic NMDA receptors
678 in the neocortex are both auto- and heteroreceptors. *NeuroReport*, 7(15–17), 2773–
679 2776.
- 680 Duque, D., & Malmierca, M. S. (2015). Stimulus-specific adaptation in the inferior
681 colliculus of the mouse: anesthesia and spontaneous activity effects. *Brain
682 Structure and Function*, 220(6), 3385–3398.
- 683 Duque, D., Wang, X., Nieto-Diego, J., Krumbholz, K., & Malmierca, M. S. (2016).
684 Neurons in the inferior colliculus of the rat show stimulus-specific adaptation for
685 frequency, but not for intensity. *Scientific Reports*, 6, 24114.
- 686 Ehrlichman, R. S., Maxwell, C. R., Majumdar, S., & Siegel, S. J. (2008). Deviance-
687 elicited changes in event-related potentials are attenuated by ketamine in mice.
688 *Journal of Cognitive Neuroscience*, 20(8), 1403–1414.
- 689 Erickson, M. A., Ruffle, A., & Gold, J. M. (2016). A Meta-Analysis of Mismatch
690 Negativity in Schizophrenia: From Clinical Risk to Disease Specificity and
691 Progression. *Biological Psychiatry*, 79(12), 980–987.
- 692 Featherstone, R.E., Melnychenko O., & Siegel S.J. (2018). Mismatch negativity in
693 preclinical models of schizophrenia. *Schizophrenia Research*, 191:35-42.
- 694 Friston, K. (2005). A theory of cortical responses. *Philosophical Transactions of the
695 Royal Society B: Biological Sciences*, 360(1456), 815–836.
- 696 Garrido, M. I., Friston, K. J., Kiebel, S. J., Stephan, K. E., Baldeweg, T., & Kilner, J.
697 M. (2008). The functional anatomy of the MMN: a DCM study of the roving

- 698 paradigm. *NeuroImage*, 42(2), 936–944.
- 699 Green, M. F., Kern, R. S., Braff, D. L., & Mintz, J. (2000). Neurocognitive deficits and
700 functional outcome in schizophrenia: are we measuring the “right
701 stuff”? *Schizophrenia Bulletin*, 26(1), 119–136.
- 702 Harms, L., Fulham, W. R., Todd, J., Meehan, C., Schall, U., Hodgson, D. M., & Michie,
703 P. T. (2018). Late deviance detection in rats is reduced, while early deviance
704 detection is augmented by the NMDA receptor antagonist MK-801. *Schizophrenia
705 Research*, 191, 43–50.
- 706 Harms, L. (2016). Mismatch responses and deviance detection in N-methyl-D-aspartate
707 (NMDA) receptor hypofunction and developmental models of schizophrenia.
708 *Biological Psychology*, 116, 75–81.
- 709 Harms, Lauren, Fulham, W. R., Todd, J., Budd, T. W., Hunter, M., Meehan, C., ...
710 Michie, P. T. (2014). Mismatch negativity (MMN) in freely-moving rats with
711 several experimental controls. *PloS One*, 9(10), e110892.
- 712 Harms, L., Michie, P. T., & Näätänen, R. (2016). Criteria for determining whether
713 mismatch responses exist in animal models: Focus on rodents. *Biological
714 Psychology*, 116, 28–35.
- 715 Homayoun, H., & Moghaddam, B. (2007). NMDA Receptor Hypofunction Produces
716 Opposite Effects on Prefrontal Cortex Interneurons and Pyramidal Neurons.
717 *Journal of Neuroscience*, 27(43), 11496–11500.
- 718 Howes, O. H., & Kaar, S. J. (2018). Antipsychotic drugs: challenges and future
719 directions. *World Psychiatry : Official Journal of the World Psychiatric*

- 720 *Association (WPA)*, 17(2), 170–171.
- 721 Hu, H., & Agmon, A. (2016). Differential Excitation of Distally versus Proximally
722 Targeting Cortical Interneurons by Unitary Thalamocortical Bursts. *Journal of*
723 *Neuroscience*, 36(26), 6906–6916.
- 724 Javitt, D. C., Steinschneider, M., Schroeder, C. E., & Arezzo, J. C. (1996). Role of
725 cortical N-methyl-D-aspartate receptors in auditory sensory memory and mismatch
726 negativity generation: implications for schizophrenia. *Proceedings of the National*
727 *Academy of Sciences of the United States of America*, 93(21), 11962–11967.
- 728 Javitt, D., Lee, M., Kantrowitz, J., & Martinez, A. (2018). Mismatch negativity as a
729 biomarker of theta band oscillatory dysfunction in schizophrenia. *Schizophrenia*
730 *Research*, 191(2016), 51–60.
- 731 Kishi, T., Ikuta, T., Oya, K., Matsunaga, S., Matsuda, Y., & Iwata, N. (2018). Anti-
732 dementia Drugs for Psychopathology and Cognitive Impairment in Schizophrenia:
733 A Systematic Review and Meta-analysis. *The International Journal of*
734 *Neuropsychopharmacology*, 21(8), 748.
- 735 Korostenskaja, M., Nikulin, V. V., Kičić, D., Nikulina, A. V., & Kähkönen, S. (2007).
736 Effects of NMDA receptor antagonist memantine on mismatch negativity. *Brain*
737 *Research Bulletin*, 72(4–6), 275–283.
- 738 Krystal, J. H., Perry, E. B., Gueorguieva, R., Belger, A., Madonick, S. H., Abi-
739 Dargham, A., ... Cyril D'Souza, D. (2005). Comparative and interactive human
740 psychopharmacologic effects of ketamine and amphetamine: Implications for
741 glutamatergic and dopaminergic model psychoses and cognitive function. *Archives*

- 742 *of General Psychiatry*, 62(9), 985–995.
- 743 Kurkela, J. L. O., Lipponen, A., Kyläheiko, I., & Astikainen, P. (2018).
744 Electrophysiological evidence of memory-based detection of auditory regularity
745 violations in anesthetized mice. *Scientific Reports*, 8(1), 3027.
- 746 Light, G. A., & Braff, D. L. (2005). Mismatch negativity deficits are associated with
747 poor functioning in schizophrenia patients. *Archives of General Psychiatry*, 62(2),
748 127–136.
- 749 Light, G. A., & Swerdlow, N. R. (2015). Future clinical uses of neurophysiological
750 biomarkers to predict and monitor treatment response for schizophrenia. *Annals of*
751 *the New York Academy of Sciences*, 1344(1), 105–119.
- 752 Lucatch, A. M., Coles, A. S., Hill, K. P., & George, T. P. (2018). Cannabis and Mood
753 Disorders. *Current Addiction Reports*, 5(3), 336–345.
754 <https://doi.org/10.1007/s40429-018-0214-y>
- 755 Malmierca, M. S. (2003). THE STRUCTURE AND PHYSIOLOGY OF THE RAT
756 AUDITORY SYSTEM: AN OVERVIEW (pp. 147–211).
- 757 Meehan, C., Harms, L., Frost, J. D., Barreto, R., Todd, J., Schall, U., ... Hodgson, D.
758 M. (2017). Effects of immune activation during early or late gestation on
759 schizophrenia-related behaviour in adult rat offspring. *Brain, Behavior, and*
760 *Immunity*, 63, 8–20.
- 761 Michie, P. T., Malmierca, M. S., Harms, L., & Todd, J. (2016). The neurobiology of
762 MMN and implications for schizophrenia. *Biological Psychology*, 116, 90–97.
- 763 Mouri, A., Noda, Y., Enomoto, T., & Nabeshima, T. (2007). Phencyclidine animal

- 764 models of schizophrenia: Approaches from abnormality of glutamatergic
765 neurotransmission and neurodevelopment. *Neurochemistry International*, 51(2–4),
766 173–184.
- 767 Musall, S., von der Behrens, W., Mayrhofer, J. M., Weber, B., Helmchen, F., & Haiss,
768 F. (2014). Tactile frequency discrimination is enhanced by circumventing
769 neocortical adaptation. *Nature Neuroscience*, 17(11), 1567–1573.
- 770 Musty, R. ., Deyo, R. ., Baer, J. ., Darrow, S. ., & Coleman, B. (2000). Effects of
771 SR141716 on animal models of schizophrenia. *In Symposium on the Cannabinoids*,
772 *International Cannabinoid Research Society. Burlington, Vermont.*
- 773 Näätänen, R., Gaillard, A. W. K., & Mäntysalo, S. (1978). Early selective-attention
774 effect on evoked potential reinterpreted. *Acta Psychologica*, 42(4), 313–329.
- 775 Näätänen, R., Paavilainen, P., Rinne, T., & Alho, K. (2007). The mismatch negativity
776 (MMN) in basic research of central auditory processing: A review. *Clinical*
777 *Neurophysiology*, 118(12), 2544–2590.
- 778 Nakamura, T., Michie, P. T., Fulham, W. R., Todd, J., Budd, T. W., Schall, U., ...
779 Hodgson, D. M. (2011). Epidural Auditory Event-Related Potentials in the Rat to
780 Frequency and duration Deviants: Evidence of Mismatch Negativity? *Frontiers in*
781 *Psychology*, 2, 367.
- 782 Natan, R. G., Briguglio, J. J., Mwilambwe-Tshilobo, L., Jones, S. I., Aizenberg, M.,
783 Goldberg, E. M., & Geffen, M. N. (2015). Complementary control of sensory
784 adaptation by two types of cortical interneurons. *ELife*, 4.
- 785 Nieto-Diego, J., & Malmierca, M. S. (2016). Topographic Distribution of Stimulus-

- 786 Specific Adaptation across Auditory Cortical Fields in the Anesthetized Rat. *PLOS*
787 *Biology*, 14(3), e1002397.
- 788 Okada, M., Fukuyama, K., Kawano, Y., Shiroyama, T., & Ueda, Y. (2019). Memantine
789 protects thalamocortical hyper-glutamatergic transmission induced by NMDA
790 receptor antagonism via activation of system xc. *Pharmacology Research &*
791 *Perspectives*, 7(1), e00457.
- 792 Olney, J., Labruyere, J., & Price, M. (1989). Pathological changes induced in
793 cerebrocortical neurons by phencyclidine and related drugs. *Science*, 244(4910),
- 794 Opitz, B., Schröger, E., & von Cramon, D. Y. (2005). Sensory and cognitive
795 mechanisms for preattentive change detection in auditory cortex. *European*
796 *Journal of Neuroscience*, 21(2), 531–535.
- 797 Oranje, B., Berckel, B. van, Kemner, C., Ree, J. van, Kahn, R., & Verbaten, M. (2000).
798 The Effects of a Sub-Anaesthetic Dose of Ketamine on Human Selective
799 Attention. *Neuropsychopharmacology*, 22(3), 293–302.
- 800 Parr, T., & Friston, K. J. (2018). The Anatomy of Inference: Generative Models and
801 Brain Structure. *Frontiers in Computational Neuroscience*, 12, 90.
- 802 Parras, G. G., Nieto-Diego, J., Carbajal, G. V., Valdés-Baizabal, C., Escera, C., &
803 Malmierca, M. S. (2017). Neurons along the auditory pathway exhibit a
804 hierarchical organization of prediction error. *Nature Communications*, 8(1), 2148.
- 805 Paxinos, G., & Watson, C. (2013). *The Rat Brain in Stereotaxic Coordinates : Hard*
806 *Cover Edition*. Elsevier Science.
- 807 Pérez-González, D., Hernández, O., Covey, E., & Malmierca, M. S. (2012). GABA A-

- 808 mediated inhibition modulates stimulus-specific adaptation in the inferior
809 colliculus. *PLoS ONE*, 7(3). <https://doi.org/10.1371/journal.pone.0034297>
- 810 Randeniya, R., Oestreich, L. K. L., & Garrido, M. I. (2018). Sensory prediction errors in
811 the continuum of psychosis. *Schizophrenia Research*, 191, 109–122.
- 812 Rasser, P. E., Schall, U., Todd, J., Michie, P. T., Ward, P. B., Johnston, P., ...
813 Thompson, P. M. (2011). Gray matter deficits, mismatch negativity, and outcomes
814 in schizophrenia. *Schizophrenia Bulletin*, 37(1), 131–140.
- 815 Rauss, K., & Pourtois, G. (2013). What is Bottom-Up and What is Top-Down in
816 Predictive Coding? *Frontiers in Psychology*, 4, 276.
- 817 Ruhнау, P., Herrmann, B., & Schröger, E. (2012). Clinical Neurophysiology Finding
818 the right control : The mismatch negativity under investigation. *Clinical
819 Neurophysiology*, 123(3), 507–512.
- 820 Schuelert, N., Dorner-Ciossek, C., Brendel, M., & Rosenbrock, H. (2018). A
821 comprehensive analysis of auditory event-related potentials and network
822 oscillations in an NMDA receptor antagonist mouse model using a novel wireless
823 recording technology. *Physiological Reports*, 6(16), e13782.
- 824 Siegel S.J., Talpos J.C., & Geyer M.A. (2013). Animal models and measures of
825 perceptual processing in schizophrenia. *Neuroscience and Behavioral reviews*,
826 37(9):2092-8
- 827 Sivarao, D. V, Chen, P., Yang, Y., Li, Y.-W., Pieschl, R., & Ahlijanian, M. K. (2014).
828 NR2B Antagonist CP-101,606 Abolishes Pitch-Mediated Deviance Detection in
829 Awake Rats. *Frontiers in Psychiatry*, 5, 96.

- 830 Slutsky, I., Abumaria, N., Wu, L.-J., Huang, C., Zhang, L., Li, B., ... Liu, G. (2010).
831 Enhancement of Learning and Memory by Elevating Brain Magnesium. *Neuron*,
832 *65*(2), 165–177.
- 833 Slutsky, I., Sadeghpour, S., Li, B., & Liu, G. (2004). Enhancement of Synaptic
834 Plasticity through Chronically Reduced Ca²⁺ Flux during Uncorrelated Activity.
835 *Neuron*, *44*(5), 835–849.
- 836 Song, X., Jensen, M. Ø., Jogini, V., Stein, R. A., Lee, C.-H., Mchaourab, H. S., ...
837 Gouaux, E. (2018). Mechanism of NMDA receptor channel block by MK-801 and
838 memantine. *Nature*, *556*(7702), 515–519.
- 839 Sterzer, P., Adams, R. A., Fletcher, P., Frith, C., Lawrie, S. M., Muckli, L., ... Corlett,
840 P. R. (2018). The Predictive Coding Account of Psychosis.
- 841 Swerdlow, N. R., Bhakta, S., Chou, H.-H., Talledo, J. A., Balvaneda, B., & Light, G. A.
842 (2016). Memantine Effects On Sensorimotor Gating and Mismatch Negativity in
843 Patients with Chronic Psychosis. *Neuropsychopharmacology : Official Publication*
844 *of the American College of Neuropsychopharmacology*, *41*(2), 419–430.
- 845 Tikhonravov, D., Neuvonen, T., Pertovaara, A., Savioja, K., Ruusuvirta, T., Näätänen,
846 R., & Carlson, S. (2010). Dose-related effects of memantine on a mismatch
847 negativity-like response in anesthetized rats. *Neuroscience*, *167*(4), 1175–1182.
- 848 Todd, J., Harms, L., Schal l, U., & Michie, P. T. (2013, December 18). Mismatch
849 negativity: Translating the potential. *Frontiers in Psychiatry*. Frontiers.
- 850 Umbrecht, D., & Krljes, S. (2005). Mismatch negativity in schizophrenia: a meta-
851 analysis. *Schizophrenia Research*, *76*(1), 1–23.

- 852 Valdés-Baizabal, C., Parras, G. G., Ayala, Y. A., & Malmierca, M. S. (2017).
853 Endocannabinoid Modulation of Stimulus-Specific Adaptation in Inferior
854 Colliculus Neurons of the Rat. *Scientific Reports*, 7(1).
- 855 Vezzani, A., Serafini, R., Stasi, M. A., Caccia, S., Conti, I., Tridico, R. V., & Samanin,
856 R. (1989). Kinetics of MK-801 and its effect on quinolinic acid-induced seizures
857 and neurotoxicity in rats. *The Journal of Pharmacology and Experimental*
858 *Therapeutics*, 249(1), 278–283.
- 859 Wacongne, C. (2016). A predictive coding account of MMN reduction in schizophrenia.
860 *Biological Psychology*, 116, 68–74.
- 861 Winer, J. A., Larue, D. T., & Huang, C. L. (1999). Two systems of giant axon terminals
862 in the cat medial geniculate body: Convergence of cortical and GABAergic inputs.
863 *The Journal of Comparative Neurology*, 413(2), 181–197.
- 864 Yu, X., Xu, X., He, S., & He, J. (2009). Change detection by thalamic reticular neurons.
865 *Nature Neuroscience*, 12(9), 1165–1170.

866

867

868

869

870 FIGURES LEGEND

871 **Figure 1. Single neuron spikes population analysis.** Results for firing rate analysis
872 and their computed differences along the thalamocortical axis. **a)** Boxplot of median

873 normalized responses for deviants (red), cascade (green) and standard (blue) for each
874 group, control (light colors) and MK801 (bright colors), within each station and the
875 statistical significance between groups (Wilcoxon signed-rank test, * $p < 0.05$,
876 ** $p < 0.001$, *** $p < 0.000$). **b-d**) Indices histograms displayed in a mirror-like manner for
877 the two groups (controls upper and in light colors; MK801 under and in bright colors),
878 showing the distribution of the three indexes for each neuronal response (ranging
879 between -1 and +1, dotted lines indicate index=0). Vertical solid lines indicate their
880 medians and the significant difference between groups is noted at the right of each
881 histogram block. **e**) Median indices of Prediction Error (orange) and **d**) Repetition
882 Suppression (blue), represented with respect to the baseline set by the cascade control
883 (green line). Thereby, iPE upwards-positive while iRS is downwards-positive. Each
884 median index corresponds to differences between normalized responses in a). Asterisks
885 inside bars denote statistical significance of these indices against zero (Friedman test),
886 while asterisks outside bars denote statistical significance between groups (Wilcoxon
887 signed-rank test, * $p < 0.05$, ** $p < 0.001$, *** $p < 0.000$).

888

889 **Figure 2. Spike Density Function.** Peristimulus time histogram along the
890 thalamocortical axis. **a-c**) Averaged firing rate profiles for each condition as normalized
891 spike-density function (light colors for control and bright color for MK801 group), and
892 their respective differences (white dotted lines). Solid horizontal white lines represent
893 the time in which the difference between groups is significant (two-sample t test
894 $p < 0.05$, Bonferroni corrected). **d-f**) Indices over time computed for 12 intervals (from -
895 50 to 190ms) compared against zero (signed-rank test and FDR corrected for 12

896 comparisons; * $p < 0.01$) for each group (light colors for control and bright color for
 897 MK801 group). Solid white lines denote differences between groups across time
 898 intervals (two-sample t test for each of the 12-time windows, $p < 0.05$).

899

900 **Figure 3. Time course for dynamical thalamocortical adaptation. a)** Averaged time
 901 course for the stimulus played in relation to the time elapsed from the beginning of the
 902 sequence. **b)** The first fifteen standard stimuli showing the three parameters of the
 903 power law fitted: a initial average response; b adaptation velocity; and c the steady-state
 904 value (dotted lines) for each group. Arrows represent the 50% of the initial responses
 905 demonstrating faster adaptation in the MK801 group and the break down in the
 906 dynamical hierarchy of adaptation.

907

908 **Figure 4. Local Field Potentials for each condition and their differences. a-c)**
 909 Population grand-averaged LFP for each condition recorded (CAS, DEV and STD)
 910 within each group (controls and MK801). Grey panels under the main LFP
 911 representations shows the instantaneous p value (white trace) of corresponding stimulus
 912 condition LFP (critical threshold set at 0.05 represented as a horizontal dotted yellow
 913 line). The thick black horizontal bars in figure 4 a-c highlights the time interval for
 914 which the LFP comparison between the control and MK801 groups is significant. **d-f)**
 915 Population grand-averaged LFP for and neuronal Mismatch (MM-LFP= LFP_{DEV} -
 916 LFP_{STD}), Prediction Error (PE-LFP= LFP_{DEV} - LFP_{CAS}), and Repetition Suppression (RS-
 917 $LFP=LFP_{STD}$ - LFP_{CAS}) respectively. Colored horizontal lines denote significant
 918 deflections (t -test, FDR corrected). Grey panels show the instantaneous p value (white

919 trace) of corresponding stimulus condition LFP (critical threshold set at 0.05
920 represented as a horizontal dotted yellow line) and black horizontal lines the time
921 interval in which MK801 and control are statistically different.

For Peer Review

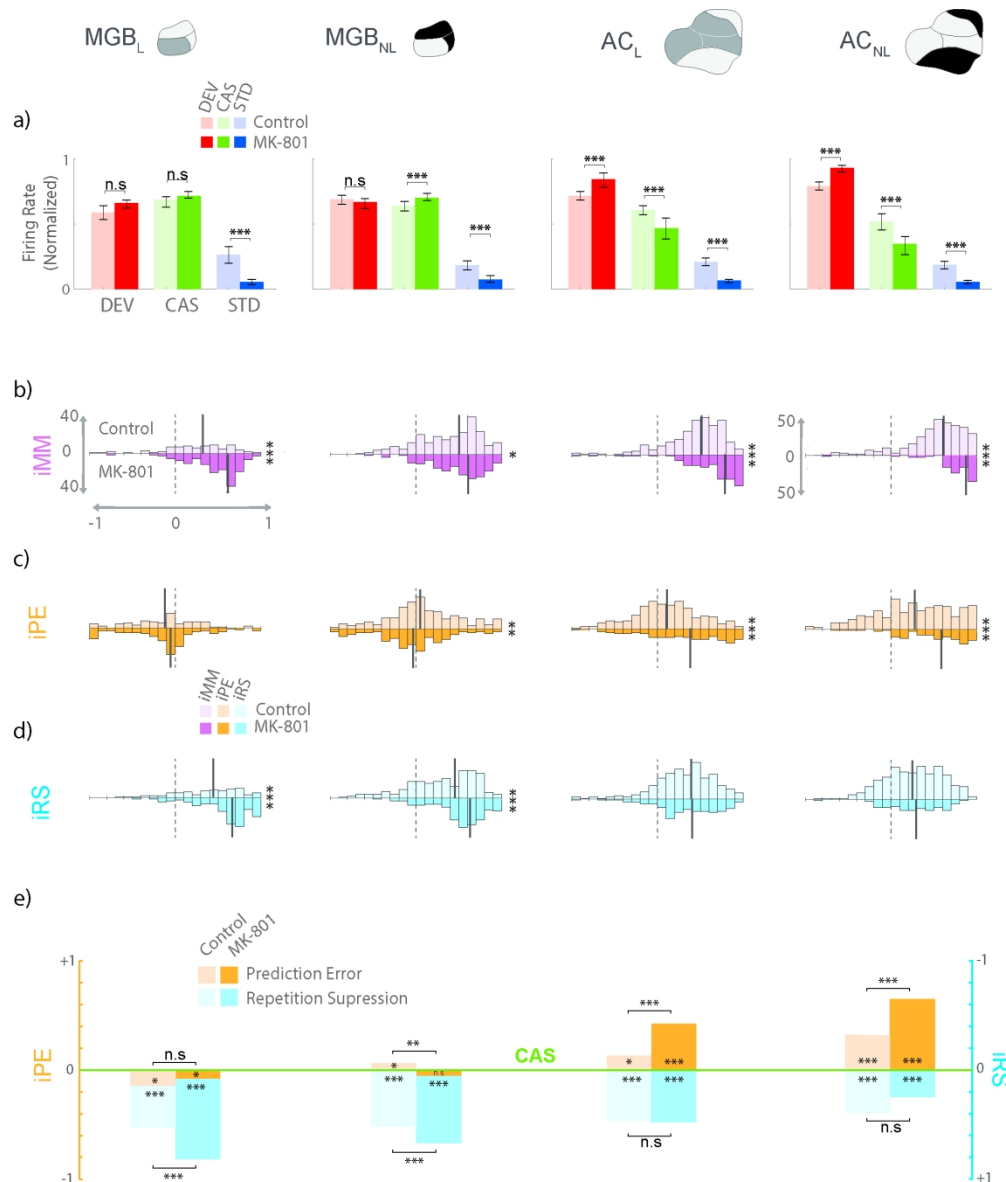
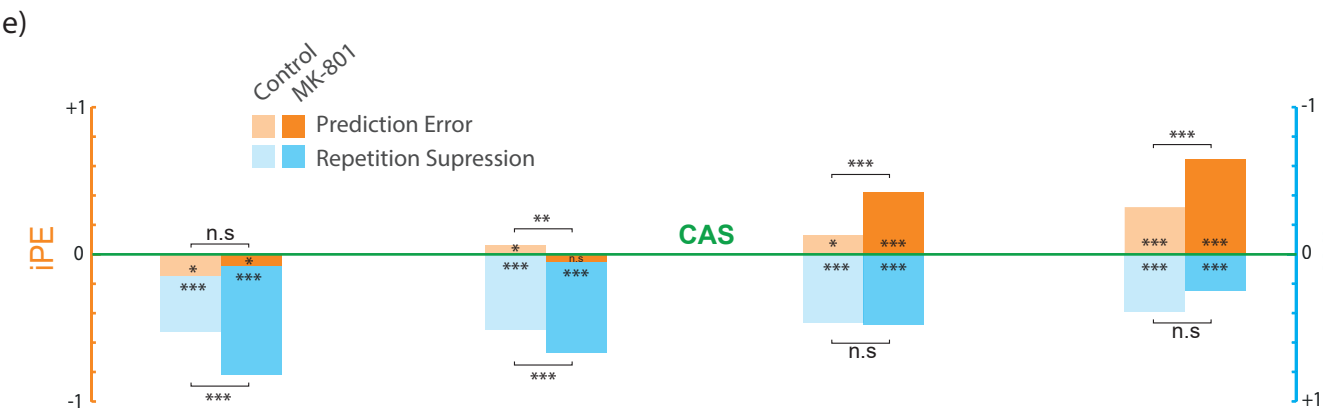
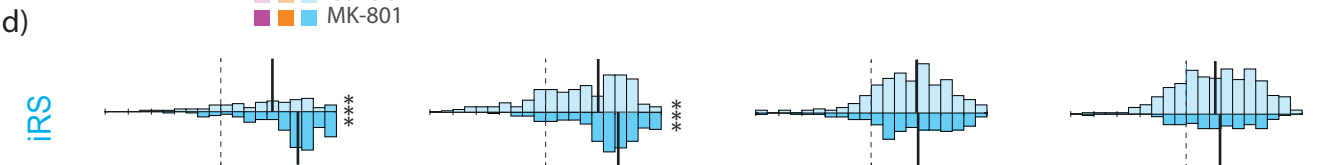
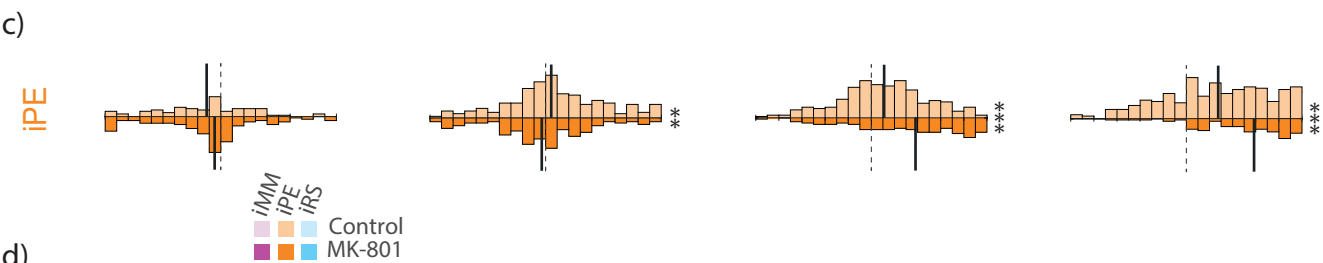
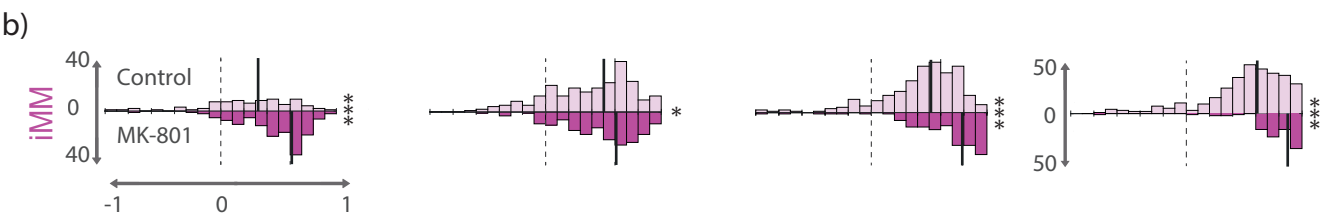
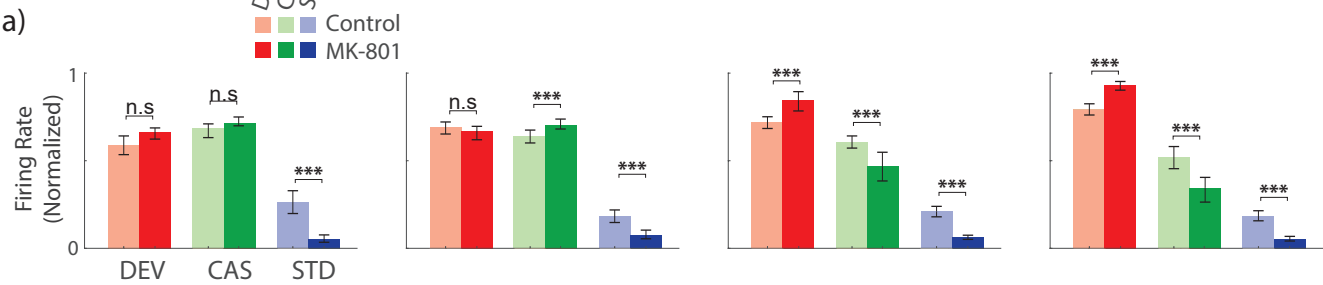


Figure 1. Single neuron spikes population analysis. Results for firing rate analysis and their computed differences along the thalamocortical axis. a) Boxplot of median normalized responses for deviants (red), cascade (green) and standard (blue) for each group, control (light colors) and MK801 (bright colors), within each station and the statistical significance between groups (Wilcoxon signed-rank test, * $p < 0.05$, ** $p < 0.001$, *** $p < 0.000$). b-d) Indices histograms displayed in a mirror-like manner for the two groups (controls upper and in light colors; MK801 under and in bright colors), showing the distribution of the three indexes for each neuronal response (ranging between -1 and +1, dotted lines indicate index=0). Vertical solid lines indicate their medians and the significant difference between groups is noted at the right of each histogram block. e) Median indices of Prediction Error (orange) and d) Repetition Suppression (blue), represented with respect to the baseline set by the cascade control (green line). Thereby, iPE upwards-positive while iRS is downwards-positive. Each median index corresponds to differences between normalized responses in a). Asterisks inside bars denote statistically significance of these indices against zero (Friedman test), while asterisks outside bars denote statistically significance between groups (Wilcoxon signed-rank test, * $p < 0.05$, ** $p < 0.001$, *** $p < 0.000$).



DEV
CAS
STD

Control
MK-801



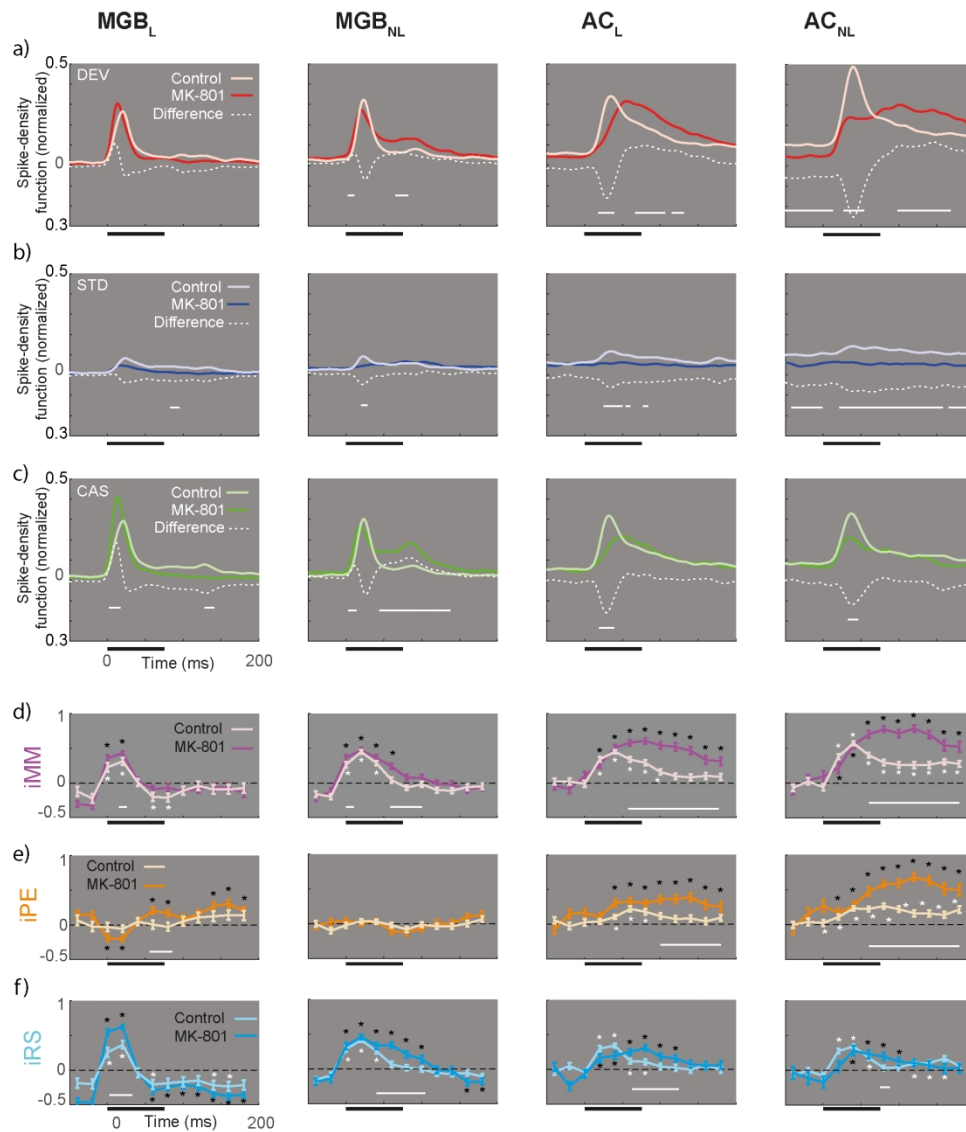
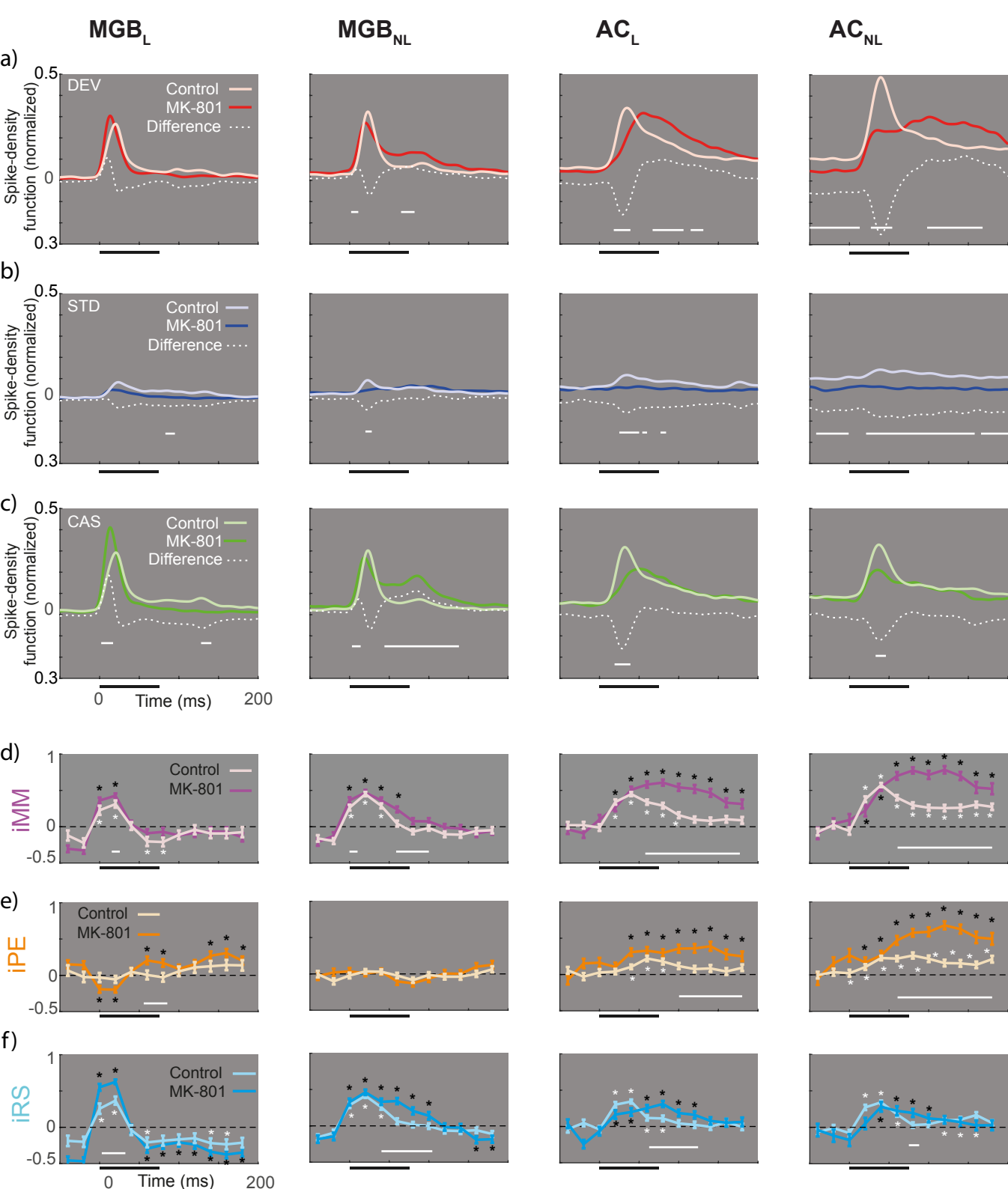


Figure 2. Spike Density Function. Peristimulus time histogram along the thalamocortical axis. a-c) Averaged firing rate profiles for each condition as normalized spike-density function (light colors for control and bright color for MK801 group), and their respective differences (white dotted lines). Solid horizontal white lines represent the time in which the difference between groups is significant (two-sample t test $p < 0.05$, Bonferroni corrected). d-f) Indices over time computed for 12 intervals (from -50 to 190ms) compared against zero (signed-rank test and FDR corrected for 12 comparisons; * $p < 0.01$) for each group (light colors for control and bright color for MK801 group). Solid white lines denote differences between groups across time intervals (two-sample t test for each of the 12-time windows, $p < 0.05$).



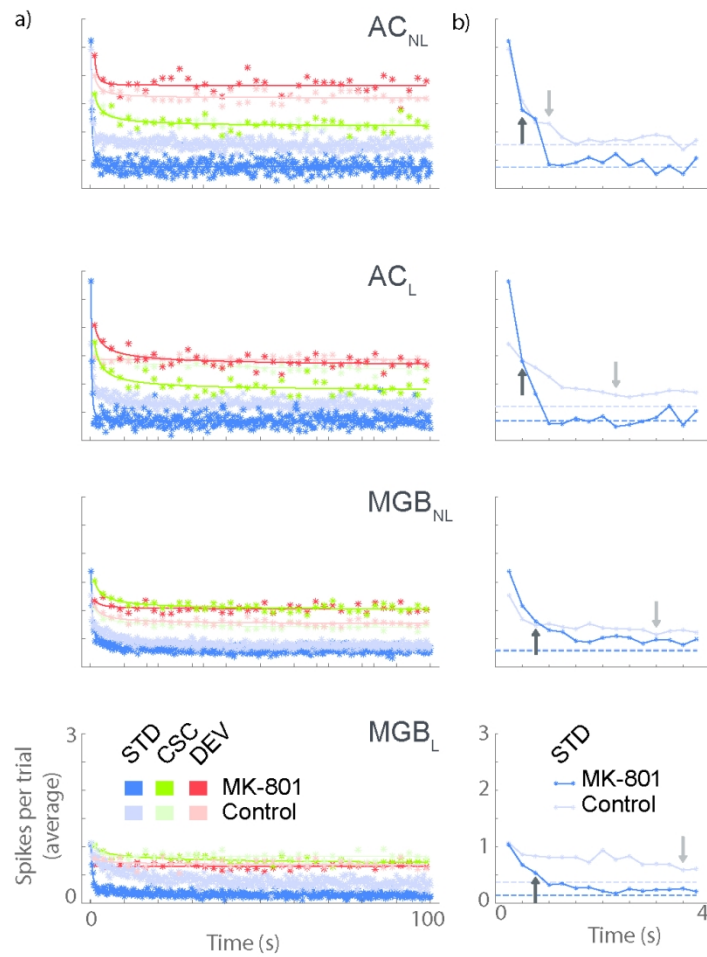
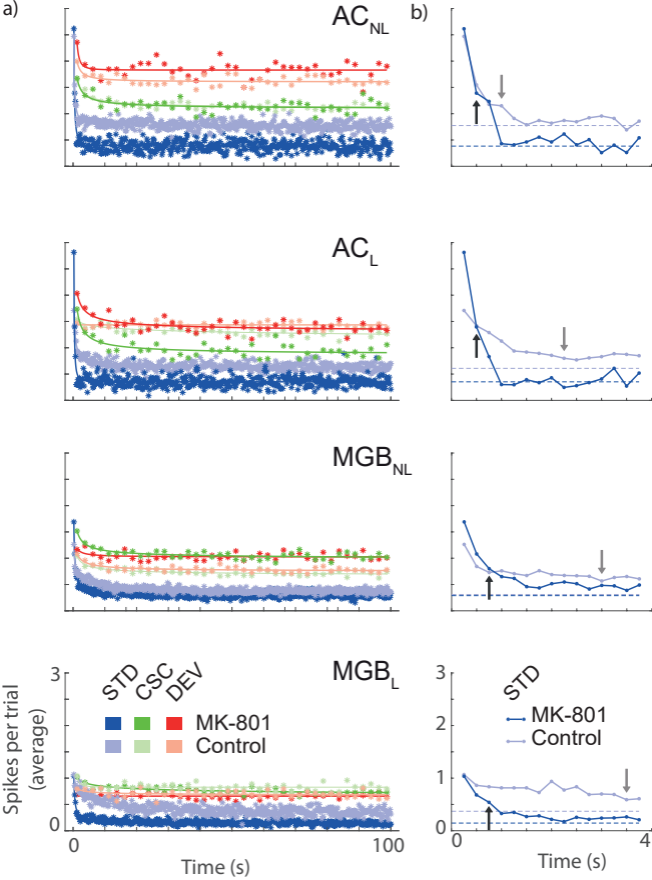


Figure 3. Time course for dynamical thalamocortical adaptation. a) Averaged time course for the stimulus played in relation to the time elapsed from the beginning of the sequence. b) The first fifteen standard stimuli showing the three parameters of the power law fitted: a initial average response; b adaptation velocity; and c the steady-state value (dotted lines) for each group. Arrows represent the 50% of the initial responses demonstrating faster adaptation in the MK801 group and the break down in the dynamical hierarchy of adaptation.



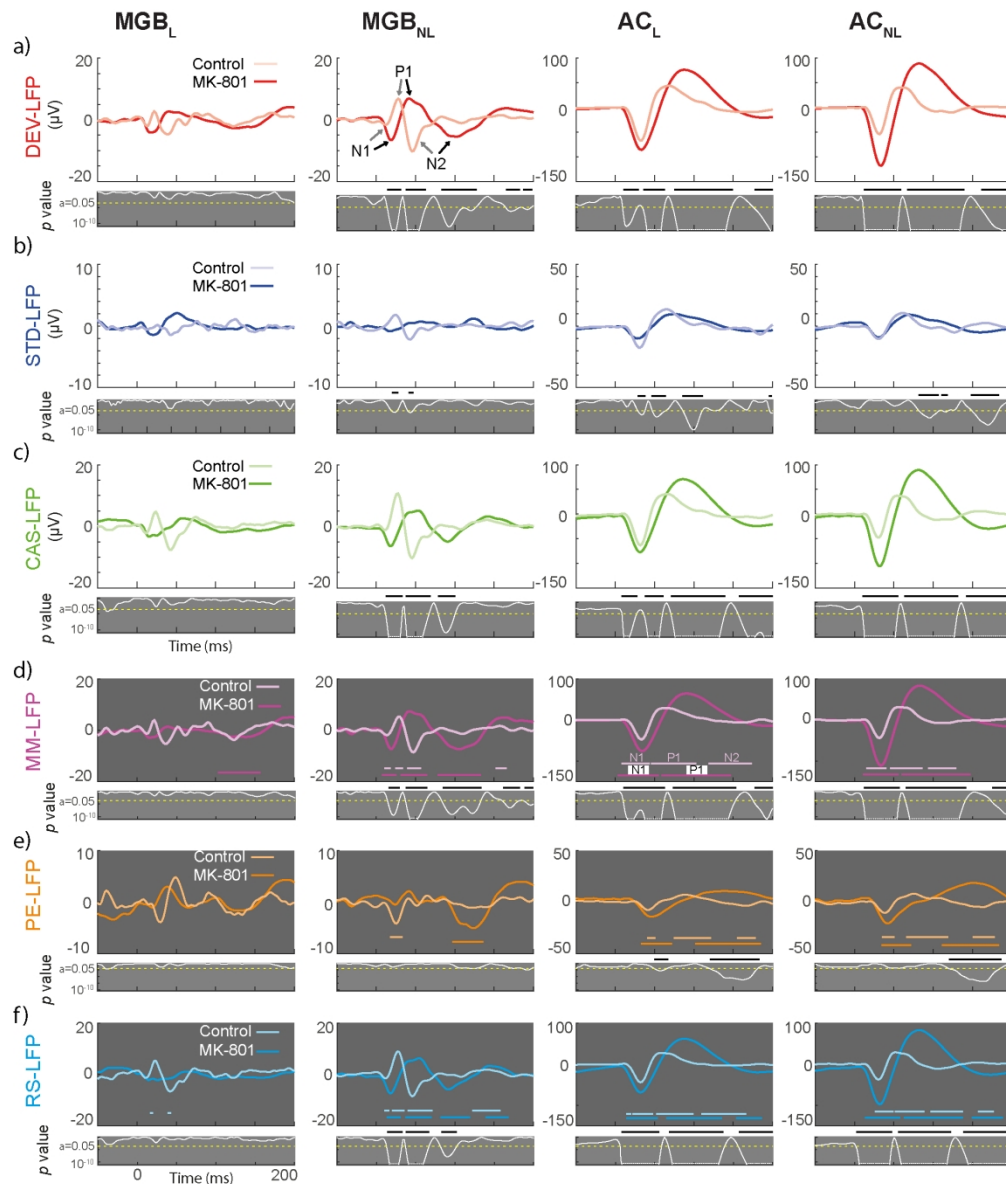


Figure 4. Local Field Potentials for each condition and their differences. a-c) Population grand-averaged LFP for each condition recorded (CAS, DEV and STD) within each group (controls and MK801). Grey panels under the main LFP representations shows the instantaneous p value (white trace) of corresponding stimulus condition LFP (critical threshold set at 0.05 represented as a horizontal dotted yellow line). The thick black horizontal bars in figure 4 a-c highlights the time interval for which the LFP comparison between the control and MK801 groups is significant. d-f) Population grand-averaged LFP for and neuronal Mismatch (MM-LFP=LFPDEV-LFPSTD), Prediction Error (PE-LFP=LFPDEV-LFPCAS), and Repetition Suppression (RS-LFP=LFPSTD-LFPCAS) respectively Colored horizontal lines denote significant deflections (t-test, FDR corrected). Grey panels show the instantaneous p value (white trace) of corresponding stimulus condition LFP (critical threshold set at 0.05 represented as a horizontal dotted yellow line) and black horizontal lines the time interval in which MK801 and control are statistically different.

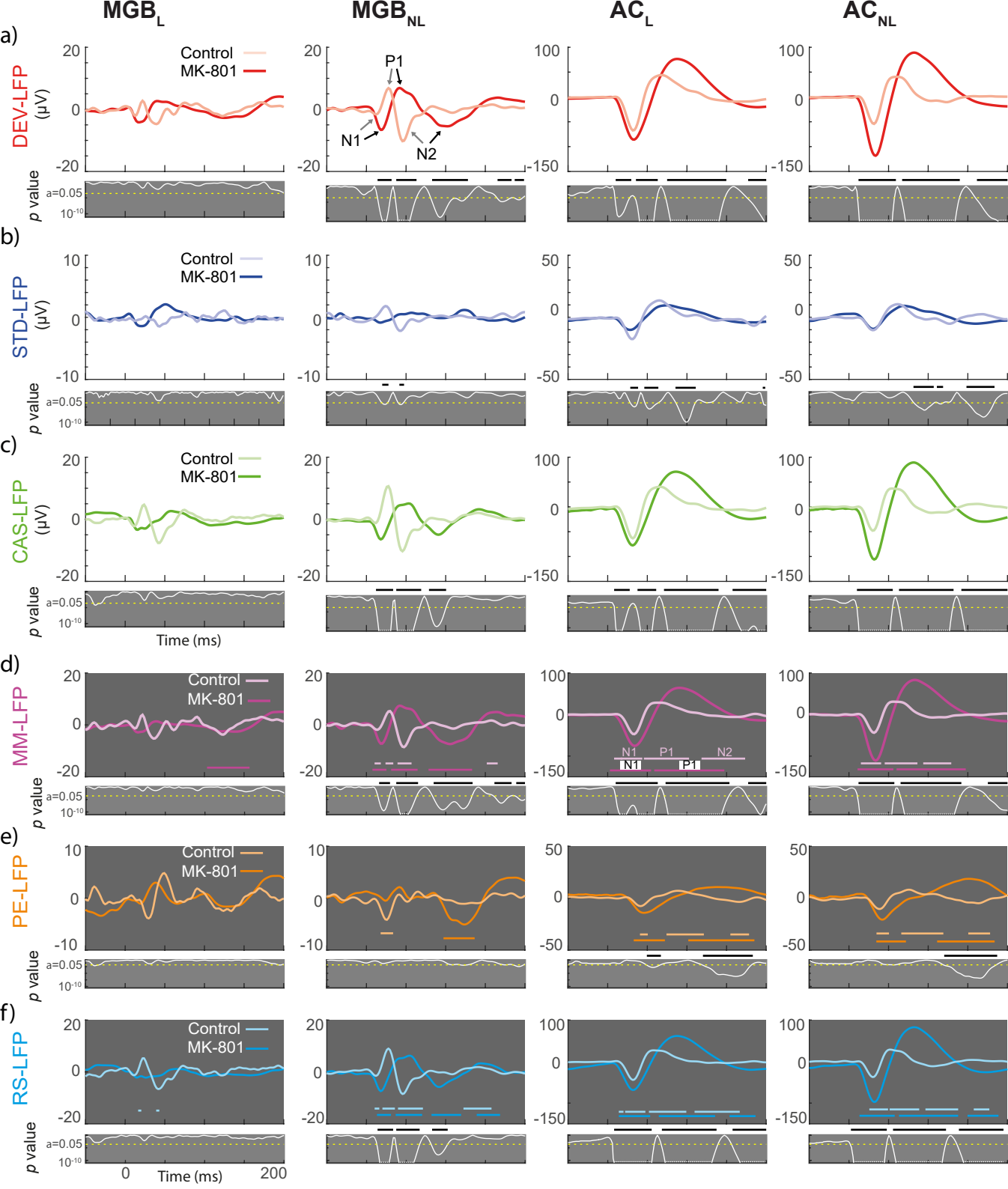


Table 1: Spike population Analysis

	CONTROL				MK801			
	MGB		AC		MGB		AC	
	L	NL	L	NL	L	NL	L	NL
# Neurons	28	38	40	37	44	42	37	24
# Points/ required	111/72	240/224	295/87	309/29	156/81	228/544	163/21	94/7
DEV (spk)	0.7249	0.6805	0.9594	0.9694	0.5970	0.6723	1.0978	1.6450
STD (spk)	0.1500	0.1504	0.2363	0.2103	0.0338	0.0837	0.0906	0.1114
CSD (spk)	0.8292	0.5601	0.7719	0.5910	0.7329	0.7889	0.5913	0.5978
	Cascade vs. Many-Standard Controls analysis (median and Wilcoxon signed-rank values)							
Many-standard	0.8982	0.6499	0.8034	0.5237	0.7855	0.9966	0.5109	0.6861
Cascade	0.7625	0.5601	0.7720	0.5911	0.7326	0.7889	0.5913	0.5979
<i>P value</i>	<i>0.2231</i>	<i>0.1567</i>	<i>0.8266</i>	<i>0.3288</i>	<i>0.4103</i>	<i>0.0286</i>	<i>0.2543</i>	<i>0.0830</i>
	Friedman test analysis							
iMM	0.4240	0.5169	0.5283	0.6073	0.6075	0.5578	0.7734	0.8699
<i>P value</i>	<i>1.01⁻⁰⁹</i>	<i>2.96⁻²⁹</i>	<i>7.52⁻⁵¹</i>	<i>7.90⁻⁵⁶</i>	<i>6.96⁻²⁴</i>	<i>5.98⁻³⁸</i>	<i>1.63⁻⁴¹</i>	<i>2.34⁻³⁰</i>
iPE	-0.0950	0.0492	0.1221	0.2734	-0.0633	-0.0445	0.3723	0.5788
<i>P value</i>	<i>0.0130</i>	<i>0.0199</i>	<i>0.0012</i>	<i>3.29⁻¹²</i>	<i>0.0092</i>	<i>0.5120</i>	<i>1.88⁻⁰⁷</i>	<i>8.84⁻¹³</i>
iRS	0.5192	0.4678	0.4062	0.3339	0.6707	0.6023	0.4011	0.2910
<i>P value</i>	<i>8.63⁻¹⁸</i>	<i>5.55⁻¹⁹</i>	<i>5.99⁻³²</i>	<i>1.68⁻¹⁸</i>	<i>7.48⁻³⁷</i>	<i>9.89⁻⁴²</i>	<i>1.16⁻¹⁶</i>	<i>1.68⁻⁰⁵</i>

1

2 **Table 1. Spike population analysis** for each experimental group and auditory station

3 independently: First row, number of recorded neurons; second row number of tested

4 neuron/frequency combinations (points), along with estimated minimum sample size (of

5 points) required for a statistical power (See Methods). Followed by median values for

6 base-line corrected spike count (spikes) to the different conditions. Comparative analysis

7 for control paradigms, median values and Wilcoxon signed-rank test values for each

8 station and group. Median indices of neuronal mismatch (iMM), prediction error (iPE)

9 and repetition suppression (iRS), and their corresponding *p* value.

10

11

12

13

14

Table 2: Firing Rate Comparisons

	MGB		AC	
	L	NL	L	NL
STD_control	0.1912	0.1717	0.1990	0.1856
STD_MK-801	0.0537	0.1047	0.0689	0.0547
<i>P value</i>	<0.000	<0.000	<0.000	<0.000
DEV_control	0.6153	0.6887	0.7274	0.7930
DEV_MK-801	0.6611	0.6620	0.8424	0.9247
<i>P value</i>	0.2309	0.2641	<0.000	<0.000
CAS_control	0.7104	0.6395	0.6052	0.5196
CAS_MK-801	0.7244	0.7063	0.4701	0.3458
<i>P value</i>	0.1169	<0.000	<0.000	<0.000
iMM_control	0.3675	0.4897	0.5124	0.5781
iMM_MK-801	0.5197	0.5221	0.7269	0.8088
<i>P value</i>	<0.000	0.0409	<0.000	<0.000
iPE_control	-0.0670	0.0513	0.1060	0.2697
iPE_MK-801	-0.0502	-0.0444	0.3592	0.5652
<i>P value</i>	0.9622	0.0035	0.000	<0.000
iRS_control	0.5300	0.3672	0.3350	0.2935
iRSdrug	0.6812	0.5632	0.3514	0.2765
<i>P value</i>	<0.000	<0.000	0.5800	0.8934

15

16 **Table 2: Comparative analysis between control and MK-801 group.** Median spikes
17 to the former measures responses to standard (STD), deviant (DEV) and cascade (CAS)
18 tones, and their corresponding *p* value (ranksum test). Similarly, medians and their
19 associates *p* value for the index of mismatch (iMM), index of prediction error (iPE) and
20 index of repetition suppression (iRS).

21

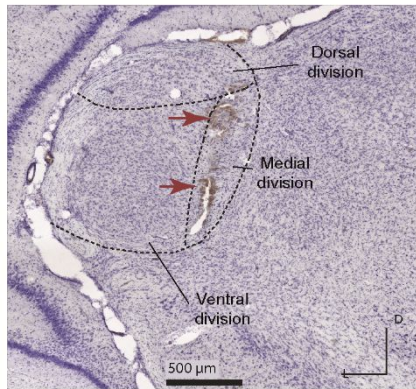
1 **Supplementary Material.**

2 **Anatomical location.** For MGB recording localization, at the end of each tract and
3 experiment, two electrolytic lesions were made to mark the end and the beginning of the
4 auditory signal. Then, animals were given a lethal dose of sodium pentobarbital and
5 perfused transcardially with phosphate buffered saline (0.5% NaNO₃ in Phosphate
6 Buffered Saline) followed by a fixative mix of 1% paraformaldehyde and 1%
7 glutaraldehyde). After fixation and dissection, the brain was cryoprotected in 30%
8 sucrose and sectioned into 40µm slices. Sections were Nissl stained with 0.1% cresyl
9 violet. Recording sites were marked on images from an adult rat brain atlas (Paxinos &
10 Watson, 2013) and neurons that were recorded from were assigned to one of the main
11 divisions of the MGB (dorsal, medial or ventral). This information was complemented
12 and confirmed by the stereotaxic coordinates as well as the depth of the neuron within a
13 tract (Supplementary figure 1a).

14 For the AC experiments, a magnified picture (25x) of the exposed cortex and the Bregma
15 references was taken at the end of the surgery with a digital single lens reflex camera
16 (D5100, Nikon) coupled to the surgical microscope (Zeiss). The picture was overlapped
17 to guide and mark each electrode placement into a micrometric grid (250-500 ~µm
18 spacing). Then we performed several tracts recording multi-unit activity frequency
19 response area (FRA), the characteristic frequency arise from each FRA was placed over
20 the picture, resulting in a characteristic frequency map of each animal. Boundaries were
21 identify following the changes in the tonotopic gradient: high-frequency reversal between
22 the ventral and anterior auditory fields (rostrally), low-frequency reversal between
23 primary and posterior auditory field (dorsocaudally) and high-frequency reversal between
24 ventral and suprarhinal auditory field (ventrally) (Nieto-Diego & Malmierca, 2016.).

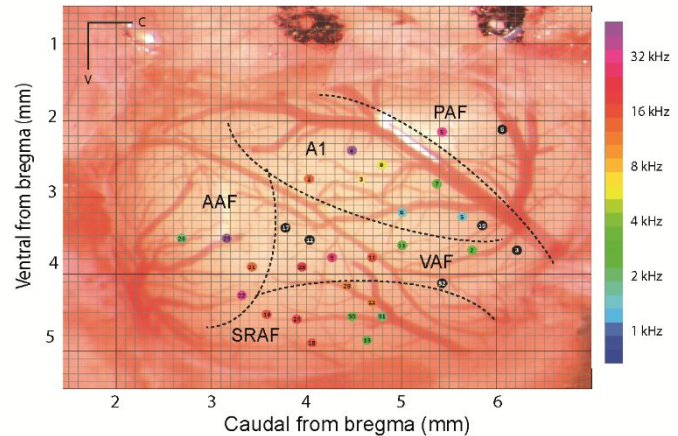
25 Then, each recording was located in one of these five fields. Nevertheless, the map was
 26 complemented during all electrophysiological recording session with the characteristic
 27 frequency of each new tract (Supplementary figure 1b).

a) Medial Geniculate Body Histology



Bregma -5.7

b) Auditory Cortex Tonotopic mapping



28

29 **Supplementary figure 1:** Anatomical recordings location. **a)** Microphotography
 30 example of Medial Geniculate Body slice (10x), red arrows point the two electrolytic
 31 lesions. **b)** Auditory Cortex photography example, each colored dot represent the
 32 characteristic frequency of each performed tract. A1: Primary Auditory Field; AAF:
 33 Anterior Auditory Field; VAF: Ventral Auditory Field; PAF: Posterior Auditory Field
 34 and SRAF: Suprarhinal Auditory Field.

35

36

37

38

39

40

41

42

43 **Electrophysiological recording and frequencies selection**: The signal recorded was
44 pre-amplified (1000x) and band-pass filtered (1-3kHz) with a medusa preamplifier
45 (TDT). This analog signal was digitalized 12k sampling rate and further band-pass
46 filtered (TDT-RX6) separately for spikes (500Hz-3kHz) and LFP (3-50Hz). We used
47 short trains of white noise bursts (30 ms, 5 ms rise-fall ramps) to search for neuronal
48 activity. To prevent neuronal adaptation during the search, some parameters (frequency
49 and intensity) and stimulus type (white noise, pure tone) were manually varied. Once a
50 single neuron was isolated a frequency-response area (FRA) of the response magnitude
51 for each frequency/intensity combination was first computed. A randomized sequence of
52 pure tones (from 1 to 44 KHz) was presented at a rate of 4Hz, with varying frequency and
53 intensity, and with 3 repetitions of all tones (Figure SI 2a). Ten frequencies were selected
54 for each neuron/FRA (0.5 octaves separation) at a fixed sound intensity (usually 20-30
55 db over the threshold) to form the control sequences, many-standard and cascade, and
56 adjacent pairs of them were used to present various oddball sequences (Figure SI 2b).

57

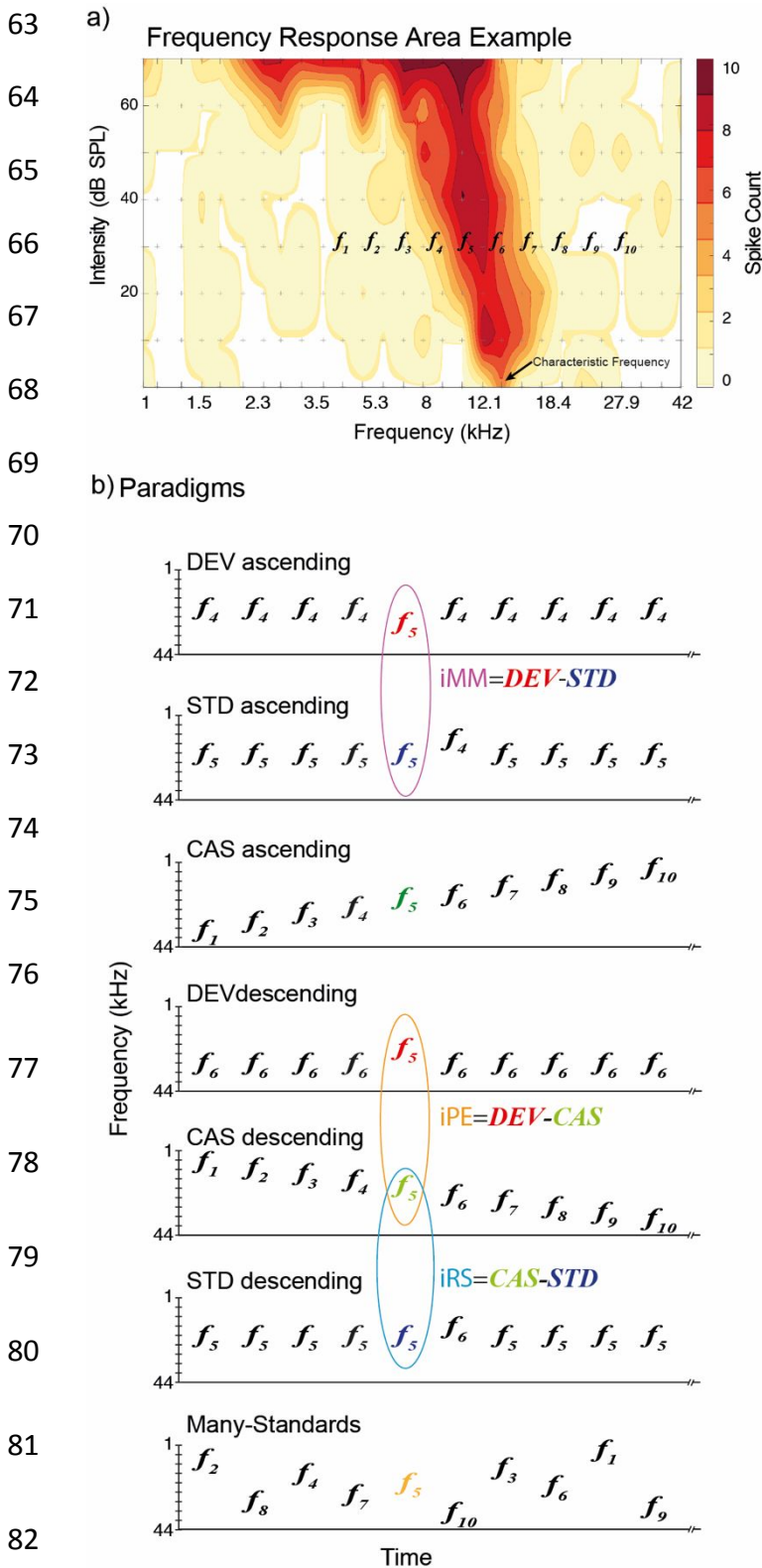
58

59

60

61

62



Supplementary figure 2:

Frequencies selection and paradigms a) Frequency Response Area, including a representation of the selected frequencies and an arrow pointing the characteristic frequency for this sample neuron.

b) Paradigms illustration formed by the frequencies selected in the frequency response area and representation for the conditions considered to calculate the indices.

view

84 **Baseline-corrected spike count and normalization.** To test for significant excitatory
 85 responses to tones we used a Monte Carlo approach, simulating 1000 peri-stimulus time

86 histogram using a Poisson model with a constant firing rate equal to the spontaneous firing
87 rate. A null distribution of baseline-corrected spike counts was generated from this
88 collection of peri-stimulus time histograms. Lastly, the p value of the baseline-corrected
89 spike count was empirically computed as $p = (g + 1)/(N + 1)$, where g is the count of null
90 measures greater than or equal to baseline-corrected spike count, and $N = 1000$ is the size
91 of the null sample. Finally, we only included in the analysis neuron/frequency
92 combinations with significant excitatory response ($p > 0.05$) after the baseline-corrected
93 spike count to at least one of the conditions (DEV, STD, CAS).

94 Normalized values were the coordinates of a 3D unit vector ($DEV_{\text{Normalized}}$, $STD_{\text{Normalized}}$,
95 $CAS_{\text{Normalized}}$) with the same direction of the original vector (DEV, STD, CAS), and thus
96 the same proportions between the three response measures.

ABBREVIATED SUMMARY

MMN is reduced in those with schizophrenia with a hypothesized mechanism of glutamate NMDA-R hypofunction. We tested whether MK-801 affects neuronal mismatch along the auditory thalamocortical pathway, and found enhanced neuronal indices of prediction error in the cortex and repetition suppression in thalamus, and altered dynamics of neuronal adaptation.

For Peer Review



175x92mm (300 x 300 DPI)

Spanish Summary

Introducción

En un ambiente continuamente cambiante, la habilidad de filtrar información irrelevante y detectar únicamente los eventos importantes determina la supervivencia. Para lograr esto, el cerebro auditivo ha desarrollado la capacidad de suprimir sus respuestas a estímulos repetitivos, permitiendo detectar solo los sonidos novedosos que inesperadamente irrumpen en la escena auditiva.

Comprender cómo el cerebro auditivo sano procesa este tipo de información nos permitirá entender el funcionamiento erróneo que se produce en condiciones patológicas. En esta tesis comenzaré estudiando cómo los estímulos auditivos novedosos son procesados a lo largo del sistema auditivo central en sujetos sanos. Continuaré analizando cómo algunas respuestas a estímulos auditivos pueden ser neuromoduladas por cannabinoides. Y finalmente comprobaré cómo esa capacidad de suprimir los estímulos repetitivos para detectar los estímulos novedosos se encuentra alterada en un modelo animal de esquizofrenia.

a. Las vías del sistema auditivo.

El sistema auditivo de los mamíferos está compuesto por varias estructuras y núcleos, a lo largo de los cuales la información es procesada y transferida desde los oídos hasta los centros auditivos superiores.

De manera resumida, después de que un sonido es convertido en señales eléctricas en la cóclea, la información auditiva es transferida a través de una serie de núcleos del tronco encefálico. Estos núcleos son: el complejo nuclear coclear, la oliva superior lateral y los

núcleos del lemnisco lateral. Desde el tronco encefálico la información auditiva llega al colículo inferior (IC, de sus siglas en inglés) en el mesencéfalo, posteriormente asciende hasta el núcleo geniculado medial del tálamo (MGB, de sus siglas en inglés), para finalmente alcanzar la corteza auditiva (AC). A lo largo de esta vía ocurren multitud de conexiones entre los diferentes núcleos, incluyendo conexiones entre ambos hemisferios del cerebro, conexiones de arriba abajo e incluso conexiones con centros no auditivos.

En esta tesis he analizado las respuestas neuronales de del IC, MGB y AC. Estas tres estructuras conforman el sistema auditivo central, siendo por tanto los niveles superiores de procesamiento de la información auditiva. Estas tres estructuras además pueden ser morfofuncionalmente disgregadas en dos vías paralelas, formando la llamada vía lemniscal y no-lemniscal (Calford & Aitkin, 1983; Jones, 2003; Lee & Sherman, 2011).

La vía lemniscal surge en el núcleo central del IC (CNIC), donde recibe información directamente desde el lemnisco lateral (de ahí su nombre), continúa ascendiendo por la división ventral del MGB (MGBv), proyectando finalmente a tres áreas de la AC: la primaria (A1), la anterior (AAF) y la ventral (VAF).

En cambio, la vía no-lemniscal recibe la información de múltiples fuentes, incluyendo centros no auditivos. La vía no-lemniscal emerge en los núcleos dorsal (DCIC), lateral (LCIC) y rostral (RCIC) del IC, proyectando a las divisiones dorsal (MGBd) y medial (MGBm) del MGB, que a su vez envía la información hasta las áreas supra-rhinal (SRAF) y posterior (PAF) de la AC (para mayor detalle ver Malmierca, 2015).

Las vías lemniscal y no-lemniscal muestran además diferentes respuestas fisiológicas, con distintos papeles funcionales. De este modo, la vía lemniscal lleva información precisa

y tonotópicamente organizada, adecuada para una transferencia fiable y eficiente de la información relativa a las propiedades físicas de los sonidos.

Por su lado, la vía no-lemniscal forma parte de un sistema integrativo, donde la información temporal y multi-sensorial es integrada y modulada (Lee & Sherman, 2011). Adicionalmente, el sistema auditivo central está organizado jerárquicamente (Malmierca, 2015), donde la información pasa desde el IC al MGB y a la AC, procesándose hacia adelante y posteriormente hacia atrás (**Figura 1**, apartado en inglés “Introduction”, pág.12). Los niveles superiores de este sistema jerarquizado, formado por el tálamo y la corteza auditiva, están además inextricablemente ligados formando una unidad funcional, que usualmente referimos como circuito tálamo-cortical, con extensas comunicaciones ascendentes y descendentes entre ellas (Bartlett, 2013; Huang & Winer, 2000; Imaizumi & Lee, 2014; Winer, 2006).

Las proyecciones tálamo-corticales ascendentes no son homogéneas, ya que diferentes neuronas del MGB proyectan a diferentes capas de la corteza auditiva (Llano & Sherman, 2008; Winer, Kelly, & Larue, 1999). Las neuronas del MGBv proyectan a las capas III y IV de la AC lemniscal; mientras que el MGBd y MGBm proyectan a las capas III y IV de la AC no-lemniscal. El MGBm también proyecta difusamente a las capas I de todas las áreas de la AC.

En cambio los axones cortico-talámicos son originados en las capas V y VI de la AC. Estas proyecciones descendentes desde la capa VI proyectan colateralmente al núcleo reticular del tálamo (TRN), un núcleo en forma de hoja, implicado también en el circuito tálamo-cortical (He, 2003; Yu *et al.*, 2009). Todas las células del TRN son GABAérgicas, reciben entradas excitatorias de los axones tálamo-corticales y cortico-talámicos y proveen

entradas inhibitorias al MGB (Conley *et al.*, 1991). Por tanto, el TRN actúa como un retroalimentador inhibitorio cuando es visto desde el tálamo, mientras que cuando es valorado desde la AC, el TRN actúa como un mediador inhibitorio del MGB (Cox & Sherman, 1999; Guillery, Feig, & Lozsádi, 1998; Ohara & Lieberman, 1985).

Las vías auditivas son normalmente descritas secuencialmente, con las conexiones ascendentes primero, seguidas por las descendentes. Sin embargo, estas conexiones serían mejor descritas como una serie de circuitos reverberantes de información ascendente y descendente (Chen, Helmchen, & Lutcke, 2015; Malmierca, 2015).

Por tanto, la importancia de estas proyecciones bidireccionales entre el tálamo y la corteza auditiva se debe a que ejercen un control retroalimentado de ambas estructuras, ya que estos bucles de transferencia de información proporcionan un control “modulatorio” o de “activación/desactivación” de las respuestas sensoriales evocadas (Sherman & Guillery, 2011).

b. Potencial de disparidad y adaptación-específica a estímulo.

El potencial de disparidad (MMN por sus siglas en inglés) es un potencial evocado que fue descrito por primera vez en 1987 por Risto Näätänen, quien definió este fenómeno como “*un cambio en la negatividad de la forma de la onda superpuesta en un potencial evocado*” que “*puede ser observado cuando se presenta un estímulo desviado de entre otros muchos numerosos estímulos estándar*” (Näätänen *et al.*, 1978).

El MMN se encuentra alterado en pacientes con esquizofrenia y otros trastornos psicóticos. Por eso es considerado como un biomarcador de deterioro cognitivo en procesos

patológicos (Todd *et al.*, 2013). Sin embargo, para comprender el MMN, es crucial entender los mecanismos neuronales que subyacen a su conformación, ya que a pesar de la gran cantidad de investigaciones dedicadas a este tema, los mecanismos neuronales que subyacen al MMN aún no se comprenden y siguen siendo confusos.

En esta tesis estudiaré el fenómeno de la disparidad neuronal (o mismatch neuronal) a lo largo del sistema tálamo-cortical, que es un fenómeno imitativo a la clásica adaptación-específica a estímulo (o SSA por sus siglas en inglés), que ha sido propuesta como el correlato neuronal del MMN (Harms *et al.*, 2014; Nieto-Diego & Malmierca, 2016; Ulanovsky *et al.*, 2003). De hecho, existe gran cantidad de evidencias que demuestran las semejanzas entre la SSA y el MMN (**Tabla 1**, pág. 15).

Ambos fenómenos son producidos de manera automática por un paradigma *oddball* y son afectados por los parámetros de los estímulos como la frecuencia, la duración y la intensidad. Al igual que el MMN, la SSA muestra mayores respuestas a los estímulos desviados o infrecuentes que a los estándar o frecuentes, cuando son presentados dentro de un paradigma *oddball* (**Figura 2b-c**, pág. 16).

En la versión más clásica del paradigma *oddball*, dos frecuencias (f_1 y f_2) son presentadas dentro de una misma secuencia de manera aleatoria y con diferente probabilidad de ocurrencia: una de las frecuencias será presentada como estándar (ej. con un 90% de probabilidad de aparición), mientras que la segunda frecuencia será presentada como infrecuente (ej. con un 10% de probabilidad; **Figura 2a**, pág. 16). Pero a pesar de las semejanzas entre SSA y MMN, algunas cuestiones quedan aún sin resolver (tabla 1) y mantienen el debate en el reconocimiento de la SSA como el correlato neuronal del MMN.

El concepto de SSA se acuña en 1979, cuando Movshon y Lennie describen unas respuestas de neuronas individuales en la corteza visual del gato cuando usaban estímulos

con patrones de rallados durante un periodo de tiempo prolongado, y reportan: “*nuestra observación más sorprendente es que la pérdida de sensibilidad de las neuronas individuales puede ser adaptación específica al estímulo*”. Pero este estudio pionero de la SSA fue ampliamente ignorado durante 25 años (Pérez-González *et al.*, 2005; Ulanovsky *et al.*, 2003). Desde entonces, muchos laboratorios han contribuido prolíficamente al estudio de la SSA, incluyendo nuestro laboratorio (Antunes & Malmierca, 2011, 2014; Antunes *et al.*, 2010; Ayala & Malmierca, 2012; Ayala & Malmierca, 2015; Ayala *et al.*, 2016; Duque & Malmierca, 2015; Duque *et al.*, 2014; Duque *et al.*, 2018; Duque *et al.*, 2012; Malmierca *et al.*, 2019; Pérez-González *et al.*, 2012; Valdés-Baizabal *et al.*, 2017).

Hoy en día sabemos que la SSA es un complejo fenómeno de adaptación diferente de una mera disminución de la velocidad de disparo (Ulanovsky *et al.*, 2004). Así la SSA implica una reducción de la respuesta a los estímulos repetitivos, mientras que la respuesta a los estímulos infrecuentes permanece intacta (Malmierca *et al.*, 2009; Ulanovsky *et al.*, 2003).

La SSA no es generada por las propiedades intrínsecas de la membrana de una neurona, lo que afectaría a todos los estímulo de manera similar, sino que necesita de la implicación de la red neuronal. La SSA ha sido encontrada en el IC (Pérez-González *et al.*, 2005), MGB (Antunes *et al.*, 2010) and AC (Nieto-Diego & Malmierca, 2016; Polley *et al.*, 2007) (**Figura 3**, pág. 17). La SSA no está homogéneamente representada en todas esas estructuras, pero muestra una organización jerárquica, manifestando un *in crescendo nivel de SSA desde el IC al MGB y alcanzando sus mayores niveles en la AC.* Igualmente la SSA aumenta desde áreas lemniscales a áreas no-lemniscales. Y es considerada una forma

de plasticidad neuronal a corto plazo (Ogawa & Oka, 2015), modulada por la acetilcolina (Ayala & Malmierca, 2015) y el GABA-A (Pérez-González *et al.*, 2012).

La SSA y el MMN fueron inicialmente descritos en diferentes especies y puntualizaban su importancia en diferentes aspectos del procesamiento de la información auditiva. Mientras que el MMN ha sido descrito durante muchos años como un proceso que refleja la detección del estímulo novedoso e infrecuente, la SSA ha sido vista simplemente como el mecanismo de adaptación a los estímulos repetitivos. Sin embargo, estudios recientes apoyan la hipótesis de que la SSA refleja también la detección del estímulo infrecuente (Ayala & Malmierca, 2012; Taaseh *et al.*, 2011), cumpliendo así un criterio fundamental de la MMN.

En este contexto, el marco teórico de la codificación de la predicción se ha convertido en una explicación atractiva de cómo se procesa la información sensorial en el cerebro auditivo (Auksztulewicz & Friston, 2016; Auksztulewicz *et al.*, 2018; Bastos *et al.*, 2012; Friston, 2005; Kort *et al.*, 2017; Shipp, 2016; Wacongne, 2016).

Conforme con este marco teórico, el MMN, y por tanto la SSA, pueden estar generados por dos mecanismos que previamente eran considerados mutuamente excluyentes: *la supresión de la repetición y el error de predicción*. Cuando un mismo estímulo auditivo es presentado de manera repetitiva, las poblaciones neuronales originalmente sensibles a ese estímulo se adaptan y sus respuestas disminuyen debido a la *supresión de la repetición*. Al mismo tiempo se crea una memoria sensorial basada en el historial de estimulación (producida por la repetición del estímulo estándar) y que es usada para crear un modelo predictivo. Cuando un estímulo raro o infrecuente aparece, una señal de error emerge, produciendo así un *error de predicción*, que incrementa las respuestas

neuronales a dicho estímulo desviado o infrecuente. Por tanto, la ruptura de la predicción que se produce al presentarse un estímulo novedoso resulta en una respuesta neuronal que es la señal de un estímulo inesperado.

En el presente trabajo trataré de desentrañar si la supresión de la repetición y/o los errores de predicción ocurren en la SSA. Además, estudiaré cómo se afectan estos mecanismos cuando se irrumpe el funcionamiento de los receptores NMDA mediante el uso de antagonistas NMDA.

c. La codificación de la predicción.

La codificación de la predicción es un marco teórico que engloba el MMN y la SSA. Aunque fue estimado hace más de un milenio por Ibn al Haytham, quien desarrolló la idea de que “*muchas propiedades visibles se perciben mediante el juicio y la inferencia*”, o cuando Hermann von Helmholtz se aferró a la idea del cerebro como un estimador de hipótesis (**Figura 4**, pág.19; Howwy, 2013), solo en los últimos años es cuando este marco teórico ha tomado fuerza dentro del campo de la neurociencia, principalmente catapultada por los trabajos de Friston (2005).

De acuerdo con este marco teórico, el cerebro trabaja como un sistema de inferencia Bayesiano (Friston, 2005) con un procesamiento jerarquizado de la información (Auksztulewicz & Friston, 2016; Friston 2005; Garrido *et al.* 2008), donde las regiones superiores estarían constantemente intentando anticipar el futuro a través de la generación de predicciones (probabilidad basada en la historia precedente) sobre lo que va a ocurrir en el futuro (Hohwy, 2013).

Este enfoque asume que las discrepancias entre las creencias anteriores y el resto de señales entrantes constituyen los errores de predicción. El MMN sería por tanto un ajuste de la suma de cientos de señales neuronales a los errores de predicción (Bendixen *et al.*, 2012). Dado que las predicciones y los errores de predicción operan de manera jerárquica (Friston, 2005; Garrido *et al.*, 2008), en términos Bayesianos, los errores de predicción corresponden a la diferencia entre la historia previa y los hechos, donde los niveles superiores envían señales predictivas hacia estructuras inferiores en la jerarquía, ejerciendo su función predominantemente a través de receptores glutamatérgicos de NMDA (Bastos *et al.*, 2012).

Por lo tanto en esta tesis estudiaré si las señales de error de la predicción se pueden encontrar en neuronas individuales y si estas señales de error de predicción muestran una organización jerarquizada a lo largo de la vía auditiva.

d. Esquizofrenia.

La esquizofrenia es un trastorno mental severo que afecta a más de 21 millones de personas en el mundo. Está caracterizada por una distorsión del pensamiento, de la percepción, de las emociones, del lenguaje, del sentido de sí mismo y del comportamiento, incluyendo alucinaciones (oír voces) y delirios (World Health Organization, 2014).

Estudios recientes sugieren que déficits en la conectividad tálamo-cortical contribuyen a la esquizofrenia (Lee *et al.*, 2017). Las teorías actuales, dentro del marco teórico de la codificación de la predicción, proponen que los síntomas positivos de la esquizofrenia, como los delirios y las alucinaciones, surgen de una alteración en la

inferencia bayesiana (predicciones) (Erickson *et al.*, 2017; Horga *et al.*, 2014; Sterzer *et al.*, 2018). Estos estudios argumentan que una predicción empobrecida de las entradas sensoriales puede ser la causa de los síntomas positivos de la esquizofrenia (Sterzer *et al.*, 2016).

En sujetos sanos, los niveles superiores, dentro de un sistema jerarquizado, codifican las predicciones y envían estas señales a niveles inferiores. Cuando los datos sensoriales entrantes rompen estas predicciones, se envía una señal de error de predicción con la finalidad de actualizar el modelo predictivo. Pero se ha propuesto que en estados de psicosis haya un desequilibrio entre las predicciones y las nuevas entradas sensoriales, con una reducida precisión de las predicciones, que produciría un aumento anómalo de los errores de predicción (Sterzer, 2018).

Se ha observado de manera consistente que las personas con esquizofrenia muestran un MMN reducido (Umbricht & Krljes, 2005). Además, también se ha visto una reducción del MMN en personas tras una exposición aguda a algún fármaco antagonista de los receptores NMDA, como la ketamina (Todd *et al.*, 2013). Una observación que permitió reforzar la hipótesis de la hipofunción de los receptores NMDA como causa subyacente a la esquizofrenia (Harms, 2016; Kantrowitz & Javitt, 2012).

Esta hipótesis se basó originalmente en investigaciones en las que la administración de antagonistas de receptores NMDA, como la ketamina o la fenciclidina (PCP) a sujetos sanos producía la gama completa de síntomas descritos en la esquizofrenia (Andine *et al.*, 1999; Krystal *et al.*, 2005). *Un deterioro similar al de los pacientes esquizofrénicos se encontró también en modelos animales tras la administración de antagonistas de los receptores NMDA, incluyendo la reducción del MMN* (Harms *et al.*, 2016) (**Figura 5**, pág.

22) . No obstante, ningún trabajo ha estudiado el impacto de estas sustancias en los errores de predicción vs. la supresión de la repetición.

Por todo ello, en esta tesis analizaré las respuestas de mismatch neuronal bajo los efectos de un antagonista de los receptores NMDA, analizando de manera independiente sus efectos en la supresión de la repetición y en los errores de predicción. También comprobaré cómo se afectan esas respuestas neuronales a lo largo de la jerarquía auditiva.

Hipótesis.

Sabiendo que el sistema auditivo central está jerárquicamente organizado con mayores niveles de SSA en las estructuras superiores de la vía auditiva y en la vía no-lemniscal. Que, además, la SSA se propone como el correlato neuronal del MMN, fenómeno alterado en pacientes con esquizofrenia y en modelos animales, y que está formado por dos mecanismos, *la supresión de la repetición y los errores de predicción*, nos planteamos las siguientes hipótesis:

- I. Los errores de predicción pueden ser registrados en neuronas individuales. Además, esos errores de predicción aumentarán conforme se asciende en la jerarquía auditiva (IC<MGB<AC), tal y como propone el marco teórico de la codificación de la predicción.
- II. La SSA en el IC puede ser modulada usando cannabinoides, ya que el colículo inferior presenta receptores endocannabinoides.
- III. Los errores de predicción y la supresión de la repetición se encuentran alterados en un modelo animal de esquizofrenia.

Objetivos.

Basados en estas hipótesis, mis objetivos fueron los siguientes:

- I. Determinar si los errores de predicción podían ser registrados en neuronas individuales del IC, MGB y AC, separando los registros entre la vía lemniscal y no-lemniscal. Para ello estimularemos con un paradigma oddball y dos paradigmas control: la secuencia de múltiples-estándar y las secuencias en cascada.
- II. Además, para evitar los posibles efectos de la anestesia en los errores de predicción, registraremos animales despiertos usando los mismos paradigmas.
- III. Determinar si la SSA puede ser modulada en el IC, usando para ello agonistas y antagonistas cannabinoides.
- IV. Por último, examinar el impacto de un antagonista de los receptores NMDA, como es el MK-801, en neuronas individuales en el eje tálamo-cortical. Descomponiendo el índice de mismatch neuronal en supresión de la repetición y en errores de predicción.

Resumen de resultados.

Nuestros resultados se basan en tres trabajos científicos publicados:

Estudio I

Registramos neuronas individuales en áreas corticales y subcorticales de ratas anestesiadas y ratones despiertos mientras eran estimulados con secuencias oddball, en cascada y de múltiples-estándar. Los datos mostraron que las neuronas individuales exhiben errores de predicción, que aumentaban a lo largo de la jerarquía auditiva, desde el colículo inferior a la corteza auditiva, y desde la vía lemniscal a la no-lemniscal. Los análisis también revelaron que esta jerarquía en los errores de predicción se presentaba independientemente de la especie (rata vs. ratón) y del estado de conciencia.

Estudio II

Los resultados mostraron que los agonistas cannabinoides incrementan las respuestas neuronales a los estímulos estándar dentro de un paradigma oddball, mientras que las respuestas a los estímulos infrecuentes permanecieron inalteradas. Produciendo, por tanto, una reducción de la adaptación-específica a estímulo (SSA).

Estudio III

Registramos una amplia muestra de neuronas individuales con condición control y animales tratados con un antagonista no-competitivo de los receptores NMDA, el MK-801. Nuestros datos muestran que el MK-801 produce un efecto diferencial sobre las respuestas a estímulos estándar (STD) e infrecuentes (DEV) dentro de un paradigma oddball en el sistema tálamo-cortical, afectando, por lo tanto, al índice de mismatch neuronal. Produciendo un incremento de los errores

de predicción a nivel de la corteza auditiva y un incremento de la repetición de la supresión a nivel talámico.

Discusión general.

En mi tesis demuestro que las neuronas individuales desde el mesencéfalo hasta la corteza auditiva muestran errores de predicción que imitan a los reportados en estudios de MMN. Este resultado apoya la hipótesis de que las neuronas individuales toman parte en la generación del MMN y de la actividad predictiva del cerebro.

Además, demostramos que los errores de predicción están jerárquicamente organizados y que son independientes de la especie y el estado de conciencia. De manera similar, mis resultados concuerdan con los que plantean que las respuestas de mismatch dependen de la actividad de los receptores NMDA (Javitt *et al.*, 1996; Garrido, 2009). Y todos ellos encajan en el marco teórico de la codificación de la predicción. Además, demuestro que la adaptación-específica a estímulo es modulada por los cannabinoides, añadiendo nuevas evidencias a la actividad neuromodulatoria de los endocannabinoides.

En este trabajo de tesis demuestro que los errores de predicción de neuronas individuales se organizan de manera jerárquica, como planteaba la teoría de la codificación de la predicción (Aukstulewicz y Friston 2016), en el sistema auditivo central de animales anestesiados y despiertos.

Por el contrario, cuando se produce una hipofunción de los receptores NMDA, esta organización jerárquica falla, como se demostró después de aplicar una dosis baja de un antagonista

de receptores NMDA (MK-801). El MK-801 aumentó la señal de error de predicción en la corteza auditiva, al mismo tiempo que aumentó la supresión de repetición en el núcleo geniculado medial.

Además, encontramos que el MK-801 altera la dinámica de la adaptación neuronal a lo largo del eje tálamo-cortical, volviéndose más rápida e intensa, especialmente a nivel del tálamo. Estos resultados están de acuerdo con otros trabajos que sugieren déficits de la actividad tálamo-cortical en la esquizofrenia (Lee *et al.* 2017). De manera similar, nuestros resultados encajan con aquellas teorías que proponen que los síntomas positivos de la esquizofrenia, como delirios y alucinaciones, surgen de la alteración en la inferencia bayesiana debido a una precisión reducida en la generación de predicciones que conduce a un aumento en los errores de predicción (Sterzer *et al.*, 2016; 2018).

Además, encontramos que los agonistas de los cannabinoides reducen la SSA en el colículo inferior, mientras que los antagonistas la aumentan. Por lo tanto, el sistema endocannabinoide puede modular la generación de SSA de manera similar a como lo hace el GABA-A y/o la acetilcolina (Ayala y Malmierca 2015; Pérez-González *et al.* 2012). Bien podría ser porque los endocannabinoides interactúan con estos neurotransmisores para dar forma a la SSA. De hecho, se ha sugerido que los neuromoduladores cannabinoides comprenden un sistema que interactúa funcionalmente con otros neurotransmisores (Lutz, 2002).

La complejidad de este sistema cannabinoide está lejos de ser entendida. Sin embargo, considerando nuestros resultados que muestran que los cannabinoides modulan el SSA y que el SSA es probablemente el correlato neuronal de MMN (Nieto-Diego y Malmierca 2016; Ulanovsky *et al.*, 2003; Harms *et al.*, 2016), sería interesante estudiar la modulación de los cannabinoides en el contexto del mismatch neuronal y la codificación predictiva. Por ejemplo, investigar si los cannabinoides desempeñan un papel en la generación de algunos síndromes psicóticos que alteran las respuestas de la MMN (Sánchez-Blázquez *et al.*, 2014; Javitt *et al.*, 2008).

En general, los datos de mi tesis doctoral muestran que las neuronas individuales a lo largo de la jerarquía auditiva tienen la capacidad de filtrar información repetitiva irrelevante para detectar estímulos nuevos, al generar señales de error mejoradas. Esta actividad es dependiente de los

receptores NMDA y modulada por los cannabinoides. Cuando estos sistemas se manipulan, por ejemplo, mediante la administración de antagonistas de los receptores NMDA, generamos un sistema patológico que altera la jerarquía normal de la supresión de la repetición y los errores de predicción, y por lo tanto un desajuste neuronal.

¿Cuáles son las implicaciones de nuestros hallazgos para la esquizofrenia? Si hubiera disponible un fármaco seguro dirigido a la subunidad relevante de los receptores NMDA, y facilitara la neuroplasticidad produciendo un aumento del MMN, incluso durante un corto período de tiempo, se ofrecería la oportunidad para una intervención que remedie los déficits cognitivos característicos de la esquizofrenia (Green *et al.*, 2000).

La memantina, por ejemplo, que se ha demostrado aumenta la amplitud de la MMN en individuos sanos y en sujetos con esquizofrenia, se ha utilizado como terapia complementaria en la esquizofrenia durante algún tiempo para mejorar la cognición en particular. Si bien los efectos de la terapia complementaria son pequeños, un meta-análisis reciente sugiere que existen mejoras en las medidas globales de cognición, pero no se observaron mejoras en las puntuaciones de pruebas cognitivas compuestas (Kishi *et al.*, 2018).

Hasta la fecha, no ha habido intentos de utilizar la respuesta de MMN a la memantina como un índice de neuroplasticidad que podría ser explotado en los estudios. Curiosamente, tanto el antagonista de afinidad moderada, la memantina, como el antagonista de alta afinidad, el MK-801, se unen a la subunidad NR2B de los receptores NMDA con uniones muy similares (Song *et al.*, 2018) pero solo se ha aprobado el uso de memantina en humanos, ya que el MK-801 mostraba efectos neurotóxicos (Olney *et al.*, 1989). Un camino para futuras investigaciones es el desarrollo de compuestos seguros para uso humano que tengan como objetivo ubicaciones de unión similares a la memantina y MK-801.

Appendix I

La Comisión Académica del Programa de Doctorado en Neurociencias de la Universidad de Salamanca, una vez examinada la solicitud enviada por D^a Gloria Gutiérrez Parra, para presentar la Tesis Doctoral en el formato de compendio de artículos cuando el número de aportaciones es inferior a tres.

Informa favorablemente sobre la calidad de las aportaciones presentadas de por la Doctoranda D^a Gloria Gutiérrez Parra, consistentes en dos artículos científicos, uno de los cuales está publicado en Nature Communication con un índice de impacto en el año de la publicación de 12,35 y del cual la doctoranda es primera autora y un segundo trabajo publicado en Scientific Report (índice de impacto de 4,12) en el que la doctoranda es segunda autora.

En Salamanca a 29 de enero de 2019



Prof^a. Aránzazu Tabernero Urbieto
Coordinadora Programa de Doctorado
en Neurociencias INCYL